Theoretical Investigations on Inorganic, Boron-containing Biradicals with a unique Structure

Dissertation zur Erlangung des naturwissenschaftlichen Doktorgrades der

Julius-Maximilians-Universität Würzburg

vorgelegt von

Eileen Welz

aus Coburg

Würzburg 2019

Eingereicht bei der Fakultät für Chemie und Pharmazie am

4.April 2019

Gutachter der schriftlichen Arbeit

1. Gutachter: Prof. Dr. Bernd Engels

2. Gutachter: Prof. Dr. Volker Engel

Prüfer des öffentlichen Promotionskolloquiums

1. Prüfer: Prof. Dr. Bernd Engels

2. Prüfer: Prof. Dr. Volker Engel

3. Prüfer: Prof. Dr. Holger Braunschweig

Datum des öffentlichen Promotionskolloquiums:

9. Mai 2019

Doktorurkunde ausgehändigt am

_____

Phantasie ist wichtiger als Wissen, denn Wissen ist begrenzt.

(Albert Einstein)

Die vorliegende Arbeit wurde im Zeitraum von Oktober 2015 bis April 2019 am Institut für Physikalische und Theoretisch Chemie der Julius-Maximilians-Universität Würzburg angefertigt.

Teile dieser Arbeit wurden bereits veröffentlicht in:

Kaiser, D.; Reusch, E.; Hemberger, P.; Bodi, A.; Welz, E.; Engels, B.; Fischer, I., The ortho-benzyne cation is not planar. *Phys. Chem. Chem. Phys.* **2018,** *20*, 3988-3996.

Légaré, M.-A.; Bélanger-Chabot, G.; Dewhurst, R. D.; Welz, E.; Krummenacher, I.; Engels, B.; Braunschweig, H., Nitrogen fixation and reduction at boron. *Science* **2018,** *359*, 896-900.

Böhnke, J.; Dellermann, T.; Celik, M. A.; Krummenacher, I.; Dewhurst, R. D.; Demeshko, S.; Ewing, W. C.; Hammond, K.; Heß, M.; Bill, E.; Welz, E.; Röhr, M. I. S.; Mitrić, R.; Engels, B.; Meyer, F.; Braunschweig, H., Isolation of diborenes and their 90°-twisted diradical congeners. *Nat. Commun.* **2018**, *9*, 1197-1203.

Seufert, J.; Welz, E.; Krummenacher, I.; Paprocki, V.; Böhnke, J.; Hagspiel, S.; Dewhurst, R. D.; Tacke, R.; Engels, B; Braunschweig, H., Isolation and Characterization of Crystalline, Neutral Diborane(4) Radicals. *Angew. Chem., Int. Ed.* **2018**, *57*, 10752-10755.

Welz, E.; Böhnke, J.; Dewhurst, R. D.; Braunschweig, H.; Engels, B., Unravelling the Dramatic Electrostructural Differences Between N-Heterocyclic Carbene- and Cyclic (Alkyl)(amino) carbene-Stabilized Low-Valent Main Group Species. *J. Am. Chem. Soc.* **2018**, *140*, 12580-12591.

Deissenberger, A.; Welz, E.; Drescher, R.; Krummenacher, I.; Dewhurst, R.; Engels, B.; Braunschweig, H., A New Class of Neutral Boron-Based Diradicals Spanned by a Two-Carbon Bridge. *Angew. Chem., Int. Ed.* **2019**, *58*, 1842–1846.

Weitere Veröffentlichungen:

Brüning, C.; Welz, E.; Heilos, A.; Stehr, V.; Walter, C.; Engels, B.; Völker, S.; Lambert, C.; Engel, V., Macrocyclic cis-lndolenine Squaraine Dyes as Efficient Near Infrared Emitters. *J. Phys. Chem. C* **2015**, *119*, 6174-6180.

Schmitt, H.-C.; Flock, M.; Welz, E.; Engels, B.; Schneider, H.; Radius, U.; Fischer, I., Electronic Structure and Excited-State Dynamic of an Arduengo-Type Carbene and its Imidazolone Oxidation Products. *Chem. Eur. J.* **2017,** *23*, 3084-3090.

Roy, D. K.; Krummenacher, I.; Stennett, T. E.; Lenczyk, C.; Thiess, T.; Welz, E.; Engels, B.; Braunschweig, H., Selective one- and two-electron reductions of a haloborane enabled by a π-withdrawing carbene ligand. *Chem. Commun.* **2018**, *65*, 9015-9018.

Danksagung

An erster Stelle danke ich Herrn Prof. Dr. Bernd Engels für die Möglichkeit, diese Arbeit in seinem Arbeitskreis anzufertigen. Die gebotenen Freiheiten, die Projektthematik, sowie der ständige Austausch mit zahlreichen Kooperationspartnern weckten vom ersten Moment an mein Interesse.

Mein Dank geht auch an die Mitarbeiter der Theoretischen Chemie, insbesondere an die der Arbeitskreise Engel und Engels. Die vielen interessanten Gespräche über wissenschaftliche, aber auch belanglose Themen, haben jeden Tag bereichert und verschönert. Auch durch das sehr familiäre Arbeitsumfeld habe ich mich stets wohl und gut aufgehoben gefühlt. Die vielen AK-Aktivitäten außerhalb der Universität waren immer lustig und haben mein Leben enorm bereichert.

Bei Herrn Prof. Dr. Holger Braunschweig möchte ich mich herzlichst für die interessanten Kooperationen und die für mich sehr aufschlussreichen Diskussionen bedanken. Besonderer Dank gilt Dr. Marc Andrè Lègarè, Dr. Julian Böhnke, Dr. Jens Seufert und Andrea Deißenberger, die mir die Welt des Bors in zahlreichen Diskussionen über Theorie und Experiment nähergebracht haben. Ein besonderer Dank gilt zudem Dr. Rian Dewhurst und Dr. Ivo Krummenacher, die mir als Theoretikerin mit ihrem immensen Wissen geholfen haben, die Borchemie besser zu verstehen.

In der Arbeitsgruppe Engels geht mein Dank an die ehemaligen und aktuellen Mitarbeiter, die mich während meiner Arbeit begleitet haben. Besonders möchte ich mich bei Dr. Johannes Becker für die vielen grandios zubereiteten Gerichte, die mir jede Mittagspause versüßt haben, bedanken. Ein großes Dankeschön geht auch an Dr. Anna Heilos, die wohl beste Büropartnerin, die man sich wünschen kann. Ich war immer wieder positiv überrascht, wie effektiv wir arbeiten und zugleich doch so viel Unsinn machen konnten. Bei Sara und Dustin möchte ich mich für die vielen wissenschaftlichen Diskussionen bedanken. Außerdem kann ich dank euch beim neuesten „Gossip" mitreden. Anh und Daniel möchte ebenfalls ich danken. Sie waren mit ihrer ruhigen, hilfsbereiten Art immer für einen da, wenn man Rat oder ein „Andechser" brauchte. Auch ein großes Dankschön für das Korrekturlesen meiner Arbeit.

Mein ganz besonderer Dank gilt Uschi. Was wäre die TC ohne eine Uschi! Du bist meine Ersatzmama und ich bin so froh und dankbar, dass ich dich kennenlernen durfte. Danke, dass

du dir immer Zeit für einen nimmst und stets versuchst, dein Bestes zu geben, sodass es jedem Mitarbeiter bei uns gut geht.

Meiner besten Freundin Corinna danke ich für die vielen Jahre der Freundschaft, die auch das Studium über eine weite Distanz überstanden hat. Ich bin sehr froh, dass ich dich habe.

Auch bei Jens, Valerie, Felix, Annika und Michel möchte ich mich bedanken. Wir haben zusammen angefangen zu studieren und ohne euch wäre das Chemie-Studium nicht so schön und lustig gewesen.

Mein größter Dank gilt meiner Familie, insbesondere meinem Papa Peter und meinen Großeltern, ohne deren Unterstützung ich heute nicht dastehen würde, wo ich bin. Danke, dass ihr immer an mich geglaubt habt und mich einfach so akzeptiert, wie ich bin.

Meinem Freund Benjamin möchte ich für einfach Alles danken. Dein Verständnis, deine Intelligenz, deine ruhige liebevolle Art, deine Geduld und vor allem dein Humor bereichern jeden Tag für mich. Danke, dass du dir die Zeit genommen hast, meine Arbeit zu korrigieren, auch wenn du mit der Thematik nicht wirklich vertraut bist.

Abbreviations

BS	Broken-Symmetry
CAAC	Cyclic Alkyl Amino Carbenes
CASSCF	Complete Active Space Self-Consistent Field
CASPT2	Multi-Configurational Second-Order Perturbation Theory
CC	Coupled-Cluster
CEPA	Coupled Electron Pair Approximation
CI	Configuration Interaction
CIM	Cluster-In-Molecule
CSF	Configuration State Functions
DFT	Density Functional Theory
DH	Double Hybrid
Dip	2,6-Diisopropylphenyl
DLPNO	Domain-based Local Pair Natural Orbitals
DSD-DFT	Dispersion corrected and Spin-Component Scaled DFT
Duryl	1,2,4,5-Tetramethylphenyl
EOM	Equation Of Motion
EPR	Electron Paramagnetic Resonance
ESR	Electronic Spin Resonance
FOIS	First-Order Interacting Space
GGA	Generalized Gradient Approximation
GH	Global Hybrid
HF	Hartree-Fock
HL	HOMO-LUMO
ISC	Intersystem Crossing
IDip	1,3-Bis(2,6-diethylphenyl)imidazoline-2-ylidene
KS	Kohn-Sham
LCAO	Linear Combination of Atomic Orbitals
LDA	Local Density Approximation
LFP	Laser Flash Photolysis
LMO	Localized Molecular Orbitals

LPNO	Local Pair Natural Orbital
LSDA	Local Spin Density Approximation
MAD	Mean Absolute Deviation
MCSCF	Multi-Configurational Self-Consistent Field
MO	Molecular Orbitals
MP	Møller and Plesset
MBPT	Many-Body Perturbation Theory
MRCI	Multireference Configuration Interaction
MR-CISD	Multireference Configuration Interaction Singles and Doubles
MRPT	Multireference Perturbation Theory
NBMO	Non-Bonding Molecular Orbital
NEVPT2	N-Electron Valence State Second-Order Perturbation Theory
NGA	Non-separable Generalized Gradient Approximation
NHC	N-Heterocyclic Carbene
NICS	Nucleus-Independent Chemical Shift
NIPES	Negative-Ion Photoelectron Spectroscopy
NO	Natural Orbital
PAH	Polycyclic Aromatic Hydrocarbon
PAO	Projected Atomic Orbital
PES	Potential Energy Surface
PNO	Pair Natural Orbital
QCCD	Quadratic Coupled-Cluster Double
SA	State-Averaged
SCF	Self-Consistent Field
SF	Spin-Flip
SIE	Self-Interaction Error
ST	Singlet-Triplet
RAS	Restricted Active Space
TB	Through-Bond
TDA	Tamm-Dancoff Approximation
TDDFT	Time-Dependent Density Functional Theory
TF	Thomas-Fermi

TME	Tetramethyleneethane
TMM	Trimethylenemethane
TS	Through-space
UEG	Uniform Electron Gas
VOO-CCD	Valence-Optimized-Orbitals CCD

Table of contents

1   Introduction

The term "radical" was used for the first time in 1789 by Antoine Lavoisier to describe the structure of organic acids.[1] In 1857, Charles Wurtz´ attempt to describe the reaction of sodium and alkyl iodides by radical intermediates was difficult to be verified as no radical species could be isolated due to dimerization effects.[2] With the discovery and synthesis of the first free organic radical, to be specific the triphenylmethyl radical by Moses Gomberg in 1900, the existence of this kind of species became subject of controversial debate,[3] in particular the idea of radicals as reactive intermediates in various reaction mechanisms. Another considerable mile stone in the area of radicals was the isolation of the first biradical by Schlenk and Brauns in 1915. The isolated bis(diphenyl)benzyl biradical showed paramagnetic properties.[4-7] Since these biradical species showed unprecedented structural, electronic and magnetic properties, they became of great interest, inter alia in this work. In the early stages of research on biradicals, an accurate description of these compounds was not possible resulting in different nomenclatures partially with the same or different meaning.[8-]

In this work, the term biradical is used and will be precisely defined and explained for an improved understanding. Biradicals can formally be described as molecules with two nearly degenerate, non-bonding orbitals with two unpaired electrons total.[9] The electrons exhibit very weak interactions and act nearly independent.[10] IUPAC's Compendium of Chemical Terminology (informally known as "Gold Book") also refers the term diradical to this species, as both names share the same meaning.[11, 12] Since the first synthesis in 1915, a multitude of different biradicals was discovered and investigated. Due to their diversity and chemical properties, they play an important role in different applications, such as optics and catalysis,[13-15] and represent a major component in bond-breaking reactions.[16-20] As silicon-based semiconductor devices exhibit high fabrication cost, the search for low-priced materials, such as organic based ones, begins. A major parameter determining the reactivity of those organic compounds is the HOMO-LUMO (HL) gap. Consequently, the main focus lies on the modification of this gap by, for example, varying the aromaticity or length of available π-systems or π-conjugated bridges. Biradicals meet the demands almost perfectly, since a small HOMO-LUMO (SOMO-SOMO+1) gap is provided. However, one of the greatest

challenges is the stability and lifetime of these biradical semiconductor compounds due to their open-shell character.

In the following section, different kinds of biradicals with their respective unique properties and applications are described. Furthermore, important parameters defining the multiplicity of the biradical and both experimental and theoretical methods to analyze the synthesis and electronic properties will be explained.

First of all, the distance between the two radical centers is of critical importance, as it determines the interaction between both radicals. For a long distance r, the electron exchange interaction J between the centers decreases tremendously leading to an almost insignificant interaction (Figure 1).[8] With the help of EPR (Electron Paramagnetic Resonance) spectroscopy, also called Electronic Spin Resonance (ESR), molecules with unpaired electrons can be identified as biradicals. Depending on the interaction J between the two radical centers, different EPR spectra are obtained. Caused by the independent behavior of the two unpaired electrons, a disbiradical refers to two doublets for one molecule in the EPR spectra. In contrast, a radical can be detected by a doublet in the EPR spectra.[21, 22] With an increasing electron exchange interaction J resulting in small interactions, a five-line signal appears in the EPR spectra representing a biradical.[8, 23, 24] Since the two electrons of a biradical should possess a similar energy and properties, they exhibit identical reactivity towards an external reagent.[22; 25]
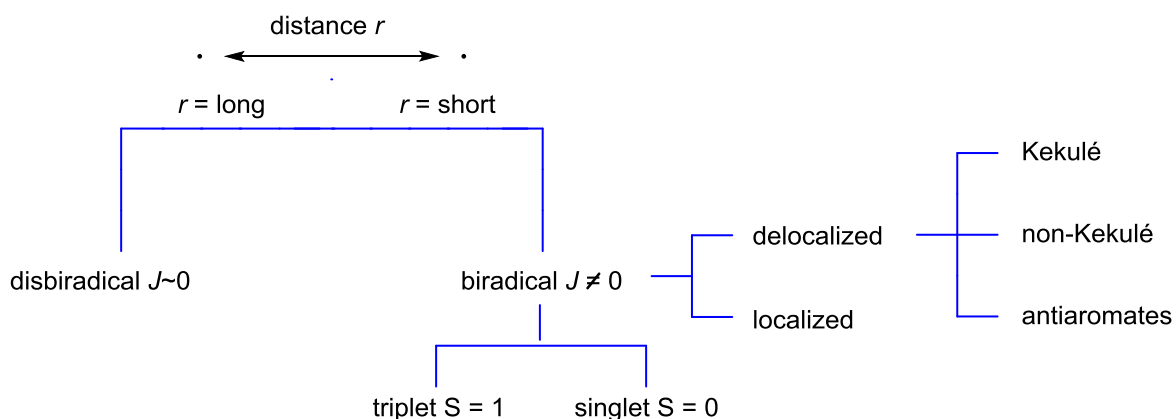

Figure 1: Definition and distinction of disbiradicals and biradicals regarding the distance r and the biradical coupling constant J of the radical centre.

Considering the occupation possibilities for biradicals as a function of the electrons and orbitals, many possible conformations can be taken. In the case of two electrons occupying two orbitals, three triplet states and one singlet state can be formed. A simplified pictured of these occupations is illustrated in Figure 2.

$$m_s = 0 \qquad m_s = 0 \quad m_s = 1 \quad m_s = -1$$
$$\underbrace{\text{singlet}} \qquad \underbrace{\qquad\qquad \text{triplet} \qquad\qquad}$$

ϕ_1
ϕ_2
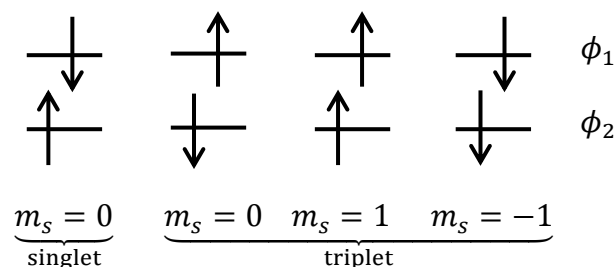
Figure 2: Presentation of the potential spin states by an open-shell occupation.

The triplet states with parallel spin components result in two degenerated states with either two up or two down spin electrons T$_1$ (m_s = 1), T$_2$ (m_s = -1). It has to be noted that the correct description of the two m_s = 0 states requires a linear combination of both states, whereas the positive combination leads to the triplet state T$_3$ and the negative combination yields a singlet wave function S$_3$. The correlation of the wave function in combination with the square of the spin operator S^2 is defined more precisely in chapter 2. Two more singlet states appear considering the closed shell occupation with every state ϕ_1 (S$_1$) or ϕ_2 (S$_2$) doubly occupied. The spin multiplicity (2S+1) of the ground state can be a low-spin singlet, with S = 0 and anti-parallel spins leading to anti-ferromagnetic spin coupling, or a high-spin triplet, with S = 1 and parallel spins resulting in ferromagnetic coupling. Whether the singlet or the triplet presents the ground state also depends on the conformation and type of biradical, as for example localized or delocalized ones. Localized biradicals, which exhibit two well defined radical centres with no conjugation through a π-system, are for instance cyclopentane-1,3-diyls or cyclobutanediyls. This kind of biradicals appears mostly in cyclic compounds or due to homolytic bond cleavage.[26] Since the triplet shows a longer lifetime than the singlet congener, substantially more experimental investigations and applications were found for the triplet species. Especially their paramagnetic properties enable a range of advantageous applications in materials chemistry, e.g. as organic magnets.[13] With just a small or nearly insignificant barrier for intersystem crossing (ISC), the singlet converts into the long-lived triplet and consequently turns into an intermediate, which is difficult to detect.[26, 27] In most organic biradicals, the singlet-triplet (ST) gap is very small and in the case of cyclobutanediyl the

biradical possesses a triplet ground state, which is experimentally proven by EPR spectroscopy.[28] This observation is quite interesting, as there are two states with different spin close by, which strongly affect the physical properties and chemical behavior.[29] This can be seen for carbenes,[14] too, and plays a considerable role in bond breaking.[16-20]

Biradicals are also used in material science, for example as graphene fragments.[15] The singlet cyclobutanediyl is very short-lived and therefore occupies a close by lying triplet, which is depicted in Figure 3. However, in contrast to the triplet, the singlet can perform a ring inversion to bicyclo[1.1.0]butane, which lies lower in energy. This ring inversion is spin forbidden in the case of the triplet state. By modifying the substituents on the cyclobutanediyl-based radicals, the lifetime of the singlet was increased.[8]
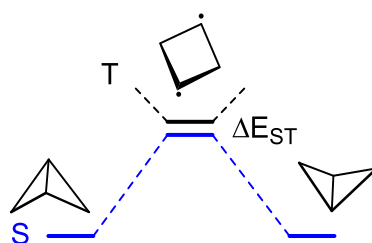
Figure 3: Different conformations of the cyclobutanediyl biradical as function of a triplet or a singlet ground state.

The ST gap and therefore the multiplicity of biradicals are determined by two parameters. On the one hand the energy gap between the two frontier orbitals and on the other hand the exchange repulsion energy. The energy gap between the frontier orbitals in turn depends on the through-space (TS) and through-bond (TB) interactions.[8, 30, 31] If the gap exceeds 1.2 eV, the singlet is expected to be the ground state.[32] For small gaps, the exchange repulsion determines the multiplicity of the system.[8] However, the 1,3-biradicals, such as cyclobutanediyl or propane-1,3-diyl, demonstrate that the amount of TS and TB plays a major role in the multiplicity of the ground state.[23, 24] While the TS interactions predict a singlet biradical as ground state, the TB interactions reveal the actual triplet multiplicity of the ground state. This behavior caused by TB interactions was already explained and proven by Hoffman in the early 1970s.[33, 34] The balance between these important parameters is of crucial importance for various kinds of localized biradicals. Since the lifetime of these biradical species can be increased by altering the energy gap between the frontier orbitals, theoretical calculations are a convenient tool to modify the size of the ST gap by varying the substituents leading to a different interaction of the TS and TB parameters.[32] In a review from Manabu Abe,

various localized biradicals and their dependencies from TS and TB interactions are examined in detail.[8]

Another biradical species is described by systems with delocalized radical centres and anti-aromatic properties, such as the $4n\pi$ annulene.[35, 36] According to the definition by Hückel, $4n\pi$ systems are supposed to be called anti-aromatic, however, the Baird determination defines aromaticity in the triplet state of $4n\pi$ annulenes (Figure 4).[35] In a theoretical analysis, this approach was confirmed, since an aromatic behavior of the triplet was observed on the basis of a nucleus-independent chemical shift (NICS) in contrast to the anti-aromatic singlet.[37, 38]
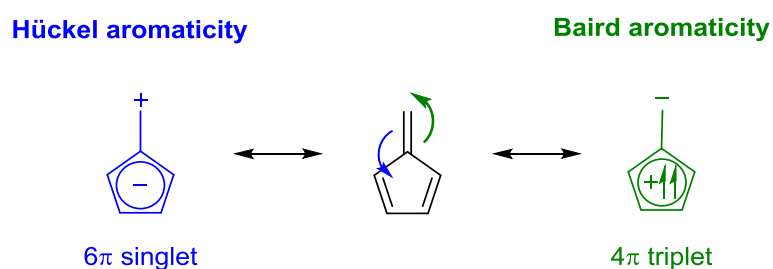
Figure 4: Schematic representation of the different definitions of aromaticity by Hückel and Baird using 5-methylene-1,3-cyclopentadiene as an example.

As a result of this analysis, fulvenes, fulvalenes and azulenes were investigated more precisely to identify those compounds as "aromatic chameleons".[39-41] These molecules, for example pentaheptafulvalene, can either appear as a Hückel aromatic singlet state or a Baird aromatic triplet state depending on the amount of conjugated π-electrons. As a function of the ground state multiplicity, the calculated dipole moments of these states are in opposite direction.[39, 40] These unique properties open up a wide field of applications, for example as starting material for various graphene-like molecules, fullerenes or large carbon systems.[42, 43] Since graphene includes Kekulé-type delocalized biradicals, understanding this type of biradical presents the main approach to control the reaction behavior of graphene.[44-46]

The most famous examples for this kind of biradicals are polycyclic aromatic hydrocarbons (PAHs) described by Tschitschibabin and Thiele (Figure 5).[47, 48] Even though the depicted molecules differ only in one phenyl spacer, they behave differently. While the electronic structure of Thiele's PAH can be described best by its closed shell structure, Tschitschibabin's PAH is outlined as biradical, both shown in Figure 5.[49, 50] In the case of the closed shell molecule of Thiele, experimental data proved the assumption of a singlet quinoid, whereas Tschitschibabin's PAH gave rise to long-lasting controversial debates about the biradical

paradox of this compound.[51-53] Depending on the structural properties and the size of the spacer in-between the two radical centres, the biradical character as well as the multiplicity of the ground state biradical can be controlled specifically. By extending the π-system of these compounds, the biradical character is assumed to increase by decreasing the HL gap.[54] Due to their switchable electronic states, those molecules can be used in a wide field of materials science, such as photovoltaics, nonlinear optics or energy-storage devices.[15, 55, 56]
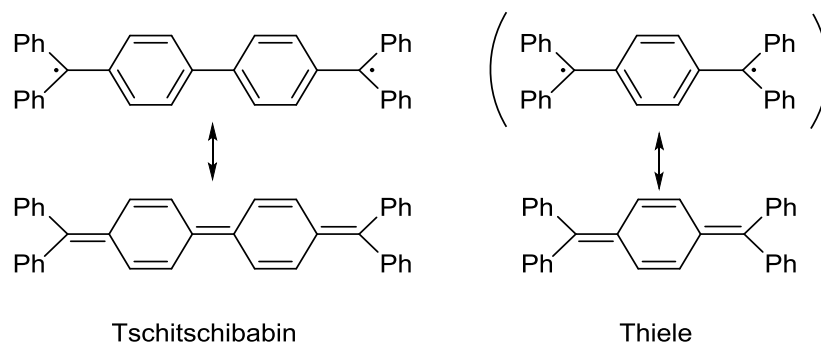
Figure 5: Tschitschibabin (left) and Thiele (right) Kekulé-type delocalized biradical in their biradical (above) and closed shell (below) structure.

Apart from the Kekulé delocalized biradicals, another quite unexplored kind of delocalized biradicals exists, named non-Kekulé biradicals.[57] Per definition, in addition to its π-electrons, a non-Kekulé biradical has to possess at least two atoms that are not included in the π-conjuagtion.[58] The best known non-Kekulé biradicals, trimethylenemethane (TMM) and tetramethyleneethane (TME), were both investigated by Paul Dowd (Figure 6).[57, 59-61]

Due to their unique bonding pattern, both molecules do not meet the requirements for the standard picture of valence resulting in new properties that need to be further investigated. Both non-Kekulé biradicals can be classified even more precisely considering the non-bonding molecular orbitals (NBMOs). TME illustrates a disjoint biradical, since the electron density is not located at the same atoms. Therefore, no particular spin-state is preferred, but mainly a singlet ground state appears. In contrast, TMM can be categorized in the class of non-disjoint biradicals, which are supposed to have a triplet ground state, since the triplet state obtains less electron repulsion.[17, 28, 62-64] In the last century, a variety of non-Kekulé biradicals was synthesized and theoretical predictions gave insight in the modification of the ST gap in the desired way.[65-67] The TME derivative for example was studied lately to tune the ST gap by modifying the TME compound with oxygen, sulphur or nitrogen, building 3,4-dimethylenefuran, 3,4-dimethylenethiophene or 3,4-dimethylenepyrroles.[65-67]

Figure 6: The two non-Kekulé molecules TMM (left) and TME (right) with their non-bonding molecular orbitals (NBMOs).

Another important species of non-Kekulé biradicals are systems with the radical center located at a heteroatom, like it is the case for benzoquinones. Those molecules play a substantial role in biological processes acting as proton-coupled electron-transfer agents.[8, 68] An interaction of biradicals with metal complexes can be observed in biological processes considering the active sites of metallo enzymes, as for example the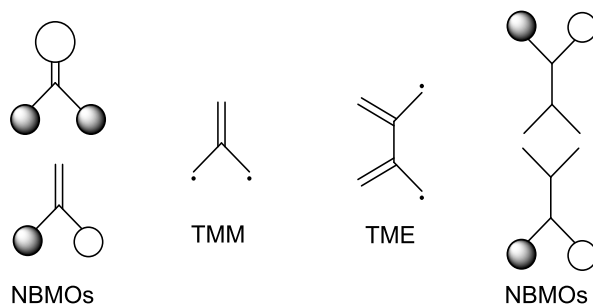 Cu(II) cation coordination to a modified tyrosyl-radical in the galactose oxidase.[69, 70] The detection and analysis of these compounds appears to be rather difficult due to the strong bonding between the radicals and the metal ion. Therefore, an enhanced understanding of those complexes illustrates a very important step in biradical chemistry. Consequently, Neese *et al.* analyzed the properties and behavior of various metal complexes with quinonato-type ligands both experimentally and theoretically to reveal their singlet biradical character.[70-72]

Due to their high energy, the associated high reactivity and short lifetime, the investigation of biradicals remains quite complicated for both theory and experiment.[73] Since the ST gap depends on the electron exchange interaction J and thus the distance of both radical centres, its magnitude provides important information about the interaction between both centres. Therefore, an accurate description of both states is necessary. One aim of this work is to develop such a method, which can reproduce the ST gap of experimentally gained biradicals correctly, even for large systems. However, not only the theoretical description of biradicals appears difficult, but the high reactivity also causes problems in experimental measurements, which are necessary to determine the ST gap of biradicals. Laser flash photolysis (LFP) and low-temperature matrix isolation methods in combination with spectroscopic techniques, such as EPR electronic emission, absorption and infrared (IR) spectroscopy, enable the detection of these short-lived species.[8] Apart from EPR spectroscopy, negative-ion photoelectron spectroscopy (NIPES) presents a suitable method to measure properties of reactive biradicals.[74, 75] By measuring the photoelectron spectrum of the anion forming both the

neutral singlet and triplet, the ST energy can be obtained directly from the spectrum.[76] As mentioned above, an important consideration of the stability and the size of the singlet-triplet energy gap ΔE_{ST} is the electron exchange interaction J, which is strongly influenced by the distance between the two spin centres. This dependency can be observed as different signals in the EPR spectra (Figure 7).
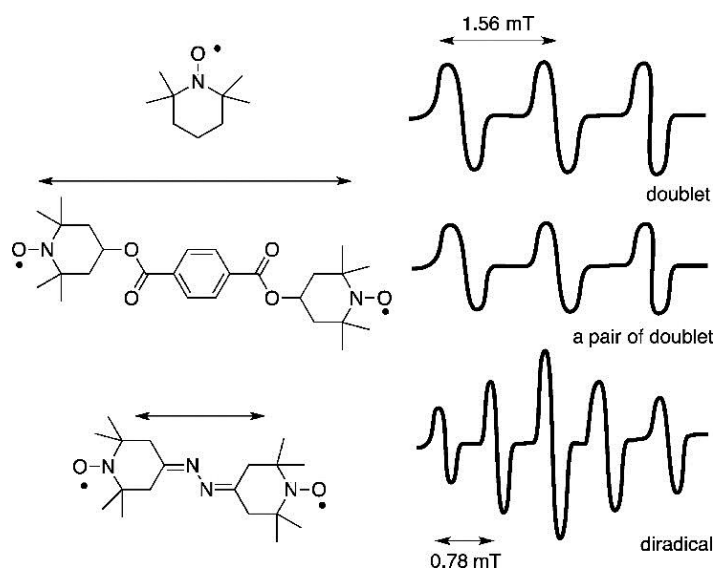
Figure 7: Differences in the EPR spectra caused by varying exchange interactions J (adapted with permission from lit.[8], copyright 2013 American Chemical Society).

To detect a doublet in the EPR spectrum of a monoradical, the measuring frequency has to be adapted to the Zeeman splitting of the molecule. Biradicals exhibit a pair of doublets in the EPR spectrum when almost no electron exchange interaction is present. With increasing interaction, a five-line signal can be seen in the spectrum, which is typical for a biradical. The singlet states are not EPR active, as their magnetic quantum number m_s is zero and thus S = 0. In contrast to the singlet, the triplet has a spin multiplicity of 3 (= 2S+1), because S = 1, in particular three magnetic quantum numbers m_s = -1, 0, 1. The singlet-triplet gap ΔE_{ST} is determined by the exchange interaction J: $\Delta E_{ST} = E_S - E_T = 2J$.[8] With a negative exchange interaction, a singlet ground state is obtained, whereas a positive interaction J leads to a triplet ground state. The magnitude of this interaction can be determined by the size of the overlap integral between both orbitals. If the overlap is insignificantly small, Hund`s rule, which states a triplet ground state, since the electrons must be half filled unpaired in two orbitals with the same energy, is no longer fulfilled.[77] This is the case for delocalized non-Kekulé molecules, such as TME. The energetic sequence of the different singlet (S$_1$, S$_2$, S$_3$) and triplet states (T$_1$, T$_2$, T$_3$) of a biradical in absence of an external magnetic field is: T$_1$ (m_s=1) = T$_2$ (m_s=-1) < S$_3$, T$_3$

(+- linear) < S_1, S_2. T_1 and T_2 represent the triplet states with unpaired electrons (Figure 2, right and second right). The positive and negative linear combined states S_3 and T_3 are lower in energy compared to the doubly occupied singlet states S_1 and S_2.

A subgroup of biradicals are the so-called biradicaloids, where the two molecular orbitals are not completely degenerated. Therefore, the molecules are called biradical-like.[78, 79] The biradical character of those molecules can be determined by an analysis of the natural orbitals obtained by a Complete Active Space multiconfigurational Self-Consistent Field (CASSCF) calculation.[79, 80] A plethora of theoreticians worked on defining a method suitable to describe the geometry, properties and behavior of biradicals correctly.[29, 55, 63, 64, 81, 82] On these grounds, the benchmark performed in chapter 4 is necessary for determining a stable and accurate singlereference method with close performance to multireference methods and suitability for large systems.

As both orbitals are not degenerated anymore, it is possible that the singlet state S_1 becomes more favourable than the triplet state. This is the case when the energy-decrease of one orbital is larger than the electron-electron repulsion interaction. With an increasing gap between the orbitals, the singlet state gets more stable.

Few attempts exist to describe the biradical character by transforming the wave function, using the natural occupation or assessing each wave function in multireference calculations. The approach developed by Ruedenberg *et al.* is based on the open-shell wave function and the coefficients that are used to describe this function by multireference methods. First of all, the negative linear combination gets recasted as depicted in Figure 8.

Figure 8: Recasting of the ψ^1 singlet wave function of unpaired electrons in terms of $\chi_\mp$.[83]

Converting the dependencies of the singlet wave function ψ^1 from φ_1 and φ_2 to χ_+ and χ_- leads to the description of the singlet electronic state, as it is used in multireferences wave functions.

$$\psi^1 = \frac{1}{\sqrt{2}}(|\varphi_1\bar{\varphi}_2\rangle) - (|\varphi_2\bar{\varphi}_1\rangle) = \frac{1}{\sqrt{2}}(|^x{}_+\bar{^x}{}_+\rangle) - (|^x{}_-\bar{^x}{}_-\rangle) \tag{1.1}$$

$$\psi^1_{MR} = \frac{1}{\sqrt{c_1^2 + c_2^2}}(c_1|^x{}_+\bar{^x}{}_+\rangle) - (c_2|^x{}_-\bar{^x}{}_-\rangle) \tag{1.2}$$

Whereas $^x{}_{\mp}$ can also be expressed in terms of spin orbitals φ_1 and φ_2.

$$^x{}_{\mp} = \frac{1}{\sqrt{2}}(\varphi_1 \mp \varphi_2) \tag{1.3}$$

Additionally, to the weighting factor of the double excited configuration, the weight coefficient of the ground state is also required to calculate the biradical character β.

$$\beta = 2c_2^2/(c_1^2 + c_2^2) \tag{1.4}$$

Within this formula, the biradical character of a singlet biradical can be determined by using the coefficients of a CASSCF calculation. Pulay and co-worker proved that systems with ten or more percentage of biradical character cannot be described correctly with single wave function methods.[84-86]

Further methods to describe the biradical character were described in literature. Yamaguchi and co-workers calculate the biradical character y_d by twice the weight of the double excited configuration c_d.[87-89] In this approach, the character can also be described by taking the overlap of the molecule orbitals T_{HO} into account.[87-90]

$$y_d = 2c_d = 1 - \frac{2T_{HO}}{(1 + T_{HO}^2)} \tag{1.5}$$

Although biradicals were studied for over hundred years, they are still difficult to synthesize, and challenging to investigate, experimentally as well as theoretically. Recent research illustrated that carbenes, especially Cyclic Alkyl Amino Carbenes (CAACs), can be suitable building blocks in order to stabilize paramagnetic compounds.[91-95] A more detailed introduction about carbenes and their stabilizing effects to biradicals is given in the initial part of chapter 5.

The unique properties of CAAC were used by the group of Prof. Dr. Holger Braunschweig, Institute of Inorganic Chemistry, University of Wuerzburg to synthesize biradical molecules

based on the main group element boron. Consequently, a further aim of this work is to find suitable theoretical methods to accurately describe some of the newly designed biradicals of the Braunschweig group. As all biradicals investigated in this work are based on boron, some interesting aspects of its behavior compared to its main group analogs are discussed in chapter 6. Due to the general high instability of biradicals, the influence of stabilizing substituents, such as various carbenes or sterically demanding substituents, is analyzed more precisely to investigate their precise effect on the stability and chemical properties of the biradicals. It is quite evident that the interaction between experiment and theory emerges as major factor in the development of new biradical species.[8]

A more precise and specific introduction is written at the beginning of each chapter. Since this work contains numerous detailed analyses, at the end of each chapter a summary is given highlighting the most important results.

2 Theoretical Foundations

2.1 Basic Principles

Apart from the findings of de Broglie regarding wave theory and the matrix mechanics from Heisenberg, Born and Jordan, one of the most important equations of the modern quantum chemistry was set up by Erwin Schrödinger in 1925, namely the so-called Schrödinger equation.[96-100] By solving the time-independent Schrödinger equation, the wave function Ψ can be obtained:[96, 101]

$$\widehat{H}|\Psi\rangle = E\,|\Psi\rangle\,.$$

<div align="right">(2.1)</div>

The Schrödinger equation contains the molecular Hamiltonian $\widehat{H}$ consisting of the kinetic (T) and potential (V) energy part of the system depending on the nuclear (R_A) and electronic (r_i) coordinates. Subsequently, the Hamiltonian depends on the number of electrons N and nuclei M and additionally on the distances between two electrons $r_{ij} = |r_i - r_j|$, two cores R_{AB} and electron and cores r_{iA}.

$$\widehat{H} = \underbrace{-\frac{1}{2}\sum_{i=1}^{N}\nabla_i^2}_{T_e} \underbrace{-\frac{1}{2}\sum_{A=1}^{M}\frac{1}{M_A}\nabla_A^2}_{T_n} \underbrace{-\sum_{i=1}^{N}\sum_{A=1}^{M}\frac{Z_A}{r_{iA}}}_{V_{en}} + \underbrace{\sum_{i=1}^{N}\sum_{j>i}^{N}\frac{1}{r_{ij}}}_{V_{ee}} + \underbrace{\sum_{A=1}^{M}\sum_{B>A}^{M}\frac{Z_A Z_B}{R_{AB}}}_{V_{nn}}$$

<div align="right">(2.2)</div>

In the course of the Born-Oppenheimer approximation, the wave function $\Omega(R,r)$ is assumed to be a product of the electronic $\Psi_{el}(r,R)$ and nuclear wave function $\Theta_{core}(R)$. The kinetic contribution of the nuclei is separated from the Hamiltonian thus the electronic Hamilton operator $\widehat{H}_{el}$ is yielded.[102]

$$\Omega(R,r) = \Psi_{el}(r,R) \cdot \Theta_{core}(R)$$

<div align="right">(2.3)</div>

Thus, the Hamiltonian can be simplified as depicted in (2.4) with the nuclear repulsion energy added after the electronic structure calculation is finished.

$$\widehat{H}_{el} = \underbrace{-\frac{1}{2}\sum_{i=1}^{N}\nabla_i^2}_{T_e} \underbrace{-\sum_{i=1}^{N}\sum_{A=1}^{M}\frac{Z_A}{r_{iA}}}_{V_{en}} + \underbrace{\sum_{i=1}^{N}\sum_{j>i}^{N}\frac{1}{r_{ij}}}_{V_{ee}}$$

<div align="right">(2.4)</div>

The electronic wave functions ψ_0 depends parametrically on the nuclear coordinates and may be modelled by slater determinants with one spin orbital χ_i per electron, thereby adhering to the Pauli principle.[103-105] A spin orbital is the combination of a spatial function and a spin dependent function $\chi_i(\vec{x}_i) = \phi_i(\vec{r}_i)\sigma(m_s)$. Since the electronic wave function depends parametrically on the nuclei, it can be solved for various conformations of the nuclei resulting in a potential energy surface.[106]

2.2 Hartree-Fock (HF)

The expectation value of the electronic energy of a molecular system, the ground state described by a single slater determinant $\langle E_0 \rangle$, can be written as follows using the Dirac notation:[101, 106, 107]

$$\langle E_0 \rangle = \langle \psi_0 | \hat{H}_{el} | \psi_0 \rangle = \sum_i^N h_{ii} + \sum_i^N \sum_{j>i}^N J_{ij} - K_{ij} \tag{2.5}$$

This represents Hartree-Fock (HF) theory. The first term, h_{ii}, is described by an one-electron operator and contains the kinetic contributions to the electronic energy, as well as the electron-nuclei attraction. The second and third term represent the Coulomb $\hat{J}_j$ and exchange operator $\hat{K}_j$ for electron-electron-interactions. Consequently, both are two electron operators. The explicit form of the operators in equation (2.5) is:[101, 106]

$$h_{ii} = \langle \chi_i | \hat{h}(1) | \chi_i \rangle \text{ with } \hat{h}(1) = -\frac{1}{2}\nabla_1^2 - \sum_{A=1}^M \frac{Z_A}{r_{1A}} \tag{2.6}$$

$$J_{ij} = \langle \chi_i | \hat{J}_j(1) | \chi_i \rangle = \langle \chi_i \chi_j | \chi_i \chi_j \rangle = \int \int \chi_i^*(1)\chi_i(1)\frac{1}{r_{12}}\chi_j(2)\chi_j^*(2)dx_1 dx_1 \tag{2.7}$$

$$K_{ij} = \langle \chi_i | \hat{K}_j(1) | \chi_i \rangle = \langle \chi_i \chi_j | \chi_j \chi_i \rangle = \int \int \chi_i^*(1)\chi_j^*(1)\frac{1}{r_{12}}\chi_i(2)\chi_j(2)dx_1 dx_1 \tag{2.8}$$

In the HF approach, the goal is to minimize the energy by optimizing the orbitals that are used in the slater determinant for the ground state ψ_0. In order to find the ideal orbitals, the variational principle is utilized:[101, 106]

$$E_{HF} = min \langle E_0 \rangle = min \frac{\langle \psi_0 | \widehat{H}_{el} | \psi_0 \rangle}{\langle \psi_0 | \psi_0 \rangle} \tag{2.9}$$

In order to obtain orthogonal molecular orbitals, this *ansatz* has to be combined with the technique of Lagrangian multipliers. The constraint $\langle \chi_i | \chi_j \rangle = \delta_{ij}$ leads to the Lagrange equation:[101, 106]

$$\delta L = \delta \langle E_0 \rangle + \sum_i^N \lambda_{ij} (\langle \delta \chi_i | \chi_j \rangle - \langle \chi_i | \delta \chi_j \rangle) = 0 \tag{2.10}$$

Thereby, so-called canonical orbitals are obtained, which are part of the solution of the diagonal matrix of the Lagrange multipliers. The resulting equation is called the Hartree-Fock equation with the Fock operator $\hat{f}_i$.[101, 106]

$$\hat{f}_i | \chi_i \rangle = \epsilon_i | \chi_i \rangle \tag{2.11}$$

$$\hat{f}_i = \hat{h}_i + \sum_j^N \hat{J}_j - \sum_j^N K_j \tag{2.12}$$

Since the HF equation for one electron depends on the averaged interaction with all other electrons, it is termed an *effective one-particle equation*. As the non-linear Fock equation is usually solved numerically using the iterative self-consistent field (SCF) procedure, a start-guess for the orbitals must be provided. However, this approach proves to be very challenging for systems with more than two electrons, if arbitrary orbital-functions are considered. Therefore, a basis set expansion is used to further simplify the mathematical problem and the molecular orbitals ϕ are approximated by a series expansion of an atomic orbital basis φ. Here, it has to be noted that all functions φ are normalized, but not orthogonalized.[101, 106]

$$\phi_i = \sum_{\mu=i}^K c_{\mu i} \varphi_\mu \tag{2.13}$$

This approach is called the Linear Combination of Atomic Orbitals (LCAO) approach. By writing the Fock equation as a function of the atomic orbital basis, the Roothaan-Hall equations are obtained as a matrix equation: [101, 106]

$$FC = SCE \tag{2.14}$$

The Fock matrix elements are part of *F*, while the *S* matrix contains the overlap elements between the basis function and the coefficient matrix *C*. The orbital energies can be found in the diagonal part of *E*.

As mentioned, the HF approach implicitly replaces the real electron-electron interaction by an average field interaction. The *ansatz* of describing the wave function as an anti-symmetrized product of one-electron wave functions does not describe the individual electron-electron interaction correctly. By expanding the basis set to its limit, the best HF result can be obtained, which does not corresponds equally to the exact energy of the system.[108] However, it turns out that the missing amount of energy appears as crucial part for describing various chemical phenomena. The missing energy is the one related to the correlated motion of the electrons due to the exact coulomb interaction. The difference between the HF estimation of the energy and the absolute energy is termed in literature as correlation energy.[108]

2.3   Post-HF methods

Since HF is known to exclude the correlation energy, different approaches were introduced to improve upon HF theory, the so-called post-HF methods.[101, 106] These methods include determinants that would identify with excited electronic states in HF theory, ϕ_i in the wave function Ψ, weighted by coefficients a_i building a multi-determinant wave function Ψ (2.15).

$$\Psi = a_0\phi_{HF} + \sum_{i=1} a_i\phi_i \qquad (2.15)$$

The various post-HF methods mostly differ in the way the additional determinants are chosen and in calculation of the coefficients a_i. The total wave function Ψ is normalized and for a system in the electronic ground-state a_0 the wave function is usually close to 1.[101, 106]

2.3.1   Configuration Interaction (CI)

In analogy to HF, CI is based on the variational principle building the trial wave function as a linear combination of various determinants weighted by expansion coefficients c_i, which differ from the LCAO coefficients $c_{\mu i}$. In CI, the coefficients are minimized, while the MOs are usually taken from a prior HF calculation. The excited state determinants can be formed by considering single excitations from an occupied orbital *i* to a virtual orbital *a* resulting in determinant ϕ_i^a. The same procedure can be performed with double or triple excitations.

$$\Psi_{CI} = \sum_i c_i \phi_i = c_0 \phi_0 + \underbrace{\sum_i^{occ} \sum_a^{vir} c_i^a \phi_i^a}_{single} + \underbrace{\sum_{i<j}^{occ} \sum_{a<b}^{vir} c_{ij}^{ab} \phi_{ij}^{ab}}_{double} + \dots \qquad (2.16)$$

Since the first term includes the HF ground state resulting in the HF energy, this part remains the main part of energy leading to a coefficient c_0 being nearly 1. It is noteworthy that the excited states determinants are not necessarily an eigenfunction of the $\hat{S}^2$ operator. By linear combination of several of these determinants, the obtained functions meet the requirements of an eigenfunction again. Functions, which are eigenfunctions of the $\hat{S}^2$ operator, like these linearly combined ones or just slater determinants, are called configuration state functions. An example of linear combinate single determinants is shown in Figure 9.

Singlet CSF   Triplet CSF
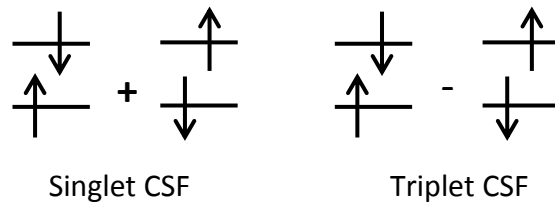
Figure 9: Configurational state functions formed from slater determinants by linear combinations.

The minimum energy can be found with the help of Lagrangian multipliers, as the total CI wave function must be normalized.

$$L = \langle \Psi_{CI} | \hat{H} | \Psi_{CI} \rangle - \lambda [\langle \Psi_{CI} | \Psi_{CI} \rangle - 1] \qquad (2.17)$$

The variational procedure is solved by considering the derivatives of the Lagrange functions with respect to expansion coefficients. For a stationary state, these need to be zero.

$$\frac{\partial L}{\partial c_i} = 2 \sum_j c_j \langle \phi_j | \hat{H} | \phi_j \rangle - 2\lambda \phi_j = 0 \qquad (2.18)$$

As seen in the Roothaan-Hall equation, the solution yields a matrix equation, which can be shortened as:

$$Hc = Ec \qquad (2.19)$$

To solve this eigenvalue equation, the CI matrix H has to be diagonalized resulting in the ground-state CI energy as lowest eigenvalue of the CI matrix, while higher lying eigenvalues are the energies of electronically excited states. The evaluation of CI matrix elements can be simplified using the Slater-Condon rules and the Brillouin theorem. The Slater-Condon rules

indicate that the CI matrix elements are only non-zero if the two determinants differ in occupation of less than two MOs. The eigenvalue of the one electron operator becomes zero for two or more mismatches and the two-electron operator for three or more mismatches. The Brillouin theorem states that singly excited states do not interact with the HF ground state. Thus, the matrix elements between the HF reference and the singly excited states is zero and only the matrix elements of the HF reference with doubly excited determinants are non-zero:

$$\langle \phi_0 | \hat{H} | \phi_i^a \rangle = \langle \phi_i^a | \hat{H} | \phi_0 \rangle = 0 \qquad (2.20)$$

Taking all kind of possible excitations into account, the CI approach is called Full-CI. For a Full-CI procedure within the limit of an infinite number of orbital functions, the Full-CI formalism yields the exact result for the energy.[109, 110] However, for N electrons $2N$ determinants are necessary and the number of CSF, which are linear combinations of the determinants, increases even more. Since apart from the occupied MOs, the virtual MOs must also be taken into account to create the different kinds of excitation, the computational cost for such methods is tremendous. By considering only a submatrix of the CI-matrix relating to finite electronically exited determinants, the computational cost can be decreased. Approximations, such as CIS (CI with singles) or CISD (CI with single and double excitations), result from this consideration. Due to the Brillouin theorem, ground-state energies obtained by CIS are identical to those evaluated using the HF approach.[111, 112] However, CIS proves suitable for the description of excited states.[113]

2.3.2 Coupled-Cluster (CC)

Another procedure to include electron correlation is the Coupled-Cluster method. While CI expands the wave function as a linear combination of determinants, in Coupled-Cluster the wave function uses an exponential expansion.[114-117] Consequently, it can also be expressed in a series expansion.

$$|\Psi\rangle = e^{\hat{T}} |\psi_o\rangle = \left(1 + \hat{T} + \frac{1}{2}\hat{T}^2 + \frac{1}{3!}\hat{T}^3 + \cdots \right) |\psi_o\rangle \qquad (2.21)$$

The cluster operator $\hat{T}$ in the exponent includes all excitations and is written as a sum of singly-excited $\hat{T}_1$, doubly-excited $\hat{T}_2$, etc. determinants:

$$\hat{T} = \hat{T}_1 + \hat{T}_2 + \hat{T}_3 + \cdots + \hat{T}_N \qquad (2.22)$$

Similar to CI, the excitation operators formally excite electrons from an occupied orbital, *i, j,* etc. to a virtual orbital *a, b*, etc. or two or more.

$$\hat{T}_1|\psi_o\rangle = \sum_{i}^{occ}\sum_{a}^{vir} t_i^a |\psi_i^a\rangle \qquad (2.23)$$

$$\hat{T}_2|\psi_o\rangle = \sum_{i<j}^{occ}\sum_{a<b}^{vir} t_{ij}^{ab} |\psi_{ij}^{ab}\rangle \qquad (2.24)$$

The coefficients t_i^a and t_{ij}^{ab} are the so-called amplitudes and differ in the calculation from the ones in CI. The excitation operators are treated within a mathematical framework, called second quantization.[118]

Coupled-Cluster has proven to be a better choice than CI, since the exponential expansion of the excitation operator gives not just the normal excitation, as for example a double excitation preserved by applying $\hat{T}_2$. There is also a mixture from the connected, such as $\hat{T}_1$ and $\hat{T}_2$, and the disconnected clusters, such as $\hat{T}_1^2$ and $\hat{T}_1^3$.[117, 119]

$$e^{\hat{T}} = 1 + \hat{T}_1 + \left(\hat{T}_2 + \frac{1}{2}\hat{T}_1^2\right) + \left(\hat{T}_3 + \hat{T}_2\hat{T}_1 + \frac{1}{6}\hat{T}_1^3\right) + \cdots \qquad (2.25)$$

In contrast to CI, the Coupled-Cluster method is size consistent. This means that both the H_2 dimer and the two disported H_2 molecules are described correctly, which is not the case for a truncated CI expansion, such as CISD.[117, 119, 120] Since Coupled-Cluster calculations are more computationally demanding than CI ones, in many cases only the numerical evaluation of Coupled-Cluster theory based approximations that assume $\hat{T} = \hat{T}_1 + \hat{T}_2$ are possible. The common nomenclature of truncated CC schemes is similar to CI, as CCS includes just the expansion to the single excitation and CCSD to single and double excitations. With a formal computational scaling of $O(n) = n^8$ (n = number of basis functions), inclusion of triple excitations exhibits very expensive computational cost and is only applicable to smaller systems.[117, 119] Consequently, CCSD offers the best choice to quantify this method. By adding the third excitations on top calculated via perturbation theory, the computationally demand increases only slightly, while the accuracy of this method increases strongly. To indicate that the third-order excitations are obtained by perturbation theory, the T is written in brackets, CCSD(T).[121-123] It is proven that even for complex multireference cases, as for example the

twist around the double bond of ethene (C_2H_4), the results of CCSD(T) lie very close to the ones obtained by multireference approaches, which include both static and dynamic correlation. CCSD fails to predict the correct energetic behaviour of this rotation. The calculation of twisting the C=C bond of ethene presents a suitable system to test the quality of the method, since the open-shell character of the system changes completely during the rotation. In such calculations, it is mandatory to consider the so-called T_1 diagnostic, which can be calculated by norming the t_1 amplitude by the amount of included electrons (2.26).[124, 125]

$$T_1 = \frac{\|t_1\|}{N_{el}^{1/2}}$$

(2.26)

Regarding the exponent T_1, the obtained value accounts for orbital relaxation or non-dynamic correlation effects.[126, 127] A large T_1 value indicates that additional dynamic correlation needs to be considered.[126-128] The amplitude t_1 is related to the coefficients of singly excited configurations and it turns out that t_1 provides a better statement than the former used reference configuration coefficient of the CI wave function c_0. However, the significance of t_1 is strongly limited to the SCF reference function. Large T_1 values over 0.02 indicate the inadequacy of the singlereference CC approach. In these cases, a multireference electron correlation method needs to be chosen instead, especially when dynamic correlation is of great influence.[126, 127] Apart from the T_1 diagnostic, the D_1 diagnostic[129] and D_2 diagnostic[130] were developed, based on the largest single excitation amplitude (D_1) or double excitation amplitudes (D_2). The best choice to examine the reliability of CC or MP2 is to consider both, the T_1 and D_1 diagnostic.[131]

The high accuracy of CC, especially CCSD(T), makes this method a suitable choice to vary and improve its performance and flexibility. A detailed review of the basic ideas of CC and of some advancement with their qualitive results, such as the multireference Coupled-Cluster (MR-CC) or equation-of-motion Coupled-Cluster (EOM-CC),[132] which was developed for excited states, is provide by Bartlett and Musial.[117] Local versions of Coupled-Cluster with second-order perturbation theory CC2 from Schütze and co-workers also yield excellent results in the field of excited states.[133-136]

In the recent years, Coupled-Cluster approaches were applied to rather large chemical systems, since various approximations were found that simplified the calculations.[137-141] Some of those approximations are based on local correlation approaches. These methodologies

were first devised by Pulay *et al.* in combination with CI, coupled electron pair approximation (CEPA) and MP methods.[142-146] This local correlation approximation reduces the number of correlated occupied MO pairs by using localized molecular orbitals (LMOs). For unoccupied MOs, projected atomic orbitals (PAO) span the virtual space but remain local.[142-146] Since AOs appear, per definition, well localized, they present a suitable choice as basis of the wave function. By projection against the MOs the correlation functions stay orthogonal to the occupied MOs. In this context, non-orthogonality of virtual orbitals exhibits just a minor issue.[142, 145, 147]

Natural orbitals (NO) are known to improve the convergence in CI tremendously.[148-150] Pair natural orbitals (PNO) are built up from a separate set of NOs for each electron pair resulting in orthonormal correlated orbitals for similar pairs, but non-orthogonal orbitals for differing pairs. Meyer used this approach to build up CEPA,[151] to which a lot of improvements were added over the time, especially to solve multireference problems.[152, 153] The PNO space for a given electron pair is local and located in the same region of space as the electron pair. In the local pair natural orbital (LPNO) approach by Neese *et al.* this locality is partially used in local fitting to the PNO.[153-155] A localization of internal orbitals reduces the number of electron pairs to be correlated, since the pair correlation energies decreases strongly with distance.[154] A problem of LPNO was the expansion of PNO in canonical virtual orbitals resulting in huge computational cost. Furthermore, the lack of truncation of single excitations results in an improvement of this approach, the domain-based local pair natural orbitals (DLPNO) approach.[156]

In the DLPNO approach, PNOs are used instead of canonical delocalized orbitals. These canonical delocalized orbitals get localized in order to classify them into domains. This reduction of computational afford. allows for the inclusion of the most important determinants to describe the electronic correlation with nearly 99.9% accuracy.[157-159] The PNOs are expanded in the basis set of projected atomic orbitals $|\tilde{\mu}\rangle$, which provide an overcomplete active space. The atomic orbitals $|\mu\rangle$ are located in the same region as their projection $|\tilde{\mu}\rangle$, thus $|\tilde{\mu}\rangle$ can be allocated to atomic centres, with $|i\rangle$ denoting occupied molecular orbitals: [156]

$$|\tilde{\mu}\rangle = \left(1 - \sum_i |i\rangle\langle i|\right)|\mu\rangle \tag{2.27}$$

Because of the exact pair correlation between distant localized orbitals, the whole pair correlation can be neglected or treated with less demanding methods. Whereby the virtual space is restricted to a subset of atomic orbitals spatially close to localized orbitals. This approach combined with CCSD or CCSD(T) is by now applicable for a large variety of systems, such as metal complexes,[138, 160] proteins[141] or different kinds of catalysis[140] and yields accurate results, even for multireference systems.[137, 157, 159-166]

Another development is the Cluster-in-molecule local correlation method (CIM) for post-HF methods.[167] In this method, the large system gets divided into a series of clusters and the thereof obtained correlation energy of each cluster is summed up. The correlation energy of the cluster can be calculated with the CC equations for a subset of occupied and virtual LMO on each cluster. Since each cluster energy can be calculated independently, the approach gets faster the better the parallelization works.[168, 169]

2.3.3 Møller-Plesset Perturbation Theory (MP)

Another methodology to evaluate correlation energy is perturbation theory.[120] For this purpose, the perturbation describing the correlation needs to be small compared to the reference system. In Many-Body Perturbation Theory (MBPT), the Hamiltonian is formally divided into two parts, the reference $\hat{H}_0$ and a perturbation $\hat{H}'$.

$$\hat{H} = \hat{H}_0 + \lambda \hat{H}' \tag{2.28}$$

The parameter λ describes the amount of perturbation. For $\lambda = 0$ the Hamiltonian is described completely by the reference system $\hat{H} = \hat{H}_0$. By applying the undisturbed Hamiltonian $\hat{H}_0$ to the zero-order wave function ψ_o, the zeroth-order energy E_0 is obtained.

$$\hat{H}_0 |\psi_o\rangle = E_0 |\psi_o\rangle \tag{2.29}$$

The number of perturbations can increase towards a finite value, as well as the obtained energy values and wave function. Both parameters can be expressed by a Taylor expansion conditional to the perturbation parameter λ^n, with n determining the order of perturbation.

$$E = \lambda^0 E_0 + \lambda^1 E_1 + \lambda^2 E_2 + \lambda^3 E_3 + \cdots \tag{2.30}$$

$$\Psi = \lambda^0 \psi_0 + \lambda^1 \psi_1 + \lambda^2 \psi_2 + \lambda^3 \psi_3 + \cdots \tag{2.31}$$

In this expansion series only ψ_o and E_0 are assumed to be known. Thus, the other perturbated wave functions ψ_n are built from the reference wave function ψ_o with the additional constraint, as the intermediaries standardization. Within this formalism all perturbed wave functions become immediately normalized.

$$\langle \Psi | \psi_o \rangle = 1 \tag{2.32}$$

Using the Taylor expansion and the normalization conditions the perturbed Schrödinger equation can be expressed in terms of λ. Whereupon terms with the same exponent of λ^n can be summarized in dependency of λ^n.

$$\lambda^0: \hat{H}_0 \psi_o = E_0 \psi_o \tag{2.33}$$

$$\lambda^1: \hat{H}_0 \psi_1 + \hat{H}' \psi_o = E_0 \psi_1 + E_1 \psi_o \tag{2.34}$$

$$\lambda^2: \hat{H}_0 \psi_2 + \hat{H}'^{\psi_1} = E_0 \psi_2 + E_1 \psi_1 + E_2 \psi_o \tag{2.35}$$

$$\lambda^n: \hat{H}_0 \psi_n + \hat{H}' \psi_{n-1} = \sum_{i=0}^{n} E_i \psi_{n-i} \tag{2.36}$$

To solve the complete perturbed equation, both, the perturbed wave function and its energy, which are both unknown, are required. By expanding the first-order wave function into a known set of functions of the reference wave function $\psi_i = \sum_i c_i \Phi_i$, the first-order correction to the energy is yielded as:

$$E_1 = \langle \Phi_0 | \hat{H}' | \Phi_0 \rangle \tag{2.37}$$

$$E_2 = \sum_{i \neq 0} \frac{\langle \Phi_0 | \hat{H}' | \Phi_i \rangle \langle \Phi_i | \hat{H}' | \Phi_0 \rangle}{E_0 - E_i} \tag{2.38}$$

Møller and Plesset (MP) propose taking the Fock operator as unperturbed part of the Hamiltonian $\hat{H}_0$ to yield a perturbation correction for the HF method. More precisely, the sum of Fock operators is used (equation (2.39)), which counts the electron-electron repulsion twice.

$$H_0 = F = \sum_{i=1}^{N} f(i) \tag{2.39}$$

To correct the double counting of the electron-electron interaction, the perturbation has to include the exact V_{ee} operator minus twice the $\langle V_{ee} \rangle$ operator. The first-order energy MP1 correction can be expressed as shown in equation (2.37). In terms of the Fock operator as unperturbed operator the energy correction gets $-\langle V_{ee} \rangle$. The designation after Møller and Plesset contains a MPn, in which n states the order of perturbation that is included.

$$E(MP0) = \sum_{i=1}^{N} \varepsilon_i \tag{2.40}$$

$$E(MP1) = E(MP0) + E(MP1) = E(HF) \tag{2.41}$$

$$E(MP2) = \sum_{i<j}^{occ} \sum_{a<b}^{vir} \frac{\langle \Phi_0 | \hat{H}' | \Phi_{ij}^{ab} \rangle \langle \Phi_{ij}^{ab} | \hat{H}' | \Phi_0 \rangle}{E_0 - E_{ij}^{ab}} \tag{2.42}$$

Investigating the unperturbed system, the results of MP0 are even worse than HF, since just the sum of the orbital energies is included. By adding first-order perturbation theory MP1, the HF solution is obtained, as MP1 includes a correction for double counting of electron-electron interaction in MP0. For second-order perturbation correction, the matrix elements between all possible excited states and the HF reference has to be taken into account. Because of the orthogonality of canonical molecular orbitals, the Brillouin Theorem, and the perturbation Hamiltonian state a 2-electron operator and only the matrix elements between the HF reference and the doubly excited state are non-zero. MP3 is empirically known to perform poorly in comparison to MP2, with results lying closer to the HF results, even if MP2 exceeds the amount of correlation. MP4 shows a performance better than MP2 and MP3; however, with a highly increased computational cost. Furthermore, the difference of the orbital energies found in the denominator of MP2 indicates difficulties of MP2 for chemical systems showing nearly vanishing HOMO-LUMO gaps.

2.3.4 Complete Active Space Methods

With Coupled-Cluster, MPn or CI the so-called dynamical correlation can be reproduced correctly. For systems with near degenerated states, such as biradicals, as well as electronically excited states or transition metal complexes, the near-degenerated correlation (also called static or non-dynamical correlation) plays a major role.[170, 171] A computational scheme to describe multireference cases and thus the statically correlation more accurately is the Multi-Configurational Self-Consistent Field (MCSCF) method. The complete wave function is therein assumed to be a linear combination of configuration state functions CSF ϕ_i weighted by mixing parameter c_i.

$$\Psi_{MCSCF} = \sum_i^N c_i |\phi_i\rangle \tag{2.43}$$

In a CI procedure working on canonical HF-orbitals, only the coefficients of the excited slater determinants get optimized. This is inadequate for the mentioned chemical systems, as the one-determinant optimized HF orbitals provide no suitable basis to form a multi-determinant wave function, even when excited electronic configurations are considered. Within MCSCF, both the coefficients c_i and the molecular orbitals themselves, more precisely the coefficients of the atomic expansion $b_{\mu i}$, are optimized:

$$\phi_i = |\psi_1 \psi_1 \psi_1 \psi_1 \dots \psi_{N/2}\rangle \tag{2.44}$$

$$\psi_i = \sum_\mu b_{\mu i}\, \varphi_\mu \tag{2.45}$$

As a simple example for a molecule requiring multireference treatment, the methylene molecule (CH_2) is presented, particularly discussing the qualitative picture of molecular orbitals developed by Walsh.[172] Considering the $\angle HCH$ angle, a different electronic arrangement appears, depending on the formation of $\angle HCH$. Since the LUMO with b_1 symmetry is a p_x orbital and thus independent of $\angle HCH$, there is no change in orbital energy if the $\angle HCH$ angle increases from 90 to 180°. Whereat the HOMO with a_1 symmetry shows a completely different behavior, since it is built from a s and a p_z orbital, which are localized at the carbon and depends on $\angle HCH$. By increasing the $\angle HCH$ angle to 180°, the percentage of the s orbital in the a_1 HOMO vanishes, resulting in an increase of the orbital energy of a_1. At

∠HCH 90°, a significant HOMO-LUMO gap and a clearly defined singlet state with a double occupied a_1 MO is observed. While for ∠HCH = 180° the HOMO a_1 and LUMO b_1 become energetically degenerate. For a correct description of every ∠HCH angle, both states have to be part of the wave function. This demonstrates the necessity to use the simplest form of a MCSCF wave function, the two-configuration SCF (TCSCF), in order to properly model the CH_2 molecule at all geometries.[173] Another example, which requires two configurations for a correct description, is the dissociation of H_2.[174]

$$\Psi_{TCSCF} = A\{a_1(\alpha)a_1(\beta)\} + B\{b_1(\alpha)b_1(\beta)\}$$

(2.46)

The molecular orbitals a_1 and b_1 are occupied by electrons with α or β spin and the amount of each state is given by the mixing parameter A or B. Thus, an easy way to describe the biradical character of a system is the use of the coefficient of the second electronic configuration in a converged TCSCF. In this case, the biradical character is given by $2B^2$. Both, the mixing parameters A and B and the atomic expansion coefficients of the MOs a_1 and b_1, need to be optimized using the variational principle. Since these additional optimizations involve a strongly increased computational effort, the amount of CSF must be kept small. A convenient idea is the restriction of the excited determinants to valence orbitals based on the principle of valence CI dividing the orbitals in external and internal sets.[170, 175-177] This concept is the basis for the Complete Active Space Self-Consistent Field method (CASSCF),[178-180] in which the most important orbitals, mainly the frontier orbitals, form the complete active space. For this active space, a Full-CI with additional orbital optimization is performed.[178, 179,-181-183]

One of the greatest challenges of the CASSCF calculation is the selection of the orbitals in the active space. If important orbitals are missing, the complete calculation loses accuracy, since all orbitals get optimized, but only the active electrons are statically correlated. The size of the space N_{CAS} including all configuration of the MCSCF wave functions depends on the number of active electrons n and orbitals m and also S, the total spin:[179, 180, 184]

$$N_{CAS} = \frac{2S + 1}{m + 1}\binom{m + 1}{\frac{n}{2} - S}\binom{m + 1}{\frac{n}{2} + S - 1}$$

(2.47)

Choosing the active space becomes even more complicated for excited state calculations, since apart from valence orbitals, more complicated orbitals, such as Rydberg orbitals, gain in importance. Roos *et al.* proposed a solution in the Restricted Active Space method (RAS), in which the active space is again divided into three sub categories, RAS1, RAS2 and RAS3.[181, 185] The RAS2 sub room is in accordance with the former active space considering all excitations, while the RAS1 space only includes a limited number of holes in a mostly double occupied space. The RAS3 orbitals contain only a limited number of electrons in orbitals that are unoccupied.[43, 44]
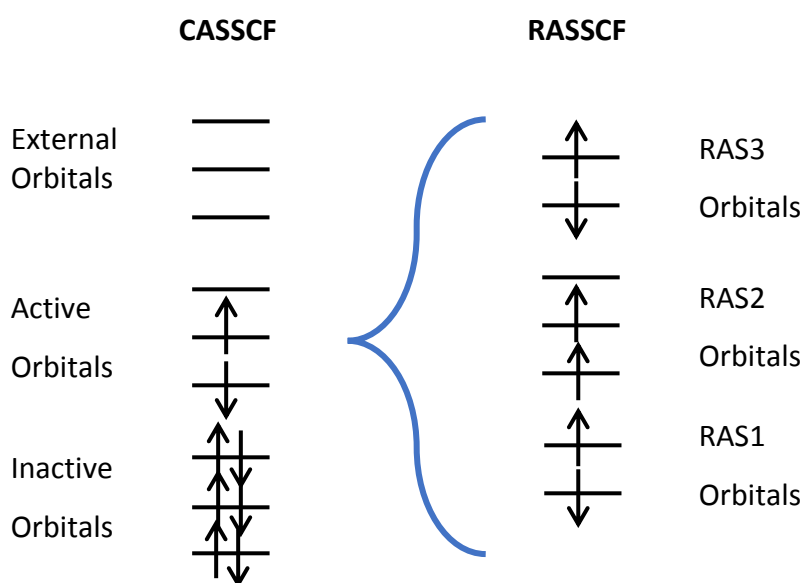

Figure 10: Scheme of a CASSCF space subspace, with an additional subdivision into the RAS space on the right.

The choice of the RAS spaces is freely selectable, thus, it is not surprising that a lot of attempts were published to simplify the choice of the active or restricted active space.[182, 186-190] In Figure 10, the room assembly of both methods CASSCF (Figure 10, left) and RASSF (Figure 10, right) is depicted.

Many roots of the same symmetry often lie energetically close to each other for excited states, which may result in issued termed root flipping.[191] A solution for this kind of problem is presented by state-averaged (SA) CASSCF, in which a set of chosen states is averaged E^{av}.[192, 193]

$$E^{av} = N^{-1} \sum_{i}^{N} E_i$$

(2.48)

Consequently, the form of the molecular orbitals has to optimized to be suitable for more than one CI vector simultaneously.[179, 194] Furthermore, the state average CASSCF method provides acceptable results in the calculation of non-adiabatic interactions, such as spin-orbit or vibronic coupling between excited states.[195]

It is noteworthy that the CASSCF wave function can be regarded as an extension of the RHF wave function capable of handling near degeneracy systems. Nevertheless, it cannot be used to accurately treat systems were dynamical correlation plays a major role. However, the CASSCF wave function and energy can be used as a reference for the inclusion of dynamical correlation.[196]

In CASSCF, nondynamical correlation is included as the wave function is modelled using a mixture of CSF. While static correlation is generally based on a limited number of states, which appear energetically close to each other near the Fermi level, dynamical correlation depends on very large number of highly excited CSF, each with a small weight. Because of the strong bonding and antibonding character of the delocalized orbitals in a near-degenerated case, the potential energy surface gets mainly effected by changes in this kind of correlation.

One of the most straight-forward methods to describe dynamical correlation is second-order Møller-Plesset perturbation theory (MP2).[197] Since MP2 depends on the energy difference of the frontier orbitals, it is known to show substantial issues for near degenerated or degenerated HL gaps. Therefore, it cannot be used in these cases.

Another method to describe both static and dynamical correlation is Multireference Configuration Interaction MR-CI.[198-201] MR-CI suffers from a number of drawbacks, which prohibit its widespread application: computational cost of reasonably truncated CI expansions rises tremendously even for small systems. Furthermore, truncated CI expansions are not strictly size-consistent.[202]

Using Multireference Coupled-Cluster both kinds of correlation can be accounted for within a size extensive methodology.[117] Although the development of these methods has a long history, there are until now hardly any routinely used variants of MR-CC available, mostly due to their unfavorable cost-benefit ratio.[203-205] Invoking MR-CC with the equation of motion *ansatz*, excitation energies and ionization potentials open-shell molecules can be obtained with very high accuracy.[206]

2.3.5 Multi-Configurational Second-Order Perturbation Theory (CASPT2)

The utilization of perturbation theory-based methods, such as MP2, is often more convenient than resorting to CI expansions due to size-extensivity and diminished computational afford. Thus, a perturbation theory-based approach for the inclusion of dynamical correlation for MCSCF wavefunctions is desirable. One of these methods is called CASPT2, and its mathematical foundation is similar to the previously mentioned singlereference formalism in Møller-Plesset theory. In CASPT2 - instead of using the HF single determinant wave function - a CASSCF wave function is used as the unperturbed reference wave function ψ_o. As one possible realization of a MCSCF wavefunction is a simple HF one-determinant solution, CASPT2 results should be equivalent to those of MP2 in these specific cases. The realization of this property turns out to be rather complicated, since the Fock operator of the spin-averaged first-order density matrix of the reference wave function is used in the CASPT2 approach.[207] One problem occurring with a MR reference wave function is the fact that this wave function does not have to be an eigenfunction of the Fock operator leading to the Fock operator as an insufficient zeroth-order Hamiltonian H_0. This problem can be solved by using Dyall's Hamiltonian - as it is the case in so-called N-Electron Valence Perturbation Theory (NEPVT2)[208-210]- or through a definition of H_0 with the projection operator *P* and its orthogonal complement *Q=1-P*. Then the Fock operator can be used as the foundation of H_0.

$$H_0 = PFP + QFQ \tag{2.49}$$

The off-diagonal elements of the subspace can be removed, while retaining the ones between the subspaces. The two reported CASPT versions differ in their neglect (older CASPT2) or inclusion (newer CASPT2) of these off-diagonal elements.

The first-order wave function Ψ^1 is obtained by applying the double substitution operator on the reference wave function Ψ^0. In contrast to MP2, which uses CSF to describe the first-order wave function, CASPT2 and NEVPT2 use internally contracted configurations to span the first-order wave function. The obtained space is called the First-Order Interacting Space (FOIS).

$$\Psi^1 = \sum_{pqrs} T_{pr}^{qs} \boldsymbol{E}_{pq} \boldsymbol{E}_{rs} \Psi^0 \tag{2.50}$$

The excitation operator E_{rs} removes an electron from the occupied orbital r, located in either the inactive or the active space, to the active or virtual orbital s. To obtain the first-order wave function Ψ^1, the linear system of equations in equation (2.51) has to be solved.

$$(H^0 - E^0)\Psi^1 = (H^0 - H)\Psi^0 \qquad (2.51)$$

The energy is subsequently calculated in analogy to the second-order energy from singlereference perturbation theory.

Excited states can be evaluated very accurately using CASPT2 providing results with a relative error of approximately ± 0.2 eV.[211-214] Since this work does not focus on excited state calculations, the basic concept and the recommended quantum methods are not described in detail. The review of Merchán and co-workers provides an overview of the quality of different computational methods for this purpose.[214] CASPT2 is also known for its reliable performance when modelling heavy elements or actinide chemistry.[215] Furthermore, open-shell systems, such as (bi)radicals, may be calculated robustly and accurately with CASPT2.[8, 73, 216] For the calculation of excited states, Rydberg states again constitute a problem. This issue can be remedied by using a multi-dimensional reference space, which is spanned by state-averaged CASSCF states. This is realized in the MS-CASPT2 approach.[217]

A seconder-order perturbation theory-based correction scheme for RASSCF calculations is also available, called RASPT2. As for a RASSCF reference state further issues appear, RASPT2 is not as widely used as CASPT2.[218] A less accurate compromise between chemical accuracy and computational practicability is offered by the generalized valence bond method combined with Møller-Plesset-Theory, termed GVB-MP2. [219-222]

2.3.6 N-Electron Valence State Second-order Perturbation Theory (NEVPT2)

Quasi-degenerate perturbation theory faces the problem of intruder states resulting in altered results for the same wave function. Rectifying this issue with the theory of intermediate Hamiltonian or Multipartitioning Perturbation Theory results in a formalism with lacking size consistency. In CASPT2, both problems are fixed by the use of a multideterminant zeroth-order CAS-CI wave function perturbed under the action of excitation operator. But the zeroth order Hamiltonian of CASPT2 does not include bielectronic interactions, while the zeroth-order wave function does.[223, 224]

By introducing partly bielectronic character in H^0 using the Dyall Hamiltonian H^D, the systematic error of the used Fock operator in CASPT2 is reduced.[225, 226] The Dyall Hamiltonian is defined as sum of the one-electron-operator H_i, the two-electron-operator H_v and a constant C, ensuring that H^D acts equivalently to H in the CAS space.

$$H^D = H_i + H_v + C \tag{2.52}$$

$$H_i = \sum_i^{core} \epsilon_i E_{ii} + \sum_r^{virt} \epsilon_r E_{rr} \tag{2.53}$$

$$H_v = \sum_{ab}^{act} h_{ab}^{eff} E_{ab} + \frac{1}{2} \sum_{abcd}^{act} \langle ab|cd \rangle (E_{ac}E_{bd} - \delta_{ac}E_{ad}) \tag{2.54}$$

$$C = 2 \sum_i^{core} h_{ii} + \sum_{ij}^{core} (2\langle ij|ij \rangle - \langle ij|ji \rangle) - 2 \sum_i^{core} \epsilon_i \tag{2.55}$$

This approach was later on realised by Malrieu *et al.* in the NEVPT2 method.[208-210] The First-Order Interacting Space (FOIS) *S* includes all determinants, which are not involved in the CAS and exhibit non-vanishing interactions with the zeroth-order wave function Ψ_m^0.
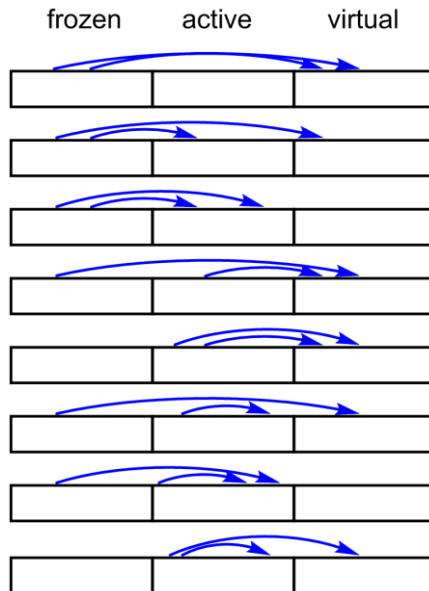

Figure 11: The eight subclasses of contracted function defining the FOIS.

S can also be described as sum of the various subspaces $S_l^{(k)}$ with *l* defining the inactive orbitals, whether from the core or virtual orbitals, and the amount of electrons *k* added or removed from the active space. A graphic representation of the eight possible typologies of

the subspaces obtained by a substitution of two core by two virtual orbitals (first row, Figure 11 or two active excited to the virtual space (last row, Figure 11) is given.

Different possibilities to form the NEVPT2 approach depend on the degree of contraction of the FOIS or the exact definition of H^0. The introduction of an internally contracted corrections function (IC) Φ_{ij}^{rs} leads to a strongly decreased dimensionality of the subspaces. Since this function is not orthogonal, they are used in the partially contracted PC-NEVPT2 approach to build multireference wave functions Φ_{ij}^{rs} being part of the various subspaces IC S_l^k.

$$\Phi_{ij}^{rs} = E_{ri}E_{sj}\Psi_m^0 \tag{2.56}$$

This contracted function spanning the FOIS is also used in CASPT2, Partially Contracted NEVPT2 (PC-NEVPT2) or contracted CI. But in contrast to CASPT2, the Dyall Hamiltonian and the multireference wave functions Φ_{ij}^{rs} appears as its eigenfunctions. Thus, the zero-order Hamiltonian for PC-NEVPT2 can be written as:

$$H_0^{PC} = P_{CAS}HP_{CAS} + \sum_{l,k} P_{S_l^k} H^D P_{S_l^k} \tag{2.57}$$

Choosing the single correction function Ψ_l^k from each IC $S_l^{(k)}$ subspace by projection ($\Psi_l^k = P_{S_l^k}H\Psi_m^0$) results in orthogonal functions, which can be easily used to form a perturbation series. Using Dyall's Hamiltonian results in a new formulation of the zeroth-order Hamiltonian in the so-called strongly contracted NEVPT2 (SC-NEVPT2).[208, 209]

$$H_0^{SC} = P_{CAS}HP_{CAS} + \sum_{l,k} |\Psi_l^{k'}\rangle E_l^k \langle\Psi_l^{k'}| \tag{2.58}$$

Although the number of correction functions needed in SC-NEVPT2 decreases significantly compared to PC-NEVPT2, the obtained results are less than 0.1 eV apart.[208, 227]

A known problem of NEVPT2 results from the Dyall Hamiltonian treating orbital differently with respect to their (arbitrary) assignment to active or inactive spaces. Thus, different results are obtained for the same reference wave function, when orbital labels are exchanged, which is unphysical.[228]

As a favorable property, NEVPT2 results are strictly size consistence and intruder states are absent. Since the formalism of the wave function is formulated spin-free, spin purity is also guaranteed.

2.4 Density Functional Theory

2.4.1 Basics

In contrast to the wave function-based methods, density functional theory (DFT) employs another idea to describe molecules with quantum mechanics, namely the use of the electron density, more precisely the probability density $\rho(\vec{r_1})$.

$$\rho(\vec{r_1}) = N \int \int \cdots \int |\Psi(\vec{r_1}, \vec{r_2}, \cdots \vec{r_N})|^2 d\vec{r_2} \cdots d\vec{r_N} \tag{2.59}$$

The electron density includes information about the number of electrons of a system by integration over the complete space: $\int \rho(\vec{r}) d\vec{r} = N$. The poles of the density correspond to the locations of the atom nuclei and the middle average density of the nuclei reveals information about the nuclei number Z. Thus, the electron density includes all necessary information about a system and the idea of using the electron density instead of the real wave function got in the focus.

In the beginning of DFT, Thomas and Fermi came up with a possible approach to describe the energy of many electron systems with a statistical model of the electron density.[229, 230] Starting point of the Thomas-Fermi (TF) theory, also called the "statistical theory", is the TF energy functional $\varepsilon(\rho)$ for a molecule with K nuclei with the charges Z_i, whereupon $Z_i > 0$ and their locations are $R_i \in R^3 (i = 1, .., K)$.

$$\varepsilon(\rho) := \frac{3}{5}\gamma \int_{R^3} \rho(x)^{5/3} dx - \int_{R^3} V(x)\rho(x)dx + \frac{1}{2}\int_{R^3} \frac{\rho(x)\rho(y)}{|x-y|}dxdy + U \tag{2.60}$$

The first term of $\varepsilon(\rho)$ describes the well-known Thomas-Fermi kinetic energy as a function of the electron density. The second term is equal to the Coulomb potential, which induces the attractive interaction of N electrons with K nuclei. The third term describes the repulsive electron-electron interaction and U resembles a constant specifying the nuclei-nuclei interaction.

The Thomas-Fermi energy E^{TF} is obtained by minimizing $\varepsilon(\rho)$ with $\rho \in L^{5/3}(R^3)$ and $\int \rho = N$:

$$E^{TF}(N) = inf\left\{\varepsilon(\rho): \rho \in L^{5/3}, \int \rho = N, \rho \geq 0\right\} \tag{2.61}$$

The solution provides the Thomas-Fermi equation:

$$\gamma \rho(x)^{2/3} = [\Phi(x) - \mu]_+ \qquad (2.62)$$

with the Lagrange multiplier μ and the TF potential Φ. In the case of $N=Z$ the more common TF equation can be applied:

$$-\Delta \Phi(x) + 4\pi\gamma^{-3/2}\Phi(x)^{3/2} = 4\pi \sum_{j=1}^{K} Z_j \delta(x - R_j) \qquad (2.63)$$

However, the solution of the TF equation provides always unstable, non-binding molecules for each $N \leq Z$.[231] By Slater, the set of self-consistent field equations involving an effective local potential defined on terms of ρ by the free-electron gas, binding in molecules was now possible.[105]

The theorems of von Hohenberg, Kohn and Sham allow for the use of a SCF scheme similar to Slater's equation to calculate the energies of atoms, molecules and solids.[232, 233] In the first theorem they proved that there is an unique relation between the electron density ρ_0 of the ground state and the ground state energy E_0, i.e the ground state energy is a functional of the ground state density $E_0 = E_0[\rho_0]$. Furthermore, they verified in their second theorem that the true ground state density ρ_0 has the lowest energy $E_0[\rho] \geq E_0[\rho_0]$. The ground state energy can be described with:

$$E_0[\rho_0] = \mathrm{T}[\rho_0] + E_{ee}[\rho_0] + E_{Ne}[\rho_0] \qquad (2.64)$$

With $\mathrm{T}[\rho_0]$ resembling the kinetic energy, $E_{ee}[\rho_0]$ the electron-electron interaction and $E_{Ne}[\rho_0]$ the electron-nucleus interaction. Since only $E_{Ne}[\rho_0]$ is known, $\mathrm{T}[\rho_0] + E_{ee}[\rho_0]$ are added in the Hohenberg-Kohn functional. The electron-electron interaction can be divided in two parts: $E_{ee}[\rho_0] = J[\rho_0] + E_{XC}[\rho_0]$. Using the known classical Coulomb energy J, only $E_{XC}[\rho_0]$ remains unidentified.

$$E_0[\rho_0] = T[\rho_0] + J[\rho_0] + E_{XC}[\rho_0] + E_{Ne}[\rho_0] \qquad (2.65)$$

With the help of Sham, Kohn (KS) described the density as a one-electron density, which can be obtained from the square of the Slater determinant.[232]

$$\rho(r) = \sum_{i=1}^{N} |\Phi_i(r)|^2 \tag{2.66}$$

$$\hat{f}^{KS}\chi_i^{KS} = \varepsilon_i \chi_i^{KS} \tag{2.67}$$

$$\hat{f}^{KS} = -\frac{1}{2}\nabla_i^2 + V_{Ks}(r) \tag{2.68}$$

The Kohn-Sham operator is divided in the kinetic part $-\frac{1}{2}\nabla_i^2$ and the effective potential $V_{Ks}(r)$:

$$V_{Ks}(r) = V_{ext}(r) + \int \frac{\rho(r')}{|r - r'|}dr' + \frac{\delta E_{xc}[\rho(r)]}{\delta\rho(r)} \tag{2.69}$$

By using a SCF scheme to calculate the energies of molecules, analog to the one for HF, they identified a way to describe the system exactly utilizing only the ground state density, if the exchange-correlation functional was given exactly.

$$E[\rho] = T_{KS}[\rho] + J[\rho] + E_{XC}[\rho] + E_{Ne}[\rho] \tag{2.70}$$

$$\text{with } E_{XC}[\rho] = T[\rho] - T_{KS}[\rho] + E_{ee}[\rho] - J[\rho] \tag{2.71}$$

As the E_{XC} functional is not known, the modern DFT is built up on finding the exact solution or a good approximation of this functional. Since there are no systematic improvements to DFT, Jacob found a way to classify the different functional into groups, which can be presented by Jacob's ladder (Figure 12). Using the slater determinant built of the electron density, the so-called non-interacting kinetic energy from the orbitals of the slater determinants can be calculated.[234] Instead of the HF exchange potential, the KS approach contains a potential *xc*, which includes the electron correlation and the electron kinetic energy beyond the non-interacting part and also tries to approximate the exchange part. The unknown E_{XC} functional can be formulated in dependencies on more factors than just the density, such as the local dimensionless reduced spin-density gradients $\nabla\rho(r)$, the local spin-labelled kinetic energy densities τ_σ or even HF exchange energy densities, constituting the single steps of Jacobs ladder (Figure 12). However, even when the dependency on τ_σ or the HF energies is included, the functional can still be declared a density functional, as orbital dependent functionals rely on occupied KS orbitals and therefore on the density.[235] Since the KS approach was formed
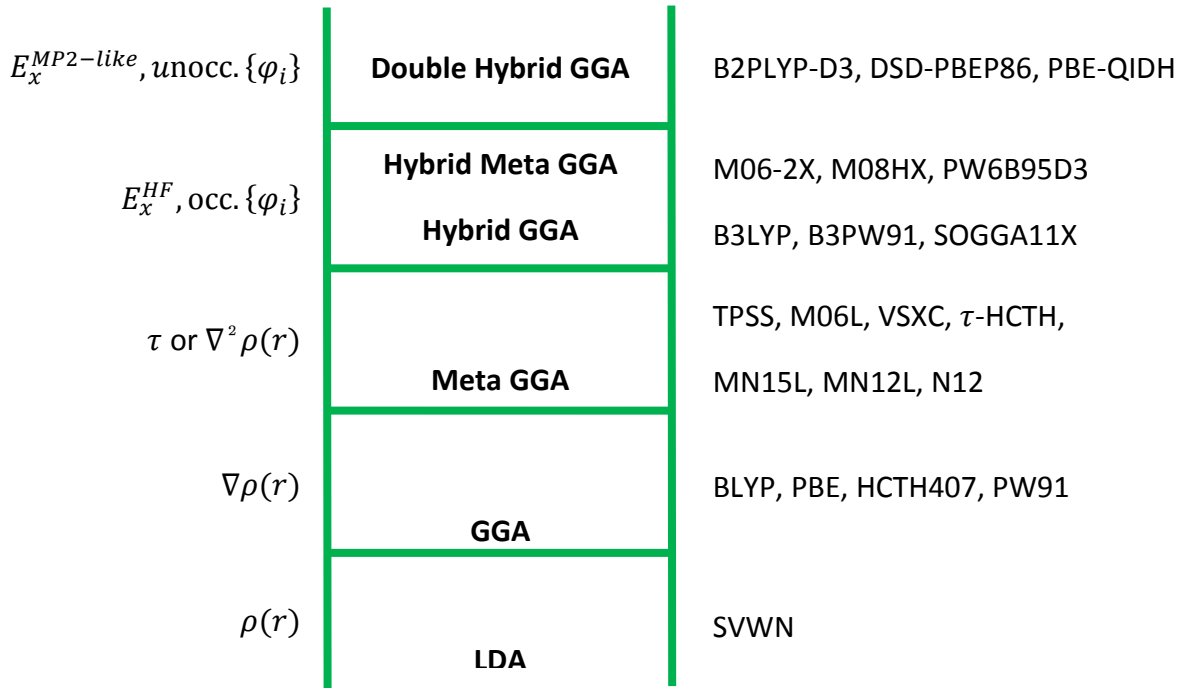
$E_x^{MP2-like}, unocc. \{\varphi_i\}$	**Double Hybrid GGA**	B2PLYP-D3, DSD-PBEP86, PBE-QIDH
$E_x^{HF}, occ. \{\varphi_i\}$	**Hybrid Meta GGA**	M06-2X, M08HX, PW6B95D3
	Hybrid GGA	B3LYP, B3PW91, SOGGA11X
τ or $\nabla^2 \rho(r)$		TPSS, M06L, VSXC, τ-HCTH,
	Meta GGA	MN15L, MN12L, N12
$\nabla \rho(r)$		BLYP, PBE, HCTH407, PW91
	GGA	
$\rho(r)$		SVWN
	LDA	

Figure 12: Jacob`s ladder classifying the different kind of functionals in DFT.

with a possible exact solution in mind, the most challenging work in DFT is to find a proper description for the exchange-correlation functional. Most of the newly developed DFT methods just focus on a better description of the exchange functional E_{XC}. Hereafter, the different steps of the Jacob's ladder are described more precisely.

2.4.2 Local Density Approximation (LDA)

Since it is possible to derive functionals for an Uniform Electron Gas (UEG), the simplest approach is represented by treating the electron density locally as a UEG at each point,[236, 237] which yields the Local Density Approximation (LDA) and Local Spin Density Approximation (LSDA), respectively.[232] In the LSDA, the total electron density can be expressed as the sum of two spin densities in the spin polarized case: spin up density ρ_α and spin down density ρ_β. For both local density approximations, the exchange energy shows an exact form and the correlation does not.[238]

$$E_x^{LDA} = -\frac{3}{4}\left(\frac{3}{\pi}\right)^{1/3}\sum \rho^{4/3} dr \qquad (2.72)$$

$$E_x^{LSDA} = \sum_\sigma^{\alpha,\beta} e_{x,\sigma}^{UEG} dr = -\frac{3}{2}\left(\frac{3}{4\pi}\right)^{1/3}\sum_\sigma^{\alpha,\beta} \rho_\sigma^{4/3} dr \qquad (2.73)$$

The correlation functions are parametrized using numerical results obtained from quantum Monte Carlo calculations,[239, 240] e.g. the formulae VWN3 and VWN5[241] from Vosko, Wilk and Nusair or the denotations in 1991 and 1992 leading to the so-called PW92[242] correlation functional from Perdew and Wan. A detailed documentation of the development and quality of these approaches can be found in various reviews.[243, 244] The combination of the exact Slater exchange S and VWN5 correlation results in the SVWN functional.[238, 242] Since no substantial difference arise when the various LDA correlation functionals are used, just the SVWN functional is examined in the Benchmark in chapter 4.[245]

Despite its conceptual simplicity, LDA performs surprisingly accurate, regardless of some typical deficiencies, such as the inadequate cancellation of self-interaction contributions.[246] A partial explanation for its accuracy lies in the systematic cancellation of errors. In fact, LDA typically underestimates E_X, but overestimates E_C resulting in unexpectedly good E_{XC} values.

2.4.3 Generalized Gradient Approximation (GGA)

For real systems, the inhomogeneous density distribution in L(S)DA gets problematic rendering this approximation rather not suitable anymore. The density inhomogeneity leads to a spatially varying density $\rho(r)$. By adding a dependency of exchange and correlation energy densities on the magnitudes s_α and s_β of the reduced gradients of ρ_α and ρ_β, these inhomogeneities lead to the Generalized Gradient Approximation (GGA).[247] The function $g_{x,\sigma}^{GGA}$ is enclosed to the former LSDA exchange functional, which is also called an Inhomogeneity Correction Factor (ICF).

$$E_x^{GGA} = \sum_\sigma^{\alpha,\beta} \int e_{x,\sigma}^{UEG} g_{x,\sigma}^{GGA} \, dr = -\frac{3}{2}\left(\frac{3}{4\pi}\right)^{1/3} \sum_\sigma^{\alpha,\beta} \rho_\sigma^{4/3} dr \tag{2.74}$$

A first attempt to improve LSDA with the $g_{x,\sigma}^{GGA}$ function was made by Herman and co-workers and has the following structure:[248, 249]

$$g_{x,\sigma}^{GGA} = 1 + c_x x_\sigma^2, \text{ where } x_\sigma^2 = \frac{|\nabla \rho_\sigma|}{\rho_\sigma^{4/3}} \tag{2.75}$$

Because of its inaccurate, asymptotical behavior, Becke invented a more suitable finite domain alternative, where x_σ was improved to u_σ and implemented in the ICF like:[250, 251]

$$g_{x,\sigma}^{GGA} = 1 + c_{x,1}u_\sigma \text{ , with } u_\sigma = \frac{\gamma x_\sigma^2}{1 + \gamma x_\sigma^2} \tag{2.76}$$

Becke extended this to the B97 exchange functional with the ICF form:[252]

$$g_{x,\sigma}^{GGA} = \sum_{j=0}^{N} c_{x,j} u_\sigma^j \tag{2.77}$$

Another possible improvement was made by Perdew with $s_\sigma^2 = \frac{1}{2(6\pi^2)^{1/3}} \frac{|\nabla \rho_\sigma|}{\rho_\sigma^{4/3}}$. In this work, a few different GGA functionals are used, such as BLYP,[253, 254] which contains the B88 exchange and the LYP correlation, and PBE,[250,255] which is composed of the PBE exchange functional and the PBE correlation functional. Additionally, it is possible to parametrize GGA functionals semi-empirically, as done for the series by Handy *et al.*, where the HCTH407[256] is used.

An enormous issue of the GGA family is that they are not able to satisfy all the theoretical constraints of the exact functional. Therefore, they do not yield accurate results for a vast area of applications. "No single GGA can describe with high accuracy the properties of both solids and molecules."[257] Truhlar and co-worker provide a possibility to improve this behavior by including the second-order coefficient in the exchange functional[258] in the flexible SOGGA11[259] functional. It is built up from SOGGA[258] and PBE,[250] both including the exact second-order coefficients.[260, 261] This functional is parametrized for a broad accuracy in chemistry[259] and provides accurate results in a wide range of areas except for lattice constants.[262]

Starting from an analysis of the low density and large gradient regions, which dominate van der Waals interactions, a modification of the exchange functional introduced by Perdew and Wang was made. This modification is obtained without increasing the number of adjustable parameters and retaining all the asymptotic and scaling properties of the original model. Coupling the new exchange functional to the correlation functional B95 leads to the *m*PWB95 model, which represents a physically very accurate generalized gradient approximation.[263, 264]

2.4.4 Meta-Generalized Gradient Approximation (meta-GGA)

As there a still several issues describing systems correctly using "only" GGAs, further improvements were done. A third level on the Jacob's ladder was found, formed by the so-called meta-GGA functionals, which are obtained when the Laplacian of the electron density $\Delta \rho_\sigma$ or the spin kinetic energy densities $\tau_\sigma = \sum_{i}^{n_\sigma} |\nabla \Phi_{i,\sigma}|^2$ are included in the functional.[265]

Since both components depend on the second-order derivation, they are related.[266] Therefore, only one of these elements is used in most cases. The typical form of a meta-GGA exchange functional can be expressed as followed:

$$E_x^{GGA} = \sum_{\sigma}^{\alpha,\beta} \int e_{x,\sigma}^{UEG} g_{x,\sigma}^{mGGA} \, dr \tag{2.78}$$

$$g_{x,\sigma}^{mGGA}(w_\sigma, u_\sigma) = \sum_{i=0}^{N'} \sum_{j=0}^{N} c_{x,i,j} w_\sigma^i u_\sigma^j \tag{2.79}$$

Apart from the non-empirical meta-GGA exchange-correlation functionals from Perdew,[267, 268] various meta-GGAs with semi-empirical parametrization exist, such as the Minnesota functionals from Truhlar, including M06L,[269] which is the only local meta-GGA of the M06 family.[234] M06L is a combination of the VSXC and M05[270] functional, but it is enforcing the right UEG limit, which is not satisfied in VSXC. Another attempt to build up semi-empirical meta GGAs is VSXC[271] from van Voorhis and Scuseria including a τ-dependent gradient-corrected correlation functional and the τ-dependent member of the HCTH family, τ-HCTH.[256, 272]

2.4.5   Non-separable Meta-Generalized Gradient Approximation (meta-NGA)

The electronic energy is separated differently for DFT and wave function-based methods, in which the energy is divided into exchange and correlation term. In the case of the non-separable GGA there is no exchange or correlation functional, instead one functional including both is applied. Therefore, the indices *x* and *c* are transcribed to *nxc* ($E_{nxc\sigma}^{NSGA}$) to illustrate that both correlation and exchange are included in this functional in a non-separable form *n*.

An attempt from Truhlar and co-workers to express the functional is $E_{nxc\sigma}^{NSGA} = E^{[1]} + E^{[2]}$ with:

$$E^{[1]} = \sum_{\sigma}^{\alpha,\beta} \int e_{x,\sigma}^{UEG} \sum_{i=0}^{m} a_{i,0} u_{x\sigma}^i \, dr \tag{2.80}$$

$$E^{[2]} = \sum_{\sigma}^{\alpha,\beta} \int e_{x,\sigma}^{UEG} \sum_{i=0}^{m'} \sum_{j=0}^{m} a_{i,j} u_{x\sigma}^i v_{x\sigma}^j \, dr \tag{2.81}$$

$E^{[2]}$ contains both, the exchange and the correlation part, since it is optimized parametrically.[273] The first functional of this kind is N12 built up from the enhancement factor for exchange from Becke B97,[252] coupling it with B97 for correlation using opposite-spin (OS) and same-spin (SS) contributions to the UEG from Perdew-Wang parametrization[274] and optimizing the $a_{i,j}$ coefficients by parametrization. MN12L,[275] the functional, which is often used in this work (see chapter 4), has 40 parameters and is based on the N12 functional with adding $\tilde{\tau}_\sigma$ to get a non-separable meta-GGA. In 2015, Truhlar *et al.* improved the MN12L functional by parametrizing it to a much larger list of databases, which gives the MN15L[276, 277] functional with a substantially broader accuracy than its predecessors.

2.4.6   Global Hybrid GGA

The local kinetic energies are local functions of the occupied Kohn-Sham orbitals.[278] Because of this locality, issues in DFT concerning the Self-Interaction Error (SIE), long-range dynamic correlation and strong correlation emerge.[279] The self-interaction error can best be explained in the simplest case of a hydrogen atom. For HF, the classical and non-classical electron-electron interactions and therefore the interactions of each electron with itself cancel each other; however, since in KS-DFT the exact exchange is replaced by the exchange-correlation functional, a substantial amount of functionals is not free from SIE.[280] This problem can be solved by applying a suggestion from Perdew *et al.*, who proved that the exact exchange function is not a local functional of the orbitals or the densities.[281] Therefore, some non-local energies need to be added. A possible option is the replacement of the local exchange functional with the exact HF exchange functional. A local version of the correlation function that results in exactly zero correlation for any one-electron system, as for example LYPO, can be used.

In the general form of a Global Hybrid (GH) functional E_{xc}^{GH}, the weight factor c_x is fitted empirically.

$$E_{xc}^{GH} = c_x E_x^{HF} + (1 - c_x)E_x^{DFT} + E_c^{DFT} \qquad (2.82)$$

Another important approach is the one proposed from Becke in 1993[282] using three fitting parameters. This attempt builds a base for some important DFT functionals, such as B3LYP or B3PW91.

$$E_{xc}^{GH} = c_x E_x^{HF} + (1 - c_x - a_x)E_x^{DFT} + a_x E_x^{DFT} + (1 - a_c)E_c^{DFT} + a_c E_c^{DFT} \qquad (2.83)$$

One of the most famous hybrid functionals is B3LYP,[253, 254, 283] which is built up from the VWN1RPA and the LYP correlation functional by adding some B88 exchange to the exact HF exchange. Further interesting hybrid functionals with a wide range of applications are the B97-3[284] (42%) and the SOGGA11X[285] (40.15%) functional differing in the amount of exact HF-exchange percentage given in the brackets. A non-empirical alternative is the PBE0[286] with 25% exact exchange. By replacing the PBE exchange functional with the revPBE exchange, the revPBE0[250] functional is obtained.

2.4.7 Global Hybrid meta-GGA

The exchange functional can also be expanded by adding Laplacian of the electron density $\Delta \rho_\sigma$ or the spin kinetic energy densities τ_σ to obtain global hybrid meta-GGAs.

In contrast to M06L, which is local, M062X[287] has the same basic structure as M06L, but the double amount of nonlocal exchange (2X). As a result, the functionals appear highly non-local. The hybrid exchange-correlation energy of this functional is a sum of non-local HF exchange E_x^{HF}, local DFT exchange E_x^{DFT} and the local DFT correlation energy E_c^{DFT}. The contributions are weighted by the factor *X*, which is optimized along with the other parameters.

$$E_{xc}^{hyb} = \frac{X}{100} E_x^{HF} + \left(1 - \frac{X}{100}\right) E_x^{DFT} + E_c^{DFT} \qquad (2.84)$$

M08HX[288] is one of the first Minnesota functionals, in which the exchange functional is based on SOGGA and contains a high HF exchange (HX) of 52.23%. Due to the improved functional form compared to the previous M06-2X, it has no self-correction term and enforces the UEG limit.

Apart from the Minnesota family, there are groups of other functionals from Truhlar and co-workers containing less parameters. One of these functionals is the PW6B95D3,[289] which includes only six parameters. It is built up on Perdew-Wang-91 exchange and Becke-95 correlation and has added the dispersion correction D3 from Grimme.[290-292]

2.4.8 Range-separated hybrid GGA

If long-range interactions play an important role, further issues appear. Since the general GGA exchange functional only depends on the electron distribution, they do not include fundamental electron-electron interactions. The HF exchange integral on the contrary, since it is an explicit two-electron integral, implies long-range exchange interaction naturally.[293]

The basic concept of this correction is to divide the exchange interactions in two parts, the short-range and long-range interactions, and adopt in both a general exchange function and HF exchange integral.[294] Savin proposed to collate long-range corrected exchange functionals with short-range correlation functionals.[295] The two electron operator $1/r_{12}$ is split into two parts and is partitioned by the standard error function *erf* with a parameter μ, which defines the division ratio.

$$\frac{1}{r_{12}} = \frac{1 - \mathrm{erf}\,(\mu r_{12})}{r_{12}} + \frac{\mathrm{erf}\,(\mu r_{12})}{r_{12}}$$

(2.85)

Instead of the equation above, CAM-B3LYP,[296] which represent the long-range corrected version of B3LYP, has two more parameters α and β implemented and can be written as:

$$\frac{1}{r_{12}} = \frac{1 - [\alpha + \beta \cdot \mathrm{erf}\,(\mu r_{12})]}{r_{12}} + \frac{\alpha + \beta \cdot \mathrm{erf}\,(\mu r_{12})}{r_{12}}$$

(2.86)

The most common values that are used are $\alpha = 19$ and $\beta = 0.81$. This functional is designed to perform more stable and precisely in the calculation of excitation energies than the simpler Hybrid GGA's without range-separation. However, other properties as atomization energies are still not described accurately enough. Additionally, long-range correction was attached in semi-empirical functionals, such as the B97 one. Based on this functional, the *w*B97X[297] was invented with the following form:

$$E_{xc}^{wB97X} = E_x^{LC(lr)} + E_x^{HF(sr)} + E_x^{B97(sr)} + E_c^{B97}$$

(2.87)

This functional contains 17 parameters that were fitted to experimental data. By adding the Van der Waals dispersion correction, *w*B97XD[297] has an even wider field of application.

2.4.9 Range-separated hybrid meta-GGA

The range-separation correction was also included in meta-GGAs. The M11[298] functional is entirely based on the M08 meta-GGA including a long-range correction proposed by Chai and Head-Gordon for GGAs.[299] Depending on the range, it contains between 42.8 (SR) and 100 (LR) percentage of non-local HF exchange. Based on the MN12L functional, which is completely local, the MN12SX[300] is formed the same adding some screened exchange and illustrating an amount of HF exchange in the range of zero to 25 percent.

2.4.10 Double Hybrid (DH)

The next step on Jacob`s ladder is represented by the Double Hybrid (DH) functionals, which contain a MP2-like perturbational correlation term in the DFT correlation. The first Double-Hybrid functional of this form is B2PLYP,[292, 301, 302] which is composed of four terms, containing a mixture of GGA (E_x^{GGA}) and HF (E_x^{HF}) exchange and the sum of the GGA (E_c^{GGA}) and MP2 (E_c^{MP2}) correlation energy. Both, the exchange and correlation parts, are portioned by two coefficients c_x and c_c.

$$E_{xc} = (1 - c_x)E_x^{GGA} + c_x E_x^{HF} + (1 - c_c)E_c^{GGA} + c_c E_c^{MP2} \tag{2.88}$$

For this functional, the same correlation and exchange functionals were used as in the B3LYP hybrid functional, in particular Becke`s exchange and Lee-Yang-Parr`s correlation functional. Another improvement to this DH functional is B2PLYP-D3,[292, 301, 302] which includes additional dispersion correction. Further features can be added to a DH, as it is the case for the DSD-PBEP86[303] functional. Apart from dispersion correction, a spin component scaling is added. This kind of functional is a so-called DSD-DFT for dispersion corrected, spin scaled Double Hybrid. This functional is built of PBE exchange and P86 correlation functional and includes the E_S^{MP2} for spin component scaling and E_D as dispersion correction.

$$E_{xc}^{\mathrm{DSD-PBEP86}} = (1 - c_x)E_x^{HF} + c_x E_x^{PBE} + c_c E_c^{P86} + c_O E_O^{MP2} + c_S E_S^{MP2} + s_6 E_D \tag{2.89}$$

Another interesting point in the development of DH functionals is presented by the parameter-free or at least nearly parameter-free DH functionals built on the adiabatic-connection formalism.[304, 305] Starting from this adiabatic-connection formalism, one-parameter Double Hybrids were derived, also known as DHs,[306-308] built on a quadratic and cubic relation between the two coefficients c_x and c_c. This assumption leads to the Quadratic

Integrand Double Hybrid (QIDH) model. In the case of PBEQIDH,[309] the PBE correlation and exchange was chosen and the functional can be described in the following way:

$$E_{xc}^{\text{PBE}-\text{QIDH}} = \frac{\lambda_x + 2}{3} E_x^{HF} + \frac{1 - \lambda_x}{3} E_x^{PBE} + \frac{2}{3} E_c^{PBE} + \frac{1}{3} E_c^{MP2} \qquad (2.90)$$

2.5 Spin Flip (SF) methods

Biradicals, molecules with two electrons occupying two (near)-degenerate molecular orbitals (see chapter 1),[8, 25] are often found in chemical reactions,[63, 310] e. g. in bond breaking. If two electrons are localized in two orbitals, there are six different possible occupation configurations (Figure 13).
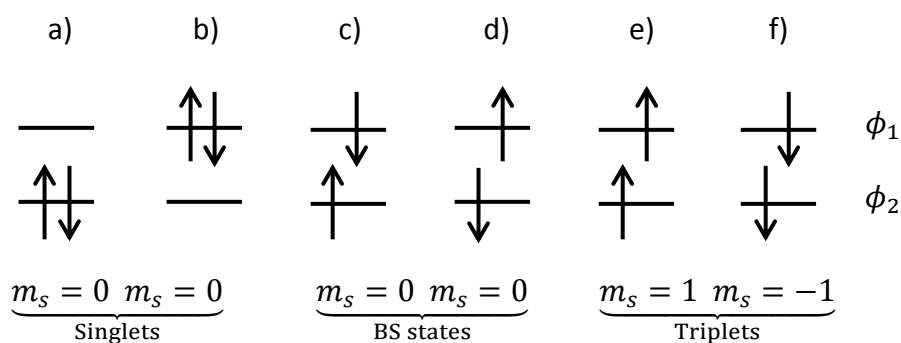
Figure 13: Possible occupations for two electrons in two orbitals with the corresponding slater determinants.

From these occupations, six different slater determinants, one for each spin-adapted configuration can be obtained. Three of these six spin-adapted configurations illustrate singlets of different energies and three triplets with the same energies. The first two singlet states, a) and b) in Figur1, are described by Ψ_1^s and Ψ_2^s shown in equations (2.91) and (2.92). The wave functions are also eigenfunctions of the $\hat{S}^2$ operator with an eigenvalue of zero and can be in general described correctly with one determinant in a closed shell case. If ϕ_1 and ϕ_2 are (nearly) degenerate, the singlet wave functions describing this arrangement consist of two equally important configurations. Therefore, the description with one slater determinant is not correct anymore.

$$\Psi_1^s = \frac{1}{2} \left[\lambda(\phi_1)^2 - \sqrt{1 - \lambda^2}(\phi_2)^2 \right] (\alpha\beta - \beta\alpha) \qquad (2.91)$$

$$\Psi_2^s = \frac{1}{2} \left[\lambda(\phi_1)^2 + \sqrt{1 - \lambda^2}(\phi_2)^2 \right] (\alpha\beta - \beta\alpha) \qquad (2.92)$$

$$\Psi_3^s = {}^1\!/_2 \, [\phi_1\phi_2 + \phi_2\phi_1](\alpha\beta - \beta\alpha) \tag{2.93}$$

$$\Psi_1^t = {}^1\!/_2 \, [\phi_1\phi_2 - \phi_2\phi_1](\alpha\beta + \beta\alpha) \tag{2.94}$$

Representations c) and d) (Figure 13) are no eigenfunctions of the $\hat{S}^2$ operator, whereas their negative and positive linear combinations are. The positive combination (2.93) describes the singlet with an eigenvalue of zero, the negative combination (2.94) the triplet with an eigenvalue of two. For these cases, a multiconfigurational model is needed, which provides an appropriate zero-order wave function. Potential methods are presented by Multiconfigurational Self-Consistent Field (MCSCF),[178, 311] Multireference Configuration Interaction (MRCI), for example MR-CISD, and Multireference Perturbation Theory (MRPT), which adds some necessary dynamical correlation.[312-314]

Configurations e) and f) in Figure 13 display the two triplet states with $S = 3$ and can be described appropriately by a single determinant. On this basis, SF methods were built. From the single reference triplet states, the closed and open shell singlets, as well as the two-configurational triplet state d), are obtained by a spin flipping excitation. In contrast to the multiconfigurational final state, the reference triplet state possesses less dynamical and non-dynamical effects. Consequently, the description of the final state is more accurate if the reference wave function is described with a complex high-level method.[315-317]

In a normal singlereference picture, the excitation is described by the multiplication of an excitation operator $\hat{R}$, which does not change the total number of electrons, to a closed-shell reference wave function $\widetilde{\Psi}_{M_s=0}^s$.

$$\Psi_{M_s=0}^{s,t} = \hat{R}_{M_s=0}\widetilde{\Psi}_{M_s=0}^s \tag{2.95}$$

The quality of the description of the excited states $\Psi^{s,t}$ strongly depends on the adequate calculation of the reference wave function. In the case of a degenerated or nearly degenerated system, the singlereference gets two-configurational, which is the case for biradicals, and a normal singlereference method is therefore not suitable anymore. This problem is addressed in the SF model by choosing a high-spin triplet state, which can be described accurately by a singlereference wave function.

$$\Psi_{M_s=0}^{s,t} = \hat{R}_{M_s=-1}\widetilde{\Psi}_{M_s=1}^{t} \tag{2.96}$$

By flipping the spin of an electron with the excitation operator $\hat{R}_{M_s=-1}$ of the reference triplet state ($\widetilde{\Psi}_{M_s=1}^{t}, \alpha\alpha$), $\Psi_{M_s=0}^{s,t}$ is yielded. Starting at this reference wave function, all three low-lying singlets, among them two closed- and one open-shell singlet, can be calculated as well as the triplet state ($M_s = 0$).[317, 318] SF-CIS can be used for biradicals due to its improved consideration of non-dynamical correlation. Even for singlet-triplet energy gaps it exhibits a great improvement compared to its spin-conserving counterpart CIS. Since the scaling and computational cost of a SF calculation is identical to the corresponding non-SF excited state calculation, the use of high-level methods, such as CCSD or CISD, is still a difficult task. Therefore, the use of SF-DFT (SF-TDDFT), introduced by Shao, is of great interest.[319] The extension to an implementation to either a collinear or a non-collinear exchange-correlation kernel, including the off-diagonal elements of the one-particle density matrix or not, was made by Ziegler and Wang.[320, 321]

DFT and TDDFT yield formally exact solutions, except for the unknown functional, which accounts for the differences of various DFT functionals (see chapter 2.4).[233, 322, 323] DFT is widely used, e.g. for its ability to describe dynamical correlation reliably.[324-326] Some of the improvements regarding the unknown functionals, like including non-dynamical correlation (CAS-DFT, Restricted Open-Shell theory for Singlets ROSS-DFT),[326-330] lead to results that are at a comparable level of quality to values calculated by MP2 or CCSD.[331] Combining DFT (dynamical correlation) with multireference models (non-dynamical correlation) results in a noteworthy improvement of the outcomes for multireference cases. However, the computational effort increases as well. The spin flip approach is the more applicable choice to include non-dynamical correlation to DFT, since the spin flip can also be assumed as linear response to the triplet reference state and is therefore treated like a single-excitation based on Kohn-Sham orbitals.[322, 323, 332, 333]

In the following, the development of TDDFT, the differences to Tamm-Dancoff approximation (TDA) and the resulting SF-TDDFT is explained more precisely. As mentioned above, the electron density $\rho(x)$ in Kohn-Sham DFT is expanded over a set of M one-electron orthonormal basis functions with x as coordinate of spin and space and the density matrix P subjecting idempotency and normalization conditions.[319]

$$\rho(x) = \sum_{pq}^{M} P_{pq} \phi_p(x) \phi_q(x) \tag{2.97}$$

In the time-dependent Kohn-Sham equation, the time development of the reference density matrix P is described by the response to an infinitesimal oscillatory perturbation $V(t)$ and the Kohn-Sham Hamilton matrix F.[332, 334]

$$[F + \lambda V(t), P] = i \frac{\partial P}{dt} \tag{2.98}$$

The linear response in the first-order of the reference state density matrix determines the excitation energies from the reference ground state and is cumulated in a non-Hermitian eigenvalue equation.[332]

$$\begin{pmatrix} A & B \\ B^* & A^* \end{pmatrix} \begin{pmatrix} X \\ Y \end{pmatrix} = \omega \begin{pmatrix} 1 & 0 \\ 0 & -1 \end{pmatrix} \begin{pmatrix} X \\ Y \end{pmatrix} \tag{2.99}$$

With the Matrix elements $A_{ia,jb}$ and $B_{ai,bj}$ depending on the derivation of F with respect to P. The element $A_{ia,jb}$ is correlated additionally on the difference of the occupied and unoccupied orbitals energies of the reference system $(\epsilon_a - \epsilon_i)$ and causes therefore the well-known problems for (near) degenerated HOMO/LUMOs.[335]

$$A_{ia,jb} = (\epsilon_a - \epsilon_i)\delta_{ab}\delta_{ij} + \frac{\partial F_{ia}}{dP_{jb}} \tag{2.100}$$

$$B_{ai,bj} = \frac{\partial F_{ai}}{dP_{bj}} \tag{2.101}$$

Considering the TDDFT approach, the numbers of α and β electrons remain the same, as only spin-conserving blocks of the response matrix X are allowed to be unequal to zero.[333, 336] Within the Tamm-Dancoff Approximation (TDA), the occupied-virtual elements of the matrix are neglected, wherefore the equation above is reduced to a Hermitian eigenvalue equation.

$$AX = \omega X \tag{2.102}$$

Because of these simplifications by neglecting the relatively small elements of B, SF-TDDFT or simply SF-DFT is based on the TDA. In contrast to TDDFT/TDA, in SF-DFT there is a change in the account of α and β electrons during the excitation, considering the $\alpha\beta$ block of X. Due to the spin flip of an electron, the Coulomb Potential J and the pure exchange and correlation

potentials do not couple single electron excitations. The potentials only depend on α- and β-electron densities and their gradients. These reference state densities show no dependencies on the $\beta\alpha$ of X. Only the HF exchange contains off-diagonal-elements of X and contributes to the SF coupling block of matrix A.[319]

Since the exchange coupling is considered to possess an extremely weak effect, it is quite intricate to calculate this parameter, especially if static and dynamical correlation are existing simultaneously. This is particularly the case if two or more nearly degenerated states exist. To get a correct description of such a system a multireference approach is useful, e.g. CASSCF or a CI expansion. Since CASSCF does not include dynamical correlation, it is therefore necessary to add multireference perturbation theory on top, like CASPT2 or NEVPT2. CI, as well as CASPT2, are both computationally demanding, especially for larger molecules.

With the help of the broken-symmetry approach, it is possible to predict the exchange coupling constants of the interacting paramagnetic centres in molecules, even for large systems.[337, 338] Because the exchange coupling J is preserved by the use of SCF methods, the approach is also applied in the field density functional methods. The exchange coupling is modelled by the Heisenberg-Dirac-van Vleck Hamiltonian $\hat{H}_{HDvV} = -2J\hat{S}_A\hat{S}_B$, with the exchange coupling parameter J and the virtual local spin-operators $\hat{S}_A$ and $\hat{S}_B$ for each interacting side.[339, 340] This Hamiltonian produces a number of spin states and is determined by the spin quantum numbers S_A and S_B with the minimum $S_{min} = |S_A - S_B|$ and the maximum $S_{max} = S_A + S_B$. Using the spin-unrestricted Slater determinants, which lead to different orbitals for different spin, results in a high-spin (HS) state with $S_{HS} = S_A + S_B$ and a broken spin symmetry with $S_{BS} = |S_A - S_B|$. The resulting energies E_{HS} and E_{BS} are subjected to calculate the parameter J in respect to the maximum spin state S_{HS}.

$$J = \frac{E_{HS} - E_{BS}}{S_{HS}^2} \tag{2.103}$$

As this formula developed by Noodleman can only be used within the weak coupling limit, another approach with modifications of Yamaguchi and co-workers is of great interest.[341, 342]

$$J = \frac{E_{HS} - E_{BS}}{\langle \hat{S}^2 \rangle_{HS} - \langle \hat{S}^2 \rangle_{BS}} \tag{2.104}$$

This formula can be employed in the complete range of coupling strength. As this is an improvement of the Noodleman approach, the formula of Yamaguchi is utilized in the following work. In addition to the usability for large molecules, another benefit of the BS approach is the "quasi-valence bond" description obtained by using the semi-localized magnetic orbitals, which reflect the interaction of singly occupied molecular orbitals of the subsystems A and B. The set of orthogonal magnetic orbitals $\eta_{a,b}$ is built from the interacting molecular orbitals $\psi_{\pm}$ of the subsystems and the orbitals are very similar to the fragment orbitals, which additionally remain from the orthogonalization.[339]

$$\eta_{a,b} = 2^{-1/2}(\psi_+ \pm \psi_-) \tag{2.105}$$

With the help of these orbitals an ionic and a neutral wave function is formed, in which the ionic state $\left| {}^1\Phi^{ion} \right\rangle$ is a superposition of two states, where both electrons are located on one side of the dimer. The neutral wave function $\left| {}^1\Phi^n \right\rangle$ outlines a pure biradical wave function with two equal contributions locating the electrons on different sides, but with coupled spin.

$$\left| {}^1\Phi^{ion} \right\rangle = 2^{-1/2}[|\eta_a\bar{\eta}_a| + |\eta_b\bar{\eta}_b|] \tag{2.106}$$

$$\left| {}^1\Phi^n \right\rangle = 2^{-1/2}[|\eta_a\bar{\eta}_b| + |\bar{\eta}_a\eta_b|] \tag{2.107}$$

This formalism of magnetic orbitals and neutral and ionic wave functions can be found in the CI language presenting a two-electron system in two orbitals.[106] Since the closed shell wave functions illustrate equal contributions from the ionic and the neutral state, it can be used to describe biradical states. The percentage of the biradical character depends on the interaction between the two states. In the weak interaction limit, the exact wave function corresponds to the neutral wave function, since the ionic one is cancelled out. The parameter W_n reflects the weight of the neutral wave function $\left| {}^1\Phi^n \right\rangle$ in the exact ground state. As the closed shell wave function exhibits an W_n value of 0.5 and a pure singlet biradical is recordable with $W_n = 1$, in an intermediate regime W_n is expressed by $W_n = \frac{1}{2} + \alpha\sqrt{1 - \alpha^2}$. By the means of this argument, the biradical character can be described as:[339]

$$R = 200\left(W_n - \frac{1}{2}\right) = 200\,\alpha\sqrt{1 - \alpha^2} \tag{2.108}$$

Translating this model into a BS wave function $|\Phi^{BS}\rangle = |\varphi_a \bar{\varphi}_b|$, the BS magnetic orbitals present a more complicated form with orthogonality only caused by their spin parts. Since the shapes of the BS magnetic orbitals are determined by a variational energy minimizing processes, these magnetic orbitals are not directly associated with the molecular orbitals ψ_+, ψ_- or magnetic orbitals η_a, η_b of the CI view. To derivate the benefits of the CI formalism, the BS magnetic orbitals are to be set into perspective with the molecular orbitals of this formalism by the two angles θ and ϑ. The values of those angles are obtained by the variational principle to provide the lowest energy.

$$\varphi_a = (cos\theta)\psi_+ + (sin\theta)\psi_- \tag{2.109}$$

$$\varphi_b = (cos\vartheta)\psi_+ - (sin\vartheta)\psi_- \tag{2.110}$$

The parameter angles θ and ϑ are functions of the coupling strength and approach zero for a strong coupling. Consequently, just the molecular orbitals ψ_+, ψ_- remain. The overlap of two BS magnetic orbitals can be calculated, in the case of $\theta = \vartheta$, as:

$$S = \langle \varphi_a | \varphi_b \rangle = cos^2\theta - sin^2\theta \tag{2.111}$$

The biradical character is now determined by the angle θ, since the BS wave function becomes a closed shell, if $\theta = 0$, as for $\theta = \pi/2$ the wave function equals the double excited state. In the BS approach, the amount of triplet plays an important role to determine the biradical character. A pure biradical (100% biradical character) exhibits 50% triplet character, whereas no triplet contribution results in 0% biradical character. Thus, the biradical character can be rewritten in dependency of the overlap integral.

$$R_{BS} = 100(1 + |S|)(1 - |S|) \tag{2.112}$$

The BS wave function is composed of a neutral $^1\Phi^n$, an ionic $^1\Phi^{ion}$ and a triplet $^3\Phi^T$ contribution.

$$|\Phi^{BS}\rangle = c_{ion}|\,^1\Phi^{ion}\rangle + c_n|\,^1\Phi^n\rangle + c_T|\,^3\Phi^T\rangle \tag{2.113}$$

In more complicated systems with more than two electrons, it is difficult to calculate the overlap of the BS magnetic orbitals. A established method used in the orca program of Frank Neese is the use of the Corresponding Orbital Transformation (COT) by Amos and Hall.[343, 344]

3   Aim of the work

The first aim of this work is to investigate suitable methods for the detailed description and characterization of biradicals regarding the energetic position of the singlet and triplet states of these molecules and the related properties. Although various multireference methods are known to describe this kind of molecules quite accurate, the accompanied computational costs make them inappropriate for huge systems. Therefore, the utilization of methods, which present a stable performance in combination with low cost, is aimed for.

In the second part of the work, the influence of variations in the electronic properties of cyclic alkyl amino carbenes (CAAC) and N-heterocyclic carbenes (NHC), more precisely 1,3-Bis(2,6-diethylphenyl) imidazoline-2yliden (IDip), substituents on the properties of the investigated boron-containing compound in terms of the singlet or triplet ground state geometry is investigated. For this instance, model systems are developed, which reveal the underlying electronic effects. These determine whether a triplet or a singlet state is formed. The various effects can be explained by a simple MO scheme including only the boron and the carbene carbon centres of the model systems. A schematic extract of some of the various boron containing systems that are investigated in this work is depicted in Figure 14.

S_c1:	-	CAAC	S-Me
S_N2:	-	NHC	S-nBu
B_2N_2:	N_2	CAAC	Dur
$B_2N_2H_2$:	N_2H_2	CAAC	Dur
A1:	C_2Me_2	CAAC	Cl
H2:	C_2H_2	CAAC	H
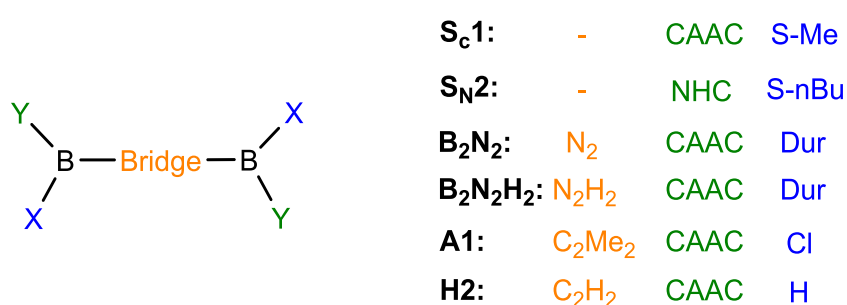
Figure 14: General structure of the various boron containing systems investigated in this work.

By expanding the boron-boron bridge with dinitrogen (**B_2N_2**, **$B_2N_2H_2$**), a completely different behavior is expected, as it is the case with a dicarbon bridge (**A1**, **H1**). Furthermore, the interaction of the bridge with the boron-carbene fragments is examined and to what extent this interaction changes the electronic properties of the whole system. The various effects should be explained by an extension of the model mentioned above including the bridge molecules and their electronic properties.

4   Benchmark

4.1   Theoretical computation of singlet-triplet gaps

As described in chapters 1 and 2, the ST gap provides a crucial parameter to determine for example the interaction and distance of the two radical centres in a biradical system. Thus, an appropriate description of both states is necessary.

The lowest triplet state can be easily calculated by unrestricted Hartree-Fock or unrestricted DFT. However, it is known that normal HF and its post methods show triplet instabilities.[345] Calculating the singlet biradical illustrates a significant problem, since more than one determinant is required to calculate this configuration in a reliable way. It is known that this causes the breakdown of singlereference post-Hartree-Fock methods, such as Møller-Plesset or Coupled-Cluster methods.[180, 221, 346] An appropriate solution is provided using multireference approaches build upon multiconfigurational self-consistent field procedure, which uses a zero-order wave function consisting of a small number of near-degenerate configurations,[173, 178, 311] such as CASSCF, CASPT2,[347] MR-CI[348] and MR-CC.[349, 350]

It is also quite intricate to obtain experimental data to compare the theoretical results with, since biradical species are barely measurable due to their high reactivity. The *ortho-*, *meta-* and *para-*benzyne molecules were proven to be excellent benchmark systems for theoretical investigations, as Wenthold, Squires and Lineberger managed to measure ST gaps for the *ortho-*benzyne and its conformers.[351] This fact was used by other groups, like Schaefer or Engels and co-workers, to perform a benchmark against experimental data with high-level *ab initio* methods.[349, 352] Therefore, it seems as if multireference Coupled-Cluster or other multiconfigurational methods must be used to obtain accurate ST gap energies. Either way, these methods exhibit enormous computational costs and difficult or impracticable application on large molecules. Through the years, some singlereference methods, such as quadratic Coupled-Cluster double (QCCD),[353, 354]valence-optimized-orbitals CCD (VOO-CCD)[355, 356] or doubly ionized equation-of-motion CCSD[357] were developed, capable of predicting some multireference problems correctly. These singlereference methods own the advantage that they are application-independent, size-consistent and show reduced computational effort.

Another possibility to diminish computational costs is the use of the so-called broken-symmetry (BS) approach (see chapter 2.5). Carpenter *et al.* compared this approach with multireference Coupled-Cluster (MkCC) and other high-level methods, such as CASPT2, CASSCF and UCCSD, by calculating the formation and rearrangement of spiropentane.[358] With a performance illustrating nearly no difference to the CASPT2 values, the BS approach can be utilized for multireference cases.

Since it is still challenging to apply these methods on larger molecules, like the ones synthesized by the Braunschweig group, a similar BS approach by Noodleman and Yamaguchi was used, too.[87, 337, 359, 360] Instead of describing the complex biradical singlet state, a BS state (see chapter 2.5, Figure 13) is characterized by unrestricted DFT (UDFT) or Coupled-Cluster (UCC). This state consists of half BS single and half BS triplet state. Therefore, the energy of the calculated state lies between these two states. A problem caused by the mixture of singlet and triplet is spin contamination, which can be corrected by the spin projection method of Yamaguchi and Schlegel.[361, 362] As this method is built up by SCF calculations on the spin-contaminated BS state, this indirect calculation of an open-shell singlet state also illustrates problems in the correct calculation of potential curves.[363] The results of DFT calculations can be improved several times over by just using the BS approach. In the following the terminus BS-DFT represents the usage of a DFT functional within the BS approach

The BS approach was improved among other things regarding the fractional-spin or variational-fractional spin method.[364, 365] Using the fractional-spin version of the delta-SCF approach,[304] the open-shell singlet state can be obtained directly preserving suitable results for ST gaps.[364, 365] A weak point of this method is the use with DFT and its failure to describe intrinsic static correlation.[366, 367] Since the static correlation is very important for disjoint biradicals, the approach fails mainly in this area.[365]

Another very interesting approach, which is based on the concept of spin flip, was developed in the early 2000 by Anna Krylov.[368, 369] Starting from a high-spin triplet state, the open-shell singlet is preserved by using the spin flip excitation operators. With the correct unrestricted start reference, the SF methods lead to better results compared to the BS approach for biradicals.[318]

This formalism was accomplished for a lot of methods (see chapter 2.5), such as spin flip configuration interaction (SF-CI),[317, 369] restricted active space spin flip configuration interaction (RAS-SCF-CI),[370, 371] spin flip equation-of-motion Coupled-Cluster theory (SF-EOM-CC)[372-374] and of course SF-TDDFT.[319-321]

However, for biradicals with small ST gaps, multireference approaches are required to obtain accurate potential energy surfaces (PES),[375] electronically excited states[376, 377] or feasible results on chemical and structural properties.[378, 379] As this work is mainly dealing with biradical species or at least with molecules consisting of an specific biradical amount, a sufficient method to describe these molecules is essential. Since singlereference approaches are often sufficiently accurate in describing multireference cases, a benchmark of different single- and multireference methods is shown in the following chapter.[380, 381]

The geometries for the benchmark were optimized using various DFT functionals within the BS approach in conjugation with the 6-311G(d,p)[382-386] Pople basis sets.[387] A further analysis of other molecules was performed to obtain the best geometry with different methods, such as CCSD or MP2, leading to geometries equal or worse compared to DFT, hence, not justifying the use of such methods for large systems. For the CASSCF[388,389,390-392] and NEVPT2[208-210] calculations, a (2,4) space, where two electrons are distributed within the HOMO and the three lowest lying unoccupied orbitals, was used. The justification for the CAS space systems lies in the more detailed analyses of the test system, which are described in the subsequent chapters. Those complete active space methods are combined with def2-TZVP[393, 394] basis sets. Other post Hartree-Fock methods, such as Coupled-Cluster theory CCSD and CCSD(t),[134, 395-397] are treated with the domain-based local pair natural orbital DLPNO[140, 154-156, 162] approximation as well as second-order Møller-Plesset Perturbation Theory[144, 398] in combination with pair natural orbitals[399, 400] and spin-scaling.[401] For these three post Hartree-Fock methods, the cc-pVTZ Dunning basis sets[402, 403] were used. To determine differences in DLPNO-MP2 and normal SCS-MP2, additional calculations with MP2/cc-pVTZ using the TURBOMOLE 7.1 programme package were conducted.[404]

The DFT, BS-DFT and CASSCF calculations were performed with latest version of Gaussian16[405], while SF-DFT, NEVPT2, DLNPO-MP2, CCSD and CCSD(t) calculations were performed with the ORCA 4.0 program package.[406] The NBO analyses were performed using the relevant NBO program.[407]

Additionally, the qualities of spin flip DFT was tested using different functionals. Since there was no substantial gap in the quality of results for employing various functionals, the most robust one, the BLYP functional, was used.[318] Another possibility, which is used in this work, is the calculation of the geometry with low cost methods, such as DFT, BS-DFT or HF, adding a high-level single point calculation (CASPT2, NEVPT2) on top.

4.2   Diboranes

The diborane system shown in Figure 15 is an experimentally proven triplet biradical, whose structure was determined by X-ray crystallography.[408] Therefore, this molecule represents a suitable model system to investigate and describe important parameters. As the geometry of the molecules, more precisely the $\sphericalangle_{SBBS}$ dihedral and the C-B, B-B bond lengths, defines whether the systems build a singlet closed shell or a biradical (with triplet ground state), it is mandatory to examine the structure in detail. It is a well-known fact that singlereference methods exhibit problems determining the correct geometry of an open shell species.[409] A consequence of the description of a biradical system using a singlereference method is in many cases an asymmetric geometry, as the treatment of the correlation of the important determinants is limited to one determinant. To describe the geometry correctly, both determinants must be included. Depending on the system the second determinant is sometimes more, sometimes less important. In case of the *ortho*-benzyne cation, the second determinant causes the out-of-plane torsion and is only poorly described by single determinant methods. However, it is difficult to calculate the geometry with high level quantum methods, as the synthesized systems are very large (more than 150 atoms).
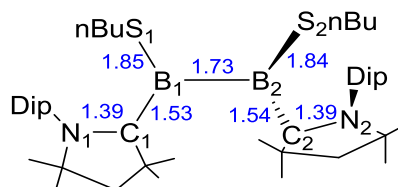
Figure 15: Synthesized biradical system with its bond lengths derived from the crystal structure (values are given in Å).

Since the ground state of the system with *n*-Butyl (nBu) groups bound to sulphur and CAAC as substituents (Figure 15) is a triplet, open shell calculations utilizing different methods were performed to get an overview of method performance. Given that the triplet can be described

correctly with one determinant, most of the methods, Post-HF or DFT, should provide proper results. The data of the crystal structure are used as a comparison to evaluate the quality of calculated structures. The 6-311G(d,p) pople basis sets were employed for density functional theory approaches.[387]

It is of utmost importance that dihedrals and bond lengths are described correctly, as, depending on its bonding patterns, the system favors a singlet (dihedral $\sphericalangle_{S_1 B_1 B_2 S_2} = 180°$) or a triplet ground state (dihedral $\sphericalangle_{S_1 B_1 B_2 S_2} = 90°$).

4.3 Geometry analysis

4.3.1 Analysis of the bond length

The most important bond length is the B-B one defining whether the system possesses a single, double or even triple bond. Considering the crystal structure, a bond length of 1.73 Å is revealed, which is in accordance with a typically B-B single bond.[410] In Table 1, the various bond lengths obtained by different DFT functionals are listed, as well as the data of the crystal structure in bold for better comparison. Furthermore, the Mean Absolute Deviation (MAD) and the maximum deviation of each functional compared to the measured values of the crystal structures are included in Table 1. The MAD values are calculated by the following equation:

$$MAD = \frac{1}{n} \sum_{i=1}^{n} |x_i - M_i|$$

(4.1)

M_i defines the measured value of the crystal structure and x_i presents calculated bond length using a functional. The MAD is obtained by adding the absolute deviations of each calculated bond length to the one of the crystal structures.

Most of the applied methods describe the B-B bond accurately. For the structure obtained with SVWN, all bond lengths are predicted too short, while for the HCTH geometry all bond lengths are too long (similar results were obtained using the HCTH147 version). The Minnesota and SOGGA functionals calculate a proper geometry, whereat the MN12L structure is very close to the crystal structure. Hence, this method seems to be the best choice for the investigated model system and for similar systems, too. Although the MN15L functional was

optimized for multireference cases and should provide the best results, it is not the case for the model system. It is quite complex to determine the best method, since all methods provide very good results close to the experimental data.

Table 1: Comparison of experimental and calculated bond lengths of the model system. The calculated structures were obtained using an unrestricted open shell calculation for the triplet ground state with 6-311G (d, p) basis sets. The values are given in Å.

	N_1-C_1	C_1-B_1	B_1-B_2	B_1-S_1	B_2-S_2	B_2-C_2	C_2-N_2	MAD	maximum deviation
Crystal structure	**1.39**	**1.53**	**1.73**	**1.85**	**1.84**	**1.54**	**1.39**	**/**	**/**
MN12L	1.38	1.54	1.72	1.85	1.85	1.54	1.38	0.01	0.02
M11	1.37	1.54	1.73	1.84	1.84	1.54	1.37	0.01	0.03
M06L	1.38	1.53	1.70	1.85	1.85	1.53	1.39	0.01	0.02
MN15L	1.39	1.55	1.73	1.86	1.86	1.55	1.39	0.01	0.02
M062X	1.39	1.53	1.71	1.85	1.85	1.53	1.39	0.02	0.04
BLYP	1.41	1.55	1.73	1.88	1.88	1.55	1.41	0.02	0.04
ωB97-XD	1.38	1.53	1.73	1.88	1.88	1.53	1.38	0.01	0.02
LC-ωHPBE	1.38	1.53	1.72	1.83	1.83	1.53	1.38	0.01	0.02
B3LYP	1.40	1.54	1.73	1.86	1.86	1.54	1.40	0.01	0.01
CAM-B3LYP	1.39	1.53	1.72	1.84	1.84	1.53	1.39	0.00	0.03
UHCTH	1.40	1.56	1.75	1.85	1.84	1.56	1.40	0.01	0.03
UHCTH147	1.40	1.56	1.74	1.86	1.84	1.56	1.40	0.01	0.02
M08HX	1.38	1.53	1.71	1.85	1.85	1.53	1.38	0.01	0.02
PBE0	1.39	1.54	1.72	1.84	1.86	1.54	1.39	0.01	0.02
PBE	1.40	1.55	1.73	1.86	1.86	1.55	1.40	0.01	0.01
revPBE0	1.39	1.54	1.72	1.84	1.85	1.54	1.38	0.01	0.01
PW6B95D3	1.38	1.52	1.70	1.84	1.84	1.52	1.37	0.01	0.03
SOGGA11	1.40	1.56	1.74	1.86	1.85	1.56	1.40	0.01	0.03
SOGGA11X	1.39	1.54	1.73	1.85	1.85	1.54	1.39	0.00	0.01
USVWN	1.37	1.51	1.68	1.83	1.83	1.51	1.37	0.02	0.05
UVSXC	1.38	1.53	1.70	1.86	1.85	1.53	1.38	0.01	0.03

With a RMSD value of less than 0.02 Å, all methods provide appropriate results compared to the crystal structure. However, taking a closer look at the obtained values it can be stated that SVWN exhibits the largest RMSD and reproduces the most important parameter, the B-B bond, incorrectly. For the optimizations, BLYP, PBE and HCTH show also one of the largest

RMSD values compared to the crystal structure; however, still within a deviation of less than 0.15 Å.

4.3.2 Analysis of the dihedrals

The same analysis was performed for the dihedrals, since they present crucial parameters to identify biradical triplets. The twisted structure ($\sphericalangle_{S_1B_1B_2S_2}$ ~90°) possesses a triplet ground state, while the plane geometry, as it is the case with NHC substituted systems, is a closed shell singlet. Thus, the $\sphericalangle_{S_1B_1B_2S_2}$ dihedral possess a major impact of the behaviour of the system and its correct arrangement influences among other things the ground state multiplicity. In Table 2, the three dihedrals obtained by different DFT functionals are listed, as well as the data of the crystal structure in bold for better comparison with their MAD values.

The calculations show that Minnesota functionals are very accurate regarding the dihedrals of the geometry. The most significant differences concerning the $\sphericalangle_{S_1B_1B_2S_2}$ dihedral is found for the SVWN and wB97-XD functional. All other methods reproduce a dihedral within an error of 1.5°. Equally important dihedrals are the $\sphericalangle_{N_1C_1B_1S_1}$ and $\sphericalangle_{N_1C_1B_1B_2}$ dihedral, which are almost plane. Considering the left side of the molecule (columns one and two in Table 2), the Minnesota functionals exhibit proper results within an error range up to 5°.

It is noticeable that the dihedral of the optimized geometry is more planar compared to the crystal structure. Only SOGGA, which delivers normally sufficiently accurate results for this kind of system, shows in this benchmark the largest error with deviations for dihedrals of about 10°. The right side of the molecule with dihedrals of 167° and 15°, is rotated more out-of-plane than the left side. These dihedrals illustrate a larger error for the calculated values compared to the crystal structure than the left side of the molecule. In the case of a triplet ground state almost all DFT functions result in structures with good agreement to the crystal structure.

Since the triplet appears as ground state, it should be sufficiently reproduced by the used DFT functionals. Furthermore, there appears no difference by calculating the geometries with or without the SF or BS approach. However, this accuracy was assumed, since the triplet only depends on one determinant and the geometry is mainly influenced by steric effects and Pauli repulsion. Consequently, some of the large deviations are not expected, as provided e.g. by SOGAA11 or VSXC.

Table 2: Important dihedrals of the calculated triplet ground state and the crystal structure. All DFT calculations were performed unrestricted with the 6-311G (d, p) basis sets.

	$\angle N_1C_1B_1S_1$	$\angle N_1C_1B_1B_2$	$\angle S_1B_1B_2S_2$	$\angle B_1B_2C_2N_2$	$\angle S_2B_2C_2N_2$	MAD
Crystal structure	**1.7**	**174.3**	**85.5**	**167.4**	**14.5**	**/**
MN12L	2.5	179.4	85.2	159.5	16.3	3.18
M11	2.7	176.7	84.9	160.5	19.1	3.10
M06L	3.1	176.6	84.5	160.8	19.2	3.20
MN15L	2.2	176.4	85.5	159.1	19.3	3.14
M062X	4.7	179.5	86.8	161.1	17.1	3.68
BLYP	4.0	179.7	84.4	167.4	18.2	2.50
ωB97-XD	2.5	178.5	87.1	160.9	18.8	3.48
LC-ωHPBE	3.9	179.3	86.6	163.7	17.1	2.92
B3LYP	3.9	179.6	85.5	164.2	17.5	2.74
CAM-B3LYP	4.0	179.4	86.2	164.1	17.2	2.82
HCTH	4.8	169.0	86.2	164.0	19.8	3.56
HCTH147	0.1	174.6	86.2	164.3	18.2	1.88
M08HX	3.4	178.9	88.0	159.7	17.6	3.92
PBE0	3.3	178.4	86.4	167.4	16.9	1.80
PBE	2.7	177.8	86.2	164.2	17.4	2.26
revPBE0	3.1	178.2	86.6	164.3	16.9	2.38
PW6B95D3	2.7	178.3	85.7	159.9	19.3	3.50
SOGGA11	11.3	161.7	85.6	161.9	22.9	7.24
SOGGA11X	4.7	179.9	85.9	163.6	17.5	3.16
SVWN	1.9	176.6	87.8	162.4	16.9	2.44
VSXC	13.9	177.1	81.1	149.0	18.8	8.42

However, if the ground state is a singlet biradical, the geometry optimization with one single determinant methods, such as DFT, gets more complex. This is the case for various benzyne molecules and their biradicals.[318, 352, 409] Thus, the adiabatic ST gap presents a considerable problem, since both geometries are needed to calculate the adiabatic ST gap. With no reference structures of the singlet state, the quality of the singlet geometry cannot be verified. Only by means of the ST gap a conclusion about the singlet can be drawn.

4.4 ST gap analysis

Both structures, the singlet and triplet state, are optimized to calculate the right ST gap from these two states. It is a quite intricate undertaking, as the singlet is a biradical, too, and no experimental geometry of this state was available for comparison. Since the triplet ground state is well described with used methods, the only complex task is the proper description of the singlet.

As this system is too large for the optimization with high-level methods, the molecule is decreased atom by atom by reducing the substituents bound to sulphur and nitrogen, as well as the steric remains of the CAAC substituents. To outline the differences in the various structures, a simplified picture of the basic structure is depicted in Figure 16.
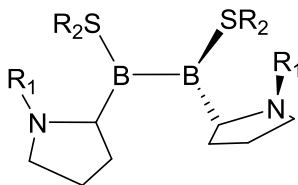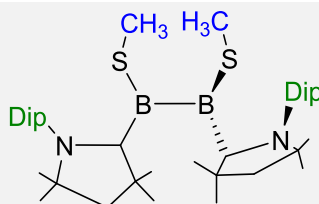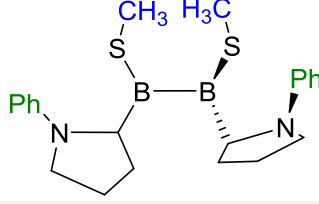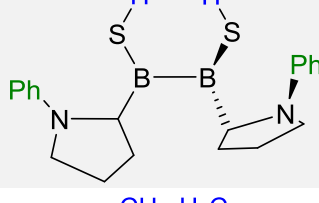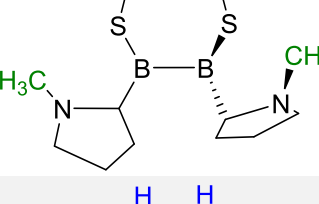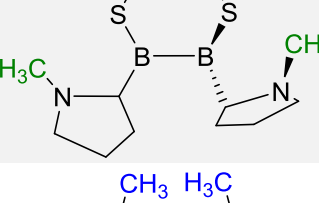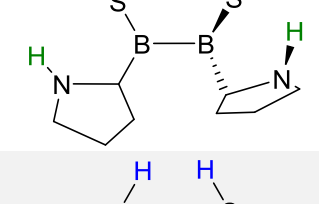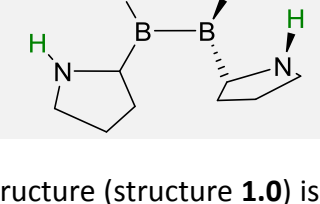
Figure 16: Basic structure of the test system with variable substituents R^1 and R^2.

It can be observed that only the substituents on the CAAC show steric effects. Therefore, if the complete system is optimized and the substituents are cut off, the ST gap stays almost unchanged.[408, 411, 412] In Table 3, the structural setup is illustrated. For structure **1.0**, only the *n*-butyl groups on the sulphur substituent are cut off to decrease the system size. It is expected to see no significant difference for substituting the *n*-butyl group with methyl, as both structures were synthesized by the Braunschweig group and show the same behavior. However, only for the *n*-butyl substituted structure a ST gap was measured providing an experimentally ST gap of 0.86 kcal/mol with a triplet ground state.[408] Since there is no substantial difference in the electronic behavior visible (still a triplet ground state), this modified structure is used for further calculations. The calculated ST gap for the reduced model system can be transferred to the originals system and shows that NEVPT2/def2TZVP performs accurately enough to serve as method to benchmark against. Thus, in the smaller subsystems only the parameters describing the substituents are reoptimized with the main geometric parameters, as the important bond length and dihedrals are kept frozen.

Table 3: Different substructures with their respective substituents R[1] and R[2] and their respective ST gap calculated with NEVPT2/def2TZVP (a negative ST gap corresponds to a triplet ground state).

Substructure		Substituents R[1] and R[2]	ΔE_{ST} [kcal/mol]	HL gap [kcal/mol]
Structure **1.0**		R[1]: Dip R[2]: Methyl	/	-6.25
Structure **2.0**		R[1]: Phenyl R[2]: Methyl	-1.23	-6.04
Structure **2.1**		R[1]: Phenyl R[2]: Hydrogen	-1.04	-5.28
Structure **3.0**		R[1]: Methyl R[2]: Methyl	-0.84	-3.49
Structure **3.1**		R[1]: Methyl R[2]: Hydrogen	-0.76	-3.14
Structure **4.0**		R[1]: Hydrogen R[2]: Methyl	-0.82	-3.37
Structure **4.1**		R[1]: Hydrogen R[2]: Hydrogen	-0.97	-3.92

The largest substructure (structure **1.0**) is very close to the experimental data, since only the alkyl substituent on the sulphur was decreased. For structure **1.0** CASSCF/ NEVPT2 calculations are already too extensive to be calculated on our clusters. In all other substructures (**2.0**-**4.1**)

the four methyl groups on the five-membered ring of CAAC were cut off. Furthermore, for **2.0** and **2.1** the isopropyl groups of the Dip-substituents, connected to the nitrogen atoms of CAAC, were replaced by hydrogen atoms forming a phenyl substituent. The only difference from structure **2.0** to **2.1** is the replacement of the methyl group bound to sulphur with hydrogen. In structure **3.0**, the phenyl group on the CAAC is substituted with a methyl group; however, there was still no substantial difference in behavior detectable. The differences in structures **3.0** and **3.1**, as well as **4.0** and **4.1**, is equal to the ones from subsystems **2.0** and **2.1** including the exchange of the substituent on sulphur. The smallest subsystems **4.0** and **4.1** show hydrogen atoms bound to the nitrogen of the CAAC substituent.

Table 4: Different substructures of the system with their calculated biradical character.

Sub structure	2.0	2.1	4.1	3.0	4.0	3.1
Biradical character β	0.31	0.29	0.41	0.42	0.43	0.44

The most significant distinctions can be seen in both the HL gap and the ST gap by cutting off the Dip or phenyl substituent of the carbene. Decreasing the substituent R^1 to methyl or hydrogen results in an energetically smaller ST and HL gap. Whereat the alterations of the ST gap are relatively small and are therefore not taken into account. The decreasing size of the HL gap on the other side shows an impact on the biradical character. The smaller the HL gap, the higher the biradical character (Table 4). Consequently, it seems that by decreasing the size of the substituent the biradical singlet gets stabilized somewhat and thus eases in energy reducing the size of the ST gap. Since each subsystem possesses a slightly changed biradical character and ST gap, the performance of the various methods is analyzed for every subsystem. Each substructure was analysed in detail focusing on the influence of the utilized functionals on the crucial parameters, in particular the ST and HL gap. To shorten the benchmark as part of this work, just the averaged over all subsystem results are shown in this work precisely.

MAD to NEVPT2

Since the applied methods provide results in various qualities regarding the description of the ST gap of the different substructures, the calculated MAD of all methods for each subsystem **2.0** to **4.1** compared to their respective NEVPT2 reference is shown in Figure 17. It is important to keep in mind that the absolute deviation is represented, thus, Figure 17 does not illustrate

the wrong prediction of the ground state multiplicity. The results of the DFT calculations are obtained applying the BS approach for each functional. Using normal closed shell DFT in contrast shows a worse performance for each subsystem (5-20 kcal/mol) depending on the HF amount of the applied functional. The use of different DFT functionals present no significant difference within the BS approach, whereas for the restricted DFT calculations, the different functionals perform quite differently depending on their composition and HF amount.
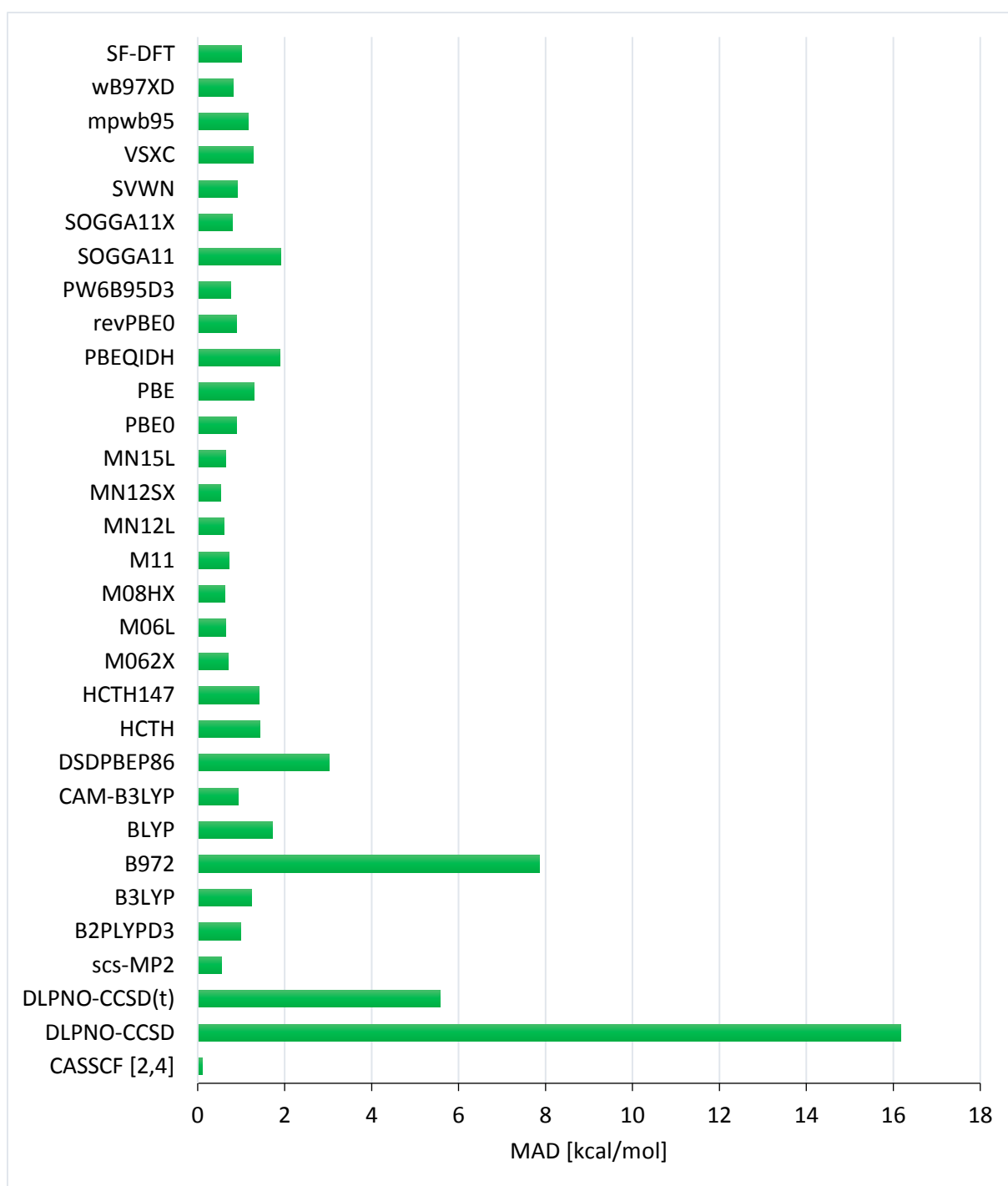
Figure 17: Calculated MAD for the different methods compared to NEVPT2 from subsystems **2.0-4.1**.

In general, it can be said that the more HF amount the functional includes, the poorer the performance of the functional using no BS approach gets. Since a DFT calculation within the BS approach does neither require nor more time or memory and always leads to a better performance, only the DFT results combined with the BS approach are shown in Figure 17 and discussed in this chapter.

Apparently, SCS-MP2 and SF-DFT provide the most stable result with a MAD of 2-3 kcal/mol. However, SCS-MP2 often predicts the incorrect ground state (singlet instead of a triplet). This is also the case for SF-DFT, although not as often as seen for SCS-MP2. SF-DFT is supposed to be a very reliable method to calculate ST gaps of multireference systems.[318, 409] One possible reason for its failure in the prediction of the correct multiplicity of the ground state is caused by the relatively small ST gap. Another possibility is the use of the BLYP functional, as the broken-symmetry singlet open-shell state is calculated from the obtained triplet state by performing a spin flip. Since SF-DFT can be used with a lot of different DFT functionals, other functionals were tested, too. However, test calculations with different methods demonstrated no substantial difference by altering the functionals.

As mentioned in chapter 2, CASSCF calculations with additional dynamical correlation by perturbation theory (NEVPT2, CASPT2) should reproduce the adiabatic ST gap accurately. Since the complete structure and also substructure **1.0** possess too many atoms to be calculated with NEVPT2, different approximations were exploited. Combining NEVPT2 with the DLPNO or LPNO approximations enable the calculations of larger systems, like **1.0**. However, this results in high deviation errors of the ST gap. This is the reason why these findings are not shown here explicitly. Using the DLPNO approximation in combination with Coupled-Cluster shows a similar behavior. The MADs obtained with Coupled-Cluster without the DLPNO approach are about 5-15 kcal/mol smaller than by the use of the approximation. Generally, Coupled-Cluster with single, doubles and triplet excitation, described by perturbation theory combined with the DLPNO approximation, always predicts the right triplet ground state and exhibits a MAD of 5 kcal/mol. As discussed in chapter 2, CCSD(t) is a more reliable method to describe multireference system in contrast to CCSD, which is clearly illustrates in these results. CCSD shows a MAD of 15 kcal/mol and underestimates the ST gap by this value.

Since the MAD of the various DFT functionals using the BS approach lead to different results, the individual DFT functionals are examined in detail in the following.

Functionals, which always predict the right ground state, have an MAD smaller than 1 kcal/mol. One of these methods is MN12L. Other functionals are presented by the very similar MAD within the Minnesota family are M06L, M11, MN12SX, M08HX, M062X and MN15L. Another Global Hybrid Meta GGA functional designed by Truhlar having less

parameters involved is the PW6B95D3 one, which provides relative constant results with a MAD of less than 1 kcal/mol. The HCTH functionals from the Handy's family HCTH and HCTH147 perform steadily with a MAD of less than 2 kcal/mol.

Other methods with a small MAD (1-2 kcal/mol), such as SVWN, VSXC, BLYP, mpwB95 and even SOGGA, predict a singlet ground state for the complete system. SVWN and mpwB95 illustrate some instabilities in the performance regarding the description of the right ground state and calculate a singlet ground state for other subsystems, too. In comparison to the GGA SOGGA, the hybrid functional SOGGA11X with 40.15% HF exchange predict the ground state correctly. Furthermore, the MAD decreases to less than 1 kcal/mol.

In the PBE family, based on PBE or *rev*PBE, PBE has the highest MAD value and also some issues in predicting the right triplet ground state. The global hybrid GGA'S PBE0 and *rev*PBE0 perform nearly identically with a MAD of about 1 kcal/mol. Other global hybrid functionals, such as B3LYP, show a solid performance with a MAD of about 1.5 kcal/mol, too. Only the B972 as global hybrid functional, illustrates issues determining the triplet ground state and provides results with a very high MAD of 8 kcal/mol.

A particularly stable performance is given by the range-separated hybrid GGA functionals CAM-B3LYP and ωB97XD. They always predict a triplet ground state in addition with a MAD of less than 1 kcal/mol.

Since B2PLYPD3 and PBEQIDH are double hybrid functionals and thus require an extremely high memory usage, it is not possible to describe system with a huge number of atoms. Therefore, system **1.0** was not calculated with double hybrid methods. For the remaining systems, the MAD for these two functionals lies in the range of 1-1.5 kcal/mol. DSD-PBEB86 was used as third double hybrid functional and has a slightly higher MAD of 3 kcal/mol. Nevertheless, the double hybrid functionals achieve no better results than the simpler GGA, meta-GGA or hybrid functionals. Due to the poor cost-efficiency of double hybrid functionals in the area of open-shell systems, they are not advisable to use in this kind of calculations.

4.5 Comparison of natural orbitals with different KS orbitals

It was recently shown in literature that the real electron density distribution gets worse by using more parameters and other improvements.[413] Although the obtained energy values may be accurate, the electron density distribution of the individual molecular orbitals might be inaccurate. DFT functionals might not present a recommendable method to apply, if the focus is set on the appearance and shape of the particular MO's. A reliable method to obtain the real electron density distribution is represented by the natural pair orbitals obtained by a CAS calculation.[409] Consequently, the natural pair orbitals NTO and the KS orbitals obtained by different DFT functionals are compared. On the basis of the electron density distribution conclusions to the behavior and reactivity can be drawn.

Since the substructures **3.0**-**4.1** possess a biradical character of nearly 50%, the electron density for the different functionals is analyzed more precisely in Table 5. The trend between the individual subsystems appears identically. In the interest of clarity, only substructure **3.0** is shown in Table 5. Since the triplets illustrate no significant differences in density and the singlet is the more challenging part, only the singlet orbitals are depicted. No difference in the orbitals of the various DFT functionals can be observed, the orbitals are almost identically.

Table 5: The four important frontier orbitals (HOMO, SOMO, SOMO+1, LUMO) of substructure **3.0** calculated applying different functionals and natural orbitals for comparison.

Methods	HOMO	SOMO	SOMO+1	LUMO
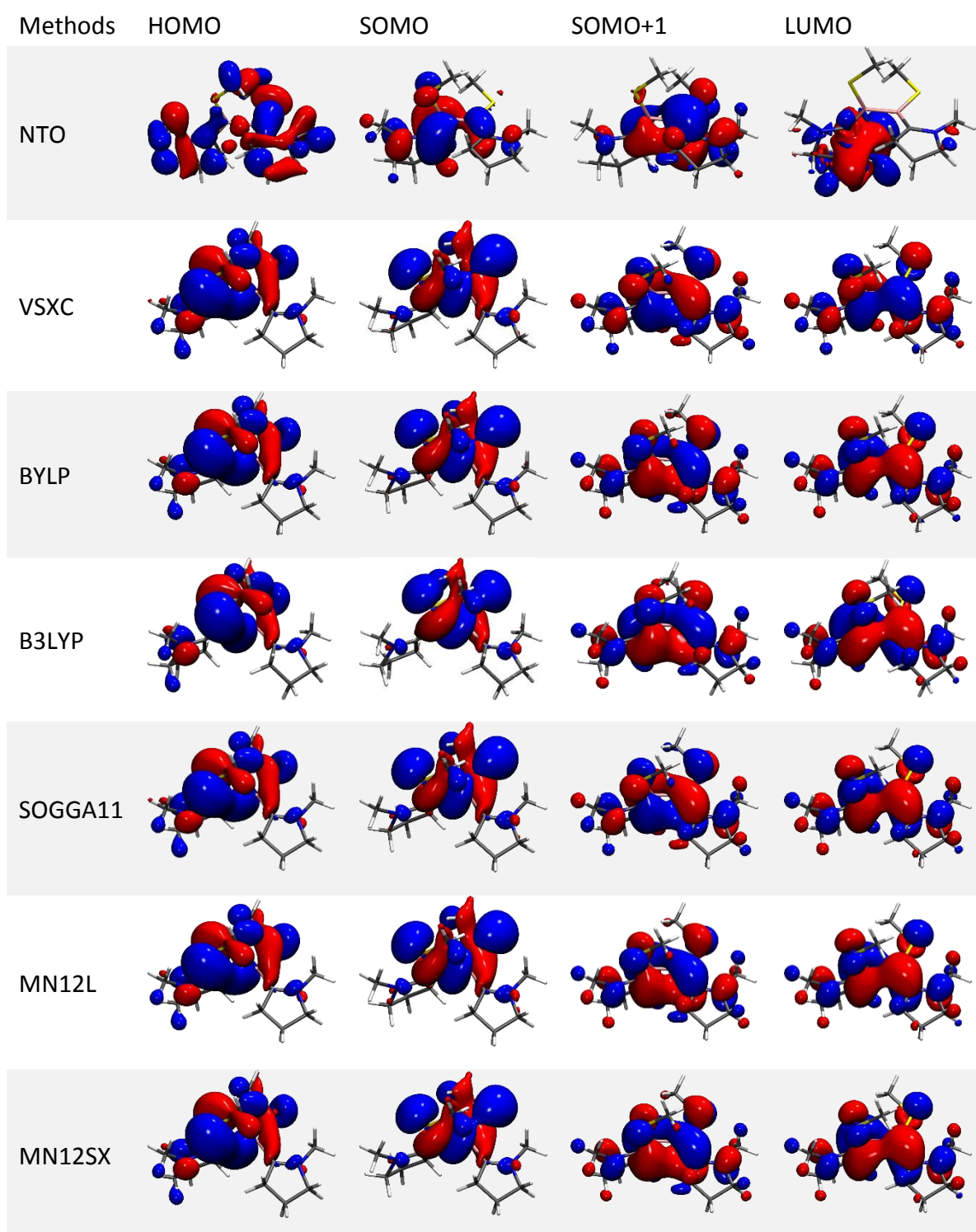
4.6   Summary

In summary, it can be stated that for biradical systems with a triplet ground state density functionals provide mostly accurate results. Special care must be taken by a singlet with biradical character, which cannot be described by singlereference methods adequately. Thus, depending on the concerning functionals DFT provides results within in an error of less than 1 kcal/mol for convenient functionals, such as MN12L, MN12SX, M06L, M062X, M08HX, SVWN, PW6B95D3 or SOGGA11X. The variance rises to up to 8 kcal/mol for inappropriate functionals, as the B972 one. Double hybrid functionals possess a poor cost-benefit ratio. Furthermore, the use of highly parametrized functionals have to be handled particularly careful, since they are sometimes not parametrized to obtain appropriate results in this area.[288]

A robust and cheap method of choice is SF-DFT providing results close to the experimental data; however, it must be noted that the quality of SF-DFT depends on the chosen functional and the description of the reference triplet state. Using the DLPNO approximation in combination with CSSD and CSSD(T) results in a poor benefit-cost ratio, since those post-HF methods are way more expensive than DFT. The method of choice is a complete active space calculation including dynamical correlation by perturbation theory, as it is the case for NEVPT2 or CASPT2, yielding results almost matching with the experimental data. Since it is not possible to calculate large sized systems with those methods, the application of SF-DFT in combination with an appropriate DFT functional (MN12L) is recommendable. However, it is highly suggested to calculate the biradical character of the system of interest. The benchmark demonstrates that the deviation to NEVPT2 increases strongly with rising biradical character of the system. But also the usually robust and accurate MN12L functional shows errors up to 5 kcal/mol for system with 100% biradical character. SF-DFT and NEVPT2 exhibit no dependencies on the biradical character.

The results obtained from the benchmark are directly applied to the following chapters. To characterize the various biradical or closed shell boron containing molecules, the most accurate and suitable methods, such as MN12L, SF-DFT combined with BLYP and NEVPT2, are mainly utilized. First of all, two diborenes are analyzed differing in their chemical and electronic properties by the use of two different carbenes.

5 NHC stabilized diborenes and their biradical analogs with CAAC

In the early 1950s, Wanzlick and Breslow investigated the improved stabilization of carbenes through amino substituents.[414, 415] The attempts to synthesize these stable carbenes as monomeric units exclusively led to the isolation of the so-called Wanzlick dimer.[414, 416, 417] In 1988, Bertrand was able to isolate the singlet phosphino-silyl-carbene **1** (Figure 18).[418] In the following years, several other carbenes were successfully synthesized differing both in the heteroatom in α-position to the carbene carbon and the (a)cyclic backbone structure. Except for the phosphino-silyl carbene **1**, which presents a π-donor (phosphorus) and a π-acceptor group (silicon), all carbenes **2**-**10** (Figure 18) involve two π-donor groups in the system.
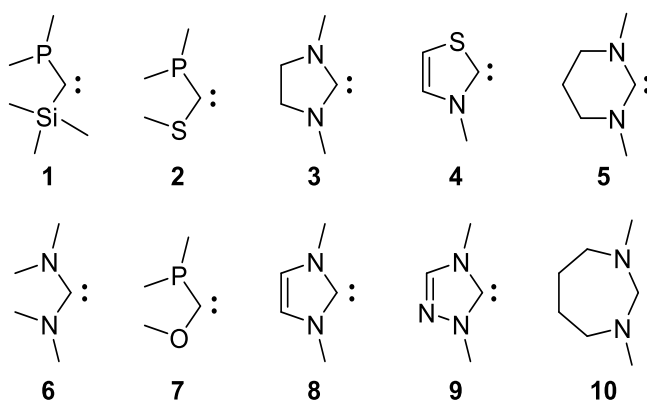
Figure 18: Variety of stable singlet carbenes **1**-**10** that were isolated over the last decades.

After Arduengo and co-workers described the isolation of the first room temperature stable N-heterocyclic carbene (NHC) in 1991, these imidazol-2-ylidene (**8**),[419] came into focus of intensive research. Only a few years later, Herrmann *et al.* discovered the similar behavior of electron-rich organophosphanes and NHCs in metal coordination chemistry, which was affirmed by spectroscopic studies.[420-424] From that moment on, numerous reaction routes to synthesize a variety of stable NHCs were investigated.[425] The groups of Arduengo and Orpen pioneered in the incorporation of nitrogen with the synthesis of imidazolidin-2-ylidene (**3**),[426] acyclic diaminocarbene (**6**)[427] and six membered ylidic diamino carbene (**5**).[428] The 1,2,4-triazol-ylidene (**9**)[429] with three nitrogens was synthesized in the year 1995 by the group of Enders. With thiazol-2-ylidene (**4**),[430] acyclic phosphino-oxy- (**7**) and phosphino-thiocarbene (**2**)[431] further stable carbenes were isolated with differing heteroatoms bound to the carbene center. In 2008, the solid state structures of the seven-membered N-heterocyclic carbene **10**

has been measured for the first time.[432] A more detailed listing of all kinds of carbenes can be found in several reviews.[425, 433-435]

In general, carbenes find relevant applications in many fields, e.g. as ligands for catalysts in homogeneous catalysis. Here, also phosphines (PL_3), a group of bulky and electron-rich ligands, are used to stabilize active catalysts and promote crucial catalytic steps, like reductive elimination or oxidative addition.[436] However, the steric environment of phosphines or NHCs was a drawback in reactions with huge steric demands.[425] NHCs replaces phosphines in some areas because of their different steric environment. One of the best-known catalysts containing both NHC and phosphine ligand is the Grubbs II one, developed by Schrock, Gauvin and Grubbs. The system is used in metathesis reactions and was rewarded the noble prize in 2005.[437]

In addition to the already mentioned application of NHCs as ligands in olefin metathesis,[438-440] carbenes can also be used in Heck and Suzuki coupling reactions,[438, 441-444] metathesis cross coupling,[445-447] Sonogashira coupling,[444, 448] Kumada couplings[449, 450] and Stille couplings[451] to name just a few. The applications of NHC in chemistry is also extensively reviewed.[425]

It is of great interest to synthesize a carbene with a stable singlet ground state and a reactive triplet state, which needs to be higher in energy. Only a large enough ST gap leads to a stable carbene. Otherwise, the more reactive triplet state is populated and the stability of the carbene decreases drastically. Therefore, several theoretical studies were made to verify and optimize the chemical properties of carbenes.[452-454] An important feature is the relative position of the HOMOs and LUMOs, which can be obtained by quantum chemical calculations. Based on the HOMO and LUMO character, it is possible to give a reliable statement about the donor-acceptor quality of a carbene. An interesting calculation in this area was made by Musavi *et. al.* comparing the calculated ST gap of various carbenes with different atoms in α-position to the free electron pair of the carbene (basic structure see **11**-**13**, Figure 19).[454] First of all, the cyclic carbene (**12** or **13**) possesses an increased ST gap compared to the acyclic one (**11**), while the unsaturated species (**13**) shows only a small destabilization of both, the singlet and the triplet state, and therefore only a minor decrease in the ST gap. The calculated ST gaps of these three types of carbenes depend on the substituent, which is included for X, Y or Z. Potential atoms for these carbenes are nitrogen, silicon, oxygen, phosphor, sulphur or carbon with an additional alkyl substituent.
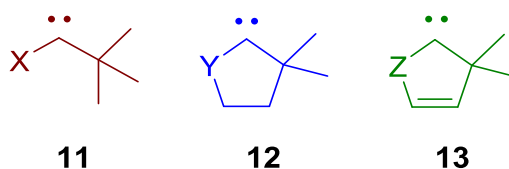
Figure 19: Basic structure of various carbenes **11**-**13** with different heteroatoms in α-position (X,Y,Z = Si, O, P, S, C or N).

Nitrogen and oxygen provide the biggest ST gap due to their good π-donating and σ-accepting qualities and the resulting stabilization of the singlet state. It is found that nitrogen stabilizes both, the singlet and the triplet state, while oxygen mainly stabilizes the singlet state and does not affect the triplet state. Since phosphorus and sulphur atoms illustrate π-donating, but no σ-accepting characteristics, the singlet state stays the ground state. But the ST gap is decreased for those two atoms.

Due to neither σ-accepting, nor π-donating properties of silicon and carbon, the triplet is favored as ground state if only these atoms are incorporated. In some cases, it can also be the singlet for the carbon containing system, due to an extremely small ST gap. In addition to isolation of singlet phosphino-silyl-carbene **1**, Bertrand and co-worker presented in 2005 a novel singlet carbene, which is similar to the known NHC, but with a small difference leading to major changes in the chemical behavior.[408, 412, 455-459] Instead of a second nitrogen atom a carbon atom is located at the α-position. Thereby, the cyclic alkyl amino carbene (CAAC) possesses unique electronic properties, which are in a various way of great interest. Because of this substitution, there is now a less σ-electron withdrawing and a less π-electron donating substituent in α-position. These properties lead to CAACs being both a better σ-donor than NHCs, caused by the energetically higher HOMO, and a better π-acceptor through the energetically lower LUMO (Figure 20). Up to this point, various changes in the substitution pattern of CAAC derivates have been established.[436, 460, 461]
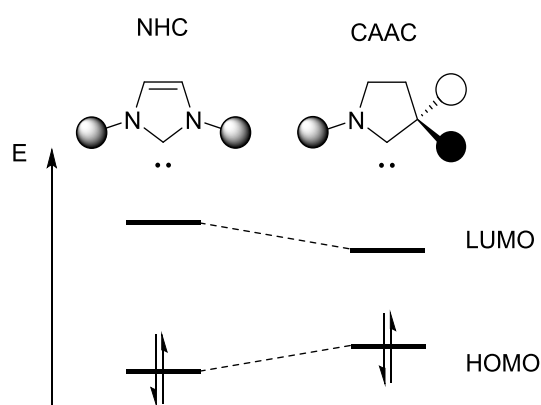
Figure 20: Illustration of the difference in the HOMO-LUMO gap between NHC and CAAC.

Another approach to assess the donor-acceptor properties of a carbene is the use of the Tolman electronic parameters (TEP). The TEP can be obtained by the changing stretching vibration of a CO ligand bound to the complex L-Rh(CO)$_2$Cl with L being either NHC or CAAC.[462, 463] By using IR spectroscopy, the strength of the CO bond can be determined by the measured wavenumber. The obtained bond strength in turn provides information about the net electronic influences of both donor and acceptor properties. Consequently, this method determines the overall electron-donating properties of the Ligand L without distinguishing between π-acidity and σ-donation.[464] To identify the ratio of the π-accepting and σ-donating properties of these carbenes a combination of TEP with ^{31}P-NMR or ^{77}Se-NMR spectroscopy is necessary.[465-468] This can be achieved by the reaction of a carbene with *P,P*- Dichlorophenylphosphine forming a carbene-phosphine adduct, or analog a carbene-selenium adduct. Depending on the strength of the π-acceptor abilities of the carbene, the electronic structure of the product can be best described with a double bond, resulting from a strong π-accepting carbene and a full π-back donation, or a single bond with a remaining lone pair on the phosphorus. This is caused by a weak π-acidity of the carbene and is accompanied by a high field shift of the phosphorus NMR signal, while a strong π-acidity yields a chemical shift to the low field. The group of Prof. Radius made an experimental and theoretical analysis of the behavior of different di-amino- and mono-amino- substituted cyclic carbenes.[469] Thereof, the assumption of CAAC being both, the better σ-donor and π-acceptor was confirmed.

Apart from the initial CAACs from Bertrand, two other derivatives were isolated (Figure 21). While Bertrand *et al.* synthesized the cyclic amino aryl carbenes (CAArCs),[470] the Bielawski group was mainly involved in the development of cyclic alkyl amido carbenes (CAAmC)[471] (Figure 21, middle).
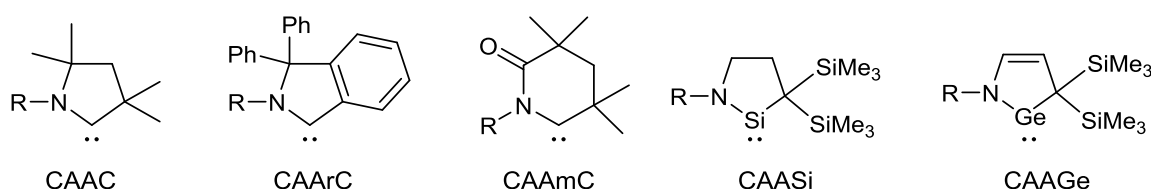
Figure 21: CAAC and some of its derivatives.

Both derivatives provide a smaller ST gap, which causes chemical stability problems. Another possible variation of CAAC is the use of heavier carbon-analogues of the same main group, namely silicon or germanium.[472, 473] These molecules were synthesized by different working

groups in the year 2016, resulting in the modification of the name CAAC to CAASi[473] and CAAGe[472] (Figure 21). Since the stability of these CAAC derivatives and their synthesis routes are still under development, in this work the focus is set on the basic CAAC ligand. Apart from their ability to stabilize radicals, CAACs are used to stabilize double bonds in main group elements. In the working group of Prof. Braunschweig, various CAAC ligated diborenes were synthesized.[455-457, 459, 474-476]

In this work, diverse diborene and diborane molecules are analyzed varying in the sulphur substituent attached to the boron centers.[477] An overview is provided in Figure 22. Instead of sulphur also selenium can be used. On the right side of Figure 22, a diborane in its biradical form with CAAC as carbene ligand is shown, while the left side shows its NHC ligated counterpart forming a diborene. The substituents bound to the sulphur can be substituted with methyl, *n*-butyl or phenyl groups and all structures could be synthesized by the Braunschweig group.[477] It is noteworthy that in the following chapters the carbene bound to the diborene is shortened as NHC, while its precise designation is 1,3-Bis(2,6-diethylphenyl)imidazoline-2yliden (IDip).
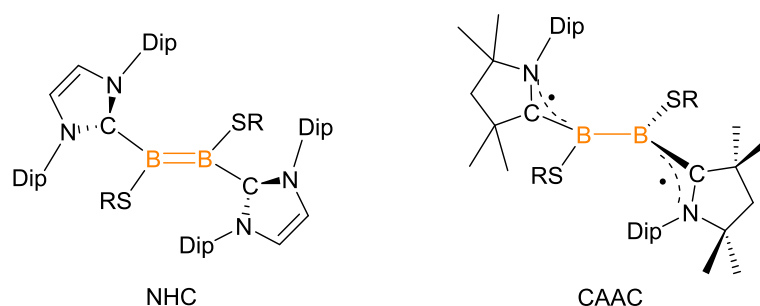
Figure 22: Basic structure of the various diborenes ligated with NHC (left) and diboranes with CAAC as ligand (right) with R = methyl, *n*-butyl or phenyl.

5.1   NHC stabilized diborenes with different substituents on the boron

As an approach to build up diborenes with a double bond, initial attempts comprised mono anionic[478] and dianionic[479-481] diborenes. The first neutral diborenes, stabilized with CAAC, were isolated by Robinson *et al.*[482, 483] The synthesis of LBrB=BBrL (**15**, Figure 23) is quite intricate, since the mono radicals with NHC ligands tend to side reactions, such as hydrogen abstraction or ligand C-H activation. The activation is favoured due to the slow dimerization process caused by the steric hindrances of the large NHC ligands, each with two 2,6-diisopropylphenyl (Dip) ligands.[482-487] Therefore, Dr. Philipp Bissinger of the Braunchweig

group synthesized diborenes from duryl (1,2,4,5-tetramethylphenyl) boranes stabilized with small NHCs (**16,** Figure 23).[476] With a B=B bond length of 1.59 Å a usual double bond length could be identified, as seen in LHB=BHL (**14**) (1.56 Å) and LBrB=BBrL (**15**) (1.55 Å).[477, 482] Diborene **14** was synthesized by the Robinson group in 2007.[482] A similar diborene with bromine, **15** was isolated in 2012 by the Braunschweig group.[476] Another attempt was made by the Braunschweig group containing different chalcogens.[477] Thereby, the influence of the substituent bound to the sulphur (**17**) and the substitution of sulphur with selenium was investigated and various systems of this kind were synthesized.
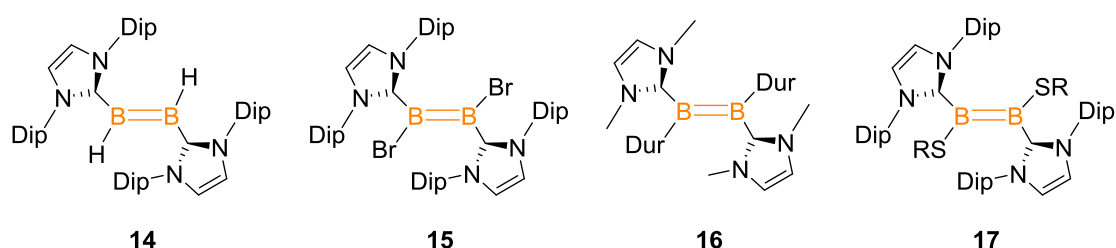
Figure 23: Different diborenes **14**-**17** synthesized over the last 15 years (R: methyl, *n*-butyl, phenyl).

In the following chapter, these molecules with the basic structure **17** are introduced and investigated, where the alkyl/aryl groups R on the sulphur are either methyl, *n*-butyl or phenyl (Figure 23). All following geometry optimizations were again performed using the unrestricted MN12L functional within the BS approach and the Pople basis sets adding diffuse and polarization functions 6-311G(d, p).

5.1.1   NHC stabilized diborenes with alkthiol substituents on the boron

To ensure a better overall view the diborenes with the basic structure **17** containing methyl groups bound the sulphur are abbreviated by **S1** and the ones with *n*-butyl with **S2** (Figure 24).
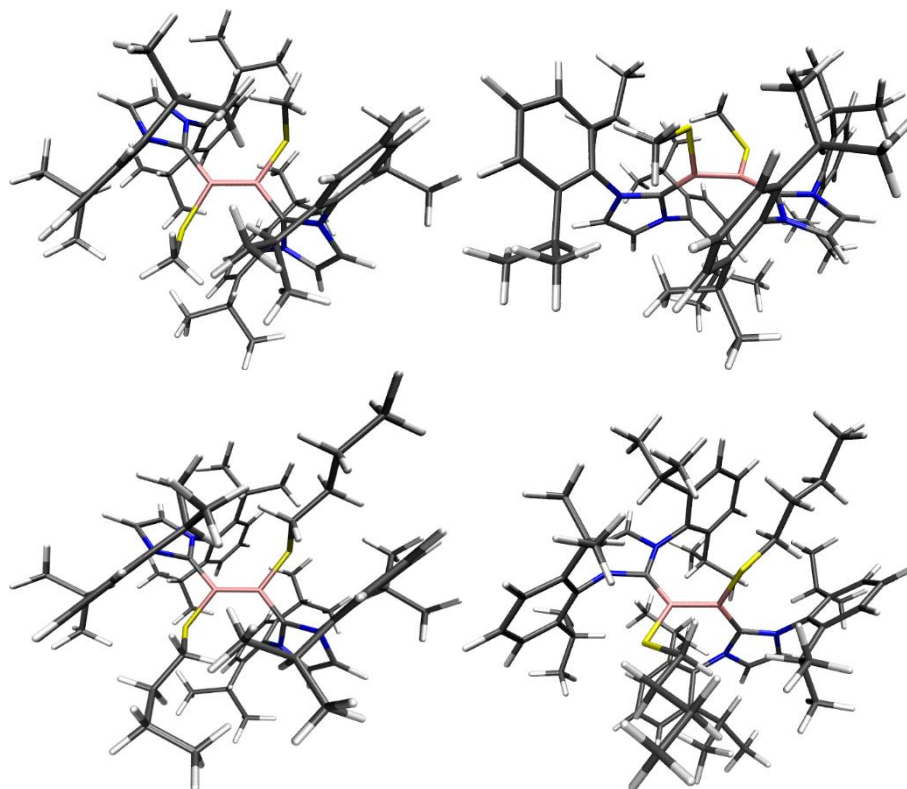
Figure 24: Singlet (left) and triplet (right) structure of the NHC systems with methyl substituents **S1** (above) and *n*-butyl substituents **S2** (below).

For both systems **S1** and **S2** the ground state is represented by a singlet with an energy gap to the lowest lying triplet of 21.2 kcal/mol (**S1**) and 22.8 kcal/mol (**S2**). This similarity in the ST gap is probably caused by the resemblance of the geometries. Some of the most important parameters, like the dihedrals of the S-B-B-S and C-B-B-C plane, are nearly identical within a difference of 5°. The same applies for the B-B bond length with 1.58 Å, which presents a B=B double bond. The same resemblances can be found in the triplet geometry, too. This parameter can be reproduced very well with the calculation of the singlet, whereat the triplet shows a slightly longer B-B single bond with 1.71 Å. The dihedrals and other angles of the singlet ground structure are in a good agreement with the data obtained from the crystal structure. Since the electron density distribution and the concerning orbital energies of both systems are nearly identical, only the molecular orbitals of **S1** are shown in Table 6. The

frontier orbitals are plotted starting from the HOMO-1 of the singlet to the LUMO+1 with each respective orbital energy in kcal/mol.

Table 6: Molecular orbitals of the calculated singlet and triplet states of **S1** with their respective energy in kcal/mol.

Singlet	Triplet

HOMO-1
-98.8

HOMO
-105.1

HOMO
-70.6

SOMO
-73.1

LUMO
-32.6

SOMO +1
-58.4

LUMO +1
-19.0

LUMO
-21.5
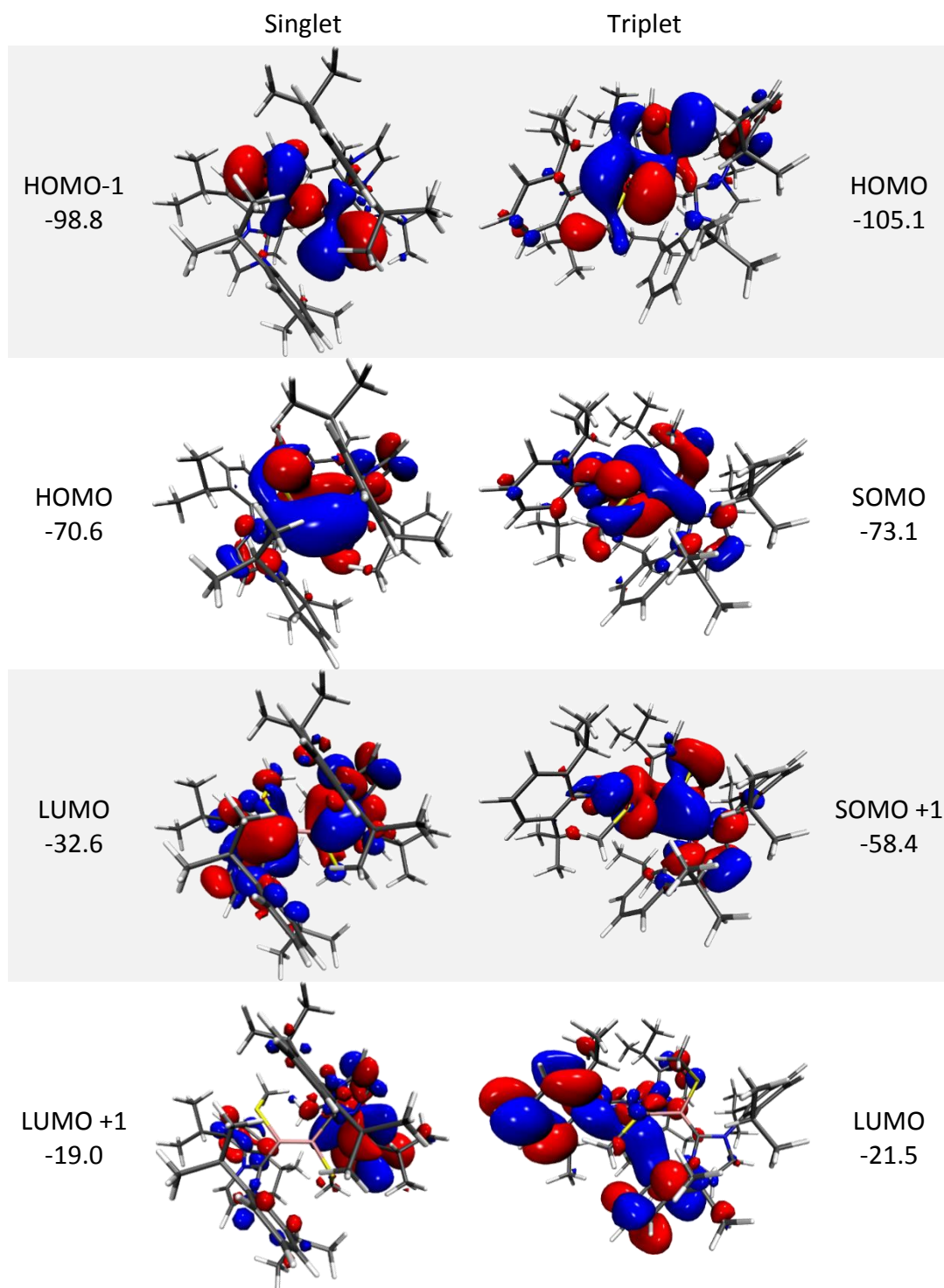
The HL gap (40 kcal/mol) is slightly bigger than the ST gap (20 kcal/mol). While the HOMO-1 of the singlet presents a σ-bond to sulphur bound methyl substituents, the remaining orbitals show mainly π-character. The HOMO shows a π-bond across the C-B-B-C moiety with an antibonding character to the nitrogens of the NHC and the methyl groups. The LUMO illustrates the same kind of π-orbital with an additional nodal plane between the boron atoms. The LUMO of the singlet is located on the substituents of the NHC ligands. Considering the triplet orbitals in Table 6, the HOMO-1 looks similar to the one of the singlet presenting a σ-bond. For the nearly degenerated SOMO and SOMO+1 the orbitals look similar to the singlet ones, too. Due to the torsion of the C-B-B-C axis there is now no conjugation between the boron centres. Therefore, the orbitals show two localized B-C π-bonds on each side with different nodal planes to the methyl substituents and nitrogen atoms of the NHC. In order to analyse these systems more precisely, a natural occupation calculation was performed to obtain the bond orders, charges and spin densities. Since **S1** and **S2** are nearly identical concerning their chemical properties and behavior, only the **S1** was included in the following analysis. The structure of the basic system can be seen in Figure 25.
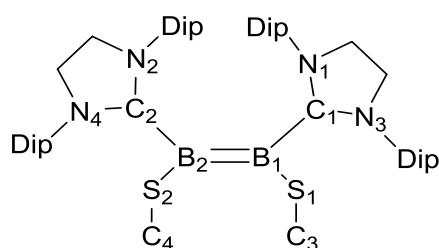
Figure 25: Basic system with the numbering of the atoms used in the following analysis.

The system is not completely symmetrical, however, the trend is on each side the same with insignificant differences. Therefore, only one side is discussed in the following analysis. The same is done for the triplet, though the changes on both sides are slightly larger. Because of the differences in the geometry of the triplet and singlet state it is assumed that the behavior of the two systems differs, too. Regarding the bond orders listed in Table 7, the main distinction can be seen in the C_1-B_1 and B_1-B_2 bond order, which fits to the differences in the bond length. While the singlet performs a double bond between B_1-B_2, the triplet performs a single bond, which in turn leads to a multiple bond character of the C_1-B_1 next to it. The changes in the other bonding situations are neglectable.

Table 7: Calculated bond orders for the singlet and triplet state of **S1** with the numeration shown in Figure 25.

	N_1-C_1	N_3-C_1	C_1-B_1	B_1-B_2	B_1-S_1	S_1-C_3
singlet	1.16	1.18	1.03	1.69	0.80	0.99
triplet	1.02	1.01	1.42	0.72	0.75	1.03

These changes in the bonding situation lead to an altered population of the electrons and charge distribution. Thus, the natural charge and natural occupation of both the singlet and triplet state, as well as the spin densities of the triplet are shown in Table 8, with numeration shown in Figure 25. Of course, the main differences can be found on C_1 and B_1 yielding a less positive partial charge on the carbon atom in the triplet, while the negative partial charge of the boron in the singlet ground states gets positive in the triplet. The spin densities of the two unpaired electrons are localized on each side of the B-B bond and can be mainly found between the boron atom and the nitrogen and carbon of the NHC ligands. Interesting is the difference between the singlet and triplet geometry and therefore the resulting changes in the population.

Table 8: Natural population and spin densities of the singlet and triplet of **S1** with the numeration shown in Figure 25.

		N_1	C_1	B_1	S_1	N_3	C_3
singlet	Natural charge	-0.52	0.42	-0.18	-0.17	-0.51	-0.46
	Natural occupation	7.52	5.58	5.18	16.17	7.51	6.46
triplet	Natural charge	-0.54	0.12	0.22	-0.13	-0.55	-0.47
	Natural occupation	7.54	5.88	5.18	16.17	7.55	6.47
	Spin density	0.17	0.33	0.30	0.03	0.16	0.01

5.1.2   NHC stabilized diborenes with arylthiol substituents on the boron

Apart from the alkyl substituted system, a molecule with an aryl group as substituent on the sulphur was also investigated. To analyze the influence of the sulphur on this kind of systems another phenyl substituted molecule was built. Instead of using sulphur as bonding partner to the boron, selenium was used. The sulphur system with phenyl is shortened **S3**, while the selenium molecule is abbreviated as **Se3** (Figure 26).
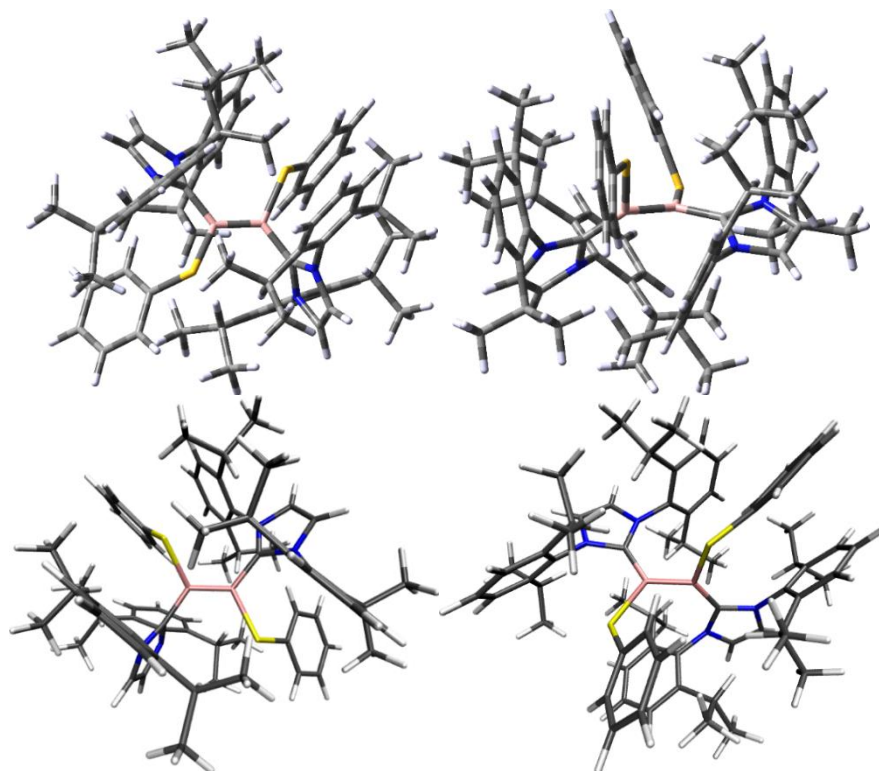
Figure 26: Above: singlet (left) and triplet (right) structure of **S3**; below: singlet (left) and the triplet (right) of **Se3**.

Since the two elements sulphur and selenium are part of the chalcogens, their behavior in these molecules is very similar. Even the geometries for the singlet, more twisted than for **S1** and **S2**, but still mostly planar, and triplet arrange likewise. For both systems a closed shell singlet is located with the triplet about 26.6 kcal/mol above the ground state for **S3** and 29.4 kcal/mol for **Se3**. As seen for the alkyl substituted systems **S1** and **S2** before, the singlet occurs as a mostly planar system, while the triplet favours the twisted structure. Since the molecular orbitals of **S3** and **Se3** are nearly identical, only the ones of **S3** are shown in Table 9.

Table 9: Frontier orbitals of the singlet ground state and the first triplet state of **S3**.
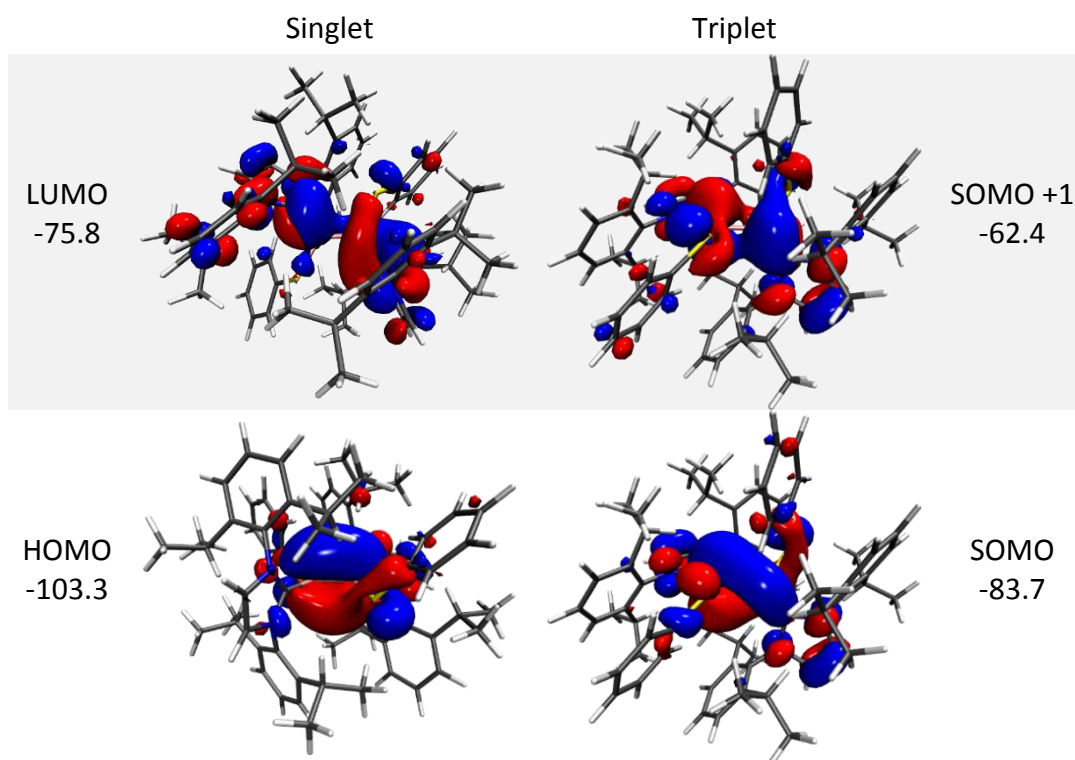
The electron distribution for **S3** and **Se3** complies more or less with the one of **S1** and **S2**. The HOMO-1 for the singlet (HOMO for triplet) constitutes a σ-orbital, while the remaining orbitals can be described as π-orbitals. In the case of **S3**, the electron density is again located at the N-C-B-B-C-N moiety and the sulphur (selenium) atoms, whereas the nitrogen and chalcogens are antibonding to the remaining system. The HL gap decreases compared to **S1/S2**, probably due to the smaller antibonding character of the HOMO and LUMO. Since these two aryl substituted systems behave analog to the alkyl ones, a more precise analysis of the bond order and natural occupation is not necessary and included here. Summarizing the so far obtained results, it can be said that the substituent bound to the sulphur does not exhibit a major influence on the behavior of the system and even the replacement of sulphur with another chalcogen, such as selenium, does not affect the arrangement and its chemical properties. Another possible modification is the variation of the carbene bound to the boron atoms, which is shown in the next chapter.

5.2   CAAC stabilized systems with different substituents on the boron

In comparison to NHC, CAAC is one of the most σ-donating and also π-accepting carbene ligand. The basic structure of the analyzed systems is shown in Figure 27.
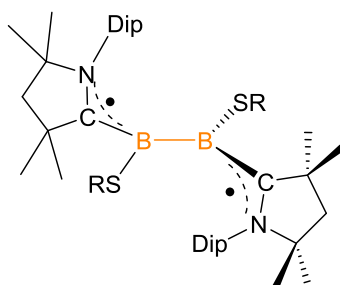
Figure 27: Basic structure of CAAC stabilized systems (R: methyl, *n*-butyl, phenyl)

5.2.1   Diboranes with alkyl substituents

The same systems as seen in chapter 5.1 were synthesized with a variation in the ligands. Instead of NHC, CAAC was used to create the following molecules. Again, a methyl group on the sulphur, shortened as **S$_c$1**, and a *n*-butyl group bound to the sulphur, with the abbreviation **S$_c$2** were synthesized and analyzed (Figure 28).
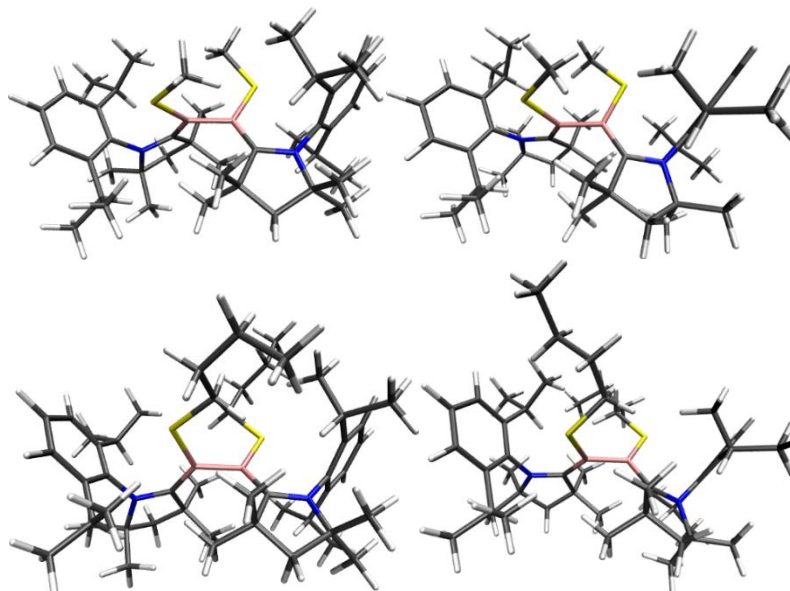
Figure 28: Singlet (left) and triplet (right) structure of the CAAC system with a methyl substituent **S$_c$1** (above) and a *n*-butyl group bound to sulphur **S$_c$2** (below).

By changing the ligands, the molecule arranges very differently compared to its NHC analog. While the triplet presents again dihedral angles C-B-B-C and S-B-B-S, which are nearly orthogonal, the singlet minimum structure is now close in energy to this arrangement. As seen for the NHC substituted systems, here, the difference caused by the variation of alkyl groups

bound to sulphur is zero. Consequently, there is no change in the geometry and the ST gap is nearly identical with a value of -6.8 kcal/mol (**S$_c$1**) and -6.4 kcal/mol (**S$_c$2**). It is obvious that a change of the ligands from NHC to CAAC directs from a singlet ground state to a triplet one. Regarding the electron density contribution reveals that the changes are caused by the triplet ground state and the twisted geometry. Again, only the molecular orbitals of **S$_c$1** are shown in Table 10, since no structural and electronic difference exists between **S$_c$1** and **S$_c$2**.

Table 10: Important molecular orbitals of the singlet (right) and the triplet (left) of **S$_c$1**.
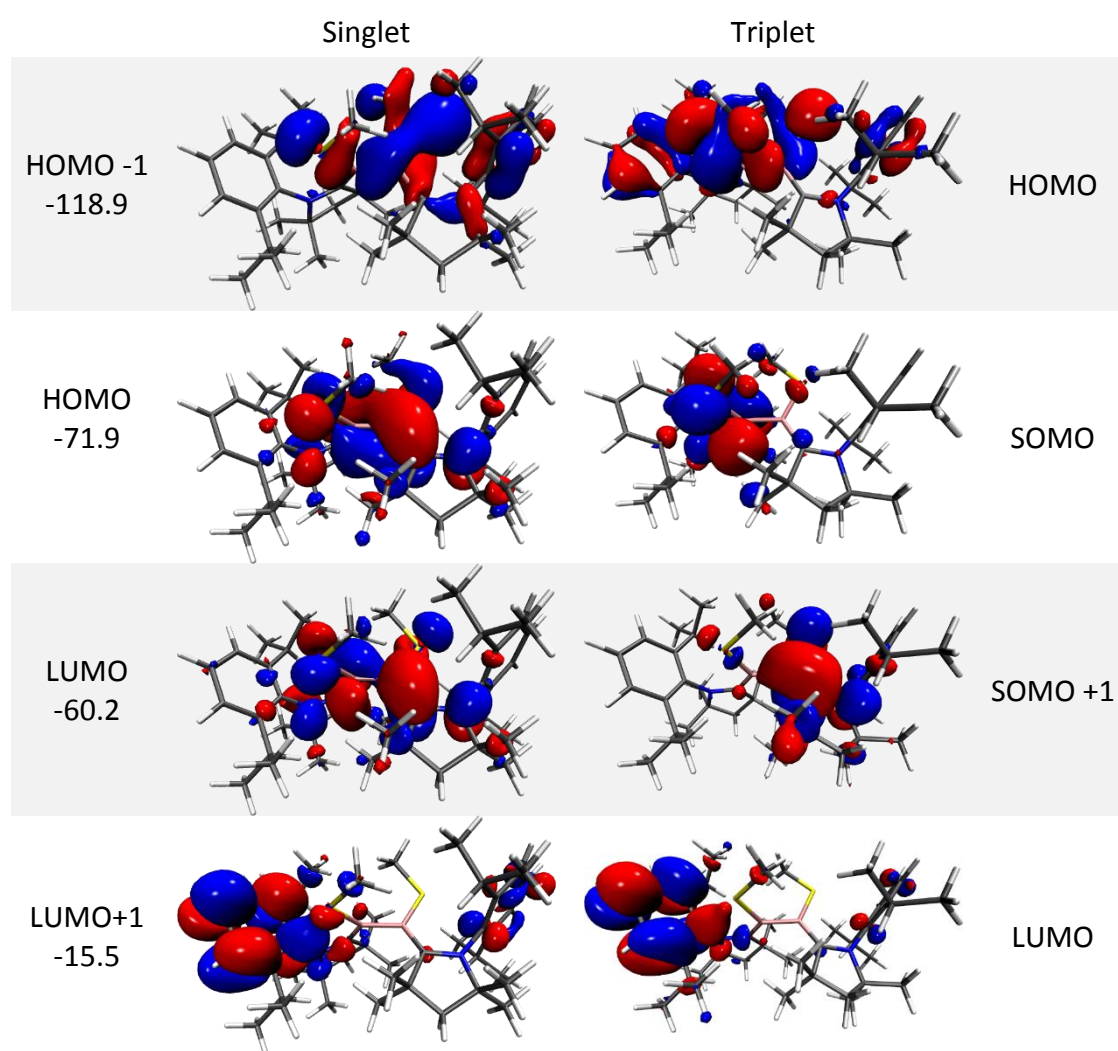
With a kind of σ -bond in the energetically lowest orbitals, the molecular orbitals of the singlet and triplet correspond to the ones of NHC. The electron density of the HOMO-1 (singlet) and HOMO (triplet) of the CAAC ligated molecules are located on the Dip-substituent of the carbene. This contribution can also be found in the NHC substituted molecules. The HOMO-1 (singlet) and the HOMO (triplet), as well as the LUMO+1 (singlet) and LUMO (triplet) look alike and both present no substantial differences to the NHC ones. Therefore, the changes in the

chemical behavior must be found in the SOMO and SOMO+1 of the triplet. The main difference in electron density can indeed be found in the HOMO and LUMO of the singlet and the SOMOs of the triplet. While the density of the singlet is located over the complete diborane, including the sulphur ligands, the triplet state has its density partial located on each side of the system over S-B-C-N-C. The size of the HL gap for the singlet decreased tremendously for the CAAC substituted systems and the SOMOs of the triplet are nearly degenerated. This is corresponding with the biradical character of the triplet state, with both radicals being located on each side of the diborane bond. Further interesting aspects are the changes in the bonding situation and the consequential natural occupation. Thus, the basic structure of this compound with the atom numbering is depicted in Figure 29.
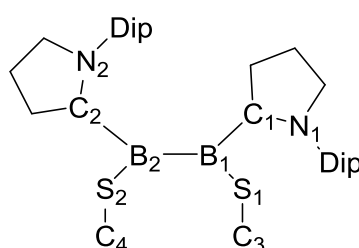
Figure 29: Basic structure of the CAAC compounds with the numbering used in the following analysis.

Since the analyzed bonding situation of S_c1 and S_c2 shows no differences, only the values for S_c1 are listed below. While the triplet shows a very symmetric behavior to each side of the B_1-B_2 bond, the singlet shows strong asymmetric tendencies. The complete bond order analysis is listed in Table 11. Because of this asymmetry, the singlet must be considered carefully, since this is an evidence for a multireference case, which cannot be described properly by DFT. This assumption is underlined by the relatively small ST gap.

Table 11: Calculated bond orders for the singlet and triplet state of S_c1.

	N_1-C_1	C_1-B_1	B_1-B_2	B_1-S_1	S_1-C_3	N_2-C_2	C_2-B_2	B_2-S_2	S_2-C_4
Singlet	1.29	1.06	1.01	1.10	1.02	1.02	1.53	0.91	1.00
Triplet	1.11	1.30	0.95	1.08	0.99	1.11	1.30	1.08	0.99

For both states, the B-B bond can be described as a single bond, probably caused by the twist between the C-B-B-C unit. In analogy to the NHC molecules, a multiple bond character exists in the triplet state between the nitrogen and carbon of CAAC and the boron atom leading to the assumption that the free electrons are localized on each side on these atoms. The other bonds can be clearly described as single bonds. In the singlet state, similar to the triplet, there is a multiple bond character. While for the singlet state on the right side of the B-B bond, the

multiple bond is located between the N_1-C_1, the bond of higher order can be found on the left side between the C_2-B_2 with every other bond showing a single bond nature. Considering the triplet, the multiple bond character is located on both sides between the carbon and boron atom resulting in a more symmetric arrangement as the singlet state. The natural occupations including the spin densities for the triplet state are listed in Table 12. For comparison, the natural occupations of the singlet state are shown in Table 13.

Table 12: Natural occupation and spin densities of the triplet ground state of S_c1.

	N_1	C_1	B_1	S_1	C_3	N_2	C_2	B_2	S_2	C_4
Natural charge	-0.59	-0.09	0.31	-0.08	-0.67	-0.59	-0.09	0.31	-0.08	-0.67
Natural occupation	7.59	6.09	4.69	16.08	6.67	7.59	6.09	4.69	16.08	6.67
Spin density	0.18	0.65	0.13	0.05	0.00	0.18	0.65	0.13	0.05	0.00

The carbon atoms C_3 and C_4 have a negative partial charge for both multiplicities, caused by hydrogens atoms bound to it, whereas the atoms of the triplet show a much higher negative partial charge as the singlet state. This partial charge decreases for S_c2. The spin densies predict the free electron delocalized on each side on the nitrogen and carbon of the CAAC and the boron atom, with a main percentage on the carbon atom of the CAAC. The boron possesses less valence electrons than it is supposed to have. This lack in electron density seems to be located on the nitrogen atoms of the CAAC, as in the conjugated system the electron density is transferred through the carbene to the nitrogen. The natural occupation of the singlet clearly demonstrates the asymmetry of each side of the B-B bond. While the right side (C_1, B_1 and S_1) possesses a positive partial charge, the left side is negative.

Table 13: Natural occupation of the singlet state of Sc1.

	N_1	C_1	B_1	S_1	C_3	N_2	C_2	B_2	S_2	C_4
Natural charge	-0.54	0.14	0.30	0.01	-0.16	-0.60	-0.05	-0.06	-0.01	-0.16
Natural occupation	7.54	5.85	4.70	16.01	6.16	7.60	6.05	5.06	16.01	6.16

5.2.2   CAAC stabilized diboranes with aryl-chalcogen substituents on the boron

As seen in the NHC section before (chapter 5.1), the CAAC ligated systems can also be synthesized with a phenyl substituent bound to sulphur or selenium. The two experimentally obtained molecules match very well with the calculated triplet geometries. Both, the singlet and the triplet minimum structures are shown in Figure 30, whereat the one with sulphur is shortened as S_c3 and the selenium substituted one is abbreviated as Se_c3.
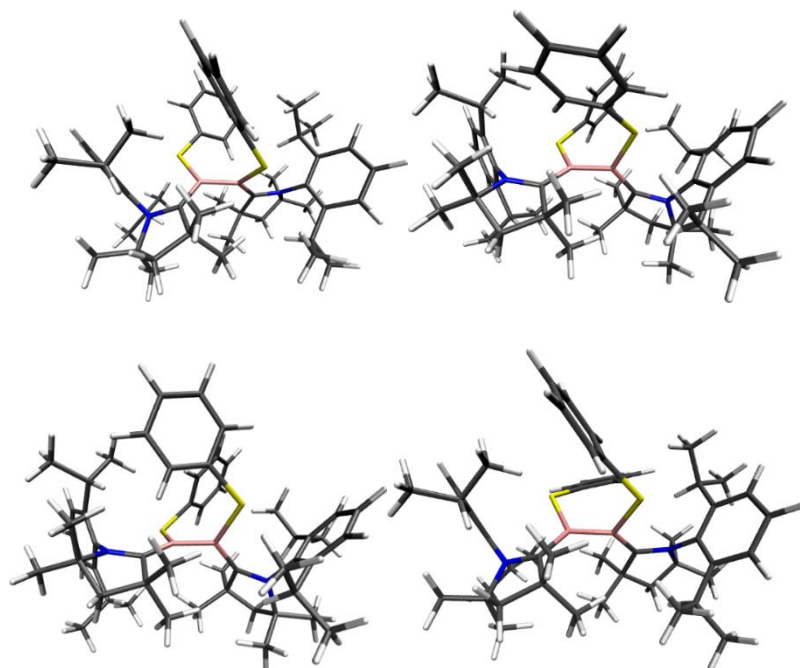
Figure 30: Geometry of the singlet (left) and triplet (right) of S_c3 (above) and Se_c3 (below).

The molecules arrange similar to the ones with alkyl substituents, irrespective of the chalcogen in between is sulphur or selenium. Consequently, both dihedrals are nearly orthogonal for S_c3 and Se_c3 in the triplet state. The dihedrals of the singlet increase slightly for both systems. Due to the similar geometries, the ST gap of all four systems is very close, too. The obtained values are 6.7 kcal/mol (S_c3) and 6.2 kcal/mol (Se_c3). For Se_c3 and S_c3 the triplet is more favourable than the singlet. For a more precise analysis, the molecular orbitals of S_c3 are depicted in Table 14.

As most interesting orbitals only the HOMO, LUMO of the singlet and SOMO, SOMO+1 for the triplet are depicted. It should be mentioned that the LUMO+1 of the singlet and the HOMO of the triplet are not only localized on the CAAC ligands, as seen for the other molecules, but also on the phenyl groups of the chalcogens.

Table 14: Frontier orbitals of S_c3.
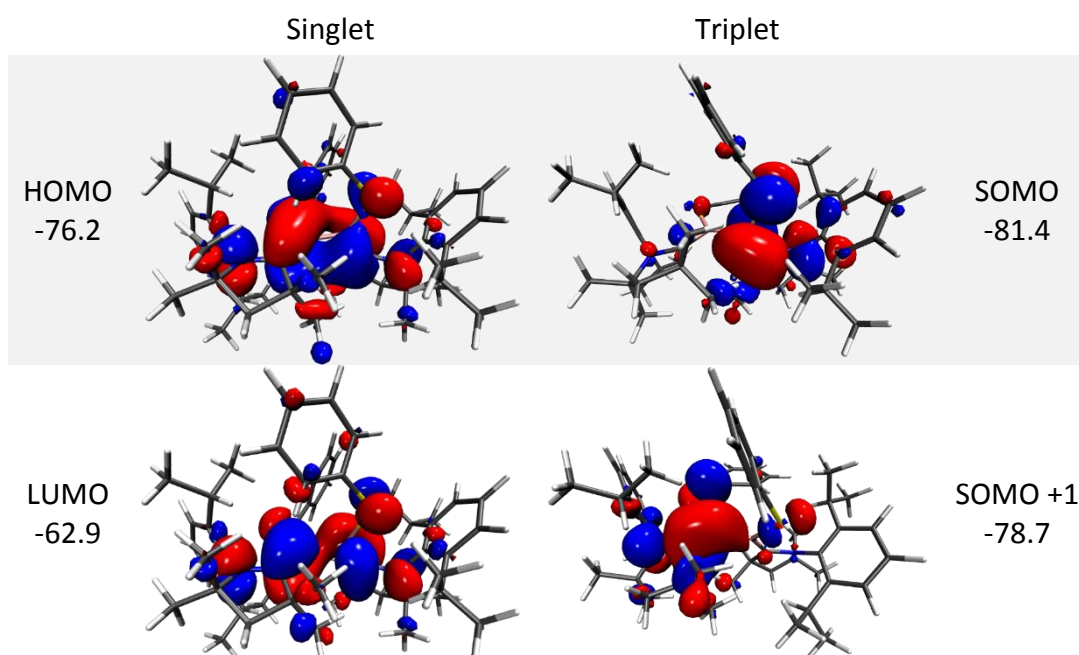
For the phenyl substituted molecules the triplet ground state illustrates two nearly degenerated SOMOs with a localization of the electron density of each side of the B-B bond on the N-C-B part. The HL gap of the singlet increases slightly compared to the molecules S_c1 and S_c2. The molecular orbitals of S_c3 look more symmetrical than the ones of the alkyl substituted systems. To further investigate this observation, the bond orders are analysed. The bond orders reveal an asymmetric behavior of the singlet (Table 15). The N_1-C_1 bond order is more symmetric in the singlet, while the C_1-B_1 and C_2-B_2 distinguish widely.

Table 15: Calculated bond orders for the singlet and triplet state of S_c3.

	N_1-C_1	C_1-B_1	B_1-B_2	B_1-S_1	S_1-C_3	N_2-C_2	C_2-B_2	B_2-S_2	S_2-C_4
Singlet	1.13	1.06	1.01	1.10	1.01	1.13	1.53	0.91	1.00
Triplet	1.13	1.31	0.93	1.06	1.01	1.13	1.34	1.05	1.00

In the case of the triplet, the same behavior as for the alkyl substituted system is found, with a multiple bond character between the N-C-B part, where the unpaired electrons are localized. The natural population was analyzed, but there are no significant differences to the alkyl substituted molecules S_c1 and S_c2, neither for S_c3 nor Se_c3. Therefore, the results are not explicitly mentioned here.

5.3   Comparison of NHC or CAAC ligated systems

Since numerous differences were seen in the molecules ligated by CAAC and NHC, a comparison of all these systems is aimed for in this chapter. To get a better overview of the disparities caused by the various substituents and the two carbenes, the changes of important parameters are figured graphically in the following section. First, one of the most important parameters, the ST gap, is described. In chapter 5.2, it was in detail described that the CAAC substituted molecules provide a triplet ground state and show a negative value for the ST gap (Figure 31, blue graph). Furthermore, the CAAC ligated systems show no substantial difference regarding the change of the substituent at the sulphur/selenium.
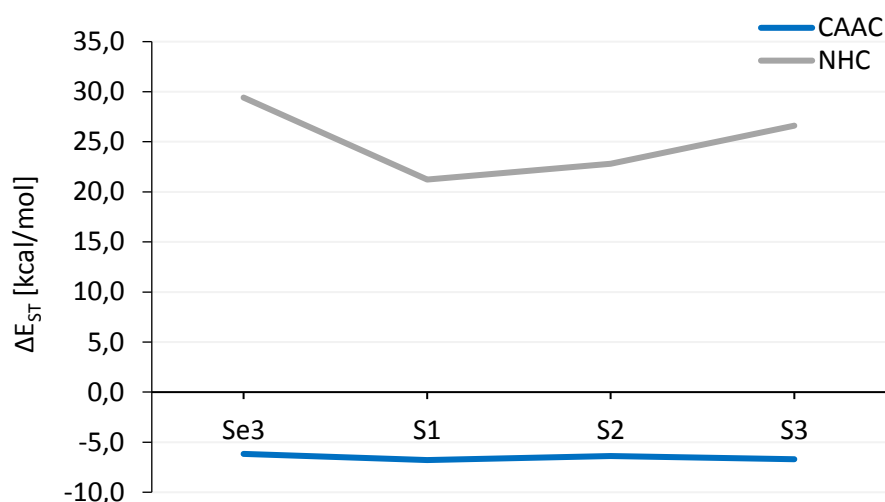
Figure 31: Energy of the ST gap for the various structures of the NHC (grey) and CAAC (blue) substituted molecules.

However, the NHC substituted systems exhibit a singlet ground state (Figure 31, grey graph). In these molecules, the ST gap provides a larger dependence on the substituents on the chalcogen. The smallest ST gap is obtained for the methyl substituted **S1** and increases with a growing size of the substituent. The reason is probably the better stabilized triplet of this molecule. Because of the smaller steric hindrance of the methyl group, the triplet is more similar to the CAAC geometry concerning the dihedrals. To be able to evaluate the steric influence of the substituents on the ST gap, some important parameters, like the B-B bond length and dihedrals, are analyzed more precisely in the following. Both the triplet and the singlet state are considered, since the ST gap depends on both multiplicities and the ground state multiplicity changes from NHC to CAAC.

As Böhnke *et al.* already summarized recently,[408] stabilizing the diborene with NHC leads to a B-B double bond and a B-B bond length of 1.59 Å. Whereupon the use of CAAC as stabilizing

carbene results in a diborane with a B-B single bond and an average length of 1.71 Å. An outline of this relation is given in Figure 32. The different systems are pointed out in the x-axis and the blue graph outlines the triplet, while the singlet is described by the green graph.
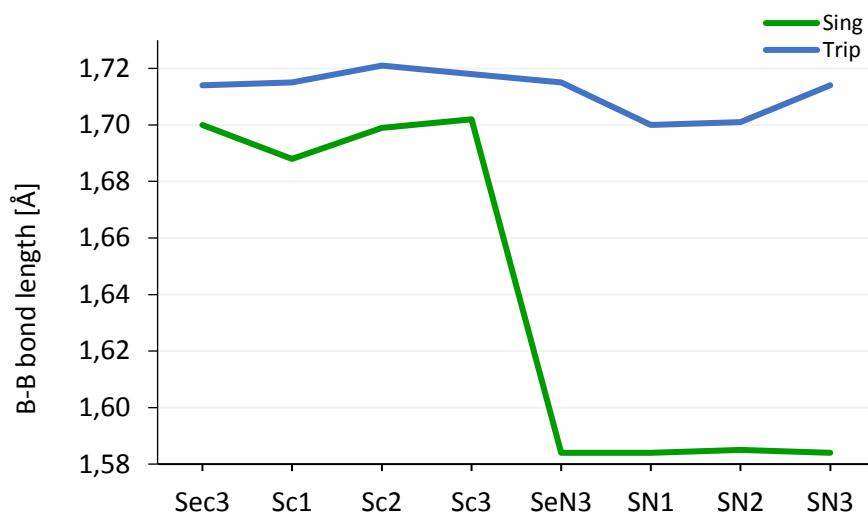

Figure 32: B-B bond length for the different molecules in the singlet (green) and triplet (blue) state.

The first four molecules represent the CAAC substituted ones (**Se$_c$3**-**S$_c$3**), the last four the NHC analogues (**Se$_N$3**-**S$_N$3**). It is apparent that the single bond character for the triplet stays the same for both systems and the value of the B-B bond fluctuates between 1.70 Å and 1.72 Å. The singlet state switches from a single to a double bond by switching from CAAC (around 1.70 Å) to NHC (around 1.58 Å) substituted molecules. This change can be directly connected to the appearance of the dihedrals, which are represented in Figure 35. The small ST gap for CAACs could be caused by the small change in geometry, since both the singlet and triplet are twisted and very similar in their geometry. This in contrast to NHC, for which the minimum singlet and triplet geometry are completely different. In Figure 31, the ST gap shows a slight decrease for **S$_N$1** and **S$_N$2** with NHC, since there is no change in the singlet. However, the triplet demonstrates a smaller bond for these two molecules, which might induce this behavior. Apart from the B-B bond, three other bond lengths exhibit great influence on the behavior of the systems: the C$_{CAAC}$-B, N$_{CAAC}$-C$_{CAAC}$ and the B-S bond length. So far, it is assumed that the B-B, the C-B and N-C bond go hand in hand with each other. With a rising B-B bond length and thus a single bond character, the B-C and N-C should decrease and induce a multiple bond character, seen in the bond order analysis in the previous chapters. Even though the singlet states of the CAAC stabilized diboranes exhibit asymmetric geometric arrangement, only one side of the molecules is shown in Figure 33, since both sides present the same trend.
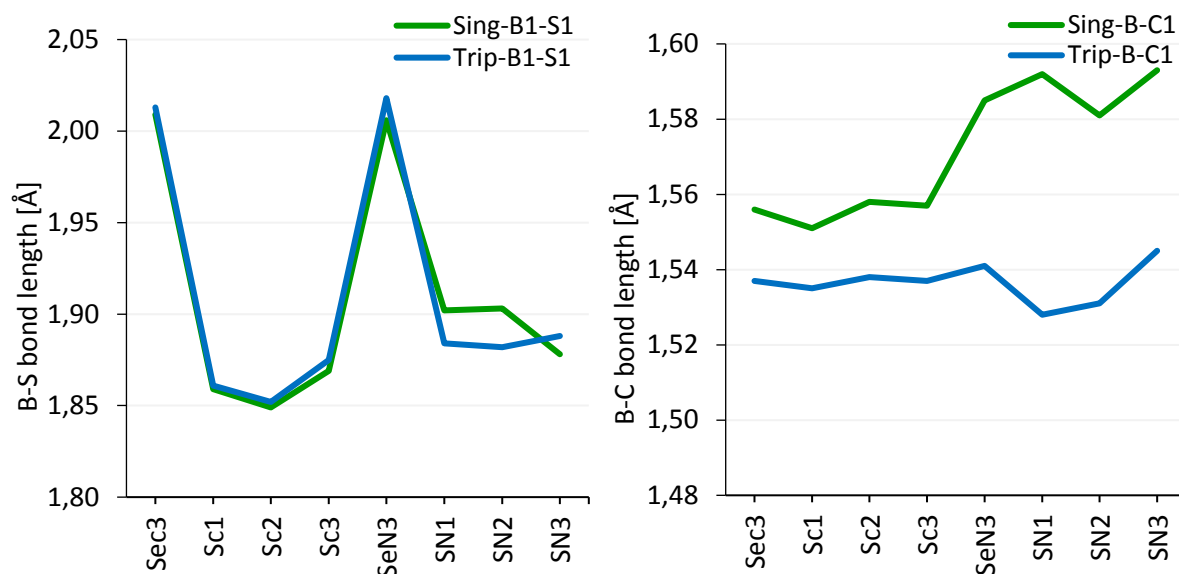
Figure 33: Variations of the boron-sulphur/selenium bond (left) and the carbon-boron bond (right) for the singlet (green) and triplet (blue) of the various NHC and CAAC ligated systems.

Considering the left graph, a longer B-S/Se bond can be found for selenium than for sulphur caused by the different size of the atoms. Changing the substituents on the sulphur leads to no visible trend in the bond length of both systems, which is in line with the assumption that the substituent bond to sulphur influences the system just slightly by its steric. The B-C and N-C bond length displays the same development for the systems, thus, only B-C is pictured in Figure 33, right graph. As seen for the B-B bond length, for the diboranes stabilized with CAAC no significant trend is visible, as the B-C bond length fluctuates about 1.55 Å for the singlet (green graph) and 1.54 Å for the triplet (blue graph). The NHC ligated diborenes possess an opposite direction regarding the triplet and singlet. While in the singlet ground state the B-B bond length (Figure 32) decreases, the B-C bond increases. The triplet shows no distinctive features for both the B-B and B-C bond length, just a very small decrease for both parameters with methyl and *n*-butyl as substituent. This may affect the ST gap and explain the small decrease of the ST gap for both systems. Additional importing parameters, which tremendously influence the behavior of the system, are the dihedrals spanned between the boron and the carbene ligands. These dihedrals are pictured in Figure 34 showing both dihedrals, the $\sphericalangle_{N_1 C_1 B_1 B_2}$ (left) and the $\sphericalangle_{S_1 B_1 B_2 S_2}$ (right). As no change between the $\sphericalangle_{N_1 C_1 B_1 B_2}$ dihedral of the one side to the $\sphericalangle_{B_1 B_2 N_2 C_2}$ dihedral on the other side of the system is detected, only one is shown. Since the C-B-B-C dihedral and the S-B-B-S dihedral provide nearly the same and show a similar behavior concerning the change of substituents R_1, only the $\sphericalangle_{S_1 B_1 B_2 S_2}$ dihedral is analyzed more precisely in Figure 35.
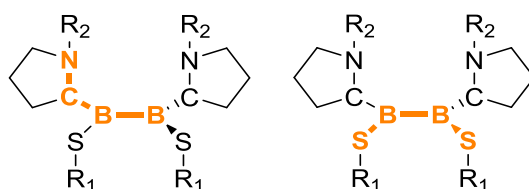
Figure 34: Important dihedrals N-C-B-B (left) and S-B-B-S (right) of both systems pictured on CAAC ligated diboranes.

As seen before in the bond lengths, there is no substantial difference for CAAC in changing the substituents on the chalcogens, neither for the $\sphericalangle_{N_1C_1B_1B_2}$ dihedral nor the $\sphericalangle_{S_1B_1B_2S_2}$ one. Only a small decrease of the $\sphericalangle_{C_1B_1B_2C_2}$ dihedral for the less sterically hindered methyl and *n*-butyl groups can be seen, insignificantly affecting the ST gap. Considering the NHC stabilized diborane, the $\sphericalangle_{C_1B_1B_2C_2}$ dihedral for the singlet ground state planarizes almost completely, while the triplet fluctuates between 90° and 120°.
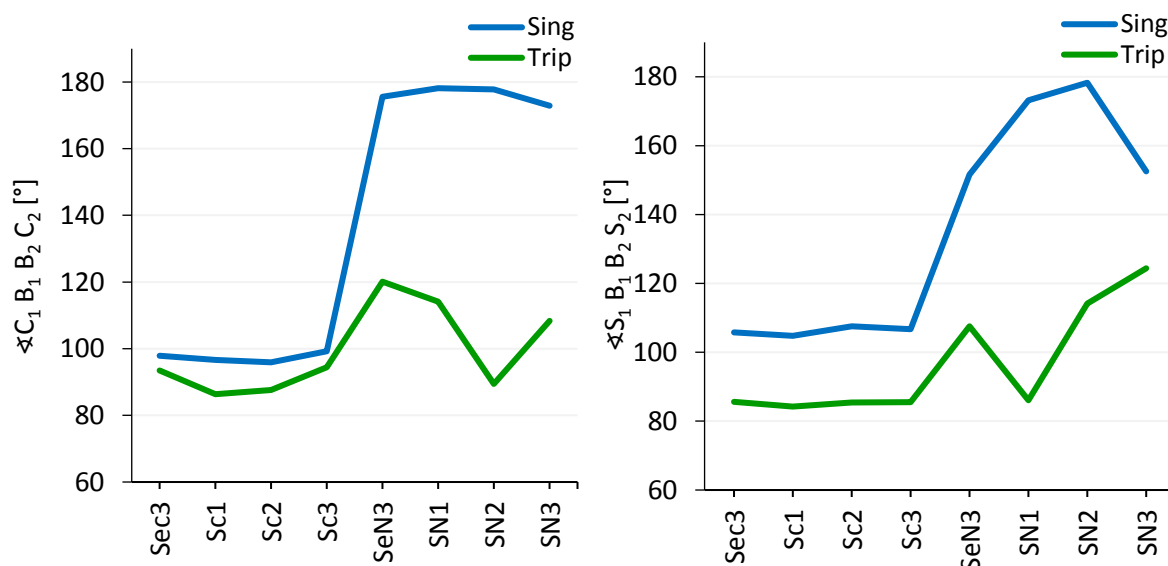
Figure 35: Graphical representation of the dihedrals C-B-B-C (left) and S-B-B-S (right) of the different systems:

The phenyl substituted NHC molecules switch the value for $\sphericalangle_{S_1B_1B_2S_2}$ and $\sphericalangle_{C_1B_1B_2C_2}$ dihedral in the triplet state. The $\sphericalangle_{C_1B_1B_2C_2}$ dihedral of **Se$_N$3** is 120° and for **S$_N$3** 110°, while the $\sphericalangle_{S_1B_1B_2S_2}$ dihedral is 110° for **Se$_N$3** and 120° for **S$_N$3**. The same trend is seen for **S$_N$1** and **S$_N$2**, with values of 90° and 115°. For the singlet, the planarity of the $\sphericalangle_{S_1B_1B_2S_2}$ dihedral is disturbed by the steric hindrances of the phenyl groups bound to the chalcogens of **Se$_N$3** and **S$_N$3**. Therefore, the dihedral decreases to nearly 150°, while the ones for the smaller molecules **S$_N$1** and **S$_N$2** are nearly plane. This may additionally influence the ST gap. The two potential curves of the two systems stabilized by CAAC or NHC show a different behavior for varying the dihedral $\sphericalangle_{S_1B_1B_2S_2}$. In Figure 36, both potential curves are outlined approximately presenting

the energetic position on the y-axis and the geometric parameter on the x-axis. It is obvious that the molecules substituted with NHC (Figure 36, left) favor a planar singlet ground state, while the CAAC ligated molecules (Figure 36, right) tend to arrange coplanar. Additionally, for both geometries of the CAAC systems the ST gap is small leading to a singlet multiplicity for the planar geometry and a slightly triplet preferred multiplicity for the twisted arrangement. Considering the NHC systems, the twisted geometry exhibits a small ST gap with a slightly favoured triplet. While the ST gap for the coplanar arrangement increases indicating a strong stabilization of the singlet combined with a destabilization of the triplet state. Apparently, the geometric arrangement of the different carbene ligated systems demonstrate a large impact on the energetic position.
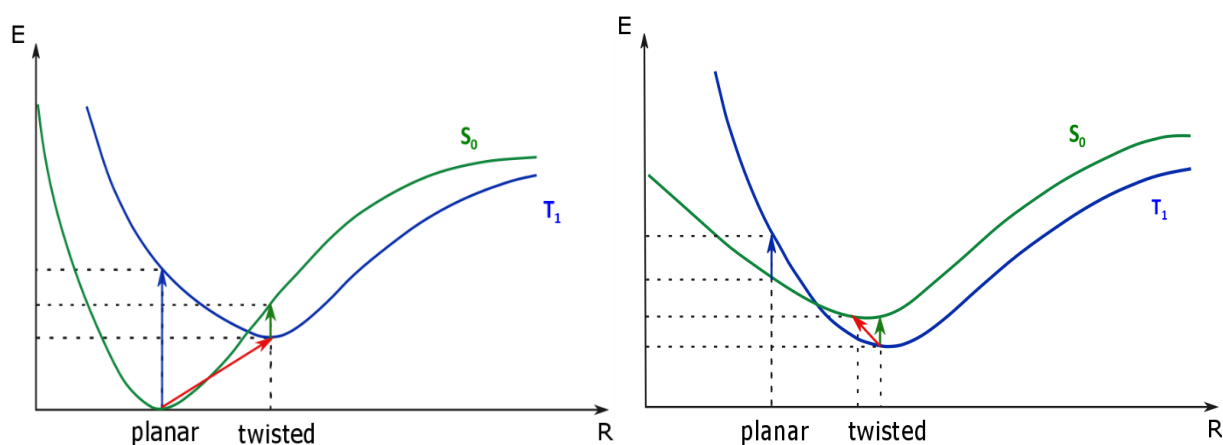
Figure 36: Schematic presentation of the energy potential of the NHC ligated systems (left) and the CAAC ligated systems (right).

5.4 Segmentation of the CAAC stabilized systems S_C3

As seen in the analysis in chapter 5.3, there is no noteworthy effect caused by the variation of the substituents bound to sulphur or selenium in the CAAC system. Since this work is about biradicals and the NHC analog shows a closed shell singlet ground state with a large HL and ST gap, in the following the focus is set on the CAAC ligated molecules.

Another interesting point is the influence of the substituents on sulphur combined with the ones bound to nitrogen and how they influence the important properties, especially the ST gap. It is shown that by decreasing the size of the steric hindrance of NHC by minimizing the alkyl substituent bound to the nitrogen atoms, a more similar behavior to CAAC is found.[459, 488] Thus, it is of great interest, if the properties of the already less sterically hindered CAAC can be influenced by the size of the substituents. The HL gap of CAAC can be affected by its structure and this should have an impact on the ability to stabilize the triplet and singlet and

consequently the biradical character.[489, 490] Another important aspect is the reduction of the atom size of these molecules. Since these kinds of systems are composed of about 150 atoms, they are difficult to handle with high quantum chemical methods Because of the previous Benchmark (see chapter 4), methods, which are able to describe the system in a good cost-benefit ratio, were in detail investigated. Consequently, the UMN12L functional (BS approach) in combination with the 6-311G(d, p) basis sets were used to optimize the various systems and also for the single point calculations. Here, it was important to control if the decreased systems can be compared to experimental data legitimating why the following analysis is necessary.

The basic structure of the following subsystems is shown in Figure 37, in which the residues R_1 and R_2 can be substituted by phenyl, methyl or hydrogen to get both electronic and steric effects.
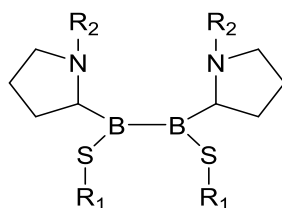
Figure 37: Basic structure of the following subsystem of the molecule with different substituents for R_1 and R_2.

In the analysis, test systems are prepared by varying the substituents R_1 and R_2 in every possible conformation. To get an overview, the composition of the various systems and their abbreviations are summed up in Table 16. By considering all possible compositions, nine subsystems are received in total.

Table 16: Different subsystem with their abbreviations and compositions of the substituents R_1 and R_2.

	S1.0	S1.1	S1.2	S1.3	S2.1	S2.2	S2.3	S3.1	S3.2	S3.3
R_1	Ph	Ph	Ph	Ph	Me	Me	Me	H	H	H
R_2	Dip	Ph	Me	H	Ph	Me	H	Ph	Me	H

Following the numeration of the different subsystems, a graphical representation of these molecules is shown in Figure 38 to improve the understanding of the composition of each system. **S1** always possesses a phenyl group bound to the sulphur in combination with varying substituent on the nitrogen (phenyl **S1.1**, methyl **S1.2** and hydrogen **S1.3**). **S2** shows a methyl group attached to sulphur and **S3** a hydrogen.
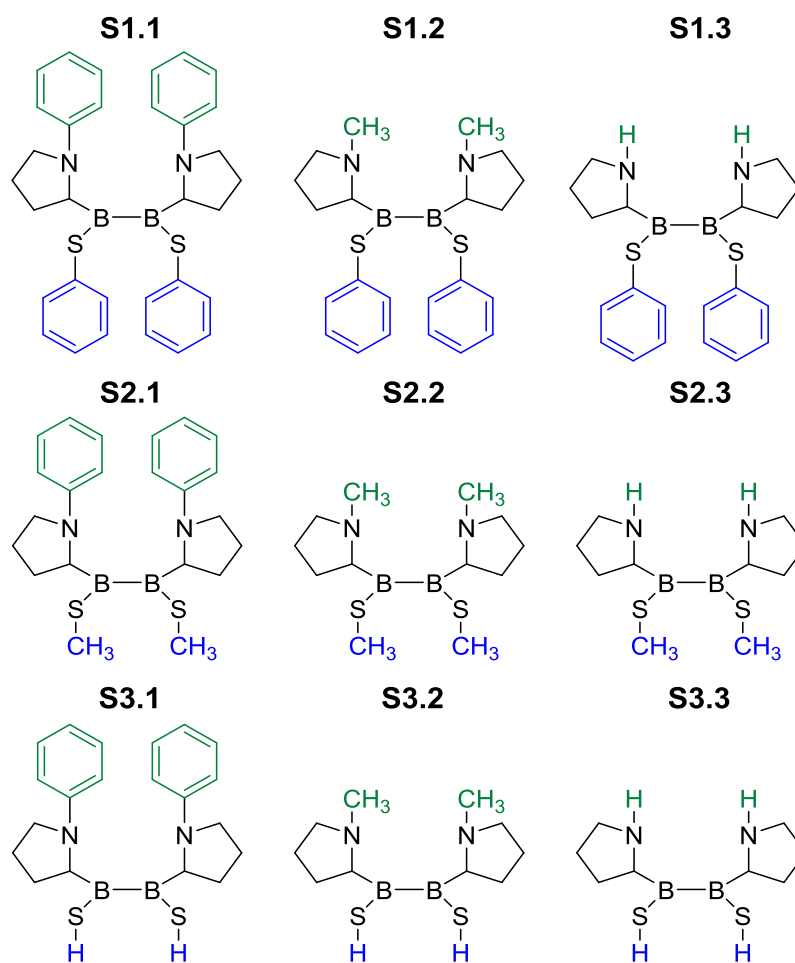
Figure 38: Depiction of the different subsystems described in Table 16.

There are two possible cases to consider. First, the geometry of the starting system **S1.0** is maintained and only the new substituents are optimized. This procedure is abbreviated as SP for single point. Therefore, the geometry is not allowed to relax due to the decreased steric hindrances and only the electronic effects should affect the behavior of the system. Second, the system is optimized completely to check the geometric adaption of the decreased size system and therefore less steric hindrances. In Figure 39, the calculated ST gap is plotted against the various subsystem **S1.1**-**S3.3**. The dotted red line represents the ST gap of the initial system **S1.0**. The blue graph constitutes the ST gap of each optimized subsystem, shortened by Opt, and includes systems adaption to the less steric. This is not the case for the green graph (SP for single point), which portrays the frozen geometry, with only small adaptions, like the changed bond length to the sp³-hybridized carbon atom of methyl compared to a sp²-hybridized carbon atom of the phenyl group.
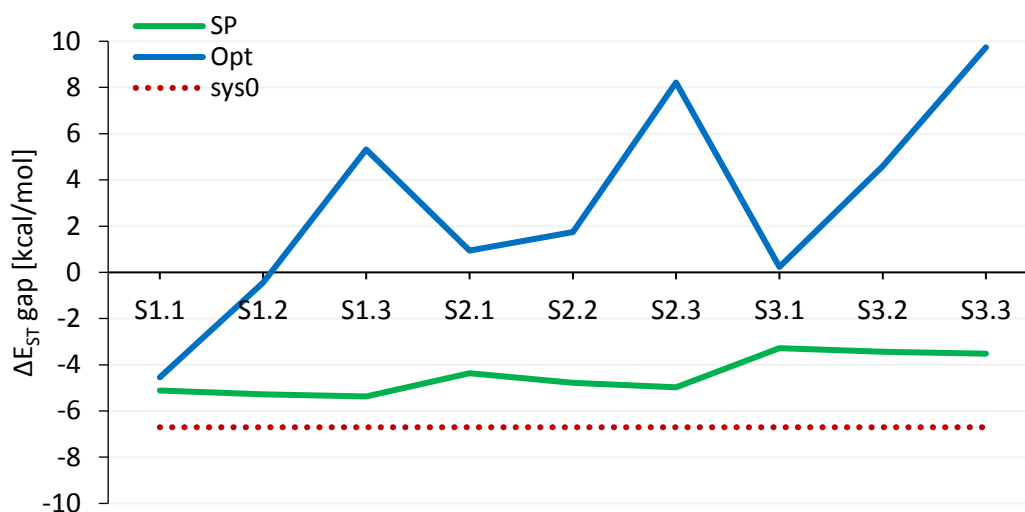
Figure 39: Calculated ST gaps for the different frozen (SP, green) and optimized (Opt, blue) subsystems with the reference value **S1.0** (red).

Considering the frozen geometries, the triplet remains the ground state for all subsystems with a decreasing ST gap of about 3 kcal/mol. There is almost no change in the ST gap if the substituents at the nitrogen are varied (Figure 40, right), while a small change in the ST gap is caused by decreasing the size of the substituent on the sulphur (Figure 40, left).

The question is, whether the singlet gets more stabilized for the smaller systems or the triplet destabilized. Therefore, an analysis of the obtained geometries is performed afterwards. Switching to the blue graph (Figure 39), a change of the ground state multiplicity is visible. After **S1.2**, the singlet gets more stable and the energetically lower ground state. To make the trends more clearly, the dependency of nitrogen and sulphur was plotted separately and can be seen in Figure 40. Here, just one dependency is pictured (e.g. **S1.1**-**S1.3**), since the trend is the same for all variations (**S2.1**-**S2.3** and **S3.1**-**S3.3**). For the optimized substructures (blue graph), the increase of the ST gap slightly rises for the decreased substituent on the sulphur (left graph) for about 5 kcal/mol. The dependency on the size of the residue bond to nitrogen (right graph) is weighted double (increase of about 10 kcal/mol).
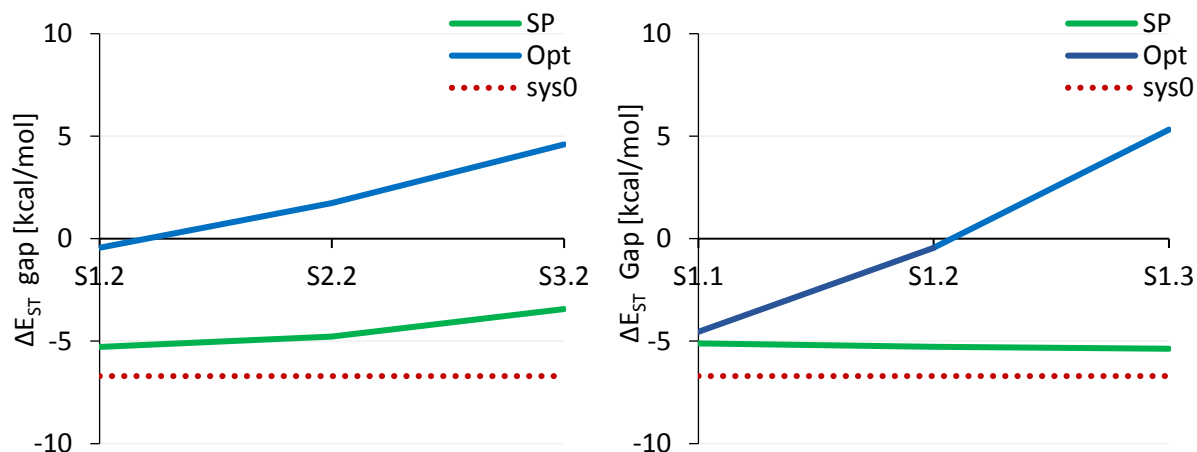
Figure 40: Specifying the individual trends of the substituent variation on the sulphur (left) and the nitrogen (right).

It can be summarized that the electronic effects received from the SP calculations illustrate barely any effect on the ST gap, while the steric influences the size of the ST gap considerably and even switches the ground state multiplicity. To reveal the nature of this behavior the obtained geometries of the subsystems are analyzed more precisely in the following. The size of the bond length goes hand in hand with the systems behavior as diborene (B-B bond length decreases, while B-C increases) or diboranes (reverse behavior to the diborene) with biradical character. Thus, the B-B, B-C and B-S bond lengths are summarized in Figure 41. To distinguish the various bonds, they are shown in different colours. The B-B bond is drawn in purple, B-S in blue and B-C in green. The dotted lines present the bond lengths of the initial state **S1.0** and should highlight the changes to the starting structure.
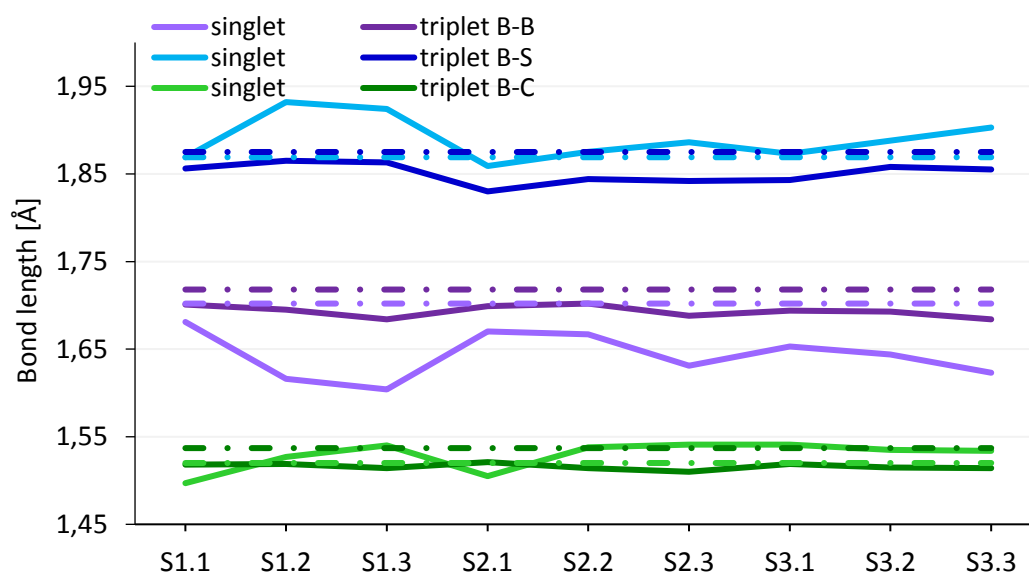
Figure 41: Different bond lengths B-B (purple), B-S (blue) and B-C (green) for the varying subsystems. The dotted lines symbolize the bond length of the initial structure **S1.0**.

The most important bond length, the B-B, represents a typical B-B single bond and remains a single bond for the triplet, while the singlet bond length decreases and shows therefore double bond character. This impact can be seen for both, reducing the size of the substituent bound to sulphur and nitrogen. Regarding the B-S and B-C bond for the triplet there are nearly no adjustment to the minimized subsystems visible. Furthermore, the singlet state also exhibits no major implications for the B-C bond of the different subsystems. It is worth mentioning that the S-B and C-B bond length of the singlet state indicate a similar trend both reverse to the B-B bond length. The dihedrals go hand in hand with the changing behavior of the subsystems and the varying bond lengths. Both dihedrals, S-B-B-S (D_S) and C-B-B-C (D_C), are illustrated in dependency on the nine substructures (Figure 42).
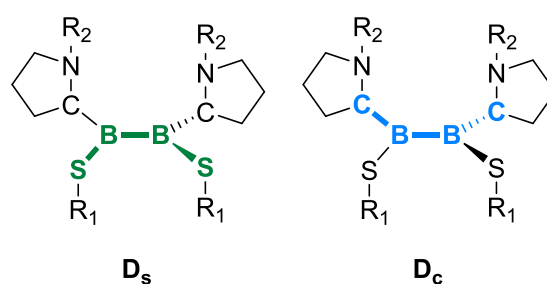
Figure 42: Presentation of the relevant dihedrals S-B-B-S (D_s) on the left and C-B-B-C (D_C) on the right.

The graphical representation of the adaption of the two dihedrals to the decreasing system size is shown in Figure 43. Considering the singlet, the initial system has a value of 100° for D_C and almost 110° for **Ds**, both aligning oneself to a nearly planar dihedral with decreasing system size. This arrangement is quite similar to the one found in the NHC substituted systems. The triplet demonstrates an exact opposite behavior. Starting at 90°, both dihedrals modify in a similar way to the various subsystems, tending to smaller dihedrals, like 50°, in the smallest system **S3.3**. Another interesting dihedral to check on is the N-C-B-B (D_{N1}) one to see if the ligand is in-plane with the boron. The variation of the dihedral to both sides is important due to the asymmetric behavior of the singlet. Therefore, the dihedral N-C-B-B (D_{N2}) on the right side is also fundamental (see Figure 44).
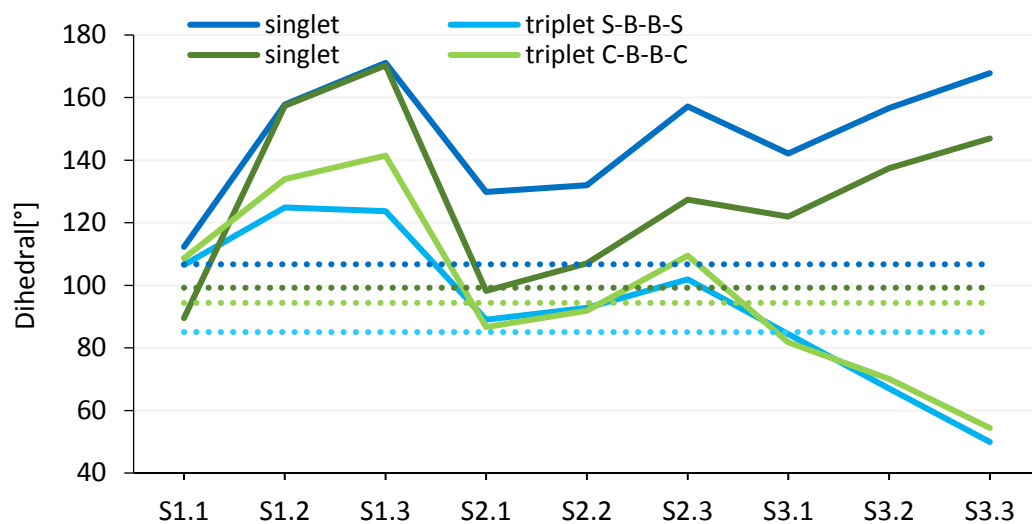
Figure 43: Change of the dihedrals S-B-B-S and C-B-B-C plotted against the nine substructures.

While the CAAC substituted systems are in-plane with the ligands of the carbene, the NHC are distorted and cannot arrange in line with carbene ligand. This is probably caused by the increased steric hindrance of the NHC molecules and the plane basic structure of **D$_C$**. The NHC systems are not able to align all substituents in one plane.

The dihedrals **D$_{N1}$** and **D$_{N2}$** (Figure 44) are very close lying for the triplet at an almost planar value of 170°. They relax to 180° for the smaller systems with just minor variations to the different systems (Figure 45).
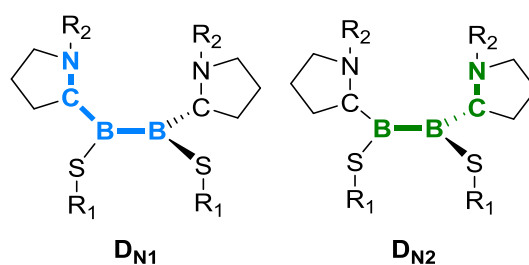
Figure 44: Two different sides of the N-C-B-B (**D$_{N1}$**, blue) dihedral on the left and its analog B-B-C-N (**D$_{N2}$**, green) on the right.

The more interesting case is the singlet state, which shows two different values for the dihedrals, particularly 150° for **D$_{N1}$** and 170° for **D$_{N2}$**. While one side is nearly plane, the other one is not. **D$_{N1}$** fluctuates between 150-180° and **D$_{N2}$** between 100-170°.
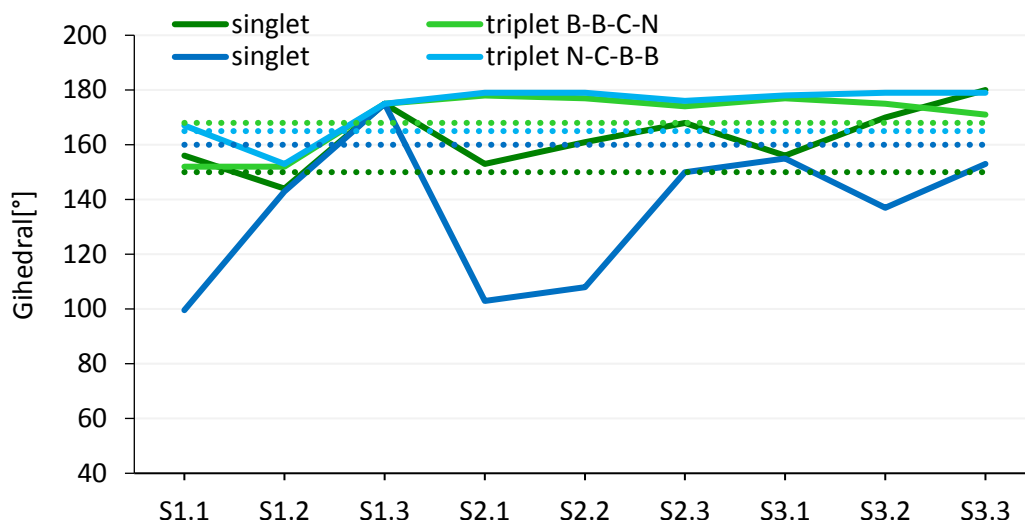
Figure 45: Relaxation of the two dihedrals B-B-C-N (**D$_{N1}$**, green) and N-C-B-B (**D$_{N2}$**, blue) as function of the decreasing system size of the substructures.

It becomes apparent that with decreasing system size the singlet arranges more planar, too, even though not as planar as the triplet. Thus, the singlet can now conjugate over the whole system including the N-C-B-B-C-N, which was hindered by the torsion before. This change in the geometric behavior is illustrated clearly in Figure 46, in which both **S1.1** and **S3.3** are depicted to make the planar arrangement of **S3.3** identifiable.
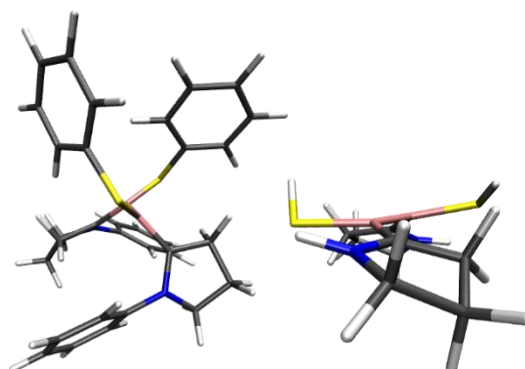
Figure 46: Depiction of the changed geometry of the twisted **S1.1** (left) compared to planar **S3.3** (right).

Both large systems, ligated by NHC and CAAC, are not able to arrange completely planar because of the high steric demands. Both systems react differently to the steric hindrances. While in CAAC the B-B bond is distorted (Figure 47, left), this part is in-plane for the NHC ligated systems (Figure 47, right). However, the NHC ligand is twisted out-of-plane, which is in-plane for the CAAC systems (Figure 47). By cutting of all steric hindrances, both systems tend to arrange in the same way, namely in a complete coplanar geometry, which enables a conjugation over the complete system. This kind of geometry is shown for the CAAC substituted case in Figure 47, middle. However, NHC containing systems respond in the same way. In the case of the CAAC ligated systems, the singlet gets stabilized by this arrangement

and therefore a switch in the ground state multiplicity results. Since this is the initial ground state multiplicity of the NHCs, only a slight increase of the ST gap is visible by the plane arrangement.
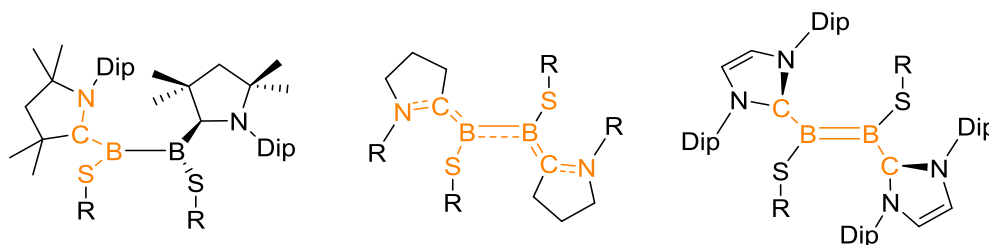

Figure 47: Exemplary presentation of the different conjugation caused by the adaption of the geometry to the decreasing size system (shown in the middle) for CAAC (left) and NHC (right).

5.5   Influences of the ligation with CAAC and NHC[412]

It is known that the stability of a radical or biradical depends on the steric hindrances and electronic properties of the substituent bound next to the radical center(s). While the steric effects play an important role on the kinetic stabilization of the radical, the electronic properties influence the thermodynamic behavior of the radical.[491] It is clearly provided that for an increasing steric hindrance the radical gets shielded from its reactants and shows therefore an extended lifetime.[492-495] Over a long period of time the state of literature claimed that the electronic properties play no major role in the stabilization, until a few small radicals were obtained with a certain chemical inertness.[491] Heinz *et. al.* explained this behavior using the cadoptive effect, which describes a system showing both electron-withdrawing (captor) and electron-releasing (donor) properties.[491] Because of these qualities of a substituent bound next to a radical centre, the radical appears more stable.[496]

Recently, carbenes,[497] more precisely CAACs, were found to fulfil this demand perfectly.[95] Due to the empty p-orbital of the carbene, a delocalization of the electron density is possible, caused by a π-back bonding interaction of the carbene. Depending on the substituents located next to carbon centre, the properties concerning the donor and acceptor abilities can be controlled.[408, 412, 458, 459, 488, 498-500] Apart from their unique ability to form paramagnetic carbene-metal complexes, the carbenes are also able to stabilize radicals.[501-503] The capability of the stabilization of different main group radicals is summarized in a review by Bertrand.[497] So far, the different behavior of the stabilization by CAAC and NHC is attributed to the various σ-donation and π-acceptance properties of CAAC and NHC.[92, 94, 95, 411, 458, 489, 504-506]

Considering the silylene and the resulting silicon biradical chemistry, Frenking and co-workers investigated, next to the donor-acceptor properties, the dependencies of the bond strength on the various carbenes. While the NHC compound provides a donor-acceptor bond between silicon and carbon of the carbene, CAAC forms an electron-sharing Si-C bond. Apart from silicon and pnictogen centred radicals, carbenes are also capable of stabilizing boron centred radicals. However, depending on the π-acidity and σ-donation of the respective carbene ligand, the radical or biradical appears more or less stable.[408, 412, 455, 458, 459, 474, 507]

As shown in chapter 5.4, CAAC ligated diboranes built a twisted C-B-B-C geometry, while the NHC substituted systems show a plane ground state structure. The CAAC system **II** (Figure 48, below) forms therefor a B-B single bond and if the C-B-B-C bond is twisted, the CAAC ligands are in-plane with each boron. A conjugation between the boron atoms and the CAAC carbene is then possible. On the contrary, NHC **I** (Figure 48, above) arranges in a planar C-B-B-C plane with NHC ligands twisted out-of-plane. Therefore, a B=B double is formed in the NHC system **I**; however, no conjugation to the NHC ligand is found, since the NHC units arrange orthogonal to the S-B-B-S plane. Due to this varied geometric arrangement, the NHC substituted system **I** possesses a closed shell singlet ground state, while CAAC **II** shows a biradical triplet ground state.
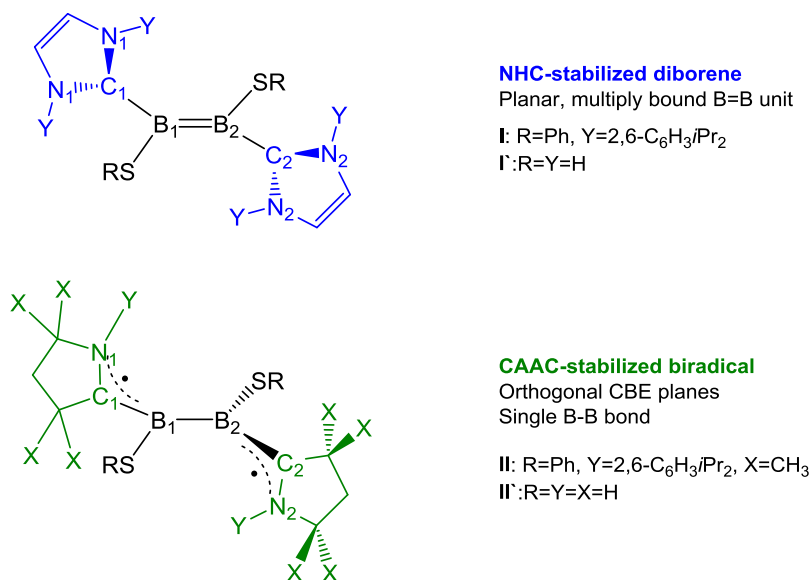

Figure 48: Basic structures of the NHC and CAAC substituted diboron molecules showing the numbering used in this chapter.[412]

In chapter 5.4, it was discussed that if the steric effects are reduced, both systems arrange all-coplanar, which enables a conjugation over the whole system and prefers a closed shell singlet

ground state. However, by increasing the steric demand, the NHC system **I** evades the steric hindrances by twisting the NHC ligands out-of-plane. In contrast, the CAAC system **II** distorts the B-B in the middle and arranges the CAAC ligands in-plane. The two systems adapt differently to the steric demand of the substituted carbenes. Since it is not possible to arrange all three dihedrals $\sphericalangle_{N_1C_1B_1B_2}$, $\sphericalangle_{S_1B_1B_2S_2}$ and $\sphericalangle_{B_1B_2C_2N_2}$ in-plane for the full systems, the molecules must sacrifice one of the favourable conjugations. A possible explanation is that system **I** is not able to rotate the bulky NHC moieties into plane and prefers therefore the planarization of the $\sphericalangle_{S_1B_1B_2S_2}$ dihedral resulting in a development of a B=B double bond. However, the slightly smaller CAAC substituents of system **II** can arrange coplanar to the boron atoms, but must twist therefore the S-B-B-S moiety. In the case of the CAAC ligated system, the formation of a N-C-B multiple bond is more favourable than the B=B double bond. This different adaption to the divergent steric effects of the two carbene is underlined by studies of Kinjo *et al.* on the arrangement of an unsymmetrical diborene (CAAC)(Br)B=B(Br)(NHC).[508] While the CAAC ligand arranges in one plane with the Br-B=B-Br moiety, the NHC substituent adapts nearly orthogonal to this plane. A similar behavior is found in another unsymmetrical molecule, (CAAC)B=B(PMe$_3$)$_2$, too.[509] One might assume that these different behaviors of the ligands can be reduced to the steric effects; however, the investigations of the smaller systems in the chapters 5.1-5.3 emphasizes a difference in the HL gap of 20 kcal/mol for the smallest systems without steric effects.

As known in literature, CAAC constitutes a better σ-donor and π-acceptor than NHC. These properties might cause the increased B-C bond strength in **II** compared to the NHC substituted system **I,** switching the relative proportion of the relevance between the B-B and both B-C bonds. Therefore, an idea to solve the differences in the geometry is that the geometry is arranged with the intention to sacrifice either the B=B double bond or the multiple bond character of both B-C bonds. In the case of **II**, the formation of both B-C multiple bond is more important than the B=B double bond, while it is the reverse case for **I**. An explanation of this observation is given by the high strain in the system, as both systems must distort, which depends on the electronical properties of the carbene, the B-B bond or the B-C$_{carbene}$ bond.

Another assumption would involve a detailed analysis of the two carbenes themselves. CAAC is known to stabilize radicals better than NHC and additionally, CAAC possesses a lower lying triplet than NHC. Because of both properties, each CAAC substituent is able to stabilize a

radical centre of **II** more easily, which is not possible for NHC and the system **I**. Previous suggestions to reveal the nature of the differences in the behavior of CAAC and NHC demonstrate that both steric and electronic properties show an effect.[412] Whereupon it appears that the electronic properties play an underlying effect, while the high strain of the steric bulk forces the system to twist their most favourable arrangement.

Motivated to find the origin of these radical changes in the geometry of **I** and **II,** which cannot be induced by the different steric effects alone, the influence of the electro-structural properties of CAAC and NHC will be discussed in this chapter.

The two main structures **I** and **II** (Figure 48) are shortened by their substituents bound to the sulphur and nitrogen to exclude the steric effects. It was proven before that by keeping the geometric arrangement of the initial systems, variations of the nitrogen or sulphur substituents illustrate almost no impact. Therefore, there should be no difference in the electronic behavior of the shortened system **I'** and **II'**, where R=Y=H, to the initial systems **I** and **II** with R=Phenyl and Y=2,6-$C_6H_3iPr_2$. These model complexes **I'** and **II'** are used to investigate the adaption of the electronic properties to the different geometric arrangement of the bond-rotated isomers. Since the steric effects are negligible in the size decreased model systems **I'** and **II'**, the impact of the rotation around certain dihedrals and ligation of CAAC or NHC can be reduced to electronic properties. By rotating one of the dihedrals ($\sphericalangle_{N_1C_1B_1B_2}$, $\sphericalangle_{S_1B_1B_2S_2}$ and $\sphericalangle_{B_1B_2C_2N_2}$) out-of-plane (90°), the electronic influence of this conjugation can be revealed, since it cannot be formed in a twisted system. To obtain an accurate picture all possible combinations concerning these three dihedrals have to be formed.

Experimental data to reduce these steric demands are not available, since it is assumed that the steric bulk is needed to control reactivity and ensure the stability of reactants and their products.[412] Most recent results prove this adoption incorrect presenting the synthesis of related, stable low-valent diboron system with the basic structure (CAAC)(R)B=B(R)(CAAC) and less steric demand with R=H, CN^{t}Bu.[455, 457, 459] Utilizing sterically less demanding substituents on the boron, such as hydrogens or cyano groups, led to stable and accessible structures from various B=B double bonds. A range of different CAACs with a changed backbone and varying steric was found by Betrand and co-workers.[433, 510, 511]

As seen in the chapter before, the sulphur and its ligand do not influence the electronic structure of the system, thus, it can be neglected in the following explanations. It was also

already demonstrated that the system favors a planar geometry; however, due to the steric demand of the ligands, the molecule must distort to reduce the steric strain. The NHC ligated system **I** releases the tension by twisting the NHC substituent out-of-plane, which is reflected in a dihedral $\sphericalangle_{N_1C_1B_1B_2} = 90°$ and a plane middle part with $\sphericalangle_{S_1B_1B_2S_2} = 0°$. The CAAC system **II** lowers the steric demand by twisting the $\sphericalangle_{S_1B_1B_2S_2}$ dihedral by 90° and in-plane positioning of the CAAC substituents ($\sphericalangle_{N_1C_1B_1B_2} = \sphericalangle_{B_1B_2C_2N_2} \sim 0°$, 180°). The important factor is to determine the influence and relevance of the B-B double bond compared to the B-C-N multiple bond. Therefore, the three relevant dihedrals $\sphericalangle_{S_1B_1B_2S_2}$, $\sphericalangle_{N_1C_1B_1B_2}$ and $\sphericalangle_{B_1B_2C_2N_2}$ are twisted on their own and in different combinations with each other to reveal the influence of each distortion and the resulting bonding properties. The energies are calculated by freezing the dihedrals $\sphericalangle_{S_1B_1B_2S_2}$, $\sphericalangle_{N_1C_1B_1B_2}$ and $\sphericalangle_{B_1B_2C_2N_2}$ in a fixed position and optimizing the residual geometric parameters to find the minimum structure of the chosen arrangement. Since some problems occurred by finding the local minimum of each conformation, different starting points were used in order to ensure the local and not a global minimum structure is investigated. For both multiplicities, the minimum structures are searched resulting in diabatic ST gaps.

The various rotated isomers are obtained by an optimization with UMN12L in combination with 6-311G(d, p) basis sets followed by an additional CASSCF/def2-TZVP optimization. The active space (2,4) was chosen according to the results obtained in the chapter before (5.1-5.4) and is described more precisely after the MO scheme shown in Figure 49 is discussed in detail. Because of the missing dynamical correlation in CASSCF calculation, on top of the obtained CAS geometry a NEVPT2/def2-TZVP calculation with the same active space was performed. Therefore, just a single point calculation is necessary to yield the relative energies of each system. As already seen in the benchmark (chapter 4), UMN12L shows some problems in systems with high biradical character, thus, inconsistencies appeared in the analysis using DFT. Using SF-DFT or CASSCF (NEVPT2), the asymmetric behaviour disappears, and solid trend can be seen observed.

The bond-rotated isomers are obtained by twisting the three important dihedrals $\sphericalangle_{N_1C_1B_1B_2}$, its analog on the other side of the B-B bond, $\sphericalangle_{B_1B_2C_2N_2}$, and the dihedral that controls the twist of the B-B bond, $\sphericalangle_{S_1B_1B_2S_2}$. This approach is an extension of the *ansatz* of Lin and Yamashita, which attempted to explain the reaction behavior and twisted CBBC arrangement

of the tetra(*o*-tolyl) diborane(4) showing a singlet ground state.[512, 513] Therefore, the energy of the LUMO and the electronic energy were computed in dependency on the $\sphericalangle_{CBBC}$ dihedral.[513] This procedure revealed the lowest LUMO energy of the system for an angle of 0°, whereat the complete electronic energy of the molecule increases to a maximum at this arrangement resulting in a destabilization.
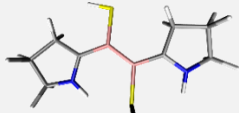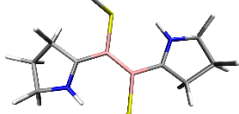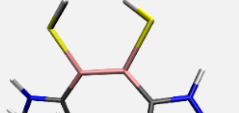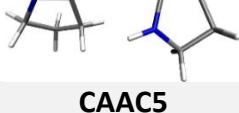
All combinations of distorting the dihedrals were investigated. However, since the system possesses symmetric elements connected with the B-B bond, only one half of the rotated isomers is shown here. Reducing the steric demand, the energetically most favorable system becomes planar regarding all dihedrals. First, all planar structures are analyzed, using dihedrals of 0° or180°. This leads to coplanar *cis* or *trans* formations of the substituents and enables to find the geometry of the real ground state. These conformers with their related singlet and triplet ground state energies of the NEVPT2 calculation are shown in Table 17.

Additionally, the dihedrals $\sphericalangle_{CN_1C_1B_1}$ and $\sphericalangle_{B_2C_2N_2C}$ are specified, too, to ascertain the arrangement of the complete CAAC ligand determining the size of the conjugated π-system. The main differences of the conformers **CAAC1-5** is the relative position of substituents bound to sulphur and nitrogen. All conformers show small energetically differences within 6 kcal/mol. The hydrogens bound to sulphur arrange in a more favorable *trans* position for a $\sphericalangle_{S_1B_1B_2S_2}$ dihedral of 180° in **CAAC1** and **CAAC2** (Table 18), both differing only in the arrangement of the $\sphericalangle_{N_1C_1B_1B_2}$ dihedral, while $\sphericalangle_{B_1B_2C_2N_2}$ remains the same (0°). Due to small steric repulsion and weak NH-S bonds in **CAAC1**, one hydrogen of the sulphur arranges itself orthogonal to the SBBS plane, while the other hydrogen is coplanar to this plane. Compared to that, in **CAAC2** both hydrogens bound to sulphur rotate about 60° out-of-plane. The main differences of both molecules are listed in Table 18 and it can easily be perceived that except the B-SH part both molecules are very similar to each other. Even if **CAAC1** is slightly more favorable for the smaller systems than **CAAC2**, **CAAC2** was chosen as starting structure of all rotamers, since the experimental obtained molecule **II** provides the same *E*-configuration of the sulphur atoms as **CAAC2**.[408]

To verify the obtained results analog calculations were made starting from **CAAC1**, resulting in the same trend as observed for **CAAC2**. As the twisting of **CAAC2** leads to more substantial and comprehensible trends, only the analysis starting from **CAAC2** is discussed in the following.

Table 17: Various B-B-coplanar conformers of model system **II'** with their important dihedrals and relative energy (kcal/mol) compared to the energy of the energetically lowest conformer **CAAC1**. The used numerations of the atoms can be seen in Figure 48.

Conformer	$\sphericalangle_{CN_1C_1B_1}$	$\sphericalangle_{N_1C_1B_1B_2}$	$\sphericalangle_{S_1B_1B_2S_2}$	$\sphericalangle_{B_1B_2C_2N_2}$	$\sphericalangle_{B_2C_2N_2C}$	E(S)	E(T)
CAAC1	179	180	180	0	179	0.0	12.7
CAAC2	-179	0	180	0	-179	2.1	11.2
CAAC3	175	180	0	180	175	2.8	13.5
CAAC4	173	180	0	0	170	4.4	12.8
CAAC5	173	0	0	0	-166	5.7	10.8

As expected, **CAAC2** prefers, if possible, a conjugation over the whole π-system. This can be seen in the HOMO and LUMO (Table 21) and also the Wiberg indices of 1.4 for C-N and B-B, listed in Table 20. The HOMO (Table 21) provides a π-conjugation from one C_{CAAC} to the other over the boron-boron bond with antibonding character to the nitrogens of CAAC and the sulphur atoms, which contrasts the high multiple bond character of C-N (1.4).
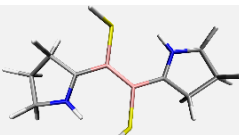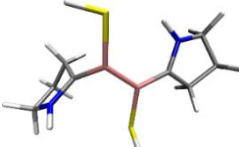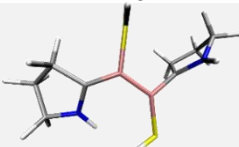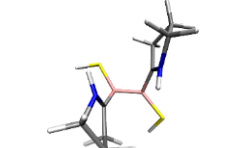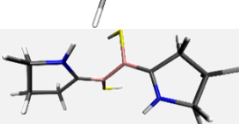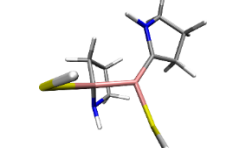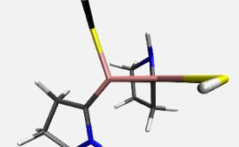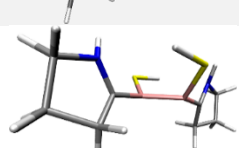
Table 18: Further geometric parameters including the dihedrals [°] and the bond length [Å] for the planar conformers **CAAC1** and **CAAC2** of **II'**.

conformer	$\sphericalangle_{B_2B_1S_1H}$	$\sphericalangle_{B_1B_2S_1H}$	N_1-C_1	C_1-B_1	B_1-S_1	B_1-B_2	B_2-S_2	B_2-C_2	C_2-N_2
CAAC1	-26	-82	1.32	1.56	1.89	1.62	1.95	1.52	1.34
CAAC2	-134	-59	1.33	1.54	1.92	1.62	1.92	1.54	1.33

However, this antibonding character can be found in many different CAAC ligated systems, as for example the Kekulé biradicaloids presented by Bertrand *et al.*,[91] as well as several diborene compounds of the Braunschweig group and a biradical diborahydrozine.[408, 412, 455-458] Due to the similar behavior concerning the molecular orbitals, the *ansatz* developed in this work may be able to explain a general behavior of CAAC, which can be transferred to various other systems.

Table 19: Summary of the relative energies of the conformers obtained from the B-B-coplanar conformer **CAAC2** ($\sphericalangle_{N_1C_1B_1B_2}$ = 0°, $\sphericalangle_{S_1B_1B_2S_2}$ = 180°, and $\sphericalangle_{B_1B_2C_2N_2}$ = 0°) by rotating the dihedral $\sphericalangle_{N_1C_1B_1B_2}$, $\sphericalangle_{S_1B_1B_2S_2}$, $\sphericalangle_{B_1B_2C_2N_2}$ by 90°. Energies are given in [kcal/mol].

Conformer		$\sphericalangle_{N_1C_1B_1B_2}$	$\sphericalangle_{S_1B_1B_2S_2}$	$\sphericalangle_{B_1B_2C_2N_2}$	$\Delta E(S)$	$\Delta E(T)$	ST gap
CAAC2		0	180	0	0.0	9.1	9.1
CAAC2.1		90	180	0	10.8	27.8	17.0
CAAC2.2		0	180	90	10.8	27.8	17.0
CAAC2.3		90	180	90	28.8	47.9	19.0
CAAC2.4		0	90	0	9.2	6.5	-2.7
CAAC2.5		90	90	0	12.3	24.9	12.7
CAAC2.6		0	90	90	12.3	24.9	12.7
CAAC2.7		90	90	90	46.7	39.1	-7.6

The LUMO provides the antibonding character to the nitrogen and sulphur and shows additionally a nodal plane between the two boron atoms. Therefore, a population of this orbital weakens the B-B bond resulting in a single bond. Consequently, the twisted structure is lower in energy. By a HL gap of nearly 30 kcal/mol, a population of the LUMO within thermal conditions appears highly improbably and, thus, the twisted structure, too. This may explain the behavior of the triplet arranging all planar, like the singlet and the therefore relatively small ST gap of 9 kcal/mol. The sulphur is bound via a single bond to the boron atom, which tributes the Wiberg indices of 0.8. This behavior is also found in the initial systems **II**. A discrepancy is found in the Wiberg indices of the B-C bond, which is nearly a single bond (1.1) with the expected multiple bond character through the π-conjugated system and also the electron density distribution of the HOMO. But taking a closer look at the orbitals (Table 21), the main part of the density is located between the boron atoms and only an extension is located at the carbon atoms of CAAC, which may explain the varying indices.

Table 20: Selected Wiberg bond indices illustrating variations in the bonding situation of the conformer **CAAC2** by twisting different combinations of the central (C-B, B-B and B-C) bonds. (S) indicates the values obtained for the singlet state, while (T) symbolizes a triplet multiplicity.

Conformer	N_1-C_1	C_1-B_1	B_1-B_2	B_1-S_1	B_2-S_2	B_2-C_2	C_2-N_2
CAAC2 (S)	1.4	1.1	1.4	0.8	0.8	1.1	1.4
CAAC2 (T)	1.2	1.4	1.0	1.1	1.0	1.3	1.2
CAAC2.2 (S)	1.2	1.4	1.3	0.9	1.1	0.9	1.5
CAAC2.4 (S)	1.2	1.3	1.1	1.1	1.1	1.3	1.2
CAAC2.4 (T)	1.2	1.3	0.9	1.2	1.1	1.4	1.2
CAAC2.5 (S)	1.2	1.3	0.8	0.9	1.4	1.0	1.1
CAAC2.7 (S)	1.0	1.4	0.8	1.1	1.3	1.2	1.1

Starting from **CAAC2** ($\sphericalangle_{N_1C_1B_1B_2} = 0°$ $\sphericalangle_{S_1B_1B_2S_2} = 180°$, $\sphericalangle_{B_1B_2C_2N_2} = 0°$), the obtained conformers and their relative energies are shown in Table 19. By twisting one dihedral by 90°, the rotated conformers are retained. For **CAAC2.1**, the left CAAC substituent is twisted by freezing the dihedral $\sphericalangle_{N_1C_1B_1B_2}$ to 90° and the remaining dihedrals correspond to **CAAC2**. The same is found by twisting the right CAAC ligand to yield **CAAC2.2** with $\sphericalangle_{N_1C_1B_1B_2} = 0°$, $\sphericalangle_{S_1B_1B_2S_2} =. 180°$, $\sphericalangle_{B_1B_2C_2N_2} = 90°$. Since the molecule **CAAC2** appears more or less symmetric, it should make no difference whether the left CAAC (**CAAC2.1**) or the right CAAC ligand (**CAAC2.2**) is distorted. This is indeed seen in Table 19, however, it is worth mentioning that caused by the slight multireference character of **CAAC2.1** and **CAAC2.2** only the most
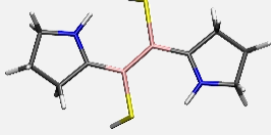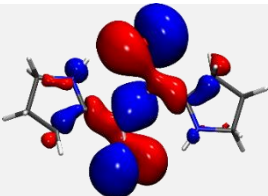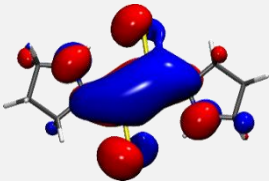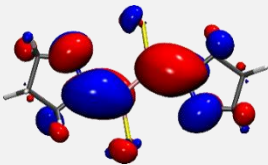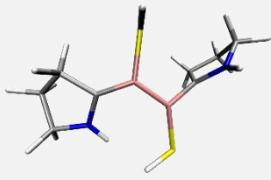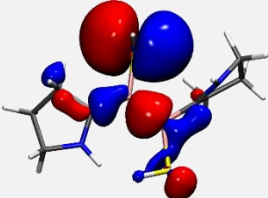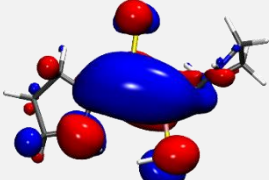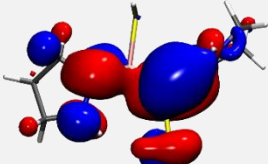
accurate method NEVPT2 reflects this symmetry correctly. While more approximated approaches, such as DFT, lead to symmetry breaking effects resulting in a slight energy shift of one conformer.

The out-of-plane distortion of a CAAC ligand in an orthogonal position leads to an energy increase of nearly 11 kcal/mol for the singlet and 19 kcal/mol for the triplet ground state, which results in a larger ST gap of 17 kcal/mol. A previous conducted variable-temperature ^{11}B-NMR spectroscopic study of a CAAC stabilized dicyano-diborene $B_2(CAAC)_2(CN)_2$ yields an estimated rotational barrier of the B-C bond of about 14 kcal/mol.[514, 515] This barrier corresponds indeed with the energy increase of 11 kcal/mol, which is slightly less caused by the less steric demand of the used test system **II'**. For this system, only the singlet can be observed, since the system favors the closed shell singlet multiplicity in this arrangement. Rotating both CAAC substituents yields **CAAC2.3** with an increased in energy of 29 kcal/mol, which is somewhat higher than the double amount of the destabilization caused by twisting one CAAC substituent. The ST gaps remains nearly the same compared to **CAAC2.1**, as both, the singlet and the triplet, are destabilized by the same amount 19 kcal/mol compared to **CAAC2.1**. Consequently, the evaluated energy to sacrifice one C=B π-interaction is about 11 kcal/mol without taking the additional steric hindrance into account. Distorting both conjugations is even more unlikely with nearly 30 kcal/mol.

The other interesting aspect is the relevance of the B-B twisting in the molecules. Therefore, using **CAAC2** as starting structure the $\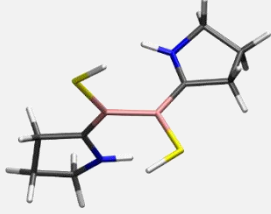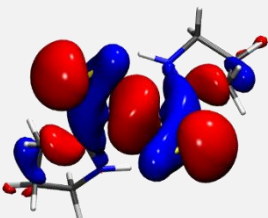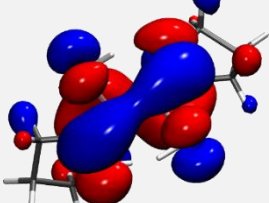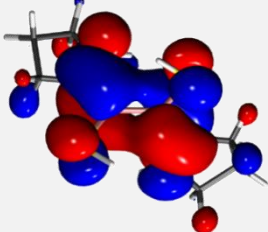sphericalangle_{S_1B_1B_2S_2}$ is twisted about 90°. **CAAC2.4** is forming an arrangement with two coplanar CAAC substituents ($\sphericalangle_{N_1C_1B_1B_2} = \sphericalangle_{B_1B_2C_2N_2} = 0°$) and an orthogonal $\sphericalangle_{S_1B_1B_2S_2} = 90°$ B-B plane. As this conformer is very similar to the initial system **II**, calculations concerning this arrangement present, as expected, a greater challenge than the previous systems caused by the high biradical character. The singlet, which is for this conformation not the ground state anymore, possesses a very high biradical character, which can be seen in occupation of the former HOMO and LUMO showing both a natural occupation of one. Since singlet biradicals are often described asymmetrical by singlereference methods, which is also the case for the investigated systems here, the geometries are optimized by CASSCF [2,4] approach. It should be noted that only this geometry shows differences between the UMN12L and CASSCF optimized structure. All other test systems illustrate the same behavior for both calculations.

Table 21: HOMO-1, HOMO and LUMO of selected conformers of compound **II'** with one broken C_{CAAC}-B or B-B-bond. The corresponding orbital energies [kcal/mol] are given below each orbital.

Conformer	HOMO-1	HOMO	LUMO
CAAC2	-119.9	-85.3	-55.3
CAAC2.2	-113.0	-76.1	-41.5
CAAC2.4	-136.1	-67.5	-66.8

Assessing the singlet structure of **CAAC2.4** compared to **CAAC2** reveals an increase in about 9 kcal/mol, while the triplet geometry only rises by 6 kcal/mol compared to the singlet ground state of **CAAC2**. Thus, the triplet of **CAAC2.4** provides a more favorable arrangement (about 3 kcal/mol) than the singlet but is still less stable than the singlet **CAAC2** coplanar geometry.

To evaluate the influence of the C=B π-interaction for this distorted structure $\angle_{S_1B_1B_2S_2} = 90°$, one CAAC is twisted by 90° obtaining **CAAC2.5** ($\angle_{N_1C_1B_1B_2} = 90°$, $\angle_{B_1B_2C_2N_2} = 0°$) and **CAAC2.6** ($\angle_{N_1C_1B_1B_2} = 0°$, $\angle_{B_1B_2C_2N_2} = 90°$). As seen for **CAAC2.1** and **CAAC2.2**, these conformers exhibit the same properties, since the molecule **II'** arranges symmetric to the B-B bond. While the singlet energy increases only slightly compared to **CAAC2.4**, the triplet gets strongly unfavorable with a difference of 25 kcal/mol compared to **CAAC2**. This observation leads to a ST gap of 13 kcal/mol and a singlet ground state. In the case of an additional distortion of the B-B bond and B-C (**CAAC2.5** and **CAAC2.6**), the obtained energies are similar to **CAAC2.1** and **CAAC2.2** with the small difference that the singlet is slightly more destabilized and the triplet in turn is less destabilized. In the highly unfavorable case, in which all three dihedrals are orthogonal (**CAAC2.7**), the singlet is about 47 kcal/mol higher in energy than in

CAAC2. The triplet energy increases about 40 kcal/mol and provides therefore the more stable conformation; however, this conformation will not be taken even by heating up the system. Considering the relative energies of the various conformers, it is obvious that apart from the coplanar singlet **CAAC2**, the B-B twisted **CAAC2.4** triplet possesses the second lowest energy. Even the torsion of one CAAC ligand yields a higher energy than the twist around the B-B bond, thus, the relative energies of the conformers explain the experimentally adapted geometry of the structure **II**.

To explain the trends detected in Table 19, the important molecular orbitals of **CAAC2**, **CAAC2.2** and **CAAC2.4** are shown in Table 21. These orbitals are on the one hand quite meaningful regarding the aligned electron density contribution and the concerning energies, but on the other hand they appear very complex. Franking *et al.* carried out the bonding pattern of group 14 elements in different environments and also the electronic structure of complexes of the type L_2E_2, with L being either NHC or CAAC and E a group 14 element by simplified orbital.[516, 517] The frontier orbitals of the whole system are obtained by combining the frontier orbitals of CAAC and NHC with the ones of E_2.

This similar concept starting from boron instead of the carbene is shown for the C-B-B-C units in Figure 49. The simplified MO scheme of the planar C-B-B-C moiety is depicted showing one rotated CAAC with no conjugation to the remaining system and an orthogonal B-B axis. As neither the sulphur atom and its ligand nor the antibonding nitrogen of the CAAC substituent influence the bonding pattern of the C-B-B-C unit, both are not included in the consideration. Therefore, the reduced MO model includes only the four π-orbitals as a result of a linear combination of the corresponding AOs of the carbene carbon atoms of the CAAC moieties and boron atoms in-between, neglecting the influence of the nitrogen and sulphur to the lower lying MOs.

The molecular orbitals are occupied by two electrons, since the residual electrons of carbon and boron atoms are involved in σ-bonds. Because of this treatment, the choice of the active space with two electrons, one occupied and three unoccupied molecular orbitals, becomes apparent. With the help of the simplified MOs, attempts are made to explain the electronic properties and behavior of the distorted and planar structures.
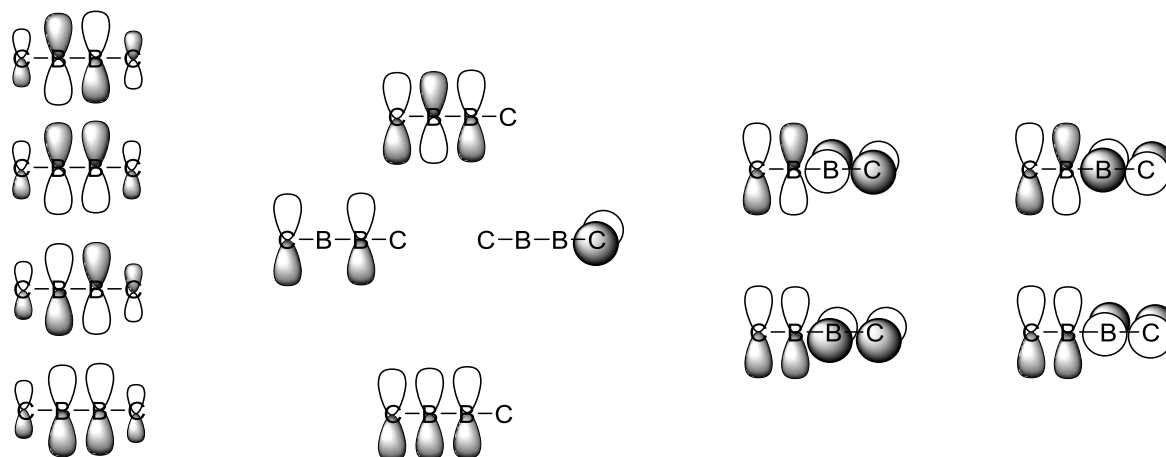
Figure 49: Variations of the MOs of the CBBC moiety of the planar system (left) upon twisting diboron species **I** and **II** around one NCBB dihedral angle (center: one CB double bond is broken) and around the SBBS dihedral angle (right: the BB double bond is broken).[412]

The coplanar arrangement with all four atoms in one plane can be seen on the left side of Figure 49 and shows a delocalization over the four π-orbitals of the CBBC unit, which is in line with the calculated HOMO of **CAAC2**, shown in Table 21. In the case of the singlet, only the lowest orbital is occupied; however, for the triplet the two lowest orbitals are singly occupied. Therefore, both states should be described appropriately by singlereference methods. Since the second lowest orbital has a nodal plane, the bond strength of the B-B bond should decrease, which facilitates the torsion of the B-B bond in the case of a triplet.

Due to the high HL gap, the ground state has to be singlet and the ST gap corresponds to the HL gap of the calculated KS orbitals. These results are examined more precisely considering the Wiberg indices of the singlet and triplet state of **CAAC2** (Table 20) revealing the same trend as expected from the MO analysis. In the triplet, the double bond character of the B-B bond decreases to nearly one, as it gets obvious that the B-B π-bond is broken. Therefore, the multiple bond character of the B-C bond rises to 1.4, which is nearly one for the singlet state, shifting the electron density into this bond. This observation can also explain the slightly decreased bond character of the N-C bond for the triplet. In sum, the triplet of **CAAC2** performs in a similar way as **CAAC2.4** presenting an orthogonal B-B bond and a completely coplanar arrangement of the structure, which is caused by the population of the B-B anti-bonding LUMO of the **CAAC2** system.

Rotating one CAAC substituent leads to a molecule orbital scheme as shown in the centered draft in Figure 49, with only three atoms in a coplanar arrangement and the fourth carbene

p-orbital orthogonal to this plane. Thus, the conjugation is delocalized over the three π-orbitals, which are in the same plane resembling the HOMO of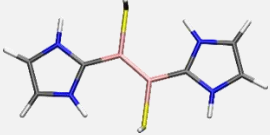 this system. This observation leads to a singlet ground state with a π-bonding character. As the single electron occupation of the triplet fills an electron in a non-binding orbital in this kind of scheme, the LUMO of **CAAC2.2** plotted in Table 21 shows this non-binding orbital with a delocalized π-system on the orthogonal CAAC ligand, which is not included in the simplified orbital picture. Therefore, both the ST gap and the HL gap increase slightly in energy compared to **CAAC2**.

By the torsion of the B-B bond **CAAC2.4** is obtained. The simplified MO scheme is illustrated for this geometry on the right side of Figure 49. The calculated electron densities for the HOMO and LUMO are shown in Table 21. A degeneration of the HOMO and LUMO leads to two SOMOs, which confirms the calculated energies of both SOMOs, and is known to favor a triplet ground state, which is the case for this geometry. Due to this degeneracy, a single wave function-based method cannot provide reliable results anymore and the use of multireference approaches is advisable, which is the case with the NEVPT2 calculations. Applying this method, a single occupation of the HOMO and LUMO leading to SOMOs was confirmed. An approach to describe the ST gap in such instance is the use of the exchange integral of both degenerated MOs. Therefore, the ST gap can be approximated by twice the exchange integral. In the case of the **CAAC2.4**, the B-B π-bond is nearly broken resulting in a Wiberg index of 1.1 for the singlet and 0.9 for the triplet ground state. The located N-C-B bond shows thus multiple bond character with values of 1.2 and 1.3. In the simplified MO scheme, the degenerated MOs are identical with changing sign of the electron density. To clarify the behavior of the electron density, both degenerated MOs have to be linearly combined. Thus, regarding the positive linear combination of the MOs, the electron density of the right side cancels itself and adds on the left side. The negative combination exhibits the same behavior the other way around, resulting in two π-bonding orbitals on boron and carbon atoms either located on the left or the right CB moiety. Caused by the orthogonal B-B bond, the CB units illustrate no interaction between each other. It is conspicuous that both the coplanar **CAAC2** and the twisted conformer **CAAC2.4** demonstrate the same properties for the triplet state considering the MOs and the Wiberg bond indices. The frontier orbitals are in line with the simplified MO picture except for appearing more complicated and thus more complex for interpretation.

To constitute the differences in the behavior of CAAC and NHC, the same analysis was performed for the truncated model **I′**, which is the analog of **II′** with NHC as substituents instead of CAAC. The NHC compound **I** was proven a closed shell singlet ground state with planar SBBS unit and orthogonal NHC ligands. In **I′**, the bulky substituents are also replaced by hydrogen atoms to neglect the steric effects mostly and to point out the electronic influence of the NHC carbenes. As seen for the truncated system **II′** before, for **I′** the most favorable ground structure is a closed shell singlet, possessing an all coplanar arrangement with an *E*-conformation of the sulphur moieties. Because of the second nitrogen of the NHC carbene, the **I′** substructure provides a higher symmetry than the CAAC substituted analog **II′** leading to less conformers. Only two different coplanar geometries (Table 22) varying in the *Z*- and *E*-configuration of the $\sphericalangle_{S_1B_1B_2S_2}$ arrangement are obtained with the same numeration, **NHC2** ($\sphericalangle_{S_1B_1B_2S_2}= 180°$) and **NHC3** ($\sphericalangle_{S_1B_1B_2S_2}= 0°$), as seen for **II′**. By rotations of the $\sphericalangle_{N_1C_1B_1B_2}$ and $\sphericalangle_{B_1B_2C_2N_2}$ dihedrals no changes appear, since NHC includes two nitrogen atoms and is therefore axisymmetric. **NHC1** possesses in analogy to **CAAC1** two dihedrals $\sphericalangle_{S_1B_1B_2S_2} = \sphericalangle_{N_1C_1B_1B_2} = 180$ and $\sphericalangle_{B_1B_2C_2N_2} = 0°$; however, caused by the higher symmetry; **NHC1** equals **NHC2**. By rotations around $\sphericalangle_{N_1C_1B_1B_2}$ or $\sphericalangle_{B_1B_2C_2N_2}$ no energetic differences appear. Thus, the numeration for the plane model rotamers **I′** starts with **NHC2** and the numeration succeeds analog to the one of **II′**.

Table 22: Comparison of the B-B-coplanar conformers of **I'**. The numbering of the atoms is as shown in Figure 48. All values are in kcal/mol and were obtained at the NEVPT2 [2,4] level of theory.

Conformer	$\sphericalangle_{CN_1C_1B_1}$	$\sphericalangle_{N_1C_1B_1B_2}$	$\sphericalangle_{S_1B_1B_2S_2}$	$\sphericalangle_{B_1B_2C_2N_2}$	$\sphericalangle_{B_2C_2N_2C}$	E(S)	E(T)
NHC2	176	0	180	0	177	0.0	28.8
NHC3	175	180	0	180	175	14.8	29.6

In contrast to **II′** with the different B-B-coplanar conformers varying just about 5 kcal/mol, the gap between **NHC2** and **NHC3** is much larger (15 kcal/mol). However, a striking difference is found in the relative position of the triplet, which is tremendously higher in energy

(29 kcal/mol for **NHC2**) than for the model system **II´** obtaining a ST gap of the complete planar arrangement of 9 kcal/mol (**CAAC2**). This increasing ST gap is nicely reflected in the rising HL gap of the MOs of **NHC2** (Table 23, first row). Compared to the MOs of the CAAC substituted system with the same geometry (**CAAC2**), the HOMO-1 exhibits nearly no change in the relative energy and the distribution of the electron density (Table 21). Regarding the HOMOs, the energies increase about 10 kcal/mol revealing a similar π-conjugated system over the CBBC system. However, significantly less electron density is located on the carbene carbon atom. The sulphur and nitrogen present the same antibonding character for both the NHC and CAAC substituted system. Since NHC possesses two nitrogen atoms on each side instead of one, the antibonding effect is therefore likely higher than in the CAAC ligated systems. This observation might explain the rise in the energies of the HOMO of about 10 kcal/mol. While the HOMO energy increases only slightly, the LUMO energy rises substantially about 30 kcal/mol compared to the CAAC substituted analog. This is on one hand caused by the doubly amount of antibonding character of the nitrogen atoms. But on the other other hand the higher shift in energy of the LUMO compared to the HOMO is caused by the larger amount of electron density on the carbene carbon atom.

Table 23: HOMO-1, HOMO and LUMO of selected conformers obtained from conformer **NHC1**. The orbital energies are given in kcal/mol.
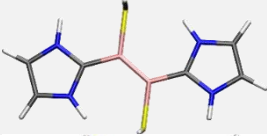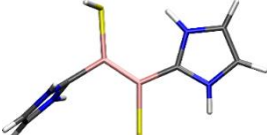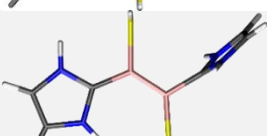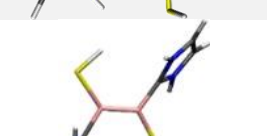
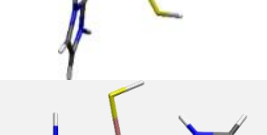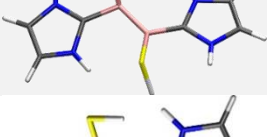| Conformer	HOMO-1	HOMO	LUMO
NHC 2	-117.6	-73.8	-30.0
NHC 2.2	-108.3	-66.9	-13.8
NHC 2.4	-129.0	-45.0	-42.6
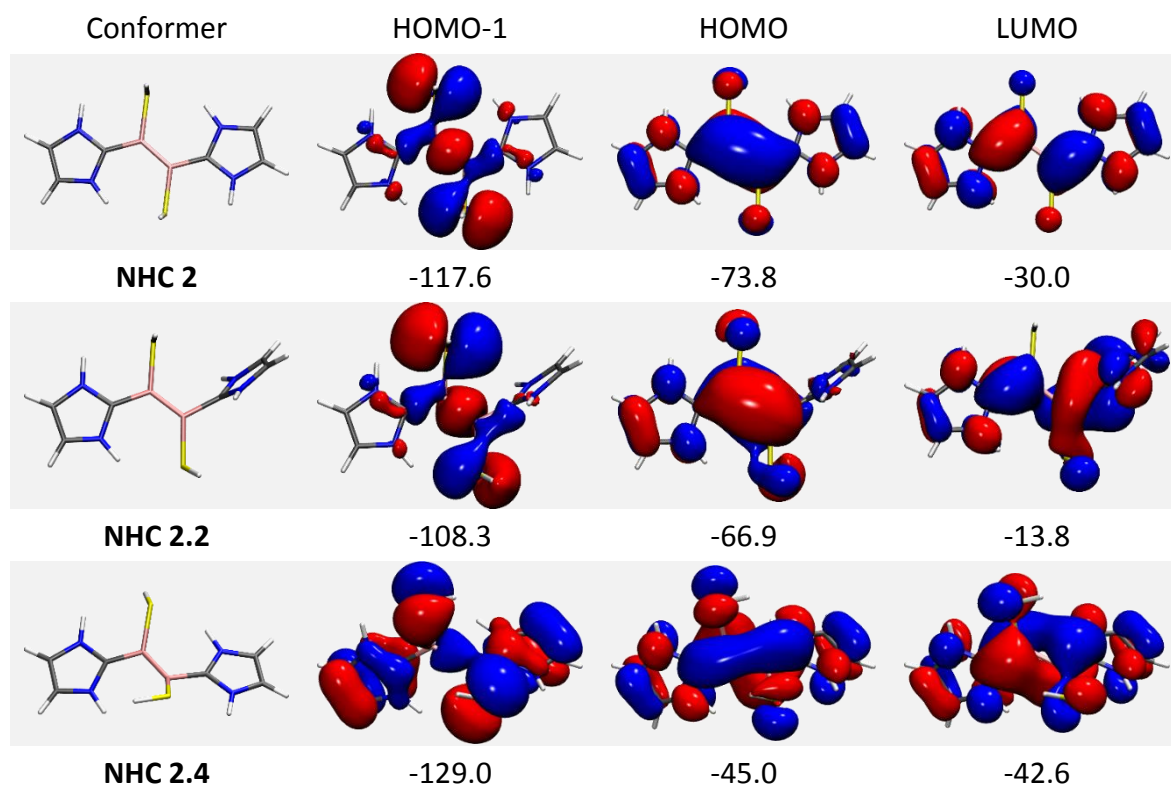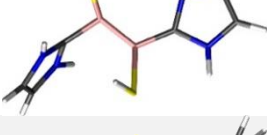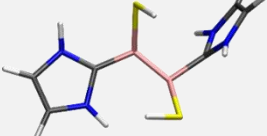
This different density distribution on the carbon center can be proven investigating the MOs and the Wiberg indices, which predict an increase of the electron density in the B-B bond of the HOMO going from CAAC (1.4) to NHC (1.6). This results in a decrease of the density between B-C and thus less electron density on the carbon atoms. The Wiberg indices of the B-C bond rises from CAAC to NHC for the LUMO, which increases from 1.1 to 1.4 looking at singlet and the triplet occupation of **NHC2**. Due to this higher amount of electron density on carbene carbon atoms, there is higher antibonding interaction between the nitrogen and the carbon. In CAAC, the same trend is found, but due to the double number of nitrogen atoms in NHC the antibonding interaction leads to a greater extend in the LUMO. Thus, the LUMO is shifted significantly to higher energy compared to the HOMO resulting in an enlarged HL gap for NHC. This change can be attributed to the shape of the MOs, especially the HOMO and LUMO. This extended HL gap of NHC compared to CAAC substituted systems is already literature-known and is found in various systems.[471, 490, 518] So far, mainly the properties of the frontier orbitals of CAAC and NHC were investigated, while in in this work the bridge between both substituents is included in the consideration of the frontier orbitals. Bertrand and co-worker demonstrated that CAAC provides more σ-electron density in the HOMO, due to its carbon atom instead of nitrogen.[519] This results in CAAC possessing an energetically higher HOMO than NHC.

While the LUMO of CAAC is decreased in energy compared to NHC, again caused by the carbon atom, which is no π-donator in contrast to the nitrogen. Therefore, the HL gap and thus the ST gap is decreased in energy for CAAC in contrast to NHC. In the truncated systems **I′** and **II′**, the σ-orbitals (HOMO) of the ligands do not influence the frontier orbitals of the system and are thus not taken into account. Instead, the focus lies on the p_{π}-orbitals forming the HOMO and LUMO in different combinations with π-orbitals of the bridge. For carbenes bound via main group elements, the HL and ST gap increases due to a greater extent of the antibonding character of the NHC ligands, as explained above. To reveal the influence of each important bond, the impact on the geometry and properties of the system, the same procedure as seen before with the CAAC ligated systems **II′** is performed. By twisting the important dihedrals $\sphericalangle_{N_1 C_1 B_1 B_2}$ $\sphericalangle_{B_1 B_2 C_2 N_2}$ and $\sphericalangle_{S_1 B_1 B_2 S_2}$ by 90°, seven conformers are obtained, of which each is listed with its relative position of the singlet and triplet in Table 24. As reported for **NHC2**, the ST gap is about 20 kcal/mol bigger than the one of **CAAC2**. By twisting one B-C bond, for **NHC2.1** and **NHC2.2** the trend stays the same as observed for the **CAAC2.1**, namely a

destabilization of the singlet by 14 kcal/mol. With both NHC ligands arranged orthogonal to the SBBS plane (**NHC2.3**), nearly the doubled amount of destabilization (29 kcal/mol) is found, as expected. In the **II′** systems, an increase of the ST gap is found by twisting one B-C bond. This can also be seen for the NHC substituted system **I′**. However, compared to CAAC the ST gap increases always about 20 kcal/mol for the NHC truncated model system.

Table 24: Summary of the relative energies of the conformers obtained from the B-B-coplanar conformer **NHC1** ($\sphericalangle_{N_1C_1B_1B_2}$ =180°, $\sphericalangle_{S_1B_1B_2S_2}$= 0°, and $\sphericalangle_{B_1B_2C_2N_2}$= 0°) by rotating the dihedral angles $\sphericalangle_{N_1C_1B_1B_2}$, $\sphericalangle_{B_1B_2C_2N_2}$ and $\sphericalangle_{S_1B_1B_2S_2}$ by 90°.

Conformer		$\sphericalangle_{N_1C_1B_1B_2}$	$\sphericalangle_{S_1B_1B_2S_2}$	$\sphericalangle_{B_1B_2C_2N_2}$	$\Delta E(S_1)$	$\Delta E(T_1)$	S-T gap
NHC2		0	180	0	0.0	28.8	28.8
NHC2.1		90	180	0	13.6	47.2	33.7
NH 2.2		0	180	90	13.6	47.2	33.7
NHC2.3		90	180	90	29.1	66.1	37.1
NHC2.4		0	90	0	29.4	28.8	- 0.6
NHC2.5		90	90	0	43.6	43.9	0.3
NHC2.6		0	90	90	43.6	43.9	0.3
NHC2.7		90	90	90	38.5	61.6	23.1

Consequently, the triplet is highly unfavorable, as seen in **NHC2.3**, with a triplet state that is 66 kcal/mol higher in energy than the minimum structure. Considering the Wiberg indices (Table 25), it is noticeable that the B-B bond shows more electron density in all NHC conformers resulting in higher B-B bond order, while the C-B present the contrary behavior possessing less electron density in most of the cases. By twisting one or two B-C bonds, the amount of electron density rises between the B-B bond, which can be seen by Wiberg indices of nearly two in the B-B bond (**NHC2.3**). This trend does not get that obvious for the CAAC substituted systems. Thus, a distortion of the NHC ligand out of the B-B plane exhibits nearly the same effect as for CAAC. The only difference is the increased ST gap. Therefore, an analysis of the B-B bond and twisting this dihedral comes more and more into focus.

In **CAAC2.4**, the destabilization of the singlet is only about 9 kcal/mol; however, twisting the B-B bond in model system **I′** leads to an increase in energy about 20 kcal/mol. Even the triplet, which is the second most likely state in the CAAC systems, is about 29 kcal/mol higher in energy for NHC. Nevertheless, the triplet remains for this arrangement (**NHC2.4**) still the ground state, as the singlet lies 0.6 kcal/mol above. Since the ST gap of **CAAC2** was declined as decisively influence the stabilization of **CAAC2.4**, the B-B distorted formation cannot be adopted for the NHC substituted systems, since the ST gap of the all coplanar geometry possesses such a high ST gap. That this influence remains the same as seen for the CAAC systems can be observed in the similar energies and geometric properties, like the Wiberg indices of triplet states of **NHC2** and **NHC2.4**.

Table 25: Selected Wiberg bond indices illustrating variations in the bonding situation of the conformers obtained from **NHC2**. (S) indicates the values obtained for the singlet state while (T) denotes the values for the corresponding triplet state.

Conformer	N_1-C_1	C_1-B_1	B_1-B_2	B_1-S_1	B_2-S_2	B_2-C_2	C_2-N_2
NHC2 (S)	1.2	1.1	1.6	0.8	0.8	1.1	1.2
NHC2 (T)	1.2	1.4	0.9	0.9	0.9	1.4	1.1
NHC2.1 (S)	1.2	1.1	1.7	0.9	0.9	0.8	1.3
NHC2.3 (S)	1.2	0.9	1.8	0.9	0.9	0.9	1.3
NHC2.4 (S)	1.1	1.3	1.0	1.1	1.1	1.3	1.0
NHC2.4 (T)	1.1	1.4	0.9	1.1	1.1	1.4	1.1
NHC2.6 (S)	1.2	1.1	1.6	1.0	0.9	0.9	1.3
NHC2.7 (S)	1.2	0.9	1.7	0.9	0.9	0.9	1.2

Following this trend, **NHC2.5**, **NHC2.6** and **NHC2.7** are highly unlikely, since both, the π-BB and B-C bond cannot be formed due to the geometric arrangement. **NHC2.5** and **NHC2.6** present the analog to **NHC2.1** and **NHC2.2** with an additional twisted B-B bond, thus, the increase in energy is substantially higher (30 kcal/mol) for the singlet state of both conformers. The difference between the corresponding CAAC analogs is only about 3 kcal/mol. The trend of the **NHC2** conformers, seen in Table 24, can also be explained by the simplified orbital scheme in Figure 49 taking the higher HL gap into account.

With the help of the results presented in Table 19 and Table 24, combined with the simplified orbital scheme, the different adaptation to the huge steric hindrances of **I** and **II** can be explained. While truncated system **II´** possesses a triplet state, B-B twisted **CAAC2.4** as lowest non-coplanar conformer, this is not the case for system **I´**. Therefore, it is reasonable that the CAAC ligated system **II´** relaxes to the steric effects by twisting the B-B bond. In contrast, **NHC2.4** provides indeed a triplet ground state; however, due to the large HL gap and therefore ST gap of the planar structure, this conformer is too high in energy. By arranging the NHC ligands orthogonal to the B-B bond, the most favorable non-planar conformer is built. Thus, a twist around the B-C bond is the most favorable way to release steric strain.

That a valid approach was used can be proven considering the calculated MOs of different CAAC stabilized system, like the various ones of the Braunschweig group, which always present a conjugated π-system between the carbene of CAAC and the included atoms.[408, 411, 455, 457, 458, 475, 485, 488, 514, 519-521] Furthermore, the arrangement of the AOs of the LUMO is found in the diradicaloids investigated by Bertrand and co-workers and induce the opportunity that this model can be generalized for different molecules built of two main group elements between two CAAC substituents.[489, 510]

Including an ethylene spacer between the carbene ligands leaves the system with two more electrons and provides therefore a HOMO that corresponds with the LUMO in the model approach. Both molecular orbitals provide a nodal plane between the carbon or boron atoms with a triple or double bond, showing thus a bonding motif to the carbene carbon atoms of the CAAC substituents. Another proof of the generality of this reduced model is presented by the orbitals of the twisted **CAAC2.4** and the associated combination of AOs (right, Figure 49). These observations correlate with the variations in the LUMO by twisting the CBBC angle of tetra(*o*-tolyl) diborane(4) described by Yamashita and Lin et al.[513]

5.6 Summary

In this chapter, four various diborenes ligated with NHC and four different diboranes ligated with CAAC were analyzed. It can be summarized, that the behavior of CAAC and NHC stabilized systems is totally different caused by the modified geometric arrangement (Figure 50). While the C-B-B-C structure of the NHC arrange planar, this part is twisted by 90° for the CAAC substituted systems. Therefore, the NHCs provide a singlet ground state with a B-B double bond and distorted NHC ligands. Whereas the CAAC systems possess a biradical triplet ground state with a conjugation through N-C-B of the CAAC ligands. A simplified illustration in Figure 50 helps clarifying the different behavior caused by the 90° twist around the B-B bond between both carbene ligands. Both systems do not dependent on the substituents bond to the sulphur or selenium. The disassembly of both systems illustrates that without the steric hindrances of the substituents bond to sulphur and nitrogen, both systems aim for a complete planar structure with a singlet ground state. However, for the smallest subsystems of both structures there is still a mismatch of 20 kcal/mol in the ST gap, which may cause the different arrangement of the whole structures. Therefore, a more precise analysis was made to find the differences regarding the electronic structure between the two carbenes CAAC and NHC.[412]
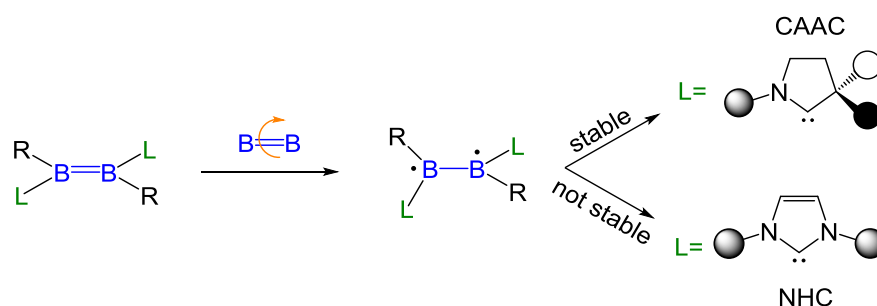
Figure 50: By a 90° torsion of the B-B double bond only the L=CAAC ligated system provides a stable ground state.

Furthermore, the influence of the steric versus electronic effects of the diborene **I** (NHC) and the diborane **II** (CAAC) was investigated, since both systems differ in their way to release steric strain caused by the huge substituents of the carbene. It was assumed that this behavior might be caused by the different steric environment of NHC and the CAAC providing a quaternary carbon atom instead of a second nitrogen.

To get an overview, which effects play major and minor roles in the interplay of steric and electronic effects, truncated model systems **I´** and **II´** are used. In these truncated systems, the huge steric substituents are substituted by hydrogens to reveal the underlying electronic

influence of the two carbenes, while neglecting the steric part. Both systems **I** and **II** differ in their geometric arrangement of the carbene substituents and the planarity of the SBBS part. Therefore, three major dihedrals ($\sphericalangle_{N_1C_1B_1B_2}$ $\sphericalangle_{B_1B_2C_2N_2}$ and $\sphericalangle_{S_1B_1B_2S_2}$) were selected with whom the systems can be characterized completely. By rotating these dihedrals to 0°, 90° or 180° a variety of conformers is obtained and calculated with high-level multireference wave function-based approaches. To figure out the importance of the electronic effects leading to the two varying twisted structures **I** and **II**, on the one hand the carbene substituents($\sphericalangle_{N_1C_1B_1B_2}$ $\sphericalangle_{B_1B_2C_2N_2}$) is rotated and on the other hand the B-B bond ($\sphericalangle_{S_1B_1B_2S_2}$) is twisted.

By means of the calculated conformers of the truncated model systems **I′** and **II′**, a completely coplanar closed shell singlet state is most likely to appear as ground state for both systems with a conjugated π-system. Thus, the huge steric strain forces the systems to sacrifice either the B-B or B-C bond. However, which bond is sacrificed is determined by the electronic effects. In the CAAC model system **II′**, it gets clear that the triplet state is readily accessible and thus can be achieved easily, in particular in the conformer twisted around the B-B bond. System **I′** shows a highly unstable triplet leading to a compound **I** with a preferable torsion of the B-C bond. Interestingly, compound **I** prefers an out-of-plane rotation of both C-B bonds, even though the electronic energy increases significantly.

An important aspect to determine the electronic effects is represented by the all-planar structure of the model compounds **I′** and **II′**. The calculations show a correlation between the ST gap of the planar structures and the relative energy of the B-B rotated conformer, indicating that these coplanar arrangements play a major role investigating the electronic effects. Especially the coplanar triplet state is of great interest, since the bonding pattern displays an analog behavior for this state and the B-B twisted structure, showing two singly occupied MOs, each located as π-orbitals on one B-C bond. The resemblance is also seen in the relative energies, while the ST gap is about 9 kcal/mol for the planar compound **II′**, the singlet B-B rotated conformer is shifted about the amount and the triplet slightly less (6 kcal/mol). Considering system **I′**, the same trend is observed, only shifted to higher energies (~30 kcal/mol for both), revealing the ST gap of the planar structure as key determinant to ascertain the cost of twisting the central B-B bond. Consequently, for system with higher steric demand this value concludes whether the B-B is twisted, leading to biradical species **II**, or stays in-plane resulting in diamagnetic diborene **I**.

Another unknown value clarifying why compound **I´** shows a ST gap about 20 kcal/mol higher than the one in system **II´** is likewise discussed and analyzed in this chapter. The differences in the ST gap of CAAC and NHC substituted compounds can be attributed to properties and relative energies of the HOMO and LUMO of the planar structure of both systems. The MOs possess π-bonding orbitals with antibonding character to the nitrogen atoms of the carbene. Because of the double amount of nitrogens in NHC, this effect is pronounced stronger for NHC than for CAAC resulting in higher energies of the MOs of **I´** compared to the CAAC compound **II´**. Since the electron density of the LUMO is shifted towards the carbene carbon, due to the additional nodal plane between the boron atoms, the antibonding C-N character increases more than in the HOMO. Consequently, the resulting shift to higher energy is very pronounced for the LUMO compared to the HOMO. The higher HL gaps leads to an increased ST gap with NHC and therefore the B-B bond is energetically more unfavorable than in CAAC.

6   Dinitrogen borylene complexes

An important contribution to the activation of dinitrogen is the π-back bonding, which is made possible by the use of transition metal (TM) complexes.[522-525] These complexes are known as one of the few compounds to fix or even activate dinitrogen (N_2).[522-525] For the industrial production of ammonia (NH_3), nitrogen is activated applying the Haber-Bosch procedure.[526-528] That process involves TM complexes, such as iron or ruthenium based catalysts in combination with a high temperature and pressure, for the activation.[528] A substantial advantage of TM complexes is that the metal centre possesses a reactive lone pair next to an unoccupied orbital.[522-525] Thus, the perfect conditions are achieved to fix and functionalize chemically inert dinitrogen. In the review of Power *et al.*, a few main group elements are highlighted, which are capable of mimicking the behavior of transition metals, in particular regarding the activation of hydrogen or the stabilization of radicals and biradicaloids.[529] Especially the carbon-based carbenes (**B**) of the Bertrand group are well investigated concerning their reaction behavior towards CO, H_2, NH_3 and radicals, revealing a performance similar to TM complexes.[95, 433, 489, 497, 511, 530-532] In addition, other carbenoids from heavier group 14 elements, namely silylenes (**C**), germylenes (**D**), stanylenes and plumbylenes and two group 15 carbenoids, such as nitrene (**E**) and phosphinidene (**F**), emerged (Figure 51).[533-539] The only representative of main group 13 is the borylene carbenoid (**A**), which was isolated first by the Braunschweig group as a terminal borylene in the ligand sphere of TM complexes.[540]
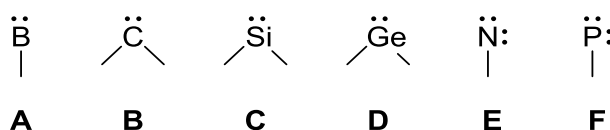
Figure 51: Various carbenoids from main group 13 (**A**), 14 (**B**-**D**) and 15 (**E**, **F**) elements.

The unique behavior and properties of those complexes open a wide field for synthesis and application of boron centred ligated metal complexes.[541, 542] While carbenes illustrate either a singlet or a triplet ground state, depending on the electronic features of the substituents bound the carbon carbene centre, borylenes appear until now only as singlet carbenoids.[543, 544] Carbenes can for example be isolated, when a vacant p-orbital of the carbene possesses electron density obtained by a p-donating nitrogen or phosphorus, which

is bound directly to the carbene centre.[543, 545-547] Since borylene exhibits not only one but two vacant p-orbitals and additionally only one substituent, the lack of electrons is even greater than for carbenes. Thus, the synthesis and isolation of stable borylenes appears more difficult.[548] In the Braunschweig group, borylenes are found as intermediates in the formation of other boron containing species.[485, 549, 550]
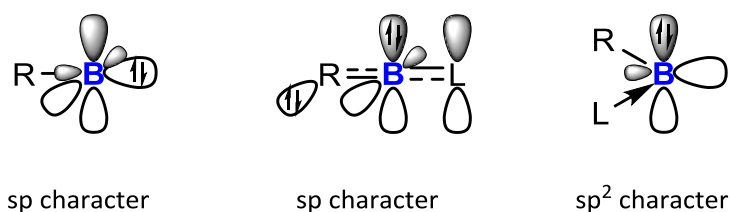
Figure 52: Orbital pictures of a borylene with one substituent (R) and two substituents (R, L) depending on the angle between the ligands and boron (R: anionic substituent, L: Lewis base).

The mono-substituted borylene possesses two sp-orbitals, one describing the bond to an anionic substituent R and the other is occupied with two unpaired electrons (Figure 52, left). Furthermore, two vacant p-orbitals are found, which are often degenerated. Since the electronic structure of these borylenes is even more electron deficient, one electron donating group is not sufficient to stabilize these systems. Consequently, the isolation of these mono-substituted borylenes appears to be nearly impossible (Figure 52, left).[551] Using additional Lewis bases, such as carbenes, an attempt is made to decrease the electrophilic character of the boron by p-donating to the vacant p-orbital of the boron (Figure 52, middle). However, even those complexes possess not enough stability to be described as borylenes, since the systems own too much electron density, which is not a preferable state for borylenes. Thus, the use of CAAC carbenes provided a suitable approach due to the more electrophilic properties of those carbenes.

The mono- or bis- (Lewis base) stabilized borylenes are reviewed by Bertrand presenting various borylenes differing in the stabilizing carbene L and the anionic substituent R (Figure 52).[551] It is also worth considering the dependency of the bonding pattern on the angle, which is included by the atoms bound directly to boron and the boron atom itself. A plane geometry features an allenic structure, in which the hybrid orbitals show a sp character (Figure 52, middle). The molecule orbitals of boron can be described as sp²-hybrid orbitals, when the CBN plane is bend, therefore becoming more electrophilic (Figure 52, right).[551] A multiple bond character between R, the carbene L and boron is given by a bonding interaction between

the lone pair in the boron p-orbital and the vacant p-orbital of the carbene, building the HOMO. An interaction of the lone pair of anionic substituents R with the empty p-orbital of boron results thereby in an unoccupied molecular orbital. The smaller stabilization of the vacant sp²-orbital and the increased electrophilicity makes those borylenes suitable main group analogues to metal complexes, which is outlined in Figure 53. This is in addition proven by their behavior against H_2 or CO.[529, 552-554]
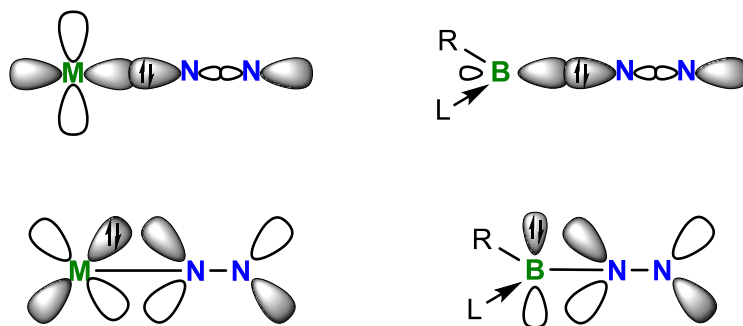
Figure 53: Scheme of the dinitrogen metal bonding (left) and the identical case for borylene instead of a metal centre (right) with a Lewis base L and an aryl substituent R.

Stabilization of borylene compounds with a second carbene allows for the isolation of the molecules and opens up a wide field of applications and variation in structural and synthetically way, like the one found by the Braunschweig group.[555, 556] In those molecules, the boron is trisubstituted and planar with B-L multiple bond distances in the range of single and double bonds, depending on the π-acceptance abilities of the carbene ligands, since boron is π-back donating. Additionally, the carbenes donate σ-electron density in the vacant in-plane orbitals of the boron. Borylene complexes exhibit strong π-back bonding to molecules, such as CO.[555, 556] This is also a requested behavior for metal centres bond to N_2. Considering these requirements, Dr. Marc Andrè Lègarè from the Braunchweig group tried to bind N_2 in a borylene-based scaffold, resulting in the first p-block element fixation of N_2, represented here as **B₂N₂** (Figure 54). For the synthesis of **B₂N₂**, [(CAAC)BBr₂Dur] (**1**) was reduced with potassium graphite (KC₈) under argon atmosphere obtaining the radical species [DurBBr(CAAC)] (**2**) as an intermediate. In the further course of the reaction, a potassium coordinated dinitrogen complex is built reacting to the dinitrogen bond molecule **B₂N₂** by oxidation in air (Figure 54). By treatment of the potassium stabilized dinitrogen complex **B₂N₂K₂** with distilled water, another dinitrogen compound is isolated, namely the paramagnetic biradical diborahydrazine **B₂N₂H₂**.
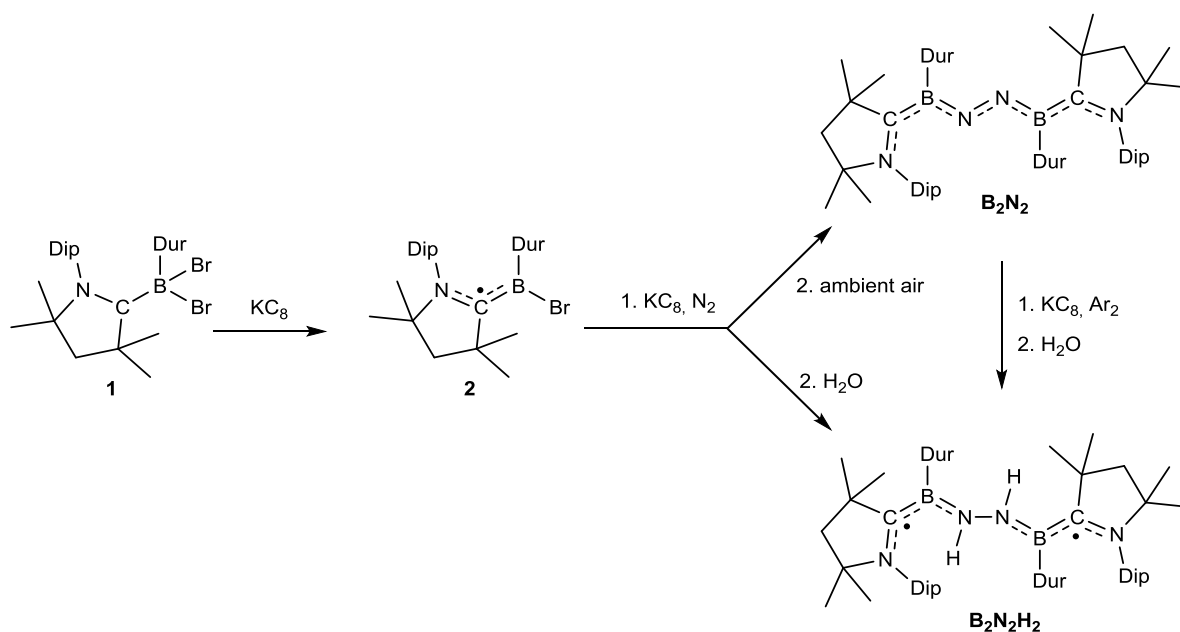
Figure 54: Synthesis of the dinitrogen fixating molecule **B₂N₂** via two electron reduction of [(CAAC)BBr₂Dur] (**1**) under N₂ atmosphere and its following reduction in water to product **B₂N₂H₂**.

Both dinitrogen compounds show completely different behavior in both the geometric arrangement and the electronic appearance. Consequently, a theoretical investigation of those molecules is of great interest to evaluate the bonding pattern and the resulting properties concerning the reaction behavior. The intermediate, the potassium coordinated dinitrogen complex **B₂N₂K₂**, could not be isolated and is therefore not investigated.

6.1 Dinitrogen fixed complex B₂N₂

A substantial shift in the B-NMR spectra indicate that the ground state of **B₂N₂** appears most likely as a singlet state. To get more insights, the singlet and triplet state are optimized, and the calculated geometry values are obtained with their experimental counterparts, taken from the available X-Ray structure. If not stated otherwise, the geometries and energy values are obtained by unrestricted calculations using the UMN12L functional in combination with the 6-311G(d, p) basis sets. This combination was tested to perform outstandingly well.[557, 558] Furthermore, the benchmark performed in chapter 4 confirms this suggestion. The computational results predict a singlet ground state with a ST gap of about 12 kcal/mol, which is in accordance with the results obtained by B-NMR spectroscopy. Furthermore, the computed geometric data of the singlet state (Figure 55) agree better with the experimental X-Ray structure than the computed triplet geometry. This is not quite obvious, since the singlet

geometry shows a slight asymmetric behavior towards the geometrical data of both sides of the dinitrogen bridge. This is probably caused by the steric hindrances of the huge substituents on the boron and carbene, coupled with the two lone pairs of the nitrogen atoms.
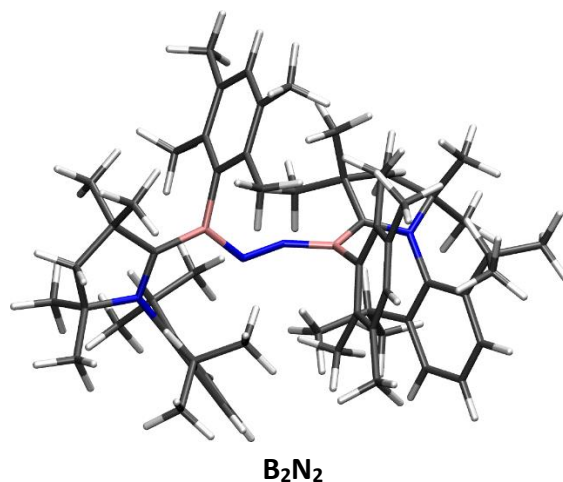
B₂N₂

Figure 55: Calculated geometry of the singlet ground state of **B₂N₂** (UMN12L and 6-311G(d, p) basis sets).

However, this asymmetry is not found in the experimental geometry. Using different functionals with the same pople basis sets, such as SOGGA11X, with a huge amount of Hartree-Fock, or the M062X and M06L functionals, which varying amount of HF, or the afore tested MN12L, results in the same geometry. In comparison, SCS-MP2 combined with def2-TZVP basis sets achieves a larger error compared to the DFT functionals.

While the carbene ligands are in-plane with one nitrogen, the BNNB dihedral ($\sphericalangle_{\text{BNNB}}$) is twisted about 90°. The N-N bond length of 1.24 Å is perfectly reproduced by theoretical calculations with DFT assuming that there is a double bond between the two nitrogen atoms. However, the $\sphericalangle_{\text{BNNB}}$ of 113°, which is not consistent with a sp²-hybridized nitrogen required for a double bond formation, slightly contradicts these findings. The equivalent TM complexes, which fix nitrogen, arrange always coplanar between two transition metal centres, as a result of the overlap of a d-orbital of the metal and the empty p-orbital of nitrogen. The asymmetry of the two angles, $\angle_{\text{BNN}}$ =146° and $\angle_{\text{NNB}}$ =132°, can also be seen in the B-N bond length varying from 1.43 to 1.40 Å (Table 26). This bond length lead to the assumption that there is a double bond between the boron and the nitrogen or at least some multiple bond character. The angles $\angle_{\text{BNN}}$ and $\angle_{\text{NNB}}$ of about 130° agree better with sp²-hybridized nitrogen centres, being close to the optimal angle of 120°.The widening of the $\angle_{\text{BNN}}$ angle might be caused by the lone

pair, which requires more space than a bond without lone pairs. Since **B₂N₂** possesses a singlet ground state, only the geometric data of the singlet state are shown in Table 26.

Table 26: Calculated (UMN12L/6-311G(d, p) bond length and bond orders for the important atoms of the singlet ground state of **B₂N₂**.

	C_1-B_1	B_1-N_1	**N_1-N_2**	N_2-B_2	B_2-C_2
Bond length (Exp.)	1.52	1.42	1.24	1.41	1.52
Bond length (Theor. Singlet)	1.52	1.43	1.24	1.40	1.54
Bond order	1.15	1.14	1.51	1.21	1.06

Another important evidence for the existence of the borylene structure is given by the B-C bond length with 1.52 Å, which is perfectly reproduced by the UMN12L singlet geometry. This result ranges between references values for a B-C single (1.59 Å) and double bond (1.44 Å).[559] This multiple bond character suggests that the boron atom exists indeed as a borylene, in which the free lone pair of the boron provides π-back bonding to both, the nitrogen and the carbene carbon. An analog case is found for the trisubstituted borylenes.[551, 559] In comparison to the CO-substituted borylene compound, also synthesized by the Braunschweig group,[555] the B-C bond increases, which might be caused by dinitrogen appearing as better π-acceptor compared to CO. Thus, the short B-N bond can be a reason for the weak N=N double bond. The same effect is found in TM complexes with N₂, which weaken the N-N bond to increase the reactivity. To prove this assumption, a Wiberg analysis (Table 27) was performed revealing a strong multiple bond character between the two nitrogen atoms (N-N: 1.5). Whereas the multiple bond character decreases going to boron (B-N: 1.1-1.2) and carbon of the CAAC ligand (B-C: 1.1).

To get a better overview of the quality of the calculated Wiberg bond indices, some nitrogen containing model systems (**3-8**) are analyzed showing different bonding patterns of the dinitrogen atoms (Figure 56). Table 27 shows the Wiberg indices, the bond length and the partial charge of the various dinitrogen containing systems. Since the natural charges of both nitrogen atom appears nearly identical, only one charge is listed in Table 27. The triple bond between the pure dinitrogen **3** shows as bond length of 1.09 Å, corresponding to the typical bond length of a triple nitrogen bond and a Wiberg index of nearly three agreeing with a third-order bond. The calculated compounds **4-6** should possess similar values as the calculated system **B₂N₂**, since they obtain a dinitrogen double bond. Different dinitrogen

double bonds are calculated by varying the substituents and the geometric arrangement. With a bond length of 1.24 Å, B_2N_2 lies in between **4** (1.25 Å) and **5/6** (1.23 Å). The molecules **5** and **6** possess a Wiberg bond order of two showing a double bond between the dinitrogen atoms. The index decreases in structure **4** to 1.77.
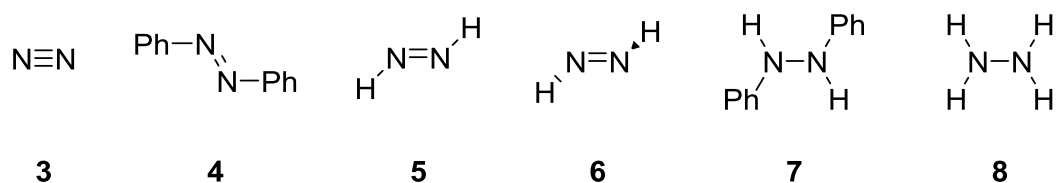
Figure 56: Dinitrogen model compounds **3-8**.

This indicates that the B_2N_2 complex with a calculated bond order of N-N=1.5 reflects more the model compound **4** than the systems **5** and **6** regarding the Wiberg index, which describes the double bond character. This may result from the electron pushing effect of the phenyl ligands, which are known to have a positive mesomeric effect.[560] Since the π-orbital is already occupied with two electrons, additional electron density is transferred to the π^*-orbital resulting in a higher antibonding character of the N_2 bond. Thus, the N-N bond length increases, while the electron density in between the two nitrogen atoms decreases, leading to a smaller Wiberg index. The even smaller Wiberg index of 1.5 for complex B_2N_2 can be described as a combination of the just mentioned electron density effect and the not perfectly arranged nitrogen atoms caused by the high steric strain in the system combined with the lone pairs on the nitrogen.

Table 27: Nitrogen containing systems **3-8** differing in the bonding pattern between the nitrogen atoms and its substituents.

Structure	3	4	5	6	7	8
Bond length	1.09	1.25	1.23	1.23	1.39	1.43
Bond order	3.03	1.77	2.06	2.06	1.02	1.04
Natural charge N_2	0.00	-0.21	-0.32	-0.29	-0.48	-0.69

The three calculated frontier Kohn-Sham orbitals of the singlet state of B_2N_2, the HOMO-1, HOMO and LUMO, illustrate an amount of antibonding character between the two nitrogen atoms. In particular, the HOMO-1 and HOMO illustrate a perfect combination of the p-orbital of the boron with the π^*-orbital of the N-N and (C-N)$_{CAAC}$ of the carbene leading to a nodal plane between the dinitrogen and the carbon and nitrogen of the CAAC substituent (Figure 57).
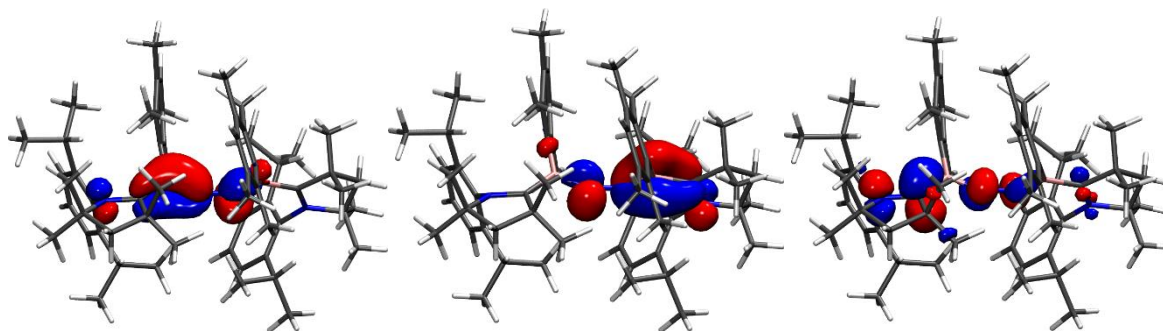
Figure 57: HOMO-1 (left), HOMO (middle) and LUMO (right) of **B₂N₂**.

The HOMO and HOMO-1 are nearly degenerated, since the molecular orbitals look alike with the electron density being located on opposite sides of the molecule. The electron density of the LUMO is located on the B-C$_{CAAC}$ π -bond with antibonding character to the nitrogen atoms of both the dinitrogen bridge and the carbene ligand. The simplified molecular orbital scheme, shown in Figure 58, represent the calculated KS orbitals perfectly
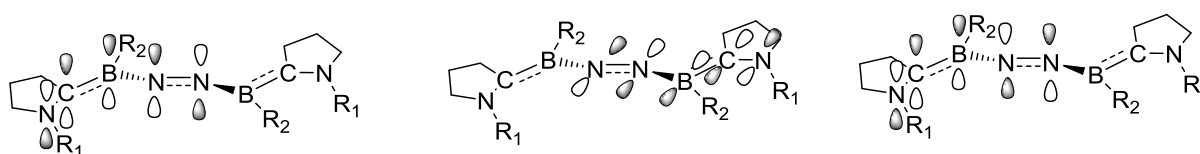
Figure 58: Schematic presentation of the HOMO-1 (left), HOMO (middle) and LUMO (right) of **B₂N₂** (R₁=Dip, R₂=Dur).

The antibonding character between the two nitrogen atoms of the frontier orbitals can be clearly seen in the schematic presentation of the MOs (Figure 58). The HOMO and HOMO-1 exhibit only two nodal planes between the two nitrogen atoms of the dinitrogen bridge and thy typical nitrogen carbon nodal plane of the CAAC ligand, which was already pointed out in chapter 5. Thus, the LUMO includes three nodal planes in the KS orbitals, which can be seen clarified in the schematic LUMO presentation in Figure 58. The additional nodal plane arises between the boron and nitrogen atom. An idea on the bonding situation considering atomic orbitals is shown in Figure 59. Both, the boron and nitrogen units, as well as the carbon atom of the carbene possess sp²-hybrid character and a vacant or unoccupied p-orbital.
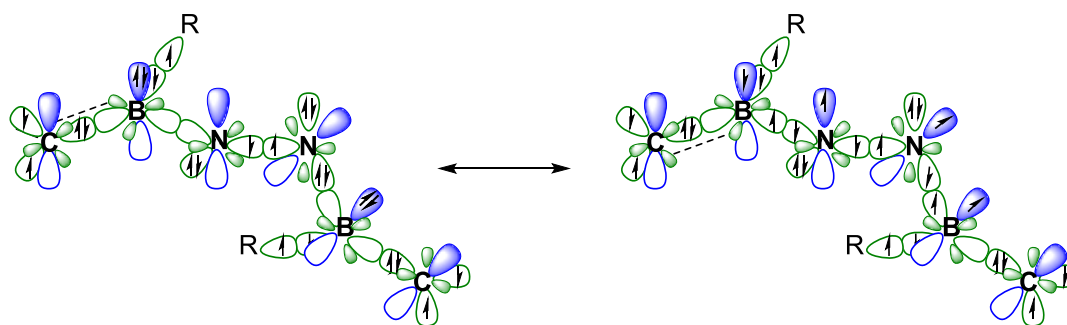
Figure 59: Schematic presentation of the bonding pattern with sp²-hybrid and p-orbitals obtained by the carbon, boron and nitrogen atoms of **B₂N₂** with R=Dur.

In Figure 59 (left), the bonding situation is described assuming a borylene bound to nitrogen mimicking a transition metal bond to N_2. This results in a double occupation of the sp²-hybrid orbital of the nitrogen donating into the empty sp²-orbital of the boron atom building up a σ-bond. The nitrogen acts as σ-donor and boron as σ-acceptor, as it is the case in TM complexes. Since the dative σ-bond between the carbene and the boron originates from the doubly occupied sp²-orbital of the carbon atom to the vacant sp²-orbital of the boron, boron possesses two free electrons, while one electron is needed to build up the bond to the duryl group. Thus, these two electrons are assumed to be in the p-orbital, which enables a π-back bonding from the boron to nitrogen and carbene carbon. A mesomeric structures with more realistic bonds can be considered in Figure 59 (right). Thereof, multiple bond character between the carbon and boron, and boron and nitrogen can be explained.

If the $\sphericalangle_{BNNB}$ dihedral is planar no double bond can be formed, since both the π- and π^*-orbital are occupied. However, by rotating this dihedral of about 120°, the sp² orbital from one nitrogen containing the lone pair and the empty orbital of the other nitrogen are in one plane. Thus, the nitrogen double bond is probably caused by an overlap of the empty p-orbital of nitrogen with and sp² lone pair containing orbital of the other nitrogen. This bond can only be formed by a rotated N-N bond of about 120°, which is the case for the **B₂N₂**. Because of this geometry, no delocalization over the complete unit including the boron and CAAC ligands can be formed.

6.2   Dinitrogen system with hydrogen B$_2$N$_2$H$_2$

By adding water to the twofold reduced **B$_2$N$_2$**, a new molecule with a different color was isolated, indicating a changed electronic behavior. The obtained complex **B$_2$N$_2$H$_2$** shows in contrast to its non-hydrogenated equivalent **B$_2$N$_2$**, a paramagnetic behavior measured with EPR spectroscopy.[411] Although a high-resolution EPR analysis and thus a determination of the ST gap was not possible, the singlet is supposed to lie close to the triplet state, as indicated by temperature dependencies of the EPR activity.[411]
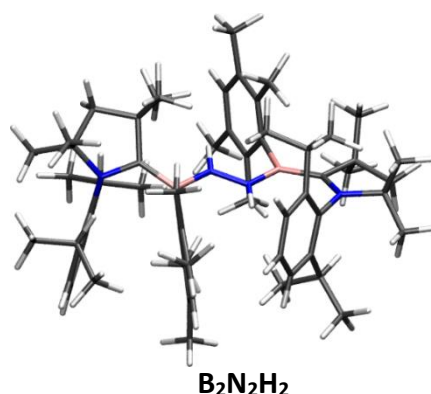
B$_2$N$_2$H$_2$

Figure 60: Triplet ground state geometry of **B$_2$N$_2$H$_2$** calculated with UMN12L in combination with the 6-311 G(d, p) basis set.

Theoretical calculations predict a triplet ground state (Figure 75), which lies about 7.8 kcal/mol lower in energy than the singlet. With an error of about 6-8 kcal/mol in the ST gap prediction for this method, the ST gap appears to be nearly zero; however, still showing a triplet ground state. Using SF-DFT, employing the BLYP functional and def2-TZVP basis sets, results in a ST gap of only 0.1 kcal/mol indicating that singlet and triplet are almost degenerate with a triplet ground state. This observation can additionally be confirmed regarding the geometries of both states, as both exhibit a very similar geometry. The crystal structure proves a N-N single bond with a bond length of 1.40 Å, which is perfectly reproduced by the triplet geometry (Table 28). The singlet bond length decreases to 1.37 Å, which still leads to a single bond between the two nitrogen atoms. The calculated Wiberg bond indices confirm a single bond with a value of 1.06 for both the singlet and triplet state (Table 28). The B-N distances of 1.43 Å refers to a B-N bond with double bond character, which is also verified by the Wiberg indices of 1.36. Furthermore, the bond lengths and Wiberg indices predict a multiple bond character which extends from the nitrogen of the bridge to the nitrogen of the carbene.

In contrast to the non-hydrogenated system B_2N_2, in which a N-N double bond is present, the multiple bond character of the N-N bond decreases, while the multiple bond character of the remaining N-C-B-N unit increases. Thus, the double bonds in the N-B-C-N unit of each side of the molecule explain the planar arrangement of the $B_2N_2H_2$ molecule, which is not favored for B_2N_2. Both calculated states arrange nearly coplanar with dihedrals of $\sphericalangle_{BNNB} = 166°$, which correspond to the crystal structure. Same applies for the dihedrals between the nitrogen and the carbene substituents $\sphericalangle_{NCBN}$ with 166° and 168°. Considering the substituents of the boron and nitrogen of CAAC, a *cis*- and *trans*-conformation of both substituents is possible. While on one side the molecule arranges in *trans*-conformation, the other side takes a *cis*-conformation. This arrangement is caused by steric effect, since for this conformation the substituents with high steric demand avoid each other.

Table 28: Calculated (UMN12L/6-311G(d, p) bond lengths and bond orders for the important atoms of the triplet ground state of $B_2N_2H_2$.

	C_1-B_1	B_1-N_1	N_1-N_2	N_2-B_2	B_2-C_2
Bond length (Exp.)	1.54	1.43	1.40	1.44	1.53
Bond length (Theor. Triplet)	1.54	1.44	1.39	1.45	1.53
Bond order	1.16	1.36	1.06	1.36	1.16

The frontier orbitals (HOMO, SOMO and SOMO+1) of the triplet ground state are shown in Figure 61. The HOMO of the singlet, which is the equivalent to the HOMO of the triplet, exhibits the same electron density distribution as its triplet analog and also the SOMOs are identical. Thus, it gets more conceivable that the singlet ground state appears as a biradical, too, which lies energetically close to the triplet ground state. This is in contrast to B_2N_2, which exhibits a closed shell singlet ground state with a much higher ST gap. The HOMO and HOMO-1 are more or less degenerated in B_2N_2 caused by the non-symmetrical behavior of the system (Figure 61). Between the boron and the nitrogen atoms a B-N π-bond is formed on each side additionally to the N=N double bond. Thus, the HOMO-1 illustrates this bond on the left side, while the HOMO represent this π-bond on the right side of N=N bridge. Since $B_2N_2H_2$ arranges almost symmetrical without a conjugation between the dinitrogen bridge, both B-N π-bonds can be formed on each side of the molecule in one molecular orbital, which represent the HOMO (Figure 61). Therefore, no degeneration is observed.
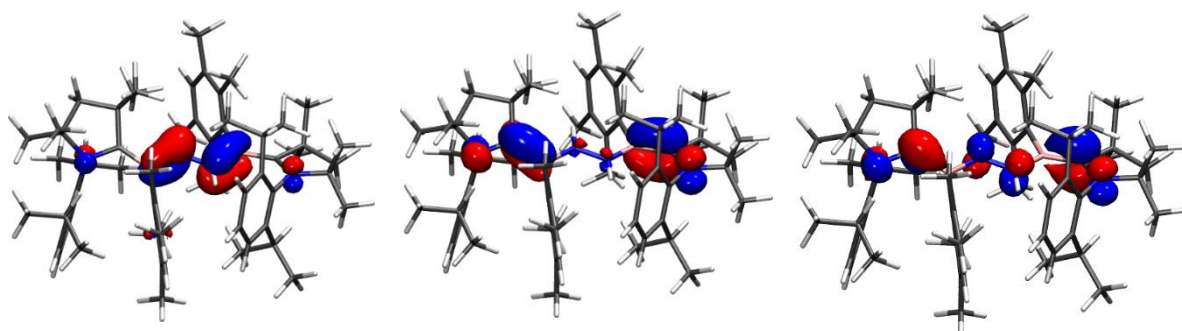
Figure 61: HOMO (left), SOMO (middle) and SOMO+1 (right) of triplet ground state of **B₂N₂H₂**.

The same trend is seen in the SOMO+1 of **B₂N₂H₂** and the LUMO of **B₂N₂**. While in the case of **B₂N₂**, the C-B π-bond is mainly located on one side, for the **B₂N₂H₂** it appears on both sides with antibonding character between the nitrogens of the dinitrogen bridge and between the nitrogen and the carbon atom of the carbene ligand. The SOMO exhibits the same behavior without a nodal plane between the dinitrogen atoms. Because of the higher amount of electron density on the nitrogen atoms next to boron, the density decreases on the boron atoms, most likely due to the antibonding character of both. By the occupation of the SOMO, the antibonding character between the dinitrogen atoms of the bridge increases, since the SOMO yields a nodal plane between those two atoms. The SOMO and SOMO+1 differ about 10 kcal/mol in energy, which increases only slightly considering the closed shell singlet with a HL gap of 13 kcal/mol. Compared to **B₂N₂**, the HL gap is about 35 kcal/mol, which hardly allows for an occupation of the LUMO. Even for the triplet of **B₂N₂** the SOMOs differ about 19 kcal/mol. The higher energy increase of the LUMO **B₂N₂** compared to the SOMO+1 of **B₂N₂H₂**, is probably caused by the minor overlap of the C-B p-orbitals in the more twisted **B₂N₂**. Furthermore, the second B-C conjugation is located in the LUMO+1 and not in the LUMO; however, the antibonding N-N interaction stays the same for the LUMO of **B₂N₂** and the SOMO+1 of **B₂N₂H₂**.
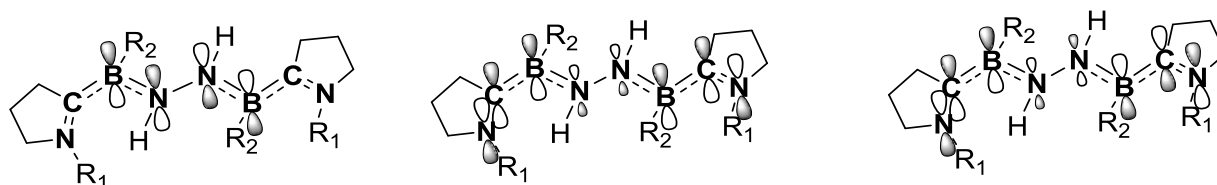
Figure 62: Schematic presentation of the HOMO (left), SOMO (middle) and SOMO+1 (right) of **B₂N₂H₂** (R₁=Dip, R₂=Dur).

The atomic orbitals of the frontier orbitals are depicted in Figure 62 to clarify the arrangement of the orbitals. Even though **B₂N₂H₂** possesses two more electrons, HOMO and LUMO state the same kind of interaction as seen for **B₂N₂**. This is caused by the asymmetric combination

of the orbitals in the case of **B₂N₂**. Because of the hydrogen bound to the nitrogen atoms in the BNNB bridge, the bonding pattern of **B₂N₂H₂** changes, since there is no lone pair located anymore at the nitrogen atoms (Figure 63). Furthermore, the free electron cannot be located in the sp²-hybrid orbital, since the third sp²-hybrid orbital is needed to form the N-H bond. Thus, the unpaired electron of each nitrogen atoms tends to be localized in the unoccupied p-orbital.
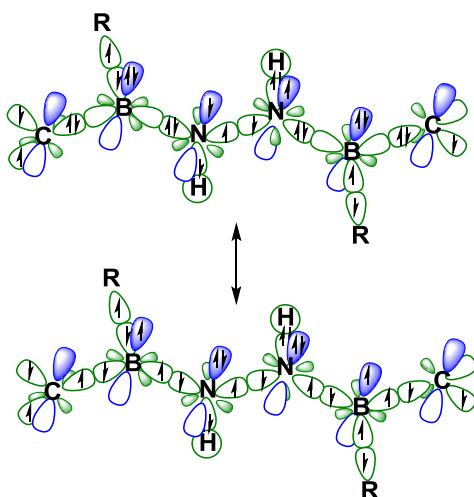
Figure 63: Schematic presentation of the bonding pattern with hybrid and p-orbitals obtained by the carbon, boron, nitrogen and hydrogen atoms of **B₂N₂H₂** with R=Dur.

Due to the high electron pushing effect of the boron atoms into the p-orbital of the nitrogen atoms, the mesomeric structure (Figure 63, below) can be formed. The σ-donating abilities of the nitrogen and the carbene carbon atom lead to an electron pushing effect towards the boron atoms. This picture explains the bonding situation, since the p-orbitals are doubly occupied, which means that both the π- and π^*-orbitals are occupied resulting in a N-N single bond. This change affects the complete electronic structure of the system, making the biradical triplet more stable, as there is no conjugation between the individual sides of the BNNB bridge. Since the π-pushing effect should also be dependent on the substituent bound to both the boron atoms and the carbenes, calculations are performed reducing the system size to provide an insight into the electronic properties as a function of the substituents.

6.3   Influence of the substituents in the B_2N_2 molecule
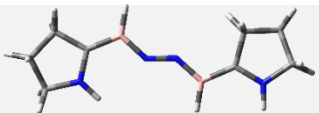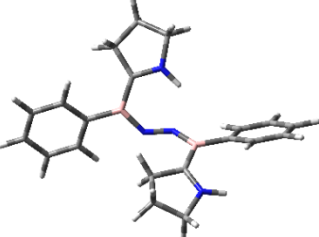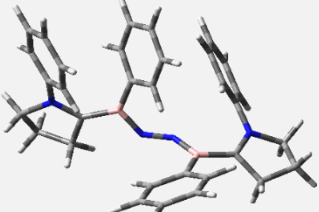
To investigate the electronic and steric effects of the substituents bound to the nitrogen of the carbene and the boron, both substituents were cut off and the obtained model structures were optimized. Again, UMN12L with 6-311G(d, p) basis sets are used to optimize the various structures, followed by a single point calculation with NEVPT2 employing the def2TZVP basis sets. The results for the relative energetic position of the different singlet and triplet states are almost identical irrespective of NEVPT2 or UMN12L being used. To identify the global minimum, a variety of geometries are modelled by varying the dihedral $\sphericalangle_{BNNB}$. Starting the geometry optimization from a twisted $\sphericalangle_{BNNB}$ geometry often results in different minimum structures, than using an all coplanar starting structure. Eight model compounds were created utilizing all combinations of substituents bound to the carbene nitrogens and the boron atoms. The former Dip ligand (R_1) on the nitrogen of the CAAC carbenes and the duryl group (R_2) on the boron are substituted by either phenyl-, methyl-groups or hydrogen atoms. Since no substantial difference was observed by changing the substituents from methyl to hydrogen, the methyl ligated substructures are not included in this work. The substituents are supposed to reflect two influences, first, a different kind of steric demand and, second, electronic effects including mesomeric (phenyl), inductive (methyl) or no effects at all (hydrogen). Since the CAAC nitrogen substituents rarely affects the remaining system, all the variations of these substituents seem to be only important for steric effects. Thus, only three substructures **9-11** are fully discussed in this work more precisely. In Table 29 the three substructures are depicted with their concerning ground state multiplicity and the diabatic ST gap.

The numeration of the various minimum geometries is abbreviated as **9-11** for each sub system, and **S** or **T** for the multiplicity of the state. The index of S_n and T_n provides information of the energetic position of this state. Consequently, the S_0 is defined as ground state, while S_1 and T_1 are higher in energy. Vice versa, with T_0 as global ground state the S_1 state illustrates an increase in energy.

Replacing the Dip- and the duryl ligands by hydrogens yields structure **9**. The different minimum structures of the singlet and triplet geometry are shown in Figure 64. Irrespective of the starting point chosen for the optimization, the singlet reaches always a minimum structure S_0 with a $\sphericalangle_{BNNB}$ dihedral of about 100° and a very small N-N double bond of 1.21 Å.

Table 29: Different substructures **9-11** of B_2N_2 with varying substituents R_1 and R_2 with their concerning ground state multiplicity, ST gap and dihedral, calculated with NEVPT2/def2-TZVP.

Substructures B_2N_2	Substituent R_1 and R_2	Ground state	∢$_{BNNB}$ [°]	ST gap [kcal/mol]
9	R_1 = Hydrogen R_2 = Hydrogen	singlet	100	15
10	R_1 = Hydrogen R_2 = Phenyl	singlet	98	14
11	R_1 = Phenyl R_2 = Phenyl	singlet	87	23

Thus, by removing the electron pushing substituents on the carbene and boron, the singlet state of system **9** arranges more symmetric with a ∢$_{BNNB}$ dihedral closer to 90°. It was tested that by rotating the dihedral ∢$_{BNNB}$ from 90° to 110° there is nearly no difference in energy resulting in a stronger dinitrogen bond combined with a weaker B-N bond, which can be seen in the bond length and the Wiberg indices of the concerning bonds. In contrast, the triplet **9T$_1$** and **9T$_2$** arrange completely planar, as the triplet of the complete system already attempted to, but was sterically hindered.

9S$_0$ **9T$_1$**   **9T$_2$**
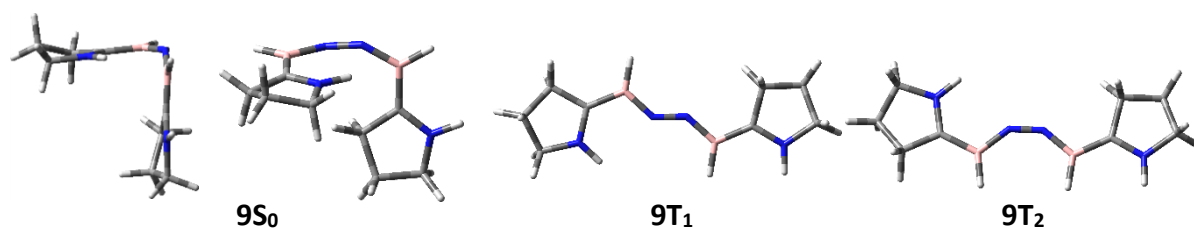
Figure 64: Structure of the global minimum of the singlet **9S$_0$** from different sights of view (two structures on the left) and the two conformers of the triplet **9T$_1$** (middle right) and **9T$_2$** (rightmost).

The minimum structure of the triplet **9T$_1$** is about 15 kcal/mol higher in energy than the singlet **9S$_0$**. The triplet also favours a N-N double bond with a bond length of 1.23 Å yielding two conformers (Figure 64). The conformer **9T$_2$** with the *cis*-transformation is about 5 kcal/mol higher in energy than the *trans* one, **9T$_1$**. However, it can be assumed that by increasing the substituent size on the boron, the energy difference between the conformers increases, as

well. The three frontier orbitals of the singlet **9S$_0$** of the smallest structure **9** illustrate the same electron density contribution as the complete system **B$_2$N$_2$** (Figure 65). This observation implies that the huge substituents do not affect the electronic behavior of the system but have an effect on the steric demand of the arrangement.

On the contrary, the triplet arranges more symmetric and coplanar for substructure **1** than for the complete **B$_2$N$_2$** molecule. Thus, combining the former HOMO and SOMO orbitals of the **B$_2$N$_2$** triplet leads to one molecular orbital for **9T$_1$** the HOMO, which is shown in Figure 65 on the right side.
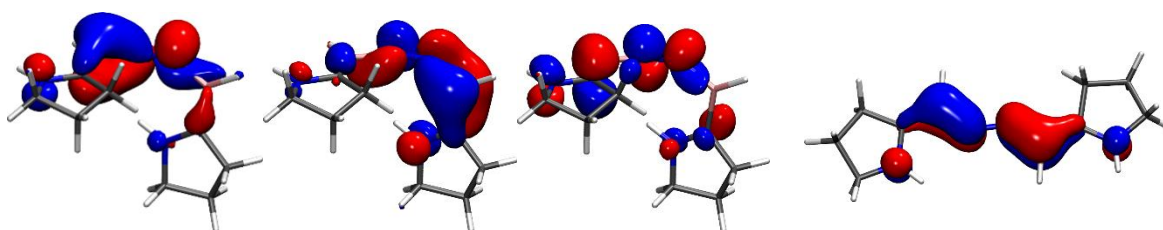
Figure 65: HOMO-1, HOMO and LUMO of the singlet **9S$_0$** and the HOMO of the triplet state **9T$_1$** of the smallest structure **9**.

The HOMO of **9T$_1$** illustrates a combination of two π-orbitals localized over the nitrogen of the left CAAC to the other nitrogen of the right CAAC. This orbitals include also the π^*-interaction of the N-N of the dinitrogen bridge and (C-N)$_{CAAC}$ of the carbene leading to a nodal plane between the dinitrogen and the carbon and nitrogen of the CAAC substituent. The singly occupied SOMOs of the triplet exhibit a π-bond between boron and carbon and strengthen this bond, which can be seen in a slightly shorter B-C bond length for this species. A more symmetric description of the triplet orbitals including the SOMOs is depicted later on, considering the conformer **B$_2$N$_2$ 2** in Table 32.

In the next step, the system size is increased by adding a phenyl group to the boron atoms yielding structure **10**. For subsystem **10**, a similar trend can be seen as for substructure **9**. The singlet **10S$_0$** arranges again nearly orthogonal and the triplet **10T$_1$** completely coplanar. By adding a stabilizing unit with mesomeric effect to the boron atoms, the N-N bond length increases to 1.25 Å, which is close to the original system **B$_2$N$_2$**. For the other bond lengths, no substantial change is visible. Similarly, there is no change visible for the triplet, as the minimum structure stays planar building up a N=N double bond with a bond length of 1.23 Å.
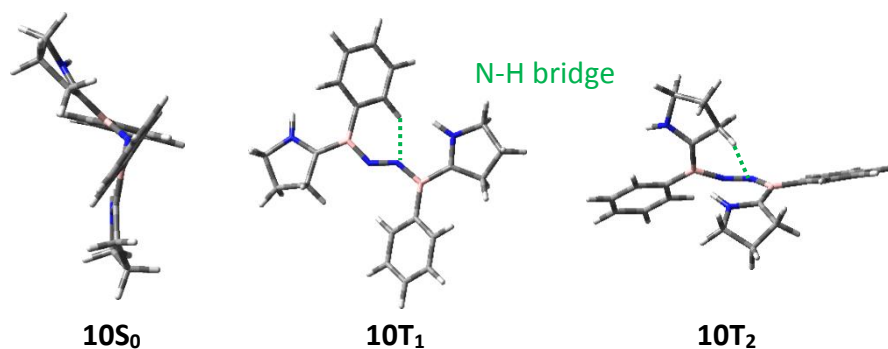
Figure 66: The global minimum structure **10S$_0$** of the singlet (left) and the triplet minimum structure **10T$_1$** (middle) and the conformer **10T$_2$** (right).

Consequently, adding substituents to the boron atom seems to have a greater impact on the electronic features of the singlet rather than the triplet. With a singlet triplet gap of 14 kcal/mol, the gap size remains the same as for the smallest (**9**) and the complete system (**B$_2$N$_2$**). Also, the frontier orbitals of the singlet and triplet stay unchanged for subsystem **10**, as the same density distribution can be seen in Figure 67, the MOs for system **11** are not explicitly shown. While it is sometimes observed that substituents containing π-system appear in the frontier orbitals, this is not the case for the **B$_2$N$_2$** system.[521] It is noteworthy that although the triplet ground state **10T$_1$** possesses a N=N double bond character, a lot of rotamers exist, which only show small energy differences of about 3-5 kcal/mol. An example is shown in Figure 66 on the right. Considering the H···N distances it gets obvious that this interaction causes the differences in the rotamers. While in **10T$_1$** the smallest H···N distance can be seen between the hydrogen of a phenyl group and the nitrogen of the dinitrogen bridge (Figure 66, middle), in **10T$_2$** it is between the same nitrogen atom and a hydrogen of the carbene (Figure 66, right).
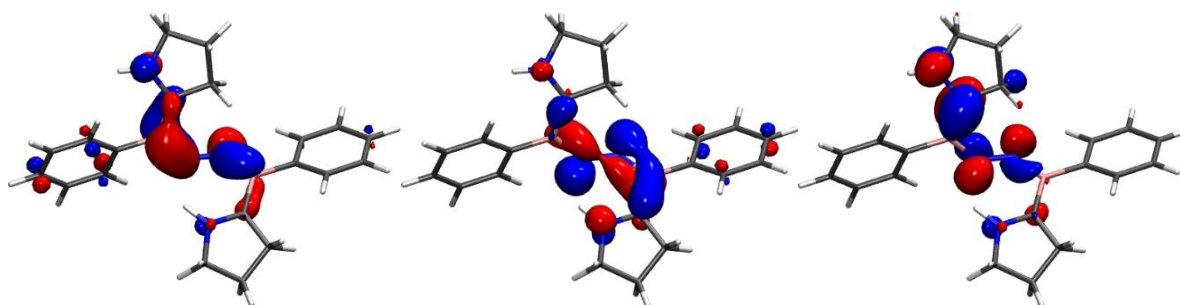
Figure 67: HOMO-1 (left), HOMO (middle) and LUMO (right) of the singlet **10S$_0$** of substructure **10**.

Structure **11** should possess similar electronic properties as the complete structure **B$_2$N$_2$**, since phenyl groups, which are quite similar to the Dip and duryl ligands of **B$_2$N$_2$**, are bound to the nitrogen and boron atoms. However, surprisingly a minimum structure is found, which is more

stabilized compared to the normally most favourable singlet and triplet geometries of substructures **9** and **10**. By arranging in a more twisted BNNB dihedral of 87°, it appears that the additional stabilization results from a π-π-interaction of three phenyl groups forming singlet **11S$_0$** (Figure 68, left). This nearly parallel arrangement with a small offset of the three phenyl groups with a distance of about 3.4 Å results in perfect conditions for π-π-interactions.[561]

11S$_0$ **11S$_1$**   **11T$_1$**
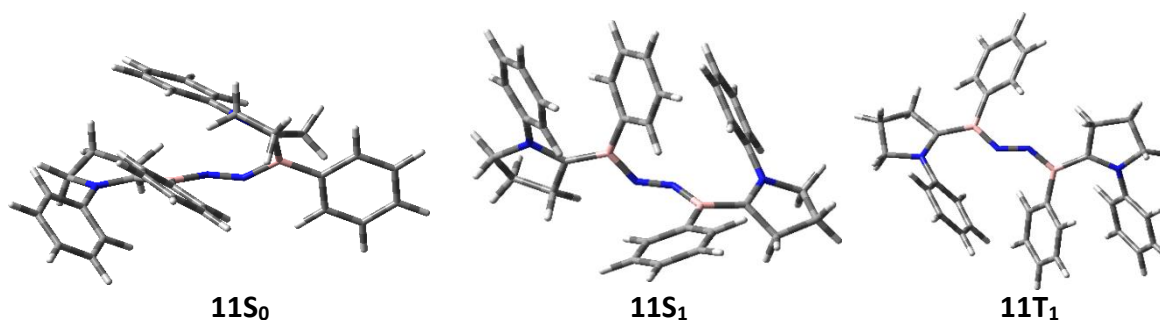
Figure 68: Geometry of singlet **11S$_0$** (left) and singlet **11S$_1$** (middle), which is higher in energy, and the triplet state **11T$_1$** (right).

If the dihedral widens up to 100°, which is the case for **11S$_1$** (Figure 68, middle), maximal two phenyl groups can interact in an increased, but feasible distance, while the third phenyl group is about 4 Å apart, as seen for structure **11S$_0$**. Thus, the second singlet structure is about 8 kcal/mol higher in energy than the first singlet structure. Except for one carbene ligand being slightly more rotated out-of-plane, in order to achieve a better conjugation, there is no further difference between the two singlet structures. The complete system **B$_2$N$_2$** arranges similar to singlet **11S$_1$**, since the geometric arrangement of singlet **11S$_0$** cannot be obtained due to addition of further steric hindrances. With increasing steric demand and the additional π-π-interactions caused by the phenyl groups, the triplet arranges not completely planar anymore forming a dihedral between 165° and 175°. However, this small distortion influences neither the energetic properties nor the electron density distribution, which remains the same as seen for the subsystems **9** and **10**.The ST gap of singlet **11S$_1$** and triplet **11T$_1$** shows a value of 14 kcal/mol, which is in the same region as for the smaller systems **9** and **10**. However, referring to the global minimum of singlet **11S$_0$**, the gap increases to 23 kcal/mol. By adding more sterically demanding alkyl groups to form the Dip or duryl groups, the gap decreases again to 12 kcal/mol, since the singlet **11S$_0$** arrangement is now not possible anymore. The KS orbitals of **11S$_0$** and **11S$_1$** correspond to the ones that were shown for the complete system **B$_2$N$_2$** (Figure 57) and the smaller subsystem **9** and **10** and are therefore not shown explicitly.

Since there are no noteworthy differences for the substructures **9-11** regarding their electronic properties, the substituents bound to the boron and to the carbene nitrogen do not influence the electronic properties of the system **B₂N₂**. The geometries of the smaller subsystems **9-11** are mainly dominated by other effects, such as hydrogen bonds or π-stacking, but these smaller changes in geometry do not affect the electronic properties of the systems themselves. Thus, the huge steric substituents are mainly needed to shield the molecule in order to improve its stability. Consequently, a more precise analysis of the smallest subsystem **9** can easily be transferred to the complete system **B₂N₂** regarding the electronic properties. The influence of the dihedral defining the bridge part $\sphericalangle_{\mathrm{BNNB}}$ seems to affect the system scarcely and by optimizing all the substructures **9**-**11** the singlet always takes a nearly orthogonal conformation, while the triplet planarizes. However, first of all, the geometry of complete system **B₂N₂** is analyzed more precisely and compared with its hydrogenated counterpart **B₂N₂H₂**.

To reveal the attempt of the complete system **B₂N₂** to arrange in the orthogonal distorted singlet minimum structure, nearby global minima are sought for and the rotational barrier of the system concerning the B-N-N-B is analyzed. Therefore, the planar conformation of the **B₂N₂H₂** system is used as starting point for the geometry optimization. By cutting of the hydrogens bound to nitrogen of the N₂ bridge of the planar **B₂N₂H₂** minimum structure, a different starting geometry for the **B₂N₂** molecule can be obtained. Thus, it can be investigated if the rotational barrier of twisting the molecule in the orthogonal singlet ground state geometry lies too high in energy to be realized or if there is another local minimum with a planar $\sphericalangle_{\mathrm{BNNB}}$ dihedral. The calculated barrier illustrates a size of about 20 kcal/mol. Consequently, room temperature seems to be enough to form the orthogonal structure independent on the starting geometry. It has to be noted that the starting structure obtained from **B₂N₂H₂** includes a N-N single bond, which changes during the optimization to a N=N double bond. The rotation around a N=N double bond requires more energy, which makes a rotation at room temperature unlikely.

Since the triplet states of both molecules **B₂N₂** and **B₂N₂H₂** are almost identical, no change in geometry is required when starting the optimization with the **B₂N₂H₂** geometry. By occupying the LUMO of **B₂N₂**, the planar structure with a N-N single bond gets more favourable, which ensures that there is no conjugation through the dinitrogen atoms. This leads to a biradical

form, in which both unpaired electrons are mainly localized on the carbon atoms of the carbene. Since the LUMO of **B₂N₂** includes a π^*-molecular orbital, occupying the LUMO weakens the N=N double bond. Because of this occupation in the triplet state of **B₂N₂**, the behavior is closely related to the one of **B₂N₂H₂.**

Shortly summarized, the singlet state favours an orthogonal formation with the carbene ligands in-plane, while the triplet tries to arrange completely coplanar independent of the substituents on the boron and the carbene nitrogen. Consequently, the $\sphericalangle_{BNNB}$ dihedral represents an important parameter, as it determines whether the singlet or triplet state is preferred.
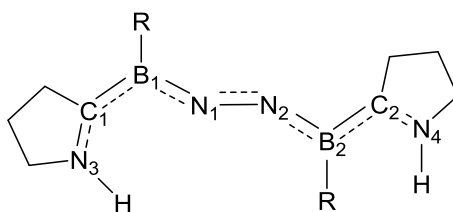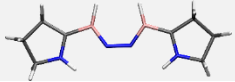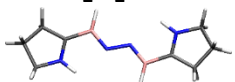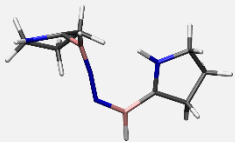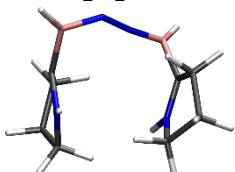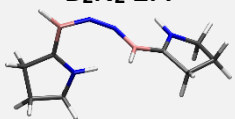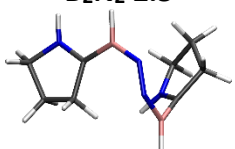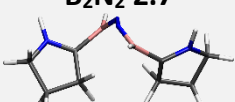
Figure 69: Basic structure of the **B₂N₂** molecule.

Therefore, the same analysis as already done for diborene in chapter 5.5 is performed for this kind of system (Figure 69). In the BNNB plane, the $\sphericalangle_{B_1N_1N_2B_2}$ dihedral is varied using values of 0°, 90° and 180°. Further important dihedrals, defining the plane between the boron-nitrogen compound and the carbene ligands, are $\sphericalangle_{N_3C_1B_1N_1}$ and $\sphericalangle_{N_1B_2C_2N_4}$. First of all, a unrestricted MN12L optimization is performed with an additional CASSCF optimization. Finally, a NEVPT2 single point calculation is performed on top to include dynamical correlation. Here, UMN12L predicts a singlet ground state for every conformation, while using CASSCF with NEVPT2 leads to a triplet ground state with coplanar structures. Considering different active spaces of the CASSCF calculation, the importance of the natural orbitals and natural occupation for a complete description, it becomes apparent that even **B₂N₂** possesses more electrons in the bridge BNNB part than the just boron containing diborene systems (see chapter 5). Only the two electrons of the HOMO play an important role, which results in an active space choice of two electrons in four orbitals. The singlet ground state of **B₂N₂** can be described by a formation of the three dihedrals with $\sphericalangle_{B_1N_1N_2B_2}$= 90° and both carbenes in-plane possessing a substituent with an angle of 0° and the other one 180°. Thus, it is not surprising that for the reduced model compound, **B₂N₂ 2.4** (Table 30) is found as the energetically lowest conformer.

Table 30: Different conformers starting from the all coplanar **B$_2$N$_2$ 2.0** by rotating one of the three dihedrals $\sphericalangle_{B_1N_1N_2B_2}$, $\sphericalangle_{N_3C_1B_1N_1}$ and $\sphericalangle_{N_1B_2C_2N_4}$ about 90°. The calculated NEVPT2/def2-TZVP energies are listed for each conformer in kcal/mol.

Conformer	$\sphericalangle_{N_3C_1B_1N_1}$	$\sphericalangle_{B_1N_1N_2B_2}$	$\sphericalangle_{N_1B_2C_2N_4}$	$\Delta E(S_1)$	$\Delta E(T_1)$	ST_{gap}
B$_2$N$_2$ 1.0	180	0	180	27.3	25.5	-1.7
B$_2$N$_2$ 2.0	0	180	0	18.8	13.9	-4.9
B$_2$N$_2$ 2.1	90	180	0	30.4	33.9	3.5
B$_2$N$_2$ 2.3	90	180	90	41.2	51.4	10.2
B$_2$N$_2$ 2.4	0	90	180	0.0	33.4	33.4
B$_2$N$_2$ 2.5	90	90	180	18.4	48.5	30.1
B$_2$N$_2$ 2.7	90	90	90	33.5	62.4	28.9

However, starting point for these various conformers is the all coplanar conformer **B$_2$N$_2$ 2.0**, with a *trans*-conformation of the $\sphericalangle_{B_1N_1N_2B_2}$ dihedral of 180°. Considering the *cis*-transformation $\sphericalangle_{B_1N_1N_2B_2} = 0°$, **B$_2N_2$ 1.0** is formed, which increases in energy for both the singlet and the triplet state compared to its *trans* counterpart. By rotating the dihedrals $\sphericalangle_{N_3C_1B_1N_1}$ or $\sphericalangle_{N_1B_2C_2N_4}$, more coplanar rotamers can be formed. Since these systems are higher in energy, they are not included in this consideration.

For the two all coplanar conformers **B$_2$N$_2$ 1.0** and **B$_2$N$_2$ 2.0** the triplet was determined to be the ground state. Furthermore, **B$_2$N$_2$ 1.0** and **B$_2$N$_2$ 2.0** show a N-N single bond with a bond length of 1.4 Å. However, the B-N and C-N bonds tend to form a double bond, which can be

seen in the bond length and also the Wiberg bond indices listed in Table 31. Despite the small ST gap and the similar geometries of the singlet and triplet for **B$_2$N$_2$ 1.0** and **B$_2$N$_2$ 2.0**, the singlet prefers the closed shell occupation. Consequently, the singlet forms a single N-N bond, too, with only a little fraction of multiple bond character and a small amount of biradical character for both conformations. Regarding the all coplanar conformers, **B$_2$N$_2$ 2.0** forms the most favorable arrangement. The *cis*-configuration of **B$_2$N$_2$ 1.0** is about 10 kcal/mol higher in energy than its *trans*-conformer **B$_2$N$_2$ 2.0**. This trend should increase for larger substituents on the boron. For both systems, the spin density of the two electrons is localized on each side of the N-N bond but delocalized over the complete N-C-B-N part with a great amount of the spin density at the carbon atoms (Table 33). It can be seen that a relative high amount of the free radicals of triplet state is located on the boron atoms, which can result in an increase of the total energy, since this is energetically unfavorable for boron atoms. An explanation for the behavior of the coplanar conformers can be seen in the KS orbitals (Table 32). Although **B$_2$N$_2$ 2.0** shows a triplet ground state, the singlet KS orbitals are shown, as the orbitals are identical to the ones of the triplets and the other conformers provide always a singlet ground state.

Table 31: Wiberg indices of the various conformers of **B$_2$N$_2$**.

Conformer	N_1-C_1	C_1-B_1	B_1-N_2	N_2-N_3	N_3-B_2	B_2-C_2	C_2-N_4
B$_2$N$_2$ 1.0	1.48	0.95	1.78	1.11	1.78	0.95	1.48
B$_2$N$_2$ 2.0	1.47	0.96	1.74	1.14	1.74	0.96	1.47
B$_2$N$_2$ 2.1	1.42	0.81	1.80	1.16	1.48	1.22	1.25
B$_2$N$_2$ 2.3	1.29	0.80	1.82	0.99	1.75	0.87	1.34
B$_2$N$_2$ 2.4	1.39	1.08	1.20	1.60	1.20	1.08	1.39
B$_2$N$_2$ 2.5	1.47	0.83	1.88	1.15	1.43	1.23	1.22
B$_2$N$_2$ 2.7	1.42	0.84	1.78	1.01	1.78	0.83	1.42

The KS orbitals of **B$_2$N$_2$ 2.0** possess similarities to the ones of **B$_2$N$_2$H$_2$**, since both states illustrate a biradical ground state with a HL gap <20 kcal/mol that is otherwise (**B$_2$N$_2$ 2.1**, **B$_2$N$_2$ 2.4**) between 30-50 kcal/mol (Table 32). For **B$_2$N$_2$ 2.0**, the occupation of the LUMO, as it is the case for the triplet, results in an increased antibonding character of the nitrogen atoms. Thus, the system **B$_2$N$_2$ 2.0** exhibits more N-N single bond than N=N double bond character with slightly extended bond length of 1.39 Å compared to all other conformers.

Table 32: Frontier KS orbitals of the singlet state of depicted conformers **B$_2$N$_2$ 2.0**, **B$_2$N$_2$ 2.1** and **B$_2$N$_2$ 2.4**. Energies are given in kcal/mol.

Conformer	HOMO-1	HOMO	LUMO
B$_2$N$_2$ 2.0	-78.2	-77.0	-60.6
B$_2$N$_2$ 2.1	-94.4	-89.3	-42.5
B$_2$N$_2$ 2.4	-94.1	-87.8	-40.4
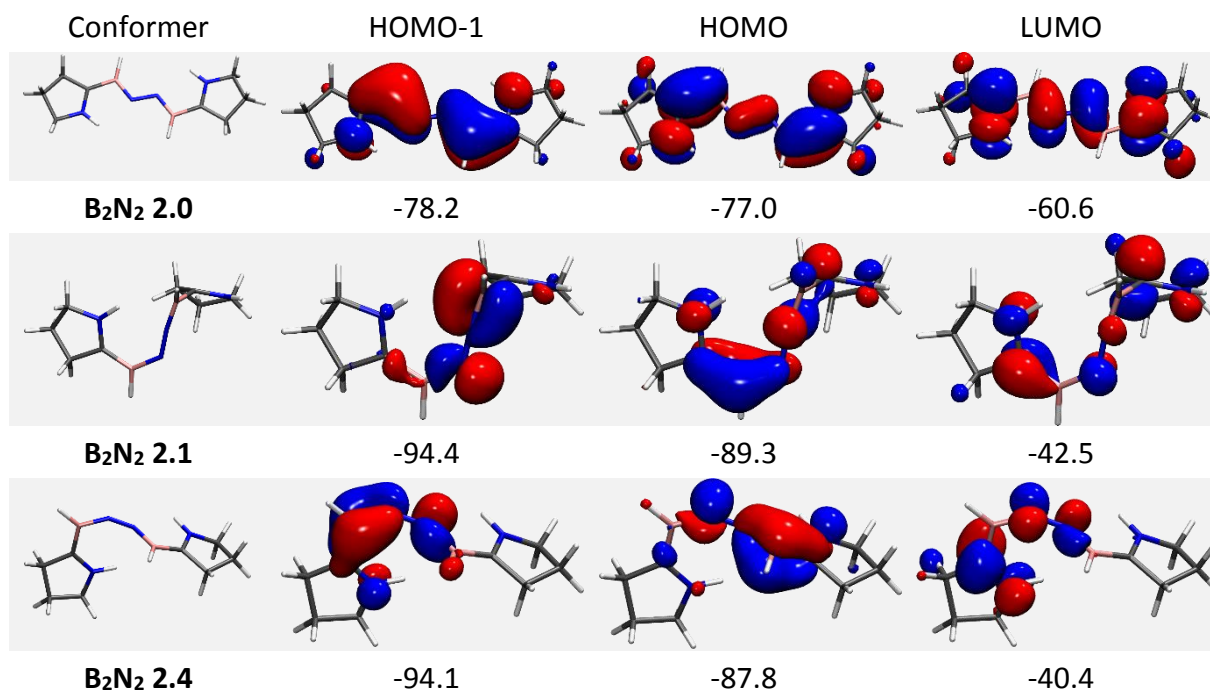
However, as the triplet ground state of **B$_2$N$_2$** exhibits this conformation, it is not surprising to find the conformer **B$_2$N$_2$ 2.0** as the one with the energetically lowest triplet.

Twisting one carbene ligand out-of-plane can be achieved by a rotation of 90° around the $\sphericalangle_{N_3C_1B_1N_1}$ or $\sphericalangle_{N_1B_2C_2N_4}$ dihedral, obtaining conformers **B$_2$N$_2$ 2.1** and **B$_2$N$_2$ 2.2**. Since both conformers show nearly identical behavior, even though the system appears to be not symmetrical to the BNNB bridge, only the first conformer is shown here more precisely. **B$_2$N$_2$ 2.1** arranges with one orthogonal carbene unit $\sphericalangle_{N_3C_1B_1N_1} = 90°$ and the remaining part stays in one plane. Caused by this twist, the singlet becomes the ground state again, as it only gets slightly destabilized (12 kcal/mol) by twisting one carbene out-of-plane. The energy of the triplet increases about 20 kcal/mol resulting in a ST gap of nearly 4 kcal/mol, in which the singlet lies energetically lower. Considering the KS orbitals, it can be noticed that the HL gap of **B$_2$N$_2$ 2.1** increases compared to **B$_2$N$_2$ 2.0** with a HL gap of 35 kcal/mol (Table 32). The HOMO and HOMO-1 show nearly the same appearance, just located on different sides of the BNNB bridge. With a conjugation over the C_1-B_1-N_2 atoms and an antibonding character to the N_1 and N_3, the orbitals look identical to the HOMO-1 of the complete system **B$_2$N$_2$**, even though one carbene is out-of-plane. It is noteworthy that on the orthogonal side of **B$_2$N$_2$ 2.1**, the B-C conjugation deteriorates, which can be seen in the decreased Wiberg index of 0.81

(Table 31). Therefore, the B-N bond illustrates a higher multiple bond character (1.80) compared to the all coplanar geometries (Table 31). However, the carbene ligand, which stays in-plane, gets also affected showing a contrary behavior with an enlarged B-N bond and decreased B-C bond length and the thereof altered bond character, which fits perfectly to the shifts of the bond length. A conjugation of the C_1 and N_2 is observable, too, and the overlap is substantial enough to obtain a Wiberg bond index of 0.1. This can be influenced by the physical proximity of C_1 and N_2 caused by the out-of-plane distortion.

By a distortion of both carbene ligands, resulting in conformer **B_2N_2 2.3**, an even higher destabilization occurs. The singlet and triplet increase again in energy (about 11 kcal/mol and 18 kcal/mol) leading to a ST gap of 10 kcal/mol, with the singlet appearing energetically more stable than the triplet. This trend completes the adoption of the destabilization of the system by twisting one or two carbene out-of-plane, with the triplet rising in energy. Because of the missing conjugation with the carbene ligands, the N-N bond length increases and the correlated Wiberg bond index decreases (Table 31). The bond length between the carbene and the boron increases leading to less π-back bonding from the boron to the carbene and vice versa. Thus, the B-N bond length gets close to a double bond on both sides of the systems. For **B_2N_2 2.1**, this was just seen on the twisted carbene side. Consequently, by twisting one or two carbenes out-of-plane, the B-N bond increases in multiple bond character affecting the N-N bond to just form a N-N single bond.

Regarding the energetically lowest conformer **B_2N_2 2.4**, the $\sphericalangle_{B_1N_1N_2B_2}$ is distorted by 90°, while the other dihedrals favors to stay in-plane. In comparison to **B_2N_2**, the ST gap increases to 33 kcal/mol for **B_2N_2 2.4**, as the triplet is forced by constrained optimizations to arrange in a BNNB twisted geometry and is not able to obtain the preferred planar structure. The KS orbitals of **B_2N_2 2.4** are identical to those of **B_2N_2** with a HL gap of nearly 50 kcal/mol. Thus, an occupation of the triplet seems to be very unlikely. For the planar structure **B_2N_2 2.0**, which arranges similar to **$B_2N_2H_2$**, the spin densities closely resemble those of the hydrogenated molecule showing a conjugation over the complete N-C-B-N part without conjugation between the two nitrogen atoms. If a conjugation between the two nitrogen atoms is existent, as it is the case for **B_2N_2 2.4**, the spin densities are not equally localized on both sides of the system anymore (Table 33). On the left side, the highest amount of spin density is localized on the carbon C_1 and nitrogen N_2 atom, with a huge amount on boron B_2, too. This trend reveals

the fact that the triplet is highly unfavorable in this conformation and the singlet possesses a completely closed shell occupation. The bonding pattern of **B_2N_2 2.4** appears in the same way as for **B_2N_2**, with a N=N double bond and multiple bond character in the N-C-B-N part. Since the frontier KS orbitals only involve antibonding parts of the N-N π- bond, the HOMO-6 and HOMO-4 are plotted in Figure 70 to emphasize the π contribution to of the N=N double bond. Considering these orbitals, two π-orbitals are formed, which are in one plane with the p-orbital of the one nitrogen and the sp²-orbital of the other one. This intensifies the assumption of the double bond being formed as an overlap of these two orbitals.

Table 33: Distribution of the amount of spin densities on the involved atoms considering the triplet states of the various conformers.

Conformer	N_1	C_1	B_1	N_2	N_3	B_2	C_2	N_1
B_2N_2 1.0	0.19	0.47	0.21	0.17	0.17	0.21	0.47	0.19
B_2N_2 2.0	0.20	0.44	0.18	0.17	0.17	0.19	0.47	0.20
B_2N_2 2.1	0.07	0.24	-0.07	0.22	0.45	0.25	0.63	0.19
B_2N_2 2.3	0.19	0.65	0.09	0.14	0.00	0.18	0.60	0.19
B_2N_2 2.4	0.18	0.68	-0.07	0.75	-0.46	0.47	0.29	0.21
B_2N_2 2.5	0.16	0.74	-0.28	0.97	-0.34	0.62	0.05	0.08
B_2N_2 2.7	0.16	0.80	-0.02	0.05	0.06	-0.02	0.80	0.16

Another interesting aspect is the out-of-plane distortion of carbene ligands starting from the singlet ground state structure with the lowest energy (**B_2N_2 2.4**). Beginning with the **B_2N_2 2.4** conformer, the influence of the carbene ligands is also analyzed. By distorting one carbene out-of-plane, resulting in **B_2N_2 2.5** and **B_2N_2 2.6**, a similar trend, as the one seen on **B_2N_2 2.1**, can be observed. It does not matter which carbene ligands is twisted since **B_2N_2 2.5** and **B_2N_2 2.6** provide identical results, wherefore only **B_2N_2 2.5** is shown. The effect is the same as seen before, irrespective of which carbene is twisted. Considering the singlet state, the energy increases about 18 kcal/mol compared to **B_2N_2 2.4**, when both carbene ligands are in-plane.

Since the triplet of **B_2N_2 2.4** is already destabilized about 33 kcal/mol compared to the singlet ground state, the triplet state of **B_2N_2 2.5** and **B_2N_2 2.6** show an energy increase of about 49 kcal/mol compared to the minimum structure. Thus, the difference between the triplet of **B_2N_2 2.4** and **B_2N_2 2.5** is about 15 kcal/mol resulting in a slightly decreased ST gap (30 kcal/mol) of the twisted **B_2N_2 2.5** conformer compared to **B_2N_2 2.4**.

In analogy to the $\sphericalangle_{B_1N_1N_2B_2}$ planar conformers, the bonding pattern changes caused by the decreased conjugation between the boron and the carbene carbon atom. This results again in an increased B-N bond character and a weakened N-N multiple bond compared to the N=N double bond in **B₂N₂ 2.4**, which can be seen in the bond length and the Wiberg indices (Table 31). Regarding the spin densities, a similar trend to **B₂N₂ 2.4** is visible with an even larger shift of the spin density to the carbon C_1, nitrogen N_2 and boron B_2 atom. Even the biradical triplet state gets highly unfavorable for **B₂N₂ 2.5** and the singlet tends to possess a higher amount of biradical character compared to **B₂N₂ 2.4**.
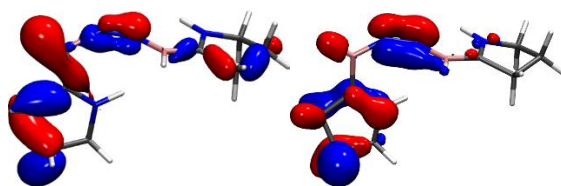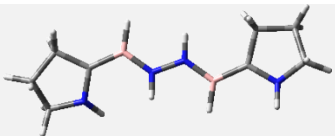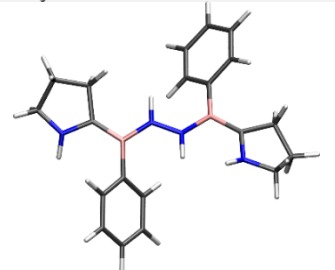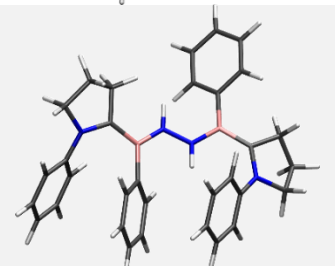
Figure 70: HOMO-6 (left) and HOMO-4 (right) of the smallest system **B₂N₂ 2.4** with a conformation close to the complete system.

To gain a complete impression, conformer **B₂N₂ 2.7** is investigated, in which both carbene ligands arrange in an orthogonal dihedral to their concerning BN part ($\sphericalangle_{N_3C_1B_1N_1} = \sphericalangle_{N_1B_2C_2N_4} = 90°$). With an energy increase of 15 kcal/mol for the singlet and 14 kcal/mol for the triplet, the same trend as for the single twisted conformers **B₂N₂ 2.5** and **B₂N₂ 2.6** is seen. Caused by the distorted carbene ligands, the C-B conjugation is lost on both sides of the system resulting in B-N double bonds and thus a N-N single bond (Table 31). Due to this prevented conjugation between the nitrogen atoms, the spin densities are again located on each side of the N-N bridge. Symmetrically distributed, the highest amount of spin density is located at the carbene carbon atoms with a small proportion at the nitrogen atoms (Table 33). This allocation provides the most favorable position of the free electrons resulting in the highest amount of biradical character of the singlet for all conformers along with **B₂N₂ 2.3**. However, as these conformations, **B₂N₂ 2.3** and **B₂N₂ 2.7**, appear as highly unfavorable due to the energetic destabilization these geometries are not likely to be adapted. For both conformers, the closed shell singlet state lies so high in energy that the biradical singlet state is close by, revealing that the true singlet state appears as a mixture of both. To exist as stable system, the molecule needs two carbene ligands, which can interact with the boron, implicating that the boron is able to shift some π-density to the carbon atoms of the carbene and the nitrogen.

6.4 Influence of the substituents in the $B_2N_2H_2$ molecule

The influence of the substituents on the novel biradical system $B_2N_2H_2$ is also investigated. For this purpose, subsystems of $B_2N_2H_2$ were established in analogy to the B_2N_2 system. First of all, only the geometry of the complete molecule $B_2N_2H_2$ was used as starting system for the smaller substructures **12-14** varying the substituents bound to the nitrogen and boron atoms. The same functionals as for B_2N_2, UMN12L with 6-311G(d, p) basis sets, are used for the optimization. The relative energies are obtained by additional NEVPT2 single point calculation on the UMN12L geometry. However, as seen for B_2N_2, NEVPT2 and UMN12L predict the same structural arrangement and energetic positions of the substructures and their conformers. In Table 34, an overview of the geometrical arrangement and multiplicity of the ground state of each substructure is depicted, as well as their concerning adiabatic ST gap.

Table 34: Different substructures **12-14** of $B_2N_2H_2$ with varying substituents R_1 and R_2 with their concerning ground state multiplicity, ST gap and dihedral, calculated with NEVPT2/def2-TZVP.

Substructures of $B_2N_2H_2$	Substituent R_1 and R_2	Ground state	$\sphericalangle_{BNNB}$ [°]	ST gap [kcal/mol]
12	R_1 = Hydrogen R_2 = Hydrogen	singlet	87	5
13	R_1 = Hydrogen R_2 = Phenyl	singlet	44	4
14	R_1 = Phenyl R_2 = Phenyl	singlet	43	2

Considering the frequencies and absorption numbers of the different obtained structures, it turned out that for the smaller structures **12-14** the global minimum was not found. Thus, apart from the optimizations with nearly the same geometry as calculated for the whole molecule **$B_2N_2H_2$**, different minimum structures are found differing strongly to the original ones. Therefore, the three structures **12-14** are analyzed more precisely. Starting with the smallest structure **12**, substituted with hydrogen atoms bound to boron and nitrogen of the carbene, different starting geometries are used to reveal the true minimum. By optimizing the system of a twisted starting structure, the singlet state **$12S_0$** appears as ground state with a dihedral $\sphericalangle_{BNNB}$ of 43° (Figure 71, left).
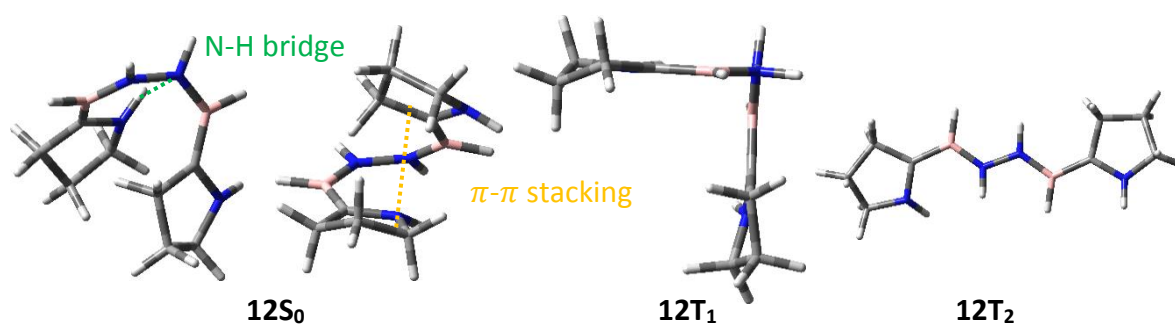
Figure 71: Singlet arrangement of **$12S_0$** for the smallest system **12** from two different views (middle left and left) and the two triplet states, one with orthogonal $\sphericalangle_{BNNB}$ **$12T_1$** (middle right) and the other one with a planar geometry **$12T_2$** (right).

The triplet state **$12T_1$** lies about 5 kcal/mol higher in energy. As assumed for the complete system **$B_2N_2H_2$**, it is also true for the smaller systems that the singlet should be a biradical or exhibits at least a significant biradical character, since the former HOMO and LUMO are singly occupied in the active space. In contrast to the complete system, the triplet **$12T_1$** of the smaller molecule **12** arranges in an orthogonal geometry with a $\sphericalangle_{BNNB}$ dihedral of 87°. Although the arrangement of the BNNB bridge partly changes, the $\angle_{CBN}$ angle stays between 124-130° for the various conformers of **12**, with a N-N single bond of 1.40 Å for **$12S_0$** and **$12T_1$**. The geometry of **$12S_0$** is depicted from different views on the left side in Figure 71. It gets clear, that even the BNNB core is distorted about 45°, therefore, the carbenes are in-plane with each side of the bridge. By this helix shaped arrangement, π-π stacking between the five membered rings becomes possible. Additionally, it can be assumed that a hydrogen bond N-H···N between the hydrogen of the carbene and the nitrogen of the BNNB bridge is built corresponding to the distance of 2.4 Å between hydrogen and nitrogen. This hydrogen bond can be perfectly seen in the illustration of **$12S_0$** (green dotted line Figure 71, left). A similar hydrogen bond can also be found in the distorted triplet **$12T_1$** (Figure 71, middle right), with a slightly increased N···H

distance of 2.5 Å. Only the complete coplanar geometry of triplet **1T$_2$** (Figure 71, right) includes no hydrogen bond, which may explain the energetic differences of 5 kcal/mol compared to the orthogonal triplet **12T$_1$**. As the singlet **12S$_1$** with the same coplanar geometry lies about 7 kcal/mol higher in energy than the orthogonal conformer, it can be assumed that this hydrogen bond stabilizes the triplet about 5-7 kcal/mol, depending on the N···H distance. Since **12S$_1$** possesses a nearly identical geometric arrangement as **12T$_2$**, it is not presented here explicitly.

To ensure that the differences in energy are caused by the hydrogen bonds and no other electronic effects, the Kohn-Sham orbitals of both, the planar and twisted singlet structure, are investigated. Therefore, the three frontier KS orbitals (HOMO, SOMO and SOMO+1) of the distorted singlet state **12S$_0$** are shown in Figure 72. Since this singlet state occurs as a biradical, too, there are no differences in the electron density distribution of the singlet **12S$_0$** and triplet **12T$_1$**. Consequently, only the KS orbitals of the singlet are shown here. In Figure 73, the frontier orbitals of the all coplanar singlet arrangement **12S$_1$** are illustrated. Considering the orbitals of the singlet and the triplet of the coplanar arrangement, it is obvious that they are nearly identical concerning their appearance and electronic localisation. The KS orbitals of the two different singlet states **12S$_0$** and **1S2$_1$** (Figure 72 and Figure 73) show that even though the structures are completely different, the electron density distribution is almost identical.
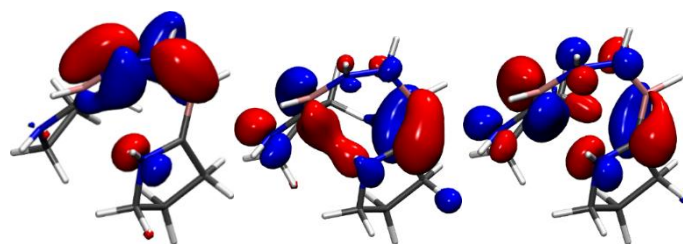
Figure 72: HOMO, SOMO and SOMO+1 frontier orbitals of the twisted singlet structure **12S$_0$**.

Compared with the KS orbitals of the complete structure **B$_2$N$_2$H$_2$**, there seems to be no differences regarding the electron density distribution of both molecules. Due to the calculated rotational barrier of only 5 kcal/mol in combination with a N-N single bond, a rotation around this bond is possible. Thus, it becomes apparent that the energetic differences of the various singlet and triplet geometries are predominated by other effects, such as hydrogen bonding (subsystem **12**) or π-stacking.
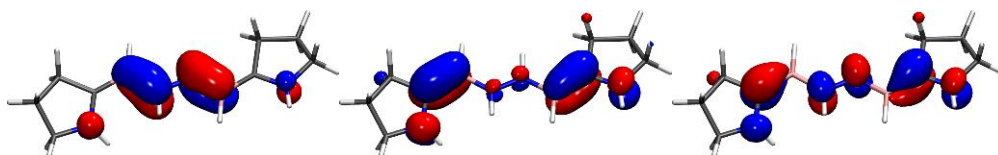
Figure 73: HOMO, SOMO and SOMO+1 frontier orbitals of the planar singlet state **12S$_1$**.

Since π-stacking is more easily possible if phenyl rings are added to the system, the same analysis was performed adding a phenyl ring to the boron atom leading to system **13** with a hydrogen atom bound to the carbene nitrogen (Figure 74). A similar behavior of the geometries, as already seen for system **12**, is found. For both multiplicities, a more favourable distorted geometry is calculated apart from the all coplanar arrangement, which is found in the complete system **B$_2$N$_2$H$_2$**. The singlet geometry **13S$_0$**, with a distorted dihedral of about $\sphericalangle_{\text{BNNB}}$= 44°, illustrates the energetically lowest conformer with a ST gap of 4 kcal/mol to the also twisted triplet **13T$_1$** ($\sphericalangle_{\text{BNNB}}$= 50°). Further properties, such as the bond lengths, the remaining dihedrals and the bonding pattern correspond to the values obtained for the smaller system **12** ($\sphericalangle_{\text{BNNB}}$= 50°). The electron density distribution also remains the same. Therefore, the KS orbitals of these geometries, which are equivalent to the orbitals of the hydrogen substituted structure **12**, are not shown here. The all planar singlet state **13S$_1$** lies 10 kcal/mol higher in energy than the singlet ground state **13S$_0$**. Both structures are illustrated in Figure 74 in order to determine the differences in the geometric arrangement and the resulting differences in energy. Since for the geometric arrangement of the triplet states of subsystem **13** no differences are found, the geometries are not shown explicitly. Analog to the singlet state, two conformers appear, a twisted **13T$_1$** conformer and an energetically higher coplanar conformer **13T$_2$**.
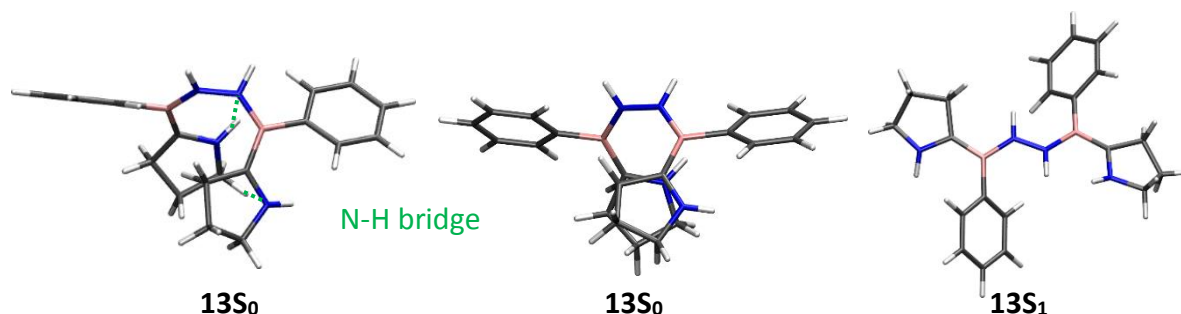
Figure 74: Illustration of both singlet states, **13S$_0$** from two different sights of view (left, middle) and **13S$_1$** (right) of subsystem **13**.

In the left singlet state (Figure 74), the N-H$\cdots$N hydrogen bond is visible, which tends to favour the geometry as seen before (**12S$_0$** of structure **12**). Additionally, π-π-interaction between

both nitrogen atoms of the carbenes is possible. This further stabilizing interaction results in a higher energy difference in comparison to the all planar structure **13S$_1$** of 10 kcal/mol. Considering the triplet geometries, the same size of the ST gap of the coplanar triplet **13T$_2$** compared to the distorted conformer of the same multiplicity **13T$_1$** is found. Thus, the differences between the biradical singlet ground state and triplet appear to be very small resulting in geometries that are mainly affected by hydrogen or π-interactions.

The last interesting aspect is the substitution of both, the nitrogen of the carbene and the boron atoms, with phenyl groups to create a significant combination of π-interaction effects and steric hindrances. Thus, conformers of structure **14** exhibit a different trend as the subsystems **12** and **13** before. Again, the KS orbitals are not illustrated, since the electronic structure of the frontier orbitals seems to be independent of both, the size of the substituents bound to nitrogen and boron and the conformation, which is taken. As seen for the smaller substructures before, mainly two conformers exist, the ones with a distorted $\sphericalangle_{B_1N_1N_2B_2}$ and the others with a complete coplanar geometry. However, for structure **14**, the twisted singlet **14S$_0$** ($\sphericalangle_{BNNB}$= 43°, Figure 75, left and middle) and the triplet geometry of the coplanar system **14T$_1$** ($\sphericalangle_{BNNB}$= 178°, Figure 75 right) are nearly degenerate, with the singlet **14S$_0$** about 1-2 kcal/mol lower in energy than the triplet **14T$_1$**. Since the mean absolute deviation of NEVPT2 is about 2-4 kcal/mol, it cannot be excluded that the singlet is the actual ground state, with an ST gap smaller than the MAD of the method.

14S$_0$ **14S$_0$** **14T$_1$**
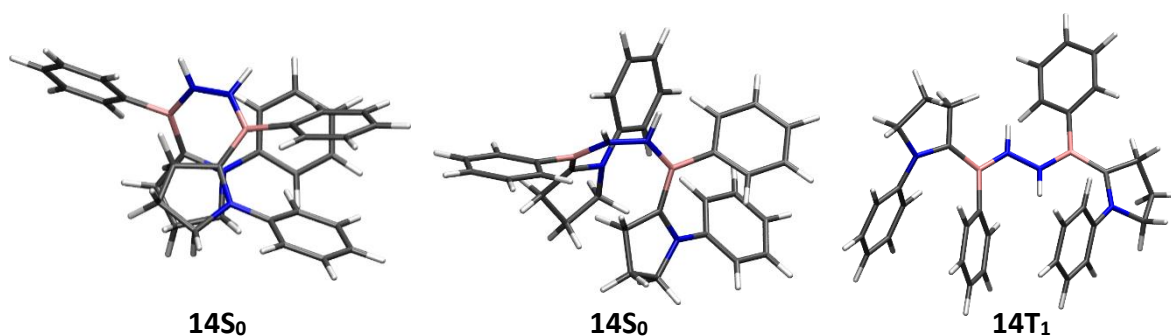
Figure 75: Geometry of the distorted twisted singlet state **14S$_0$** of two different sights of view (left and middle) and the planar triplet **14T$_1$** on the right side.

The triplet **14T$_2$** (not explicitly shown) with the same distorted arrangement as shown for **14S$_0$** lies about 4 kcal/mol higher in energy than its planar conformer **14T$_1$**. As singlet **14S$_1$** with the coplanar geometry is identical to the planar **14T$_1$**, it is not explicitly shown here. The conformer **14S$_1$** possesses the highest energy with a difference of 8 kcal/mol to **14S$_0$**. Regarding the

π-interaction between both geometries, the twisted structure (Figure 75, left and middle) shows a conjugation along the phenyl group of the carbene and the boron atom close to the involved carbene. With a distance of about 3.4 Å between the phenyl groups, a stabilization effect caused by π-stacking is highly possible. In addition to the sandwich π-stacking, the phenyl group of the second carbene arranges in a T-shape respective to the two phenyl groups of **14S$_0$** to form another form of π-stacking.[561] For the all coplanar triplet geometry **14T$_1$** (Figure 75, right), it can be clearly seen that the same three phenyl groups perform π-stacking. Caused by the different structural arrangement all three phenyl groups order in a sandwich conformation with 3.5-4.1 Å between the single phenyl units. Thus, it appears that both geometries, the distorted and the coplanar structure, show the same stabilizing interactions. This leads to the assumption that the singlet prefers the twisted structure, where the steric strain is released, while the triplet attempts to arrange all coplanar. With a slightly decreased rotational barrier between both conformations of subsystem **14** of about 8 kcal/mol, it is most likely that a combination of the various conformers is present.

To investigate the rotational barrier of the complete system and the stabilities of both conformers, an optimization starting from the distorted **B$_2$N$_2$** geometries was performed. Both, the starting structure (left) and the final minimum (right), are depicted in Figure 76. While the smaller subsystem **12**-**14** tend to arrange in the distorted geometry and the **B$_2$N$_2$** molecule demonstrates that is possible to take this conformation despite steric hindrances, the **B$_2$N$_2$H$_2$** favours an all coplanar geometry for the complete system. This might be caused by the additional steric hindrances appearing in the whole system, which prevents the assembly in a geometry, which favours π-stacking. Irrespective of the starting structure, the dihedral ($\sphericalangle_{BNNB}$) was varied between 40° and 120°.
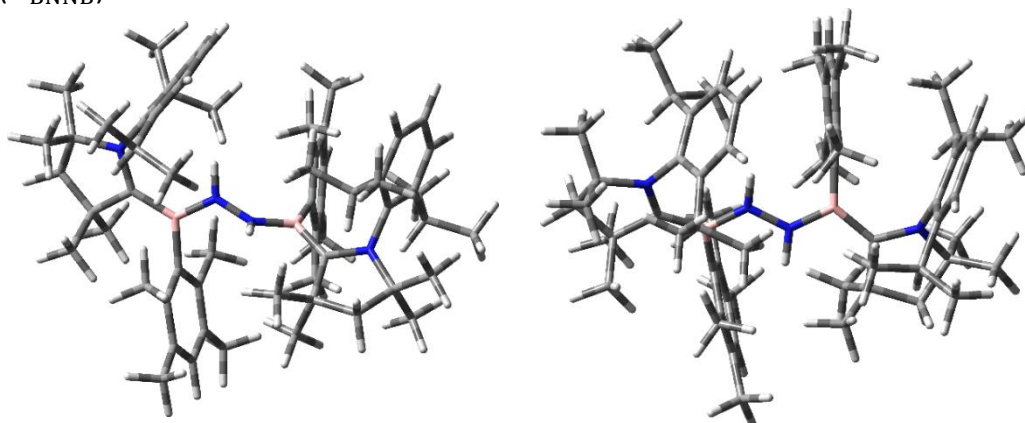
Figure 76: Starting structure with a $\sphericalangle_{BNNB} = 50°$ (left) and the optimized geometry with $\sphericalangle_{BNNB} = 170°$ (right) of the complete system **B$_2$N$_2$H$_2$**.

The minimum structure always arranges coplanar with a dihedral of $\sphericalangle_{BNNB}= 167°$. Since the molecule can rotate freely around the N-N single bond and the barrier was calculated to be only 10 kcal/mol, it is most likely that the molecule arranges always in the all coplanar geometry for both the singlet and the triplet state.

Considering the smaller substructures **12-14**, it can be assumed that the geometries and their corresponding energetic location does not depend on the electronic influences of the conjugated system. Thus, only the smallest structure, with hydrogen atoms as substituents, was further investigated concerning the importance of the conjugation of the BNNB compound or the carbene stabilization. This analysis was performed analog to the one performed in chapter 6.3 by rotating the important dihedrals. A schematic representation of the basic structure is given in Figure 77 with the numbering of the important atoms to define the dihedrals.
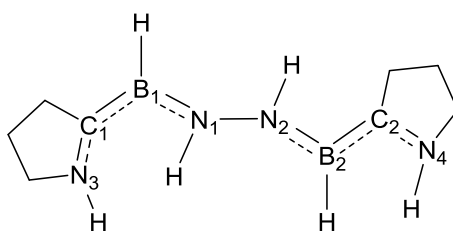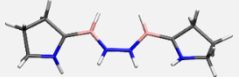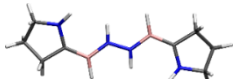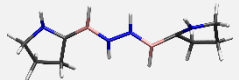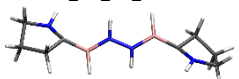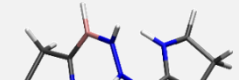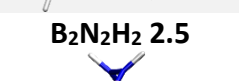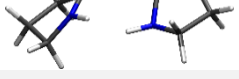
Figure 77: Basic system of the smallest substructure of **$B_2N_2H_2$** numbering all important atoms.

In analogy to the previous analysis, three important dihedrals, $\sphericalangle_{N_3C_1B_1N_1}$, $\sphericalangle_{B_1N_1N_2B_2}$ and $\sphericalangle_{N_2B_2C_2N_4}$, are twisted around 0°, 90° or 180° to investigate the influence of the related conjugation. The structures are obtained with a constrained optimization using UMN12L or CASSCF and by freezing the three dihedrals in their respective position. On top a NEVPT2 calculation with def2TZVP was performed. The various conformers differing in the frozen dihedrals ($\sphericalangle_{N_3C_1B_1N_1}$, $\sphericalangle_{B_1N_1N_2B_2}$ and $\sphericalangle_{N_2B_2C_2N_4}$) are shown in Table 35. Additionally, to the geometric parameters, the relative singlet and triplet energies with respect to the minimum energy of conformer **$B_2N_2H_2$ 2.4** are listed. In the right column of Table 35, the adiabatic ST gap obtained by NEVTP2/def2-TZVP calculation is presented. Only the NEVPT2 results are shown, as all three results, SF-DFT, NEVPT2 and UMN12L, agree excellent with each other and show no discrepancies.

Table 35: Different conformers obtained from the all coplanar **B₂N₂H₂ 2.0** by rotating one of the three dihedrals ($\sphericalangle_{N_3C_1B_1N_1}$, $\sphericalangle_{N_1B_2C_2N_4}$ and $\sphericalangle_{B_1N_1N_2B_2}$) about 90°. The calculated NEVPT2/def2-TZVP energies are listed for each optimized singlet and triplet state with respect to the energy of the energetically lowest conformer. Also, the adiabatic ST gap is given.

Conformer	$\sphericalangle_{N_3C_1B_1N_1}$	$\sphericalangle_{B_1N_1N_2B_2}$	$\sphericalangle_{N_2B_2C_2N_4}$	$\Delta E(S_1)$	$\Delta E(T_1)$	ST_{gap}
B₂N₂H₂ 1.0	180	0	180	14.5	13.9	-0.5
B₂N₂H₂ 2.0	180	180	180	8.7	8.6	-0.1
B₂N₂H₂ 2.1	90	180	180	22.9	16.9	-6.0
B₂N₂H₂ 2.3	90	180	90	40.1	32.0	-8.0
B₂N₂H₂ 2.4	0	90	0	2.0	0.0	-2.0
B₂N₂H₂ 2.5	90	90	0	21.5	18.4	-3.2
B₂N₂H₂ 2.7	90	90	90	38.4	34.4	-4.4

Since the complete system is all coplanar (Figure 60), this arrangement is chosen as the starting system. However, the twisted arrangement obtained by a full optimization of the smallest system is not considered. There are two main arrangements that are possible for a planar BNNB geometry, either the substituents bound to the boron atoms take a *cis-* or a *trans*-conformation. With a $\sphericalangle_{B_1N_1N_2B_2}$ of 0° the less favourable *cis*-transformation is obtained resulting in **B₂N₂H₂ 1.0** (Table 35). By twisting the dihedral of about 180°, the more favourable *trans*-geometry **B₂N₂H₂ 2.0** results (Table 35). This arrangement is about 6 kcal/mol lower in energy than its *cis*-conformer, whereas this difference is supposed to increase further with the size of the substituents bound to boron. The ST gap of the *trans* **B₂N₂H₂ 2.0** appears close

to zero, with a triplet ground state. However, it must be noted that within the small mean error of NEVPT2 it cannot be excluded that the singlet is the real ground state.

Considering the bonding pattern or rather Wiberg indices of these systems, it is obvious that in the smaller system a N-N single bond is formed (Table 36). The multiple bond character extends from the carbene carbon over the boron to the nitrogen atom of each side of the N-N bridge; however, without a conjugation over the N-N bridge. The NEVPT2 calculation reveals a strong biradical character of nearly 90% in the energetically lowest singlet state of **B$_2$N$_2$H$_2$ 2.4** and for most of the other conformers. This explains the small singlet triplet gaps, and the fact that the singlet and triplet arrange nearly in the same geometry and exhibit both a tremendous amount of biradical character. Only for **B$_2$N$_2$H$_2$ 2.7** this character decreases to 36%.

Furthermore, by combining the frontier orbitals (SOMO and SOMO+1, see Table 38) linearly, orbitals, which only possess electron density on one side of the BNNB bridge, arise. The positive combination of these orbitals shows a conjugated π-system located on N$_1$-C$_1$-B$_1$-N$_2$, whereas the negative analog is located on the other side N$_3$-C$_2$-B$_2$-N$_4$. This results in an almost non-existing overlap of both orbitals leading to a very small exchange energy J, which determines the size of the ST gap.

Table 36: Wiberg indices of the important bonds for the different conformers of **B$_2$N$_2$H$_2$**.

Conformer	N$_1$-C$_1$	C$_1$-B$_1$	B$_1$-N$_2$	N$_2$-N$_3$	N$_3$-B$_2$	B$_2$-C$_2$	C$_2$-N$_4$
B$_2$N$_2$H$_2$ 1.0	1.08	1.17	1.30	0.94	1.30	1.17	1.01
B$_2$N$_2$H$_2$ 2.0	1.17	1.19	1.35	0.95	1.34	1.18	1.15
B$_2$N$_2$H$_2$ 2.1	1.03	1.01	1.44	0.95	1.33	1.20	1.12
B$_2$N$_2$H$_2$ 2.3	1.04	1.01	1.44	0.94	1.43	1.01	1.04
B$_2$N$_2$H$_2$ 2.4	1.17	1.25	1.10	0.94	1.10	1.25	1.17
B$_2$N$_2$H$_2$ 2.5	1.06	1.02	1.33	0.92	1.23	1.20	1.10
B$_2$N$_2$H$_2$ 2.7	1.05	1.00	1.36	0.93	1.38	1.00	1.06

Starting from **B$_2$N$_2$H$_2$ 2.0**, two possible rotamers concerning the $\sphericalangle_{N_3C_1B_1N_1}$ and $\sphericalangle_{N_1B_2C_2N_4}$ dihedrals exist, with the dihedrals ($\sphericalangle_{N_1B_2C_2N_4}$, $\sphericalangle_{N_3C_1B_1N_1}$) either arranged at a geometry of 180° or 0°. The geometry of **B$_2$N$_2$H$_2$ 2.0**, with all dihedrals possessing a value of 180° ($\sphericalangle_{N_3C_1B_1N_1} = \sphericalangle_{N_1B_2C_2N_4} = \sphericalangle_{B_1N_1N_2B_2} = 180°$), proves to be the coplanar arrangement with

the lowest energy. Thus, the other planar rotamers are not mentioned in this work and all other conformers are obtained by rotating one, two or all three dihedrals of **B₂N₂H₂ 2.0** by 90° or 180°.

As seen for the optimization of the complete system **B₂N₂H₂** and the various subsystems **12-14** before, the all coplanar geometry does not represent the most favorable arrangement for all conformers. This is the case for **B₂N₂H₂ 2.4**, which is twisted 90° for the $\sphericalangle_{B_1N_1N_2B_2}$ dihedral. In **B₂N₂H₂ 2.4**, the ST gap illustrates a value of about 2 kcal/mol with the triplet being the more favorable state. This result is in contrast to the optimization without frozen dihedrals of the subsystem **12**, in which the singlet appears to be the ground state with a twisted $\sphericalangle_{B_1N_1N_2B_2}$ dihedral. The dihedral, which is chosen here (90°), does not correspond to the preferred dihedral of the minimum singlet structure of **12** (nearly 40°) and lies closer to the preferred 87° dihedral of the triplet. **B₂N₂H₂ 2.4** possesses a N-N single bond with a Wiberg bond index of 0.94 (Table 36), which agrees approximately with the values of the all coplanar conformers **B₂N₂H₂ 1.0** and **B₂N₂H₂ 2.0.**

Because of the twist in the $\sphericalangle_{B_1N_1N_2B_2}$ dihedral for **B₂N₂H₂ 2.4**, the multiple bond character in the N-B unit decreases, while the multiple bond character between the N-C of the carbene and C-B increases. In both cases, the spin density is mainly located at the carbon atoms of the carbene with a small amount on the neighboring nitrogen and B-N atoms of the bridge (Table 39). With the rising N-C conjugation of **B₂N₂H₂ 2.4**, the spin density is shifted to the nitrogen atom. In contrast to the all coplanar geometry **B₂N₂H₂ 2** with $\sphericalangle_{N_3C_1B_1N_1} = \sphericalangle_{N_1B_2C_2N_4} = 180°$, the carbene substituent decreases to a dihedral of 0°, defining the plane of the carbene, nitrogen and boron of the BNNB bridge ($\sphericalangle_{N_3C_1B_1N_1}$, $\sphericalangle_{N_1B_2C_2N_4}$). Thus, only the most favorable geometries concerning the dihedrals $\sphericalangle_{N_3C_1B_1N_1}$ and $\sphericalangle_{N_1B_2C_2N_4}$, switching between 0° and 180°, are shown here. The substituents illustrate three possible conformations concerning their CAAC ligand and the substituent bound to boron, which must be taken into account (Table 37). In particular, the molecule can form a *cis*-conformation regarding the substituent bound to nitrogen of CAAC and the one next to boron atom, namely N₃-C₁-B₁-H, or even H-N₃-C₁-B₁-H. A simplified picture of these *cis*/*trans*-configuration that can be formed is depicted in Figure 93.

Considering the *cis*-conformation, not only the nitrogen of the carbene and the substituent on the boron illustrate a *cis*-conformation, but also the substituent bound the nitrogen atom (Figure 78). For the model system, hydrogen atoms or Dip ligands for the complete system arrange in the same direction as the substituent bound to boron (see Figure 60 in chapter 6.2). The three rotamers of **B₂N₂H₂ 2.4** are depicted in Table 37. With both substituents arranging parallel to each other, the energetically most unfavourable conformation **B₂N₂H₂ 2.4 *cis*** is reached. By increasing the substituent size, the steric demand rises tremendously, forcing the carbene to twist out-of-plane. Hence, the conformation **B₂N₂H₂ 2.4 *cis*** becomes energetically not desirable. Another possible conformation is represented by the *trans*-configuration (**B₂N₂H₂ 2.4 *trans***), which seems to be the conformation with the lowest energy for both the triplet and the singlet state. The configuration **B₂N₂H₂ 2.4 *cis/trans***, in which one side forms a *trans*-arrangement and the other a *cis*-geometry, appears to be 2 kcal/mol higher in energy for the triplet.
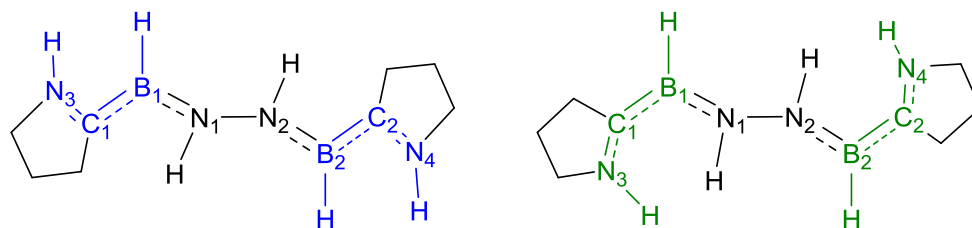
Figure 78: Two rotamers of **B₂N₂H₂ 2.4** with different configurations concerning the substituent bound to the boron and the orientation of the CAAC ligand, forming either two *cis*-conformations (left) or *trans*-conformations (right) on both sides of the molecule.

It is noteworthy that the complete molecule **B₂N₂H₂** arranges in a mixture of one side *cis* and the other one *trans* (compare Figure 60). The π-interactions of the parallel phenyl groups of the complete molecule cause this arrangement, although it shows a higher steric demand. This geometry seems to implicate the best π-interactions between three phenyl groups caused by their advantageous position to each other, whereas only one *cis*-transformation increases the steric demand.

Each of the three conformers of subsystem **B₂N₂H₂ 2.4** are described by a triplet ground state with a ST gap of 2-5 kcal/mol and an increase in energy about 3 kcal/mol from **B₂N₂H₂ 2.4 *trans*** to **B₂N₂H₂ 2.4 *trans/cis*** to **B₂N₂H₂ 2.4 *cis***. Considering the singlet geometry there is almost no difference to the triplet geometry, which results again in the assumption of

biradical singlet states, which is confirmed by the natural occupation numbers. These states increase about 5-8 kcal/mol compared to the lowest state.

Table 37: Different conformers of **$B_2N_2H_2$ 2.4** with an orthogonal $\sphericalangle_{B_1N_1N_2B_2}$=90° dihedral and the CAAC substituents in-plane $\sphericalangle_{N_3C_1B_1N_1}$= $\sphericalangle_{N_1B_2C_2N_4}$= 0, varying the arrangement of the CAAC substituents concerning the substituent on the boron atom (*cis* or *trans*).

Conformer		$\sphericalangle_{N_3C_1B_1N_1}$	$\sphericalangle_{B_1N_1N_2B_2}$	$\sphericalangle_{N_2B_2C_2N_4}$	$\Delta E(S_1)$	$\Delta E(T_1)$	ST_{gap}
$B_2N_2H_2$ 2.4 *trans/cis*		0	90	0	5.1	2.2	-2.9
$B_2N_2H_2$ 2.4 *trans*		0	90	0	2.0	0.0	-2.0
$B_2N_2H_2$ 2.4 *cis*		0	90	0	8.0	3.4	-4.5

Since the complete molecule possesses an all coplanar structure (Figure 60), the investigation starts from the planar structure with an arrangement of all three dihedrals of 180° (**$B_2N_2H_2$ 2.0**) A rotation of the $\sphericalangle_{N_3C_1B_1N_1}$ dihedral about 90° results in **$B_2N_2H_2$ 2.1** with an energy increase of about 23 kcal/mol for the singlet and 17 kcal/mol for the triplet (Table 35). Thus, the ST gap rises to 6 kcal/mol. A rotation of the other dihedral $\sphericalangle_{N_2B_2C_2N_4}$ yields the conformer **$B_2N_2H_2$ 2.2**, which shows the exact same results and properties as **$B_2N_2H_2$ 2.1**. This is due to the symmetric geometry of the molecule. A twist of one side of the molecule affects just the twisted side and has no influence on the remaining system, as it is the case for **B_2N_2**. The multiple bond character of the N-C and C-B decreases to a single bond and due to the twisted side with a $\sphericalangle_{N_3C_1B_1N_1}$ dihedral of 90° the B-N bond character increases only on the distorted side of the molecule. The increased ST gap corresponds to the energetic shift of the two SOMOs and their distribution. While the SOMOs for **$B_2N_2H_2$ 2.0** appear nearly degenerate and the linear combination of those orbitals show a localization on each side of the BNNB bridge, the orbitals of **$B_2N_2H_2$ 2.1** show a completely different appearance (Table 38). The planar side looks like the SOMO of **$B_2N_2H_2$ 2.0** with a N-C π-bond, whereas the orthogonal carbene does not form this bond. This leads to antibonding orbitals for the SOMOs between boron and carbon and carbon and nitrogen (Table 38).

By twisting both dihedrals, $\sphericalangle_{N_3C_1B_1N_1}$ and $\sphericalangle_{N_2B_2C_2N_4}$(**B₂N₂H₂ 2.3**), the energy of the singlet increases about 17 kcal/mol, while the triplet is destabilized by only 15 kcal/mol, resulting in a further increased ST gap of about 8 kcal/mol with a triplet ground state. By this distortion, **B₂N₂H₂ 2.3** arranges even more symmetrically and exhibits the same conjugation on both sides. As seen in the previous system (**B₂N₂H₂ 2.2**), the multiple bond character between N-C and B-C decreases and therefore the remaining B-N bond strengthened (Table 36). In contrast to the **B₂N₂** molecule, twisting one carbene out-of-plane does not affect the complete system. Considering the geometry of **B₂N₂H₂ 2.3** it is obvious that despite the planar arrangement of the BNNB bridge, the system is distorted in such a way that the nitrogen atoms cannot interact. Consequently, the electron density in between the nitrogen atoms decreases, resulting in a Wiberg index smaller than one (Table 36). Furthermore, the π-back-bonding from the p-orbital of the boron atom to the nitrogen increases, which can be seen by the natural occupation numbers of the system, the slightly decreased B-N bond length and the increased Wiberg indices. This might explain the destabilization in energy of about 30 kcal/mol in comparison to the complete coplanar conformer **B₂N₂H₂ 2.0**. Regarding the spin densities, a decrease of the delocalization of the unpaired electrons can be detected (Table 39). For the all coplanar system **B₂N₂H₂ 2.0**, the unpaired electrons are mainly located on the carbene carbon, with a delocalization on the nitrogen of the carbene and even less spin density on the nitrogen atoms N_1 and N_3 of the $B_1N_1N_3B_2$ bridge. By twisting the carbene ligand to the B-N unit, the conjugation over the B-N increases, while the C-B conjugation disappears completely. Thus, the amount of spin density increases on the carbon and nitrogen atoms of the carbene and decreases on the boron atom and the bridging nitrogens N_1 and N_2. This localization of the unpaired electrons constitutes another effect, which leads to a destabilization of the distorted systems **B₂N₂H₂ 2.1**, **B₂N₂H₂ 2.2** and especially **B₂N₂H₂ 2.3**. It should also be noted that in contrast to the distorted conformers **B₂N₂H₂ 2.1** - **B₂N₂H₂ 2.3**, the planer conformer **B₂N₂H₂ 2.0** cannot form hydrogen bonds. Consequently, it can be concluded that the resulting destabilization in energy by the distortion is even larger; however, it is partly compensated by hydrogen bonds, which present stabilizing effects.

A twist around the $\sphericalangle_{B_1N_1N_2B_2}$ dihedral exhibits only a small influence on the energy of the system, which is mostly induced by hydrogen bonds and not caused by differences in the electronic structure. That there are no electronic differences between **B₂N₂H₂ 2.0** and

B₂N₂H₂ 2.4 is due to the N-N single bond and the thereof resulting not-existent π-conjugation of these conformers. This not alternating behavior can also be seen in the MOs of both systems (Table 38). The electron density distribution of both conformers appears almost identical. Only small variations can be found in the energies of the important KS orbitals, in particular for the HOMO.

Table 38: Kohn-Sham orbitals of the different conformers **B₂N₂H₂ 2.0**, **B₂N₂H₂ 2.1** and **B₂N₂H₂ 2.4** and their corresponding orbital energies for the triplet states.

Conformer	HOMO	SOMO	SOMO+1
B₂N₂H₂ 2.0	-119.4	-58.0	-51.9
B₂N₂H₂ 2.1	-118.9	-54.8	-42.6
B₂N₂H₂ 2.4	-135.7	-61.1	-50.2
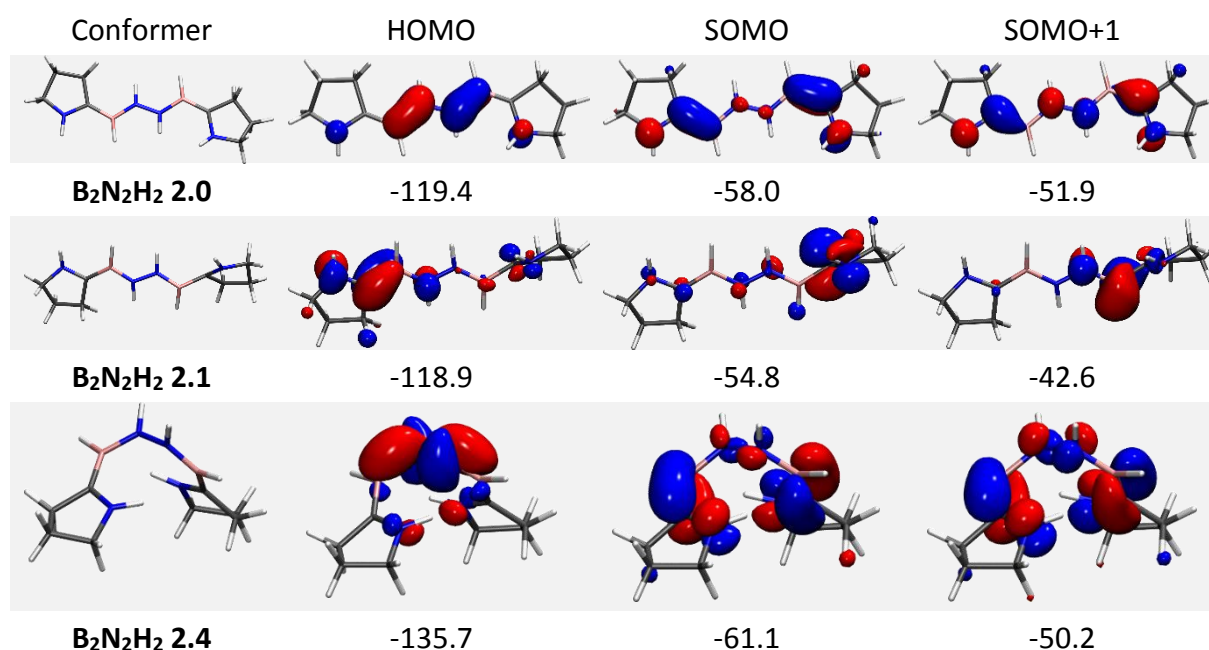
The KS orbitals of **B₂N₂H₂ 2.4** show a stabilization and thus a decrease in energy, which can be explained by the twisted $\sphericalangle_{B_1N_1N_2B_2}$ plane and the resulting decreased antibonding interaction between the two nitrogen atoms. However, the antibonding character increases for the all planar system **B₂N₂H₂ 2.0**, in which the two π-orbitals of the HOMO are perfectly in line and thus spatially closer to each other. Since the antibonding between the bridging nitrogen atoms is not detected in the SOMOs, their energies are not changing substantially.

By rotating the carbene ligands of the planar conformer **B₂N₂H₂ 2.0**, the system is energetically destabilized. Therefore, an interesting aspect is the influence of the carbenes on **B₂N₂H₂ 2.4**, which was analyzed by rotating one or both dihedrals ($\sphericalangle_{N_3C_1B_1N_1}$, $\sphericalangle_{N_2B_2C_2N_4}$) resulting in the conformers **B₂N₂H₂ 2.5** and **B₂N₂H₂ 2.6** (Table 35). By twisting one carbene out-of-plane, both the singlet and the triplet state of **B₂N₂H₂ 2.5** and **B₂N₂H₂ 2.6** are destabilized by nearly 19 kcal/mol. Since both conformers differ solely in the side of the rotated carbene ligand and

respond in the same way, only conformer **B₂N₂H₂ 2.5** is shown here. As seen for the conformers with one carbene twisted out-of-plane (**B₂N₂H₂ 2.1**), the bonding pattern of conformer **B₂N₂H₂ 2.5** changes in a similar way. The B-N bond length decreases slightly, induced by a larger amount of π-back bonding of the boron atom to the nitrogen. Due to this observation, the side with the distorted carbene illustrates a smaller multiple bond character between the boron and carbon and additionally between the nitrogen and the carbon atom of the carbene. This can be seen in the increased bond length and the lower Wiberg coefficients (Table 36). For the conformer with the carbene in-plane, the bonding pattern shifts in a similar, but less pronounced way. Again, the spin density cannot be delocalized over the nitrogen and boron of the BNNB bridge for the twisted unit resulting in an increased spin density on the carbon atom, which destabilizes the system compared to its not twisted counterpart **B₂N₂H₂ 2.4**. By distorting both carbenes out-of-plane (**B₂N₂H₂ 2.7**), this trend is even more distinctive. As seen for the planar conformer with both carbenes orthogonal to the BNNB bridge (**B₂N₂H₂ 2.3**), the spin density can be located almost exclusively on the carbon atom. For this reason, the energetically lowest singlet state shows nearly no biradical character and prefers a closed shell arrangement.

Table 39: Spin densities of the important conformers of the **B₂N₂H₂** substructures.

Conformer	N_1	C_1	B_1	N_2	N_3	B_2	C_2	N_4
B₂N₂H₂ 1.0	0.13	0.75	0.06	0.07	0.07	0.06	0.75	0.13
B₂N₂H₂ 2.0	0.12	0.77	0.03	0.09	0.09	0.03	0.75	0.12
B₂N₂H₂ 2.1	0.11	0.89	-0.04	0.02	0.11	0.04	0.70	0.17
B₂N₂H₂ 2.3	0.11	0.89	-0.05	0.02	0.03	-0.04	0.88	0.11
B₂N₂H₂ 2.4	0.19	0.66	0.10	0.06	0.07	0.10	0.65	0.19
B₂N₂H₂ 2.5	0.10	0.90	-0.03	0.01	0.07	0.09	0.71	0.16
B₂N₂H₂ 2.7	0.08	0.91	-0.05	0.02	0.02	-0.03	0.88	0.11

This is also confirmed by the KS orbitals. While the other systems present a HL gap of 10-15 kcal/mol, it strongly increases to 30 kcal/mol for **B₂N₂H₂ 2.7**. Here, it should be considered that this system is further stabilized by hydrogen bonds. Without those hydrogen bonds, the system would be even more unfavourable. Furthermore, interactions between the two carbon atoms of each carbene are possible, as well as the boron and the carbon atom, which can be seen in the KS orbitals, too.

Considering the **B₂N₂H₂** molecule, a very small ST gap appears with the singlet and triplet arranging in a similar geometry caused by the high open shell character of the singlet. Consequently, it cannot be determined unambiguously whether the singlet or the triplet occurs as real ground state, since both states should be populated at room temperature. The composition of the $\sphericalangle_{B_1N_1N_2B_2}$ dihedral influences the molecule just slightly, since **B₂N₂H₂** exhibits a N-N single bond, which allows for free rotation. By decreasing the system size, the substructures arrange with an orthogonal $\sphericalangle_{B_1N_1N_2B_2}$ dihedral, which is not affecting the electronic properties of the system. Influences on the electronic properties can be attributed to hydrogen bonding or π-stacking interactions. Irrespective of the system size, the dihedrals $\sphericalangle_{N_3C_1B_1N_1}$ and $\sphericalangle_{N_2B_2C_2N_4}$ remain always in a plane arrangement. By twisting one or both dihedrals, the system gets highly destabilized due to the non-delocalized spin density over the whole system. The density localizes on the carbon atoms of the carbene, which is highly unfavorable. Consequently, the substituents on the boron atoms and carbene ligands can be reduced without influencing the stability of the whole system. Considering these theoretical results, an interesting aspect for the synthesis of those BNNB bridged molecules is the use of carbene ligands with modified push-pull behavior in order to stabilize the systems even more.

6.5   Summary

Two different molecules, **B₂N₂** and **B₂N₂H₂**, were synthesized by the Braunschweig group as an attempt to explore a boron containing system mimicking transition metals to activate chemically inert molecules, such as N_2.[411] On the one hand, the singlet closed shell molecule **B₂N₂** arranges in a $\sphericalangle_{B_1N_1N_2B_2}$ twisted conformation showing a N=N double bond and multiple bond character between the remaining system and the carbene ligands. On the other hand, the hydrogenated counterpart **B₂N₂H₂** possesses a biradical ground state, in which singlet and triplet are nearly degenerated exhibiting an almost coplanar geometry. With hydrogen bonding to nitrogen due to one additional unpaired electron on each nitrogen, the antibonding π^*-orbital of the N-N gets occupied resulting in a N-N single bond.

Since the amount of electron density located on the main BNNB bridge presents an important parameter, both the substituents on the boron and carbene nitrogen atoms are varied to investigate whether they influence the system sterically or electronically. The various subsystems of **B₂N₂** exhibit no differences in the bonding pattern and small changes in

geometry are predominated by other electronic effects, such as hydrogen bonds (N···H) or π-stacking of phenyl substituents. The geometry of the **B₂N₂** substructures illustrates no changes upon replacing the sterically demanding substituents with hydrogen. The minimum geometry of the **B₂N₂H₂** subsystems appears as a twisted geometry concerning the $\sphericalangle_{BNNB}$ dihedral with a singlet ground state, which is planar for the complete system. An in-detail study reveals that the electronic properties remain the same as seen for the substructures of **B₂N₂** and the minimum structures are those with the highest amount of hydrogen bonds or π-stacking.

Since **B₂N₂H₂** possesses a N-N single bond, a rotation around the dinitrogen is possible at room temperature. By varying the three important dihedrals $\sphericalangle_{B_1N_1N_2B_2}$, $\sphericalangle_{N_3C_1B_1N_1}$ and $\sphericalangle_{N_2B_2C_2N_4}$ between 0°, 90° and 180°, the detailed influence of the geometry on the electronic properties is investigated. As seen before, the orthogonal structure is the most favorable for the smallest substructures of **B₂N₂H₂**. With a difference of 8 kcal/mol compared to the all coplanar geometry and no substantial differences regarding the KS orbitals, the size of the energy gap can be reduced due to interaction effects, such as hydrogen bonds, which can also be formed in the orthogonal case. On the contrary, the conjugation of the BNNB bridge with the carbenes and thus the planarity of the $\sphericalangle_{N_3C_1B_1N_1}$ dihedrals play a more important role regarding the electronic properties. When the carbene ligands arrange orthogonally to the B-N part, the bonding pattern is shifted resulting almost in a B=N double bond and a C-B single bond. Consequently, the spin density is mainly localized on carbon. This kind of bonding pattern reveals a destabilization of the system up to 40 kcal/mol.

The substructures of **B₂N₂** show that the system has to arrange orthogonally regarding the $\sphericalangle_{B_1N_1N_2B_2}$ dihedral to form the N=N double bond. By forcing the system to a coplanar structure, the nitrogen bond becomes a single bond with a triplet ground state. If the carbenes are twisted out-of-plane, the singlet and triplet get highly unfavorable, in particular for $\sphericalangle_{B_1N_1N_2B_2}$ = 90°. Caused by the missing conjugation from boron to carbon, the p-orbital of the boron donates electron density only to nitrogen leading to a B=N double bond and a N-N single bond. Since a N-N single bond is easier to break than a N=N double bond or even a N≡N triple bond, this formation is in accordance with the desirable nitrogen activation. By pushing more electron density to the boron atom and thus to the nitrogen, the π^*-orbital of the N-N bond is occupied. Another attempt to activate N₂ includes reducing the π-donating properties from

boron to the empty p-orbital of the carbene carbon by adding steric hindrances. This way, the B-N π-back bonding is increased. Thus, the system is forced to an energetically more unfavorable geometry caused by steric hindrances.

7 CAAC stabilized biradical diborylalkenes

7.1 Synthesis of diborylalkene biradicals

As seen in the previous chapters 5 and 6, boron-based biradicals with both a direct boron-boron[408] bound and those with a dinitrogen bridge[411] were successfully synthesized. Since various radical species exist for carbene ligated boranes and borenes, it is obvious that a biradical could be based on the same basic structure.

An example for this kind of radical is the 9-borylated acridinyl radical (**1**, Figure 79), which was synthesized by Gabbai in 2007 via reduction of a cationic borane.[562] Another interesting radical (**2**) was presented in 2008 by Lacote and Curran *et al.* investigating a new class of radical hydrogen atom donor.[563] In 2014, Bissinger *et al.* from the Braunschweig group synthesized a neutral CAAC stabilized boryl chloride radical (**3**) with duryl or thiophene substituents on the boron.[458] An overview of these radicals is shown in Figure 79.
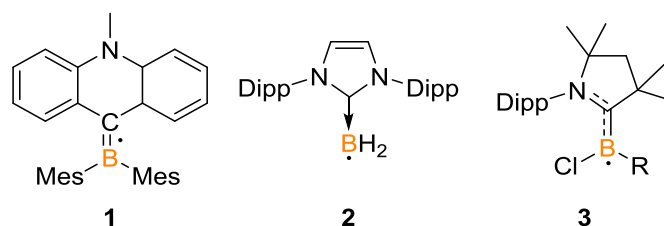
Figure 79: Carbene ligated boryl radicals synthesized by Gabbai (**1**), Lacote and Curran (**2**) and the Braunschweig group (**3**, R: duryl or thiophene).

Origin of the idea to synthesize a carbene bridged diboryl biradical was the CAAC stabilized boryl chloride radical **3** of the Braunschweig group, as this radical is stable and was analyzed precisely.[458] In contrast to the mono-radical, which was generated from an arylhaloborane that stabilizes a boryl-radical and prevents dimerization by radical homo-coupling, for the biradical a tetrahalodiborane was used as an starting material.[519] Combining tetrachloro-diborane (**4**) with an alkyne at low temperature leads to the *cis*-diborylalkene in an addition reaction (Figure 80), which was verified by the characteristic signal in the ^{11}B-NMR spectra.
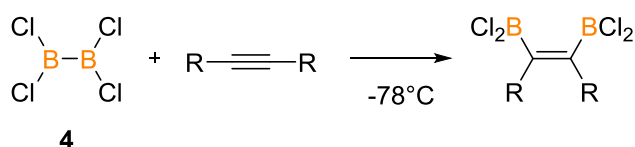
Figure 80: Reaction of tetrachlorodiborane (**4**) with an alkyne (R: methyl, ethyl or hydrogen).

Adding an equimolar amount of cyclic carbene CAAC yields a diborylalkene, stabilized by one CAAC unit (Figure 81). In the ^{11}B-NMR spectra, the values are shifted to 30 and 2.5 ppm, with a slight variation depending on the substituent R. This confirms the assumption of both sp^2-and sp^3-hybridized boron atoms.
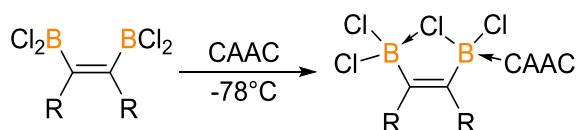
Figure 81: Adding stabilizing CAAC to the diborylalkene (R: methyl, ethyl or hydrogen).

Last step of this synthesis is the reduction of CAAC stabilized diborylalkene with potassium graphite and another equimolar amount of CAAC resulting in a CAAC stabilized *E*-Bis(monochloroboryl)alkene with two planar boron centres (Figure 82). With R being a methyl or ethyl group, the synthesized compound is NMR silent, suggesting that the synthesized molecule could be a biradical. This is affirmed by the connectivity and planarity of the two boron atoms.

A1/A2/H1
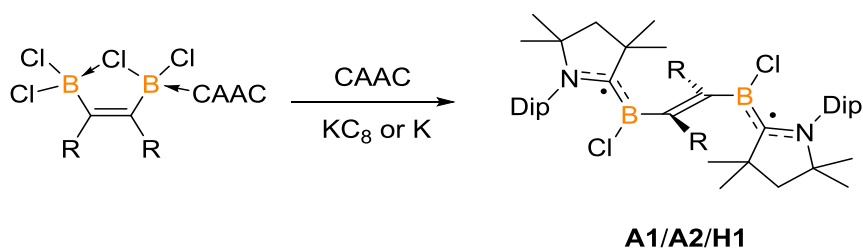
Figure 82: Reduction to the CAAC stabilized diborylalkenes **A1** (R: methyl), **A2** (R: ethyl) and **H1** (R: hydrogen).

The basic structure of these compounds, synthesised by Andrea Deißenberger from the group of Prof. Dr. Holger Braunschweig, are two boron atoms, which are bridged by an alkene.[564] The system is stabilized by two CAACs next to each boron atom. In three of the four compounds, a chloride is attached to boron, just in one compound the chloride is substituted by a hydrogen atom. Therefore, a completely different synthesis was performed. Starting with tetrabromodiborane (**5**), CAAC was added for stabilization reasons and a subsequent reduction leads to the permanently CAAC stabilized diboracumulene **6** (Figure 83).[565]
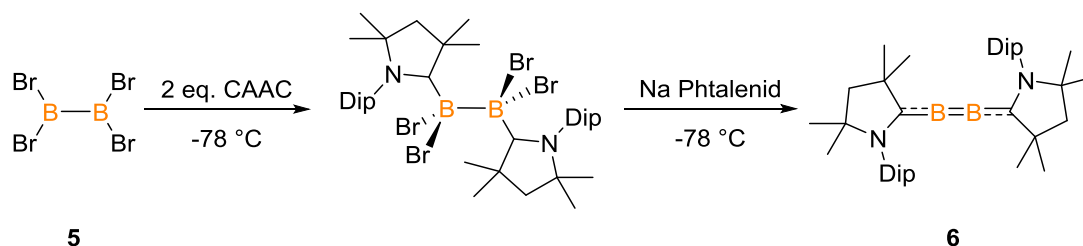
Figure 83: Realization of the diboracumulene precursor **6**.

This molecule enables various reaction paths, which were studied by Dr. Julian Böhnke in his doctoral thesis at the Braunschweig group.[520, 566] **6** exhibits a singlet closed shell character with an extended π-system from one carbene to the other. This conjugation can also be seen in the HOMO and LUMO, showing a π-system from nitrogen of the CAAC to the other nitrogen of the CAAC.[565] Whereat the N-C bond illustrates an antibonding character for both molecules, analog to the previous investigated molecules in this work. Interestingly, by changing the ligands from CAAC to NHC the synthesis yields a similar molecule; however, instead of a conjugated double bond the system shows now a B≡B triple bond.[459, 565] Via selective hydrogenation, the dihydrodiborene **7** was obtained (Figure 84).[459] **7** can also be synthesized by reductive coupling of a CAAC stabilized dichloroborane.[455] Furthermore, **7** shows interesting behavior towards carbon monoxide.[474] Since it is known that alkene analogs of the 13th main group, such as dialumine or digallene, react under an addiction reaction with an unpolar alkyne,[567, 568] the same was tried with a diborane.[520] Therefore, acetylene was added to the synthesized dihydrodiborene **7** and in a [2+2]-cycloaddition the hydrogenated diborylalkene **H2** was synthesized (Figure 84).
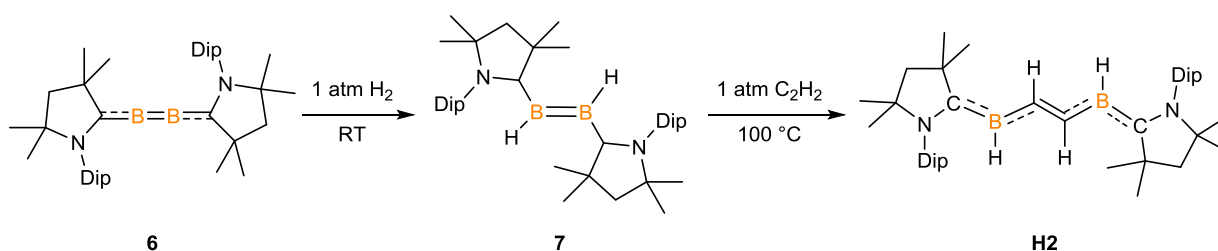
Figure 84: Synthesis of the hydrogenated diborylalkene **H2**.

Figure 85 depicts the basic structure of the four analyzed molecules **A1**, **A2**, **H1** and **H2**. The methyl substituted system is abbreviated as **A1** and the one with ethyl groups as **A2**. The other two molecules show a hydrogen instead of an alkyl substituent and are shortened by **H1** and **H2**, whereat **H1** has two chlorides at the boron centers and **H2** has only hydrogens bound to boron.[564]
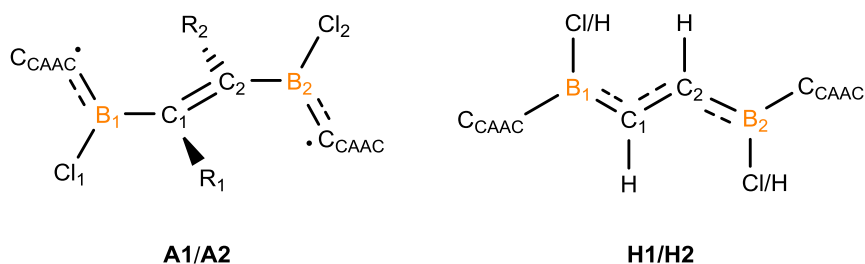
Figure 85: Basic structure of the CAAC stabilized diborylalkenes with the alkyl substituted ones **A1** (R: methyl) and **A2** (R: ethyl) on the left, the hydrogen substituted **H1** (R: hydrogen) and the "all"-hydrogen system **H2** on the right

There is nearly no difference between the compounds with a methyl or ethyl substituent bound to the carbon-bridge. In the following, all four molecules are theoretically analyzed in detail to identify the differences concerning the substituent R and to investigate the role of the halogen substituent.

7.2 Systems A1 and A2 with alkyl substituents

A1 and **A2** are two very similar molecules, which only differ in the chain length of the alkyl substituent R bound the alkene carbon atoms (Figure 86). While system **A1** has a methyl group bound to the carbon of the dicarbon bridge, it is ethyl for **A2**.

A1   **A2**
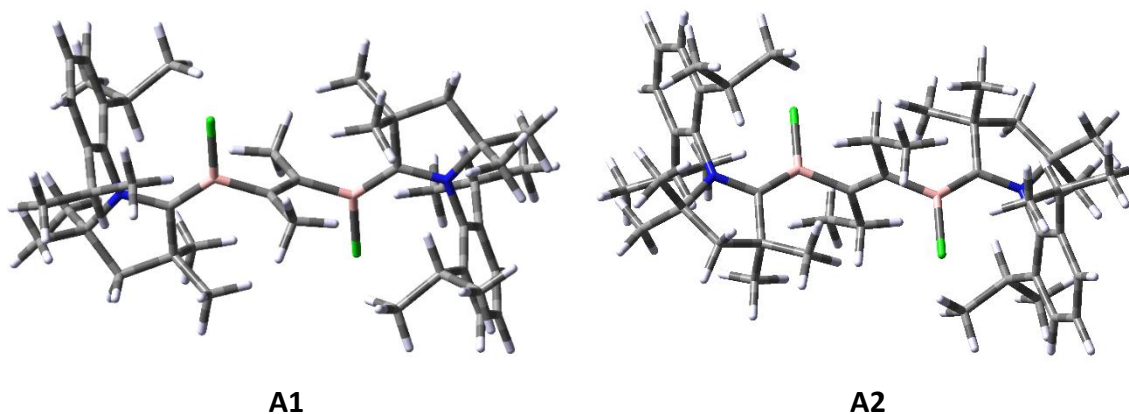
Figure 86: 3D-structure of diborylalkenes with methyl groups **A1** (left) and ethyl groups **A2** (right) as substituent R.

As shown in the Benchmark chapter 4, using the UMN12L functional provides an appropriate choice to calculate a suitable ST gap energy with the correct multiplicity of the ground state. For both systems, the ground state is calculated as a triplet, which is 9 kcal/mol (**A1**) and 12 kcal/mol (**A2**) more favourable than the singlet. Comparing this result with SF-DFT, which yields better results according to the Benchmark (chapter 4), a different multiplicity of the ground state is predicted. According to the spin flip BLYP calculation, the singlet is about 0.39 kcal/mol (**A1**) and 0.22 kcal/mol (**A2**) lower in energy. This leads to the assumption of a

small ST gap, which is experimentally measurable.[564] With a Bleaney-Bowers fit of the temperature-dependent EPR measured data, a singlet ground state with a low lying triplet (0.017 kcal/mol) is revealed.[564]

Since the calculated singlet and triplet geometry of these molecules are very similar, the singlet possesses most likely a huge amount of biradical character. Even though the singlet appears as slightly favoured ground state, the triplet is analyzed in detail, as this state represents the singlet biradical geometry more closely and is in particular more symmetric than the singlet geometry calculated by unrestricted DFT. To ascertain the quality of the calculated geometries, a comparison to the crystal structure was made. The designation of the different geometrical parameters is simplified by labelling the different atoms of the molecules **A1** and **A2** according to Figure 87.
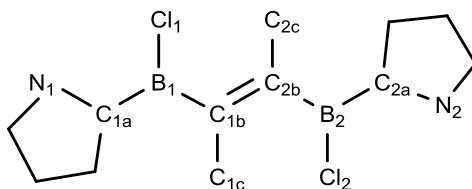
Figure 87: Labeling of the atoms of molecule **A1** and **A2**.

At first, the bond length of both structures is examined. The obtained values are listed in Table 40 with the numbering shown in Figure 87. It is obvious, that both theoretical and experimental data are in good agreement and the two systems appear to have a very similar structure. The C_{1b}-C_{2b} bond length with ~1.35 Å indicates a C=C double bond, as it was expected, while the C_{1b}-C_{1c} bond length suggests a typical C-C bond from a sp³ to a sp² carbon atom.[569] By comparing the two boron-carbon bond lengths of C_{1a}-B_1 and C_{1b}-B_1, the length between boron and alkene carbon (C_{1b}-B_1) exhibits a typical distance for a single bond (1.58 Å), see Table 40. However, the length between boron and carbene carbon (C_{1a}-B_1) has a slight multiple bond character (1.51 Å). The bond length of carbene nitrogen and carbon (N_1-C_{1a}), with a value of 1.37 Å, indicates a double bond character, too. Therefore, it can be assumed that the two radicals are delocalized over the nitrogen and carbon of the CAAC and the boron atom of each side, since there is apparently no conjugation over the ethylene bridge between the boron atoms.

Table 40: Comparison of experimental and theoretical (triplet state) bond lengths of the **A1** and **A2** with the numbering shown in Figure 87.

Bond length [Å]	N_1-C_{1a}	C_{1a}-B_1	B_1-Cl_1	B_1-C_{1b}	C_{1b}-C_{1c}	C_{1b}-C_{2b}	N_2-C_{2a}	C_{2a}-B_2	B_2-Cl_2	B_2-C_{2b}	C_{2b}-C_{2c}
Exp. **A1**	1.37	1.51	1.81	1.59	1.52	1.35	1.37	1.51	1.81	1.59	1.52
Exp. **A2**	1.37	1.50	1.82	1.58	1.52	1.34	1.37	1.50	1.82	1.58	1.52
Theor. **A1**	1.36	1.52	1.82	1.57	1.51	1.36	1.36	1.52	1.82	1.57	1.51
Theor. **A2**	1.36	1.51	1.83	1.57	1.52	1.35	1.36	1.51	1.83	1.57	1.52

Apart from the bond length the dihedral illustrates another important parameter. Based on the planarity of the system, it can be determined whether there is a conjugation through the system or not. In analogy to the bond lengths, there is no substantial difference in the dihedrals between the singlet and triplet geometry. Therefore, the triplet geometry was used to compare the dihedrals with the crystal structure. The dihedrals of both sides of the system are fully symmetrical for the crystal structure, as well as the calculated triplet. Only the singlet shows slight asymmetric properties in the geometry, caused by the high biradical character. Since the symmetric triplet structure is used, only the left side of the system is listed in Table 41. For the first dihedral built by the nitrogen and carbon of the CAAC, B_1 and the alkene carbon ($\sphericalangle_{N_1C_{1a}B_1C_{1b}}$) an almost plane (170°) geometry is obtained. The middle part of the molecules ($\sphericalangle_{C_{1c}C_{1b}C_{2b}C_{2c}}$) forms a planar dihedral of 180°. The reason why there is no conjugation between the CAAC ligand, and the alkene is a twist of the C_{1b}-C_{2b} atoms, which can be seen in the dihedral $\sphericalangle_{C_{1a}B_1C_{1b}C_{1c}}$ with an angle of nearly 90°. The distortion of the alkene in combination with the bond length evidences a conjugation over CAAC to the boron atom and the first alkene carbon, which is bond to the boron via a single bond.

Table 41: Different dihedrals for **A1** and **A2** with the numbering shown in Figure 87

Dihedral [°]	$\sphericalangle_{N_1C_{1a}B_1C_{1b}}$	$\sphericalangle_{B_1C_{1b}C_{2b}B_1}$	$\sphericalangle_{C_{1a}B_1C_{1b}C_{1c}}$	$\sphericalangle_{Cl_1B_2C_{2b}C_{2c}}$	$\sphericalangle_{C_{1c}C_{1b}C_{2b}C_{2c}}$
Exp. **A1**	169.6	180.0	-97.7	93.3	180.0
Exp. **A2**	178.1	180.0	96.7	83.3	180.0
Theor. **A1**	174.2	180.0	-84.5	93.5	180.0
Theor. **A2**	174.9	180.0	-97.4	79.3	180.0

So far, the results are just based on geometry analysis of the molecules. Additional calculations regarding the bond order, natural occupation, charge and spin densities are performed either to verify these assumptions or give new insights for these systems. The analysis of the bond

order (Table 42) confirms the suggestion of a multiple bond character between the nitrogen, carbon and boron atom.

Table 42: Calculated bond orders for molecules **A1** and **A2** with the numbering shown in Figure 87.

Bond order	N_1-C_{1a}	C_{1a}-B_1	B_1-Cl_1	B_1-C_{1b}	C_{1b}-C_{1c}	C_{1b}-C_{2b}	N_2-C_{2a}	C_{2a}-B_2	B_2-Cl_2	B_2-C_{2b}	C_{2b}-C_{2c}
Theor. **A1**	1.18	1.23	0.95	0.99	1.00	1.91	1.18	1.23	0.95	0.99	1.00
Theor. **A2**	1.18	1.35	0.95	0.96	0.98	1.98	1.18	1.35	0.95	0.96	0.98

This can be seen by a bond order higher than 1.00, but not even close to two. Whereat the alkene atoms in the middle, C_{1b}-C_{2b}, share a double bond with a bond order of nearly two. In the ethyl substituted molecule **A2**, the double bond character is slightly more pronounced, probably caused by the higher inductive effect of the ethyl group. Due to this little increase of the C_{1b}-C_{2b} bond order of 0.07, the bond order to the boron atom decreases in the same range (Table 42). The other evaluated bond orders (~1.00) present single bonds, whereat the carbon-chloride bond shows a smaller value caused by the high electronegativity of the chloride.

To get an overview of the localization or delocalization of the free electrons, the natural occupation, charges and spin densities were analyzed. Since the two sides of the molecule show the exact same values for these variables, only the left side of the system is listed in Table 43.

Table 43: Natural occupation, charge and spin density of the important atoms of **A1** and **A2**.

A1	N_1	C_{1a}	B_1	Cl_1	C_{1b}	C_{1c}
Natural charge	-0.54	-0.03	0.66	-0.30	-0.39	-0.57
Natural occupation	7.54	6.03	4.33	17.30	6.39	6.57
Spin density	0.24	0.49	0.27	0.02	-0.01	0.01
A2	N_1	C_{1a}	B_1	Cl_1	C_{1b}	C_{1c}
Natural charge	-0.55	-0.12	0.81	-0.30	-0.39	-0.39
Natural occupation	7.55	6.12	4.18	17.30	6.39	6.39
Spin density	0.24	0.49	0.27	0.02	-0.01	0.02

It is irrelevant, whether **A1** or **A2** is considered, since the obtained values are very similar, and the trend is completely the same. Whereby the natural charge and the natural occupation go hand in hand. The charge and occupation of chloride and nitrogen is increased due to their

high electronegativity. On the contrary, boron has a positive charge due to its small electronegativity and therefore less than its normal occupation. The high negative charge of alkyl C_{1c} is probably caused by the hydrogen atoms and affects its neighbour C_{1b}, too.

By means of spin density it emerges that the two unpaired electrons of compound **A1** and **A2** are mainly delocalized over the N-C-B bond of each side. The main part of the unpaired spin can be found on the carbon atoms (C_{1a}, C_{2a}) between nitrogen and boron. This can be seen in the spin density distributions (Table 43), which illustrate the highest amount localized on the carbon atoms with a small amount on the neighbouring nitrogen and boron atoms. In the EPR spectra of both molecules, an interspin distance if 5.8 Å can be approximated with the point dipole approximation.[564] This distance lies in between the C_{CAAC}-C_{CAAC} distance of about 6.3 Å and a B-B distance of about 4.1 Å with tendencies to the carbon atom distance. Considering the EPR spectra of both molecules, the signal resembles more a CAAC supported boron monoradical than an interacting biradical signal, suggesting a very weak coupling between the two radicals. One factor is the relatively long distance; however, the most important factor is the distortion of the ethylene bridge regarding the two CAAC ligands (Table 42), which makes a conjugation over the bridge impossible. Thus, these radicals exhibit a small coupling. This is in contrast to related systems, which contain also two radicals coupled by an ethylene bridge, but an all coplanar geometry.[570, 571]

Since the triplet MOs present the highest similarity with the natural orbitals, in contrast to the singlet orbitals, the SOMOs of the triplet state are shown in Figure 88. For **A1**, the energy of the SOMO+1 is 3.46 kcal/mol higher than the SOMO, which is slightly smaller than the one of **A2** with a gap of 6.00 kcal/mol. This small distinction of 3 kcal/mol for the HL gap corresponds to the difference in the ST gap, which is 3 kcal/mol smaller for **A1**. The electron density of the SOMO is localized over the N-C-B-Cl bond with antibonding character to the nitrogen and the chloride. The SOMO+1 appears with the same distribution except an additional reversion of the electron density for one side. As already observed in the examined parameters before, the frontier MOs demonstrate also no differences comparing systems **A1** and **A2**.
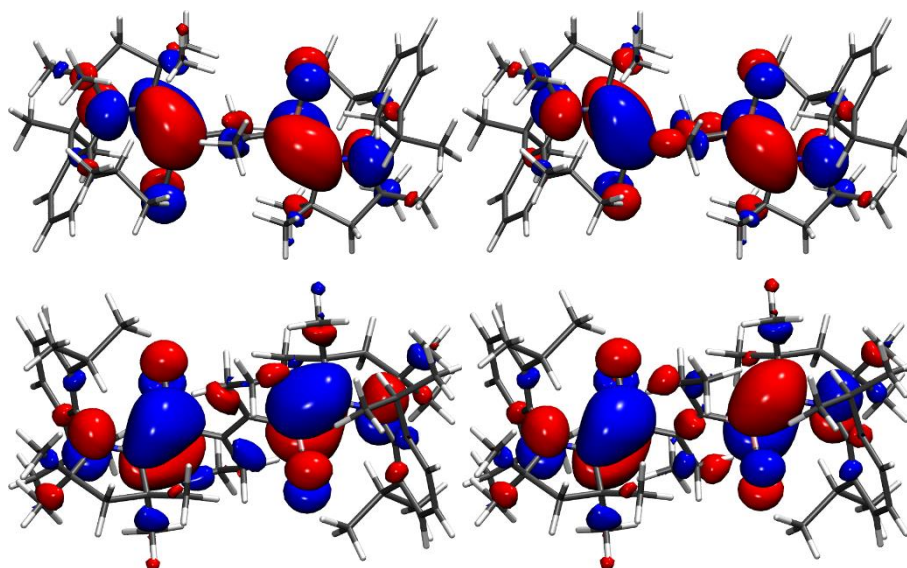
Figure 88: SOMO (left) and SOMO+1 (right) of the triplet ground state of **A1** (above) and **A2** (below).

This results, as seen analogously for the biradical systems of chapter 5 and 6, in orbitals with the electron density just localized on one side of the C=C bridge, if the linear combination of the SOMO and SOMO+1 is formed. The HOMO characterizes the π-electrons of the π-bond of the ethylene group in the middle, while the electron density of the LUMO is just localized on the CAAC ligands.

These systems were experimentally analyzed by EPR resonance spectroscopy and therefore a value for the ST gap and the antiferromagnetic coupling was obtained. The antiferromagnetic coupling J was calculated after the improved *ansatz* of Noodleman and Ginsberg:[360]

$$J = \frac{-(E[HS] - E[BS])}{S_{max}^2}$$

With $E[HS]$ as the energy of the High-Spin state (triplet), $E[BS]$ equals the energy of the broken symmetry state (singlet) and a maximal value of two for S². The necessary parameters for this equation were obtained by a SF-DFT (BLYP/ def2TZVP) calculation. Since the electron is supposed to be delocalized over N_1, C_{1a} or B_1, a coupling of J=136.89 cm⁻¹ can be achieved by a spin flip on N_1, C_{1a} or B_1 for **A1**. Flipping the spin on the same atoms leads to an antiferromagnetic coupling of J=76.97 cm⁻¹ for **A2**. These calculated coupling constants are predicting slightly too high, as the experimental ones are about 6 cm⁻¹.[564] This leads to an even smaller ST gap of 0.02 kcal/mol, which is hardly capable within the theoretical approaches. Thus, the calculated ST gap of 0.2-0.4 kcal/mol seems to describe the system in line with the experimental data.

7.3 Hydrogenated systems H1 and H2

During the description of the synthesis, it was already mentioned that the substituent R can also be a simple hydrogen. In contrast to the alkyl substituted molecules, the hydrogen substituted system **H1** (Figure 89, left) shows a diamagnetic behavior and appears probably as a closed shell system in the ground state. Another molecule can be synthesized in an additional hydrogenation reaction, in which the chlorides are replaced by hydrogen atoms. This system **H2** possesses four hydrogen atoms at the alkene center (Figure 89, right).

H1 **H2**
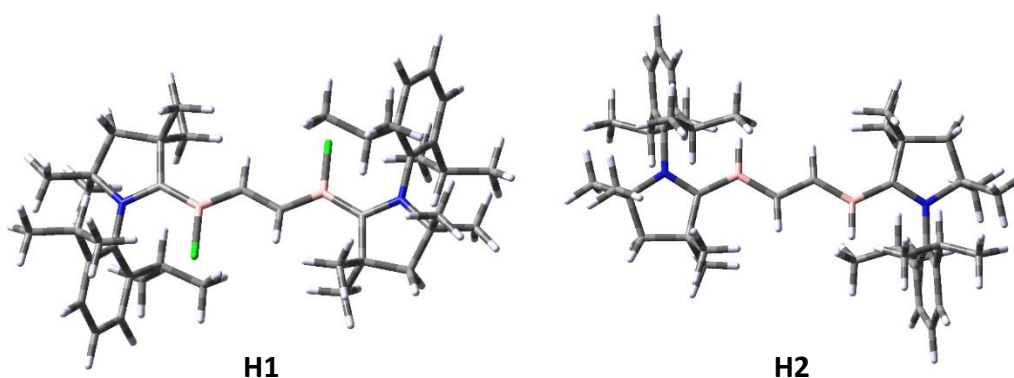
Figure 89: 3D-structure of the hydrogen substituted system with chloride **H1** (left) and the fully hydrogenated molecule **H2** (right).[564]

The geometries of both molecules appear to be very similar (Figure 89), though the behavior shows differences. Calculations of the adiabatic ST gap with the UMN12L functional yield a singlet ground state, which is about 11 kcal/mol more favourable than the triplet for **H1**. The use of SF-BLYP decreases the ST gap to a value of 7.8 kcal/mol. **H2** exhibits a singlet ground state, too, with a slightly larger ST gap of 12 kcal/mol using UMN12L and 10.4 kcal/mol with SF-BLYP. It should be noted that the unrestricted MN12L results are very similar to the SF-DFT findings for this closed shell case, which are denoted as an excellent choice for multireference and non-multireference cases.[318, 319, 409]

Since for **H1** and **H2** the ground state is the singlet, it was analyzed more precisely if this ground state illustrates a multireference character.
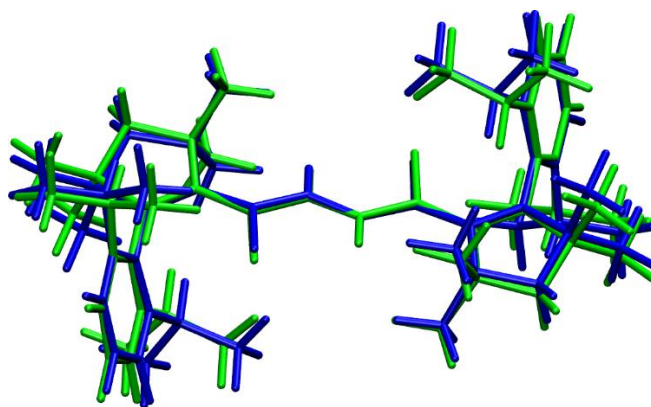
Figure 90: Different geometries of the triplet (green) and the singlet (blue).

Considering the singlet and triplet geometries shown in Figure 90, it is evident that all important aspects of the geometry of the triplet are close by the singlet, only some rotational permitted twists in the substituents of the carbenes can be found. To shorten this analysis, the triplet is not shown here, since both the geometry and electron density appears to be very close to the singlet one, indicating a possible biradical character of the singlet.

The electron density for **H1** and **H2** is delocalized on the nitrogen and carbon of the CAAC, the boron and now additionally on one of the carbon atoms of the ethylene between the boron atoms (Figure 91). Like for **A1** and **A2** there is an antibonding character to the nitrogen of the CAAC. This can be seen in the HOMO and LUMO of **H1** and **H2**, which are depicted in Figure 91.
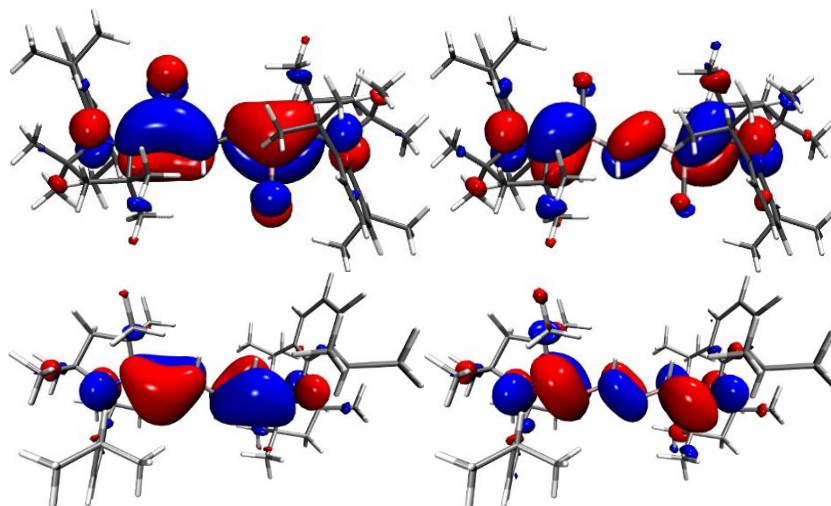
Figure 91: HOMO (left) and LUMO (right) of the singlet for **H1** (above) and **H2** (below).

It gets obvious that there are different bonding situations compared to the alkyl substituted molecules, since the alkene carbon is now in conjugation with the CAAC. Apparently, the centred carbon atoms are in-plane with the B-C-N unit and subsequently a conjugation over the whole system is possible. The electron density of the HOMO is mainly localized in the

N_1-C_{1a}-B_1-C_{1b}-C_{2b}-B_2-C_{2a}-N_2 units with nodal planes between the C_{1b}-C_{2b} double bond and the nitrogen atoms of CAAC. The LUMO is localized on the same atoms, just with different nodal planes. In this case, now between B_1-C_{1b} and symmetrically on the other side C_{2b}-B_2, too. For **H1** and **H2**, the electron density distribution is very similar, only the conjugation to the chloride is missing in **H2**. In both systems, the HL gap is about 25.4 kcal/mol, which makes a population of the triplet or open-shell singlet very unlikely.
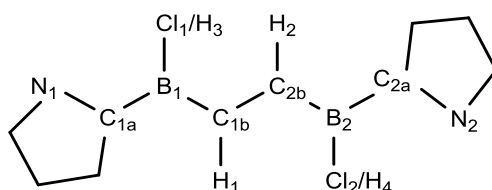
Figure 92: Denotation of the atoms needed for the important parameters of **H1** and **H2**.

The different behavior of the molecules **H1** and **H2** compared to **A1** and **A2** is probably caused by a change in the geometry and therefore resulting in an altered bonding situation. On this account, the important parameters, like the bond length and dihedrals, are collected to obtain the differences. Figure 92 contains the denotation used in the analysis.

The calculated bond lengths are in good agreement with the measured values (both depicted in Table 44), which is expectable for a normal closed shell ground state. In general, the bond lengths, shown in Table 44, remain the same for **H1** and **H2**, except the different ones between hydrogen or chloride and boron. The bond lengths C_{2b}-H_2 and C_{1b}-H_1 are smaller for **H2** than for **H1**. Compared to the alkyl substituted systems, there is a decrease of the bond length B_1-C_1 and thus an increase of the C_{1b}-C_{2b}.

Table 44: Comparison of experimental and theoretical bond lengths of the two molecules **H1** and **H2** calculated with UM12L/6-311G(d, p).

Bond-length [Å]	N_1-C_{1a}	C_{1a}-B_1	B_1-Cl_1/H_3	B_1-C_{1b}	C_{1b}-H_1	C_{1b}-C_{2b}	N_2-C_{2a}	C_{2b}-B_2	B_2-Cl_2/H_4	B_2-C_{2a}	C_{2b}-H_2
Exp. **H1**	1.34	1.53	1.83	1.49	0.93	1.40	1.34	1.50	1.83	1.53	0.93
Exp. **H2**	1.35	1.53	1.10	1.51	0.95	1.40	1.35	1.51	1.10	1.53	0.95
Theor. **H1**	1.34	1.54	1.84	1.49	1.09	1.40	1.34	1.49	1.84	1.54	1.09
Theor. **H2**	1.35	1.53	1.10	1.51	0.95	1.40	1.35	1.53	1.10	1.51	0.95

The change of the bond length is in both cases probably caused by the larger conjugation within **H1** and **H2**. This conjugation needs a planar system to exist, therefore a closer look at the dihedrals is taken. Considering the dihedrals of the theoretical calculated singlet, it appears that the dihedrals of both sides of the ethylene spacer are not completely symmetric. This is in particular the case if the singlet has a biradical character and the perfect symmetric geometry can only be achieved by using multireference methods, since more than one state has to be included. However, the triplet is always slightly more symmetric and closer to the experiment, since it can be described sufficiently with one determinant. Since the difference is only about 1-3° for **H1** and **H2**, only the dihedrals of one side of the singlet state are listed in Table 45. In analogy to the bond length only the dihedrals of the left side of the molecules are shown.

Table 45: Different measured and calculated (UMN12L/6-311G(d,p) dihedrals for **H1** and **H2**.

Dihedral [°]	N_1-C_{1a}-B_1-C_{1b}	B_1-C_{1b}-C_{2b}-B_2	C_{1a}-B_1-C_{1b}-C_{2b}	Cl_1-B_2-C_{2b}-C_{1b}	H_1-C_{1b}-C_{2b}-H_2
Exp. **H1**	164.7	180.0	-175.2	-178.5	-180.0
Exp. **H2**	170.0	180.0	-176.5	-179.1	-179.9
Theor. **H1**	164.8	179.2	-171.6	-177.6	-179.8
Theor. **H2**	170.1	180.0	-176.5	-179.1	-179.9

In contrast to the alkyl substituted systems, the ones with hydrogen are completely planar with a maximum out-of-plane torsion of 20°. As seen for the investigated system without or with a dinitrogen bridge (chapters 5 and 6), the singlet gets more stable, as the system is in-plane and the electron density is conjugated over the whole N-C-B-C-C-B-C-N system. Considering **H1**, the N_1-C_{1a}-B_1-C_{1b} dihedral is more distorted out-of-plane compared to **H2**. However, it is still plane enough to yield a conjugation over the whole system. This conjugation should affect the bond orders of the molecules and their other properties. Consequently, a closer look is taken at the bonding situation and again only the left side is discussed more precisely (Table 46). For this analysis, the bond orders and the natural composition of the systems are investigated. The bonding situation in **H1** and **H2** is almost identical, only small differences are observed caused by the replacement of the strongly electron withdrawing chloride by hydrogen in **H2**. Compared to **A1** and **A2**, the bond order of N_1-C_{1a} increases, while the C_{1a}-B_1 order slightly decreases (Table 46). The main difference can be found in the B_1-C_{1b} and the C_{1b}-C_{2b} bond. While the B_1-C_{1b} bond order is getting stronger (nearly a double bond), the C_{1b}-C_{2b} double bond character decreases to a bond with a slight multiple bond character.

Thereby, the continuous conjugation of the π-system over the entire molecule can be demonstrated. If there exists no explicit double bond, but a conjugation over the whole N-C-B-C-C-B-C-N system, the involved atoms possess a multiple bond character, which represents the conjugated π-system. Since the hydrogen substituted molecules exist as closed shell singlet ground state, there are no spin densities measurable or calculable. However, the spin densities of the triplet state are not delocalized over the whole system, as expected (Table 48). The delocalization of the radicals appears similar to the one found in **A1** and **A2**, where the radicals are just localized on each N-C-B unit.

Table 46: Calculated bond orders of the singlet geometry for **H1** and **H2**.

Bond order	N_1-C_{1a}	C_{1a}-B_1	B_1-Cl_1/H_3	B_1-C_{1b}	C_{1b}-H_1	C_{1b}-C_{2b}
H1	1.31	1.13	0.89	1.54	0.94	1.28
H2	1.27	1.14	0.93	1.54	0.94	1.28

The natural charges (Table 47) primarily demonstrate a decrease of the positive natural charge of the boron caused by the less electronegative hydrogen in **H2** compared to the chloride in **H1**. This difference marginally influences the characteristics of the other atoms justifying why the trend stays the same for both molecules. Compared to **A1** and **A2** (Table 43), C_{1a} illustrates a positive charge for the hydrogenated systems, probably caused by the increased delocalization. Another effect of this conjugation is presumably the decreased positive charge of the boron atoms and the increase in the negative charge of C_{1b} and its counterpart C_{2b}.

Table 47: Natural occupation and charge of the important atoms of **H1** and **H2**.

H1	N_1	C_{1a}	B_1	Cl_1	C_{1b}	H_1
Natural charge	-0.54	0.19	0.44	-0.33	-0.55	0.20
Natural occupation	7.54	5.81	4.56	17.33	6.55	0.80
H2	N_1	C_{1a}	B_1	H_3	C_{1b}	H_1
Natural charge	-0.56	0.22	0.13	-0.10	-0.42	0.13
Natural occupation	7.56	5.77	4.87	1.10	6.42	0.87

Due to the small ST gap of the alkyl substituted systems, a relatively small coupling constant *J* was calculated and confirmed by experiments. Since the ST gaps increase strongly, the constant *J* increases to 2770.92 cm^{-1} for **H1** and 3609.35 cm^{-1} for **H2**. Both energies are achieved in a similar way to the alkyl substituted systems. It is noteworthy that the same

coupling constant J is yielded irrespective of the spin being flipped on N_1, C_{1a} or B_1. This is in line with the assumption of the delocalization of the unpaired electrons over these three atoms on each side.

Experimentally, **H2** possesses definitely a singlet ground state, while **H1** exhibits tendencies to have a close lying triplet next to the singlet (based on EPR and NMR signals). In theory, the ST gap and the energy difference between the HOMO and LUMO are close to each other. Furthermore, the geometry of both systems and the electron density distribution are very similar, too. Therefore, the question remains, why these molecules interact differently in the experiment. In order to find the reason for the behavior, both molecules were analyzed more precisely.

Single point (SP) calculations were performed with the multiplicity of a singlet and triplet on both ground state geometries, R(S_0) and R(T_0). R(S_0) states the minimum geometry of the singlet state and R(T_0) the one for the minimum triplet. By means of the relation between the relative energetic positions of these states in dependency on the ground state geometry another aspect is included. In Figure 93, the calculations are presented with the relative energy difference in eV on the y-axis. As a reference, the energy of the singlet ground state energy of each system, **H1** and **H2**, was taken. The x-axis presents the different geometries depending on the core coordinates R in Å.
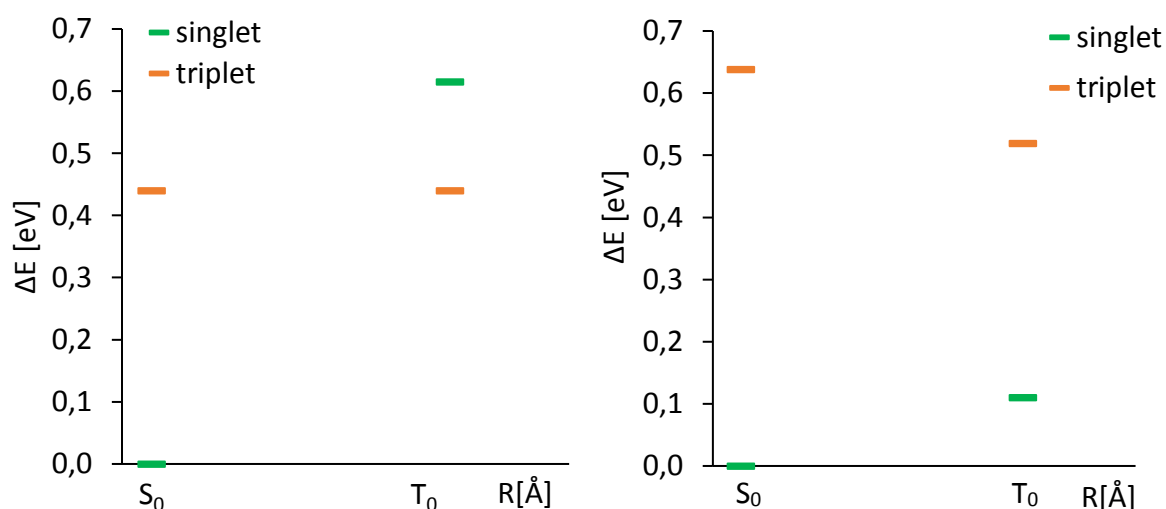
Figure 93: Calculated energies of the singlet and triplet for different minima structures of **H1** (left) and **H2** (right).

The SP calculated for a singlet with the multiplicity of one is always green, the states coloured orange present the triplet with a multiplicity of three. The energy difference of the singlet on

the S_0 structure and the triplet on the T_0 geometry resembles the adiabatic ST gap mentioned above. In the case of **H2**, the singlet stays always more favourable than the triplet, independent on the ground state geometry. The diabatic ST gap (calculating the energy vertical without geometry changes) of **H2** (Figure 93, right) decreases from 0.63 eV of the S_0 structure to 0.39 eV for T_0. For **H1**, the triplet of the minimum triplet structure is more favourable than the singlet calculated on this structure and the other way around. The diabatic ST gap of the S_0 structure is also very small (0.45 eV) and does not change compared to the adiabatic ST gap (0.45 eV). In this case, the triplet state could be thermally populated of little account at room temperature, which effects the spectroscopic behavior of the system.

However, this is not the case for the **H2**, since the diabatic ST gap is about 0.64 eV. Though, even the adiabatic ST gap is similar on both sides, the diabatic ST gap on the ground state singlet geometry differs about 0.2 eV. To find an explanation of the different behavior of the triplet on the singlet geometry, the spin density of this geometry was analyzed. The spin densities of both systems are shown in Table 48 to determine the difference in the relative position of the energy concerning the triplet.

Table 48: Spin densities of **H1** and **H2** calculated with UMN12L/6-311G(d,p) for the triplet.

Spin densities	N_1	C_{1a}	B_1	Cl_1/H_3	C_{1b}	H_1
H1	0.21	0.51	0.28	-0.01	0.03	0.00
H2	0.22	0.51	0.25	-0.02	0.03	0.00

However, there is no difference in the contribution of the spin between **H1** and **H2**, which could explain why the systems differ in their behavior. Although there is only a slightly noticeable change in geometry of **H1** and **H2**, the triplet is better stabilized in **H1** for both the singlet S_0 and the triplet T_0 geometry. There is no spin density on the chloride, which points out the only difference between these systems. Consequently, by an additional chloride instead of a hydrogen next to the boron (**H1**), the triplet seems to get stabilized better, which is caused by the higher electro-positivity of the boron atoms. The most remarkable difference is the energetically decreased triplet of the S_0 geometry of **H1**, whereat **H2** exhibits the reverse trend, which might cause the changed experimental behavior of **H1** compared to **H2**.

7.4   Comparison of A1 and H1

Another interesting aspect is the difference between **A1** (or **A2**) and **H1,** since the only difference is the substituent at the carbon atoms in the middle. While **H1** has a hydrogen atom bound to the ethylene bridge, in **A1** a methyl group replaces the hydrogen atom. The resulting disparity between the alkyl substituted **A1** and **H1** is the twist around the C-B bond and the consequent conjugation, which is outlined in Figure 94. While **A1** has a dihedral of nearly 90° in the C_{CAAC}-B_1-C_1-C_2 plane, the same dihedral is nearly planar (172°) in the case of **H1**.
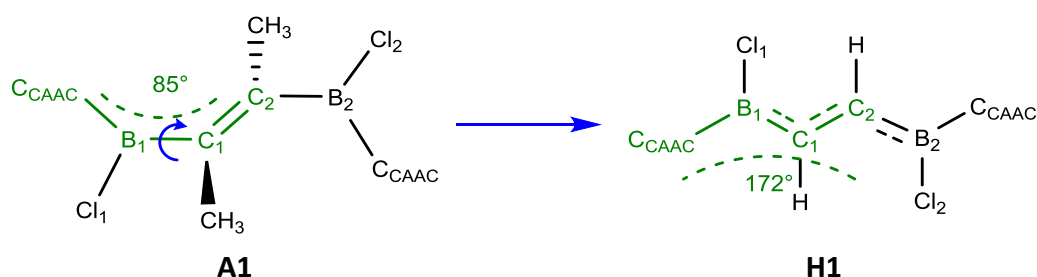
Figure 94: Illustration of the differences in the dihedrals between **A1** (left) and **H1** (right).

By rotating this dihedral $\sphericalangle_{C_{CAAC}B_1C_1C_2}$ about 90°, the molecules can be transferred into each other. Since the rotational barrier is too high due to the steric hindrances, the systems were analyzed without rotations. To evaluate the role of this rotation around the C-B axis, the two structures were calculated in the ground state geometry of the other structure. Thus, both dihedrals $\sphericalangle_{C_{CAAC}B_1C_1C_2}$ = 90, 180° can be preserved.
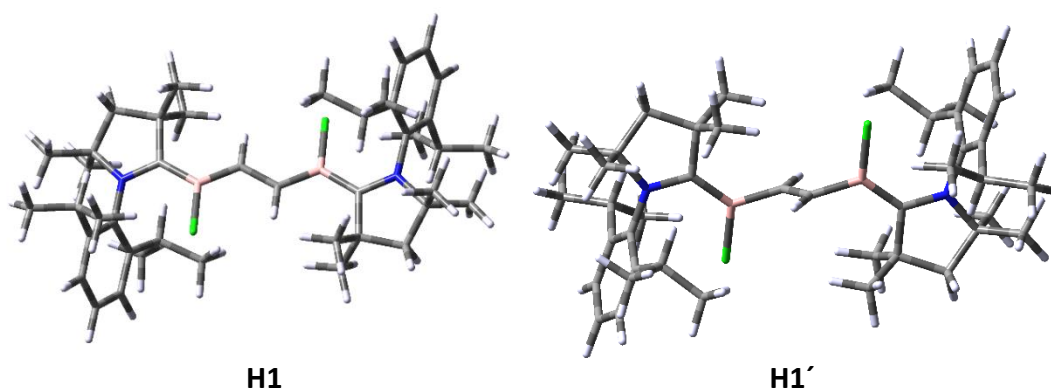
Figure 95: Ground state singlet structure of **H1** (left) and the twisted structure **H1'** (right).

Due to the steric hindrances, a distortion to the global minimum is prevented and a local minimum for the distorted structure is observed. It is noteworthy, that nearly the same results are yielded for both, a geometry optimization with and without constrains concerning the $\sphericalangle_{C_{CAAC}B_1C_1C_2}$ dihedrals. **H1**, which possesses a planar singlet ground structure (Figure 95, left

side) and its twisted conformer **H1'** (Figure 95, right side) were obtained from the **A1** geometry by substituting the methyl groups with hydrogen atoms. With the twisting of **H1** in an orthogonal geometry, the ground state switches the multiplicity and a triplet ground state is obtained. The triplet is located 13 kcal/mol lower in energy than the singlet, which is a similar gap as found for **A1** and **A2**. This result is in line with former systems of chapters 5 and 6 containing no bridge or a dinitrogen bridge. While the complete planar system provides a closed shell singlet structure, the twisted geometry states a biradical arrangement with a very small ST gap.
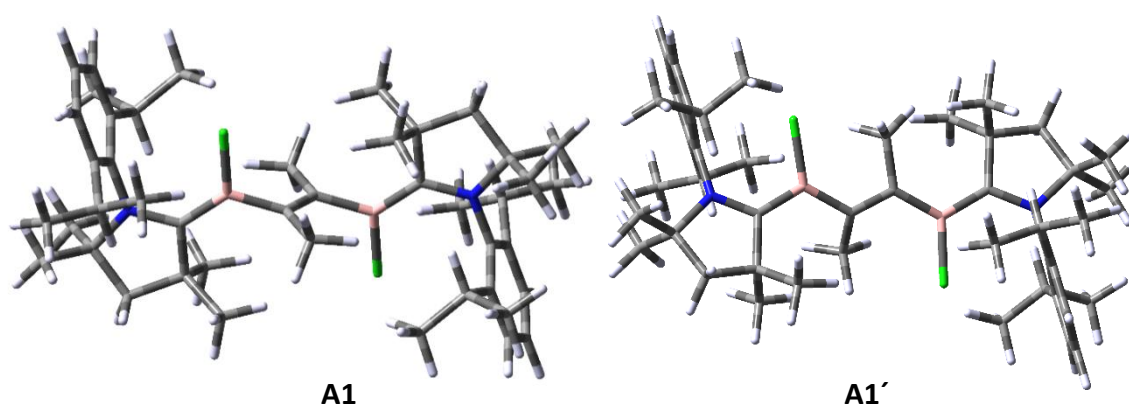
Figure 96: Ground state singlet structure of **A1** (left) and the twisted structure **A1'**(right).

The same procedure was performed for **A1** yielding the coplanar arrangement **A1´** (Figure 96). Therefore, for the planar structure the triplet is still the ground state; however, the ST gap decreases to 7 kcal/mol. Considering the spin densities of the twisted **A1'** yields a contribution similar to the orthogonal systems **A1** and **A2**. The spin densities of the planar systems **H1** and **H2** are also quite similar to the orthogonal systems **A1** and **A2**. However, the molecular orbitals of the rotated **A1'** show a population comparable to **H1** and **H2** and a conjugation over the whole system. For this reason, it is not consistent that the triplet remains the ground state for **A1'**. Thus, the reason for the different arrangements are on the one hand the small steric difference of the methyl group compared to the hydrogen atoms. On the other hand, additionally hydrogen bridges between the chloride and the hydrogen atom can be formed in **H2**.

7.5 Analysis of single system B1 for comparison

Another interesting topic is the behavior of the single system with only one boron, one chloride and one CAAC substituent, since for the twisted structures of **A1** and **A2** there is no conjugation between the two sides of the B-C-C-B bond. If **A1** and **A2** react like the single system on both sides, an understanding of this system is of great interest for the biradical system. A substitution with different atoms might lead to an even more stabilized radical and therefore to a biradical. The molecule was also synthesized in the Braunschweig group by Dr. Philipp Bissinger and is shortened here as **B1** (Figure 97).[458] As there is no second boron atom in the single system, a duryl group is needed to stabilize the mono radical system. Because of its mono radical ground state, the molecule illustrates a normal doublet multiplicity.[458]

B1
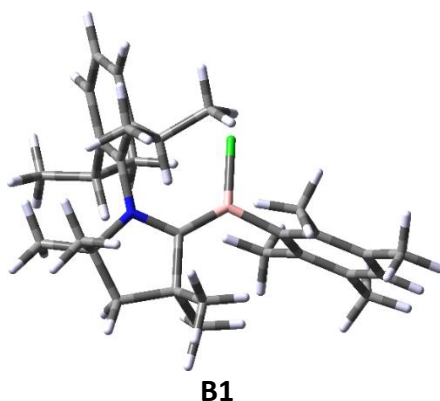
Figure 97: The smaller **B1** system with just one boron-chlorine unit and a duryl ligand attached to boron.

The system is analyzed more precisely and compared to **A1**, since there is no difference between **A1** and **A2**. The values of both systems are summarized in Table 49.

Table 49: Bond lengths and dihedrals of the mono-radical **B1** and its biradical dimer version **A1**

Bond length [Å]	N_1-C_{1a}	C_{1a}-B_1	B_1-Cl_1	B_1-C_{1b}	Dihedral [°]	N_1-C_{1a}-B_1-C_{1b}	Cl_1-B_1-C_{1b}-C_{1c}
B1	1.36	1.52	1.82	1.58	**B1**	173.6	-84.5
A1	1.37	1.51	1.81	1.59	**A1**	174.9	-84.5

The bond lengths of **B1** are very similar to the systems **A1** and **A2** (especially B_1-C_{1b}), since the duryl ligand is rotated and there is no conjugation between this ligand and the rest of the system. The dihedral between the CAAC ligand and the duryl is twisted by nearly 90°, which corresponds to the twisted double bond of **A1**. The other dihedral, N_1-C_{1a}-B_1-C_{1b}, resembles the one of **A1**, too. Apparently, the geometry of the mono radical system **B1** is equal to one half of the biradical **A1**.

The electron density of **B1** and the three frontier orbitals are plotted in Figure 98. The density of the HOMO is located at the duryl ligand. This kind of HOMO is often seen for systems with a π-system as ligand.[572]
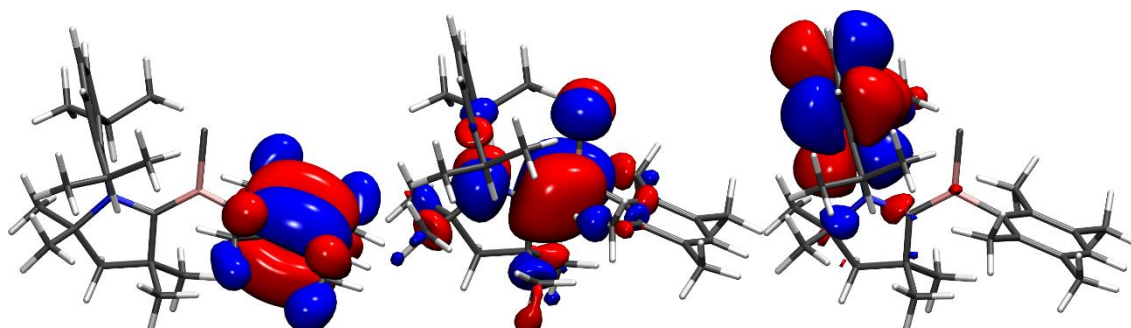
Figure 98: The HOMO (left), SOMO (middle) and SOMO+1 (right) of **B1**.

The SOMO presents similarities to the alkyl substituted system **A1** and **A2** (Figure 88). The SOMO and SOMO+1 of these systems seem to be built of the SOMO of **B1**. They exhibit the same density distribution on the $(N-C)_{CAAC}$ with boron and chloride, even with the same antibonding character to nitrogen and chloride. The SOMO of **A1** and **A2** can be outlined as a positive combination, in which both sides have the same value of the electron density. Whereas the SOMO+1 is the negative combination showing a nodal plane between the two sides of the double bond. The density of the LUMO is mainly localized on the Dip substituent of the CAAC ligand. This kind of orbital can be found in **H1**, **H2**, **A1** and **A2** in a higher order, like the LUMO+1 or LUMO+2.

Taking a closer look at the bond orders (Table 50) reveals that the assumption that **A1** is a combination of twice **B1** linked via a double bond is right. The bond orders of **B1** are very close to the biradical system demonstrating that neither the double bond of **A1** nor the duryl substituent of **B1** influence the stability of the radical centers.

Table 50: Bond orders of **A1** and **B1** calculated with UMN12L/6-311G(d,p)

Bond order	N_1-C_{1a}	C_{1a}-B_1	B_1-Cl_1	B_1-C_{1b}
A1	1.18	1.23	0.95	0.99
B1	1.19	1.34	1.09	0.97

This assumption is affirmed by an analysis of the natural occupation and spin densities (Table 51). The only difference is the charge and occupation of C_{1a} and B_1. C_{1a} shows a smaller partial positive charge for **A1**, i.e. it has a higher natural occupation than in **B1**. Thus, the atom

next to it, C_{1a}, possesses a less negative partial charge for **A1**. In **B1**, the carbon has a slightly increased negative charge.

Table 51: Depiction of the natural occupation, charge and spin density of **A1** and **B1**

Molecule	**A1**					**B1**				
Atoms	N_1	C_{1a}	B_1	Cl_1	C_{1b}	N_1	C_{1a}	B_1	Cl_1	C_{1b}
Natural charge	-0.54	-0.03	0.66	-0.30	-0.39	-0.55	-0.12	0.81	-0.30	-0.42
Natural occupation	7.54	6.03	4.33	17.30	6.39	7.55	6.12	4.19	17.30	6.30
Spin density	0.24	0.49	0.27	0.02	-0.01	0.25	0.50	0.26	0.02	-0.02

This differences in the partial charges seem to have no influence on the spin densities, as the spin density distribution is nearly the same for both molecules. The largest spin density proportion is at the carbon atom of CAAC with one quarter on the nitrogen and the other on the boron atom. Hence, varying the single system **B1** influences the biradical systems, whereat the substituents are apparently of minor relevance. The substitution of chloride with another ligand offers a possibility to control the behavior of the mono radical and its analog dimer.

7.6 Different substituents on the carbon atom

Further molecules with different alkyl substituents were tried to be synthesized in the working group of Prof. Braunschweig yielding either more steric hindrance or different electronic effects. Although two molecules with methyl (**A1**) and ethyl (**A2**) substituents were successfully synthesized presenting a stable biradical behavior, systems with *iso*-Propyl (iPropyl) or phenyl substituents could not be isolated, yet. Therefore, these systems are investigated theoretically to reveal potentially existing destabilizing effects originating from steric or electronic properties yielding unstable molecules. To provide a better overview, the molecule with the iPropyl substituent is labelled as **A3** and the phenyl substituted molecule as **A4** (Figure 99). There is no opportunity to compare the calculated structures with experimental data due to the molecules not been synthesized, as discussed above. The two systems **A3** and **A4** provide geometries similar to **A1** and **A2** with a twisted C-B bond and no conjugation over the C=C double bond.
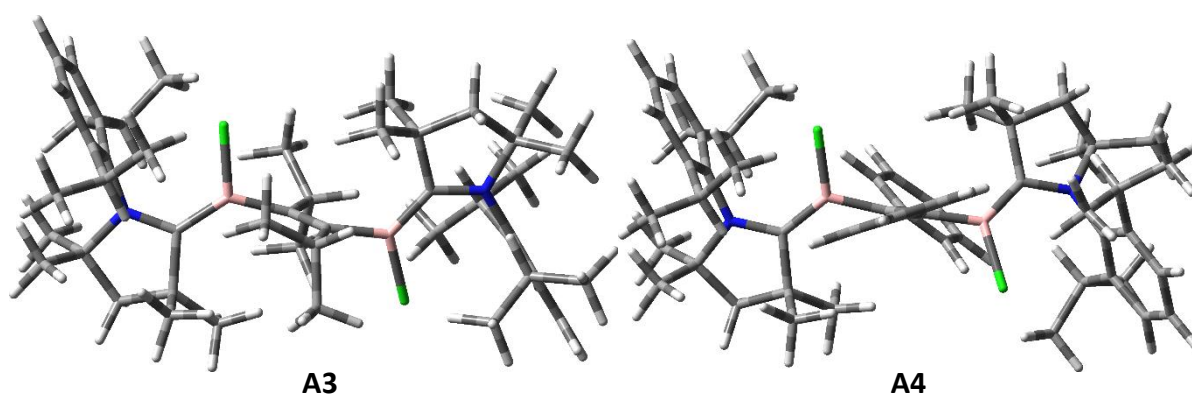
Figure 99: Calculated geometry (UMN12L/6-311G(d, p)) of the singlet ground state of **A3** (left) and **A4** (right).

While **A3** is closer to the synthesized systems **A1** and **A2** with a dihedral of 99°, **A4** shows a rotation towards a more planar structure with a dihedral 122° and a smaller ST gap of nearly 4 kcal/mol. There are two possibilities, why these reactions cannot take place. One is the increasing steric hindrance of the two substituents and the other is the instability of the starting materials, which are synthesized with phenyl and iPropyl as alkyl group substituents. Since the reaction path of such large molecules is challenging to model, only the second possibility is discussed here. Therefore, the absolute energies of the systems were calculated in their respective minimum structure. Since it is meaningless to compare absolute energies of systems with a varying number of molecules, all possible combination of molecules **A1-A4** with the pure substituents methyl, ethyl, iPropyl and phenyl were considered. To establish the affiliation between the substituents and their concerning molecules, the pure substituents were abbreviated analogously by **S1-S4**, whereby **S1** equals methyl and **S4** phenyl.
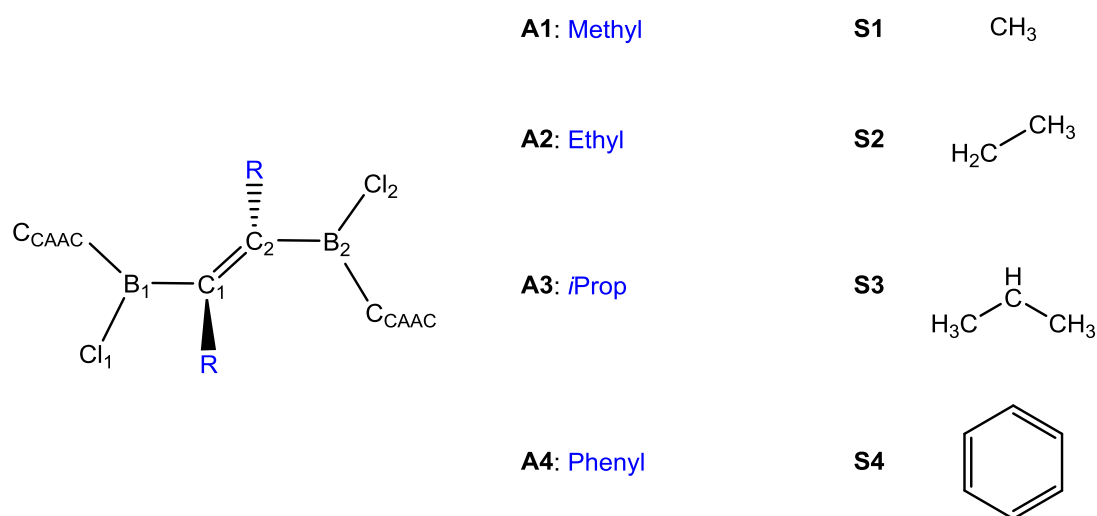
Figure 100: Schematic depiction of the four system **A1-A4** and the substituents **S1-S4**.

For reasons of clarity, an overview of the abbreviated systems **A1-4** and their concerning substituents **S1-4** is shown in Figure 100. Taking the stoichiometry into account, the substituents have to be multiplied by two, since each system **A** contains two substituents **S**, which are bound to the carbon atom of the ethylene bridge. The sum of each combination is shown in the respective box of Table 52. To provide a better overview, the two values, which are supposed to be identical, are marked in the same colour.

Table 52: Different absolute energies in kcal/mol for each combination of the molecules **A1-A4** with the pure substituents **S1-S4**.

	A1	A2	A3	A4
2·S1		-1854329,01	-1903602,88	-2045532,55
2·S2	-1854326,24		-1952885,77	-2094815,44
2·S3	-1903612,66	-1952898,33		-2144101,86
2·S4	-2045509,74	-2094795,41	-2144069,28	

As seen in Table 52, the sum of the different molecules with the substituents are not the same, which provides more favorable and less stable molecules. As the absolute energies are high in value and incomprehensible, the relative energy of each reaction path is illustrated. It should be noted that the reaction does not take place as shown. The illustration just helps to identify the difference in energy of the "starting materials" and "products".

Comparison of A1 with A2

First, the different stability of **A1** and **A2** was assessed. A negative ΔE gives a "product" side, which is more favorable than the "starting materials" on the left side. As mentioned above, the same number of molecules must be on each side. Therefore, the following equation is set up, in which **A1** is summed up with twice the substituent **S2** and on the other side **A2** is summed up with twice **S1**.

$$\mathbf{A1} + 2\,\mathbf{S2} \rightarrow \mathbf{A2} + 2\,\mathbf{S1} \quad \Delta\mathrm{E} = -2.78\,\mathrm{kcal/mol}$$
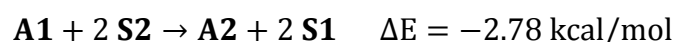
With a slight discrepancy of less than 3 kcal/mol, there is no substantial difference between the two systems **A1** and **A2.** This is in line with the expectations and the calculations made. Nevertheless, this first calculation helps to prove that the quality of this approach is in good agreement with the experiment and can be applied on the other system without experimental

data. It must be mentioned that the stabilities of the pure substituents are not included in this consideration, since there should be no significant disparity between these systems.

Comparison of A1 with A3

The same method was applied to the other molecules and their stabilities were calculated. Herein, the methyl substituted **A1** is compared with the iPropyl substituted **A3**.

$$\textbf{A1} + 2\,\textbf{S3} \rightarrow \textbf{A3} + 2\,\textbf{S1} \quad \Delta E = 9.79\,\text{kcal/mol}$$

In this case, the difference between the two molecules is more significant. With a positive ΔE of about 10 kcal/mol, **A1** is about this value more stable than **A3**. This indicates an energetic destabilization of **A3** caused by the rising steric hindrances of the iPropyl group.

Comparison of A1 with A4

The same comparison was made for the phenyl substituted molecule **A4**, which provides a similar steric hindrance as **A3**.

$$\textbf{A1} + 2\,\textbf{S4} \rightarrow \textbf{A4} + 2\,\textbf{S1} \quad \Delta E = -22.81\,\text{kcal/mol}$$

In contrast to the sterically equal systems **A3**, **A4** shows a more stable ground state than **A1**. Apart from the steric hindrance, the electron pushing effect of the phenyl group seems to stabilize the system.

Comparison of A2 with A3 and A4

In order to assure the quality of the performance the same calculations were performed comparing **A3** and **A4** with **A2**.

$$\textbf{A2} + 2\,\textbf{S3} \rightarrow \textbf{A3} + 2\,\textbf{S2} \quad \Delta E = 12.56\,\text{kcal/mol}$$

$$\textbf{A2} + 2\,\textbf{S4} \rightarrow \textbf{A4} + 2\,\textbf{S2} \quad \Delta E = -20.03\,\text{kcal/mol}$$
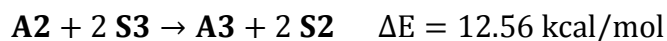
The trend of **A2** to be about 2 kcal/mol more favorable than **A1** can be seen here, too. Compared to the results with **A1**, the tendency is the same with a difference of 2 kcal/mol. While **A3** is somewhat higher in energy, because of its rising steric, **A4** is again much more favorable due to its +M-effect that apparently stabilizes the system significantly.

Comparison of A3 and A4

The systems with the same steric environment are investigated to point out the electronic effects of these substituents.

$$\mathbf{A3} + 2\,\mathbf{S4} \rightarrow \mathbf{A4} + 2\,\mathbf{S3} \quad \Delta E = 32.58\ \text{kcal/mol}$$
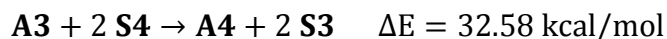
As expected, **A4** is more favorable. Taking the steric effects not into account leads to an electronic stabilization of about 33 kcal/mol by using a phenyl substituent. Since this difference in energy corresponds to the sum of the energy gaps before, the effect of the steric hindrance is, as expected, the same for both systems **A3** and **A4**. While it is plausible that the more unstable **A3** cannot be synthesized, **A4** should actually be synthesizable. One possible explanation could be that the reaction path is hindered and significantly higher in energy due to the phenyl group. This could be the case in the substitution reaction of chloride and CAAC or the last step, the reduction of CAAC-stabilized diborylalkene with potassium graphite, seen in Figure 82.

7.7 Summary

In this chapter, similar molecules, as the one from chapter 6, are investigated. By substituting the dinitrogen with carbon atoms, forming an ethylene bridge, a different behavior is found. For this kind of system, four various molecules were synthesized in the Braunschweig group. An overview of this molecules is provided in Figure 101.
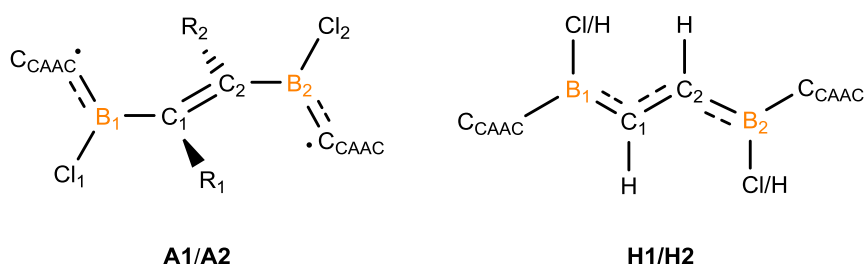
Figure 101: Basic structure of the CAAC stabilized diborylalkenes with the alkyl substituted ones **A1** (R: methyl) and **A2** (R: ethyl) on the left, the hydrogen substituted **H1** (R: hydrogen) and the "all"-hydrogen system **H2** on the right

The systems **A1** and **A2** are formed with alkyl substituents R_1 and R_2 bound to the bridging carbon atoms and chlorides on the boron atoms (Figure 101, left). Both systems form a C=C double bond with a coplanar $\sphericalangle_{\mathrm{BCCB}}$ dihedral. However, the carbene is twisted out-of-plane by nearly 90° and ensures that there is no conjugation between the ethylene bridge and the CAAC

ligands. As already seen for this kind of twisted systems, the ground state is a biradical with a very small ST gap (0.22 kcal/mol for **A2**, 0.39 kcal/mol for **A1**). The two radicals are mainly located on the carbon atom of each CAAC unit, which is proven by experiment and theoretical calculations. Because of the multiple bond character of N-C-B, the radical is slightly delocalized over these three atoms, too.

When hydrogens are attached to the bridging carbon atoms, a slightly different picture appears (**H1**). System **H2**, which is completely substituted by hydrogen atoms, arranges completely coplanar equal to **H1** (Figure 101, right).

On the first look, **H1** and **H2** are very close in energy and both systems exhibit a singlet with a ST gap of 8-10 kcal/mol. The different bonding pattern can be explained by completely coplanar systems, in which the C-C bond order decreases and shows only a slight multiple bond character, while the B-C bond illustrates a nearly double bond character. Both systems demonstrate almost the same geometry and electronic properties. However, they substantially differ in experiments, with **H2** being a singlet and **H1** appearing as triplet. This can be attributed to the close lying diabatic triplet of **H1** to the singlet minimum structure, which is highly increased for **H2**. Thus, by substituting boron with hydrogen, it gets less electropositive, which results in a slightly destabilization of the triplet.

The difference between **H1** and **A1** is observed in the substituent bound to the carbon atom in the center of the molecule. Since both systems arrange in another way concerning the B-C-C-B bridge, even this small steric influence resulting from the substitution of a hydrogen to a methyl is enough to cause this change. Besides the steric effects, the hydrogen bond of chloride, which can be formed in the planar **H1**, is one of the significant differences, since it cannot be formed in **A1**.

The single system **B1**, which depicts a mono radical and shows the same properties as just one side of the molecules **A1** and **A2**, confirms the suggestion that both radicals centered on each side of the ethylene bridge do not interact. Hence, variations of the single system **B1** influences the biradical systems, whereas the substituents are apparently of minor relevance.

The idea of attaching bulkier substituents, as iPropyl or phenyl, to the carbon atoms could not be realized in the laboratory so far. An analysis of the stability of these compounds shows that the increase of system size with iPropyl destabilizes the ground state about 10 kcal/mol, while

a substitution with phenyl leads to a more stable compound of about 20 kcal/mol. Nevertheless, both systems are found to be stable and should be synthesizable in the laboratory. In particular, the phenyl substituted system seems to be a very interesting molecule to study in future works.

8   Summary

In this work, biradical boron containing systems with various structures are investigated to reveal the dependency of the biradical character on the ligated carbene (NHC, CAAC) and the related steric demands of the substituents. An overview of all investigated systems with their concerning ST gaps, ground state multiplicities and geometric appearances is given in Table 53.

The findings of the benchmark clearly indicate that the use of conventional DFT approaches are satisfactory to generally provide quite accurate results for the triplet ground state of diborane systems. On the contrary, the singlet state with rising biradical character is poorly described by most of the utilized functionals, as they describe the geometry of the singlet biradical incorrectly. By using the BS approach this error can be decreased tremendously with a MAD of less than 5 kcal/mol for most of the DFT functionals. The most suitable functionals with a small ST gap error of 1 kcal/mol are MN12L, MN12SX, M06L, M062X, M08HX, SVWN, PW6B95D3 and SOGGA11X.

Apart from calculations with broken-symmetry DFT and its specific functionals, spin flip DFT is employed. In particular, this application demonstrates the ability to describe both, closed shell and open shell systems, with multireference character accurately. Another additional benefit of SF-DFT is the combined application with different DFT functionals and, therefore, its utilization for huge systems. However, it needs to be considered that the quality of the SF calculation depends on an accurate description of the triplet state. As known before, CCSD(T) provides mostly accurate results in contrast to its Coupled-Cluster counterpart, CCSD, without taking triplet excitations into account. However, for a larger system size, Coupled-Cluster methods are only applicable with the DLPNO approximation. The use of this approximation increases the calculable system size, but reduces the quality of the obtained ST gap compared to NEVPT2 or experimental results.

Table 53: Overview of the investigated molecules with their ground state multiplicities and ST gaps according to their geometrical appearance.

Molecules	R	Ground state	ΔE_{ST} [kcal/mol]	Dihedrals [°]
	phenyl methyl *n*-butyl	triplet	6-7	SBBS: 90 NCBB 170
	phenyl methyl n-butyl	closed shell singlet	22-30	SBBS: 160 NCBB: 100
		closed shell singlet	12	BNNB: 110 NCBN: 160
		triplet	0.1	BNNB: 170 NCBN: 170
	methyl ethyl	closed shell singlet	0.3	BCCB: 180 CBCC: 90
	hydrogen chloride	singlet	8	BCCB: 180 CBCC: 180

It turned out that complete active space methods with perturbation correction terms for dynamical correlation, such as CASPT2 or NEVPT2, illustrate the best methods to describe biradicals. As these methods exhibit major issues with the system size of the investigated, inorganic biradical systems, a combination of the UMN12L functional and SF-DFT using the BLYP functional represents the method of choice for huge biradical systems. These functionals provide highly accurate results for both, the triplet and the biradical singlet state.

This obtained knowledge is used in the calculation of CAAC and NHC stabilized diborenes **I** or diboranes **II** (Figure 102). The basic structure of molecule **I** and **II** are depicted in Figure 102 with various substituents bound to the sulphur next to the boron atoms.
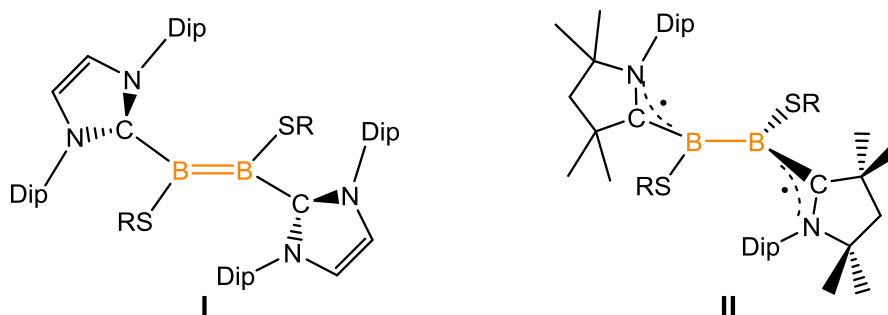
Figure 102: Basic structure of investigated diborenes ligated with NHC (left) and diboranes with CAAC ligands (right) and with R= methyl, *n*-butyl or phenyl.

The CAAC substituted diborane arranges in an orthogonal C-B-B-C plane and forms a biradical with no conjugation between the boron atoms, which are connected by B-B single bonds. In contrast, the diborene with NHC ligands builds a coplanar C-B-B-C corpus with a B=B double bond. Thus, the CAAC diborane possesses a triplet ground state with a biradical singlet state lying close by, while the NHC diborene forms a closed shell singlet with no biradical character. The triplet CAAC systems shows a conjugation through the N-C-B of the CAAC ligands leading to a spin density, which is delocalized over the carbon and nitrogen of the carbene and even partially over the boron atoms on each side. With a plane C-B-B-C unit, the carbene ligands of the NHC are twisted out-of-plane making a conjugation with the complete carbene ligand impractical. A variation of the size of the sulphur bound substituents R (Figure 102) demonstrates that this part seems to have no influence on the electronic structure of both systems. However, by decreasing both the sulphur and the nitrogen substituents of the carbene ligands, the CAAC and NHC ligated systems tend to arrange all coplanar. Thus, without the steric hindrances forcing the molecules out-of-plane, both systems arrange as diborene.

This leads to the assumption that by increasing the steric hindrances, the molecules are forced to either give up the conjugation through the C-B-B-C component or the one build by the boron atoms and the carbene ligands, B-C-N. The question, why the CAAC ligated system **II** sacrifices the C-B-B-C conjugation, whereas the NHC ligated system **I** abandons the B-C-N conjugation was analyzed more precisely considering the influence of the different conjugations in a decreased model system (Figure 103).
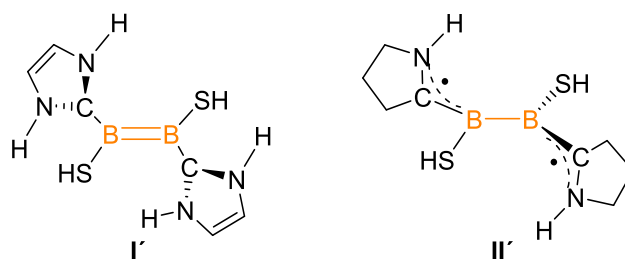
Figure 103: Model systems for the analysis of the influence of the different carbene ligands NHC (left) **I'** and CAAC(right) **II'**.

Forcing the system into a planar or twisted dihedral of the C-B-B-C plane or the B-B-C-N dihedral to the carbene, conjugations are either possible or unfeasible. It is obvious that the triplet ground state can be achieved by **II**, since the HL gap appears significantly smaller compared to the one from **I**. As this trend continues in the model systems, it seems consistent that the ST gap for model compound **II'** decreases, as well. This difference in energies of the HOMO and LUMO for both model compounds can be attributed to the fact that the LUMO of **I** is energetically unfavorable compared to **II**, while the HOMOs of both systems show nearly no difference in their energetic behavior. The increase in energy of the LUMO of **I** can be explained by the enhanced antibonding character in the NHC, since the nodal plane appears between N and C of the carbenes and a NHC possesses twice the number of nitrogen atoms compared to CAAC. Additionally, the B-B rotation is of great interest, since the cost of a rotation around the B-B bond correspond to the ST gap of each compound. Thus, the small ST gap for the B-B single bond in **II** and the highly increased ST gap for the B=B double bond in **I** can be explained thereby.

Figure 104 emphasizes the different stabilizing effects of the two carbene ligands. By rotating the diborene around the B-B-axis, a biradical with a B-B single bond is obtained. This biradical possesses a stable structure ligated by CAAC, but with NHC the molecule is not stable.
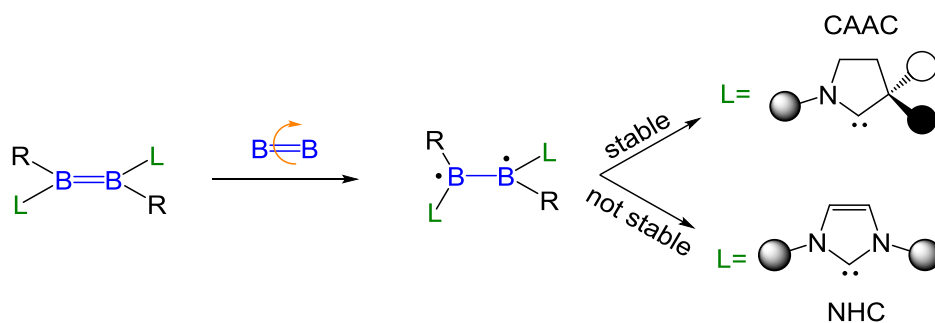
Figure 104: By a 90° torsion of the B=B double bond only the CAAC ligated system provides a stable ground state.

Another boron-containing species that was synthesized by the Braunschweig group shows almost the same structural properties compared to the investigated diborane and diborene systems with the substantial difference that additionally these species illustrate a dinitrogen bridge between the two boron atoms (Figure 105). By this change in the structural and electronic properties, a different behavior is observed.
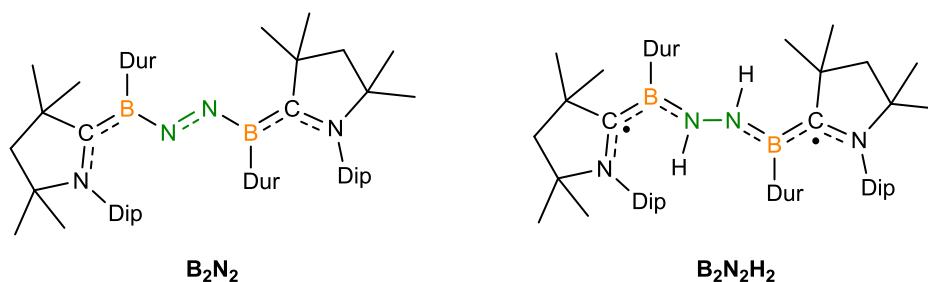
Figure 105: Two different dinitrogen complexes without hydrogen (left) and with hydrogens atoms bound to the bridging nitrogen (right).

On the one hand, the singlet closed shell molecule **B$_2$N$_2$** arranges in a $\sphericalangle_{B_1N_1N_2B_2}$ (numeration depicted in Figure 106) twisted conformation showing a N=N double bond and multiple bond character between the remaining system and the carbene ligands. On the other hand, the hydrogenated counterpart **B$_2$N$_2$H$_2$** possesses a biradical ground state, in which singlet and triplet are nearly degenerate, illustrating an almost coplanar geometry. With hydrogen bonding to nitrogen due to one additional unpaired electron on each nitrogen, the antibonding π^*-orbital of the N-N gets occupied resulting in a N-N single bond.

Since the amount of electron density located on the main B-N-N-B bridge presents an important parameter, both substituents on the boron and carbene nitrogen atoms are varied to investigate whether they influence the system sterically or electronically. The various subsystems of **B$_2$N$_2$** illustrate no differences in the bonding pattern and small changes in geometry are predominated by other electronic effects, such as hydrogen bonds (N···H) or

π-π-stacking of phenyl substituents. While the geometry of the **B₂N₂** substructures exhibit no changes, the minimum geometry of the **B₂N₂H₂** subsystems appears in contrast as twisted geometry at the $\sphericalangle_{B_1N_1N_2B_2}$ dihedral with a singlet ground state. An in-detail study reveals no significant differences in the electronic properties for the substructures of **B₂N₂** and the minimum structures are those with the highest amount of hydrogen bonds or π-stacking. Since **B₂N₂H₂** possesses a N-N single bond, a rotation around the dinitrogen is possible at room temperature.

B₂N₂   **B₂N₂H₂**
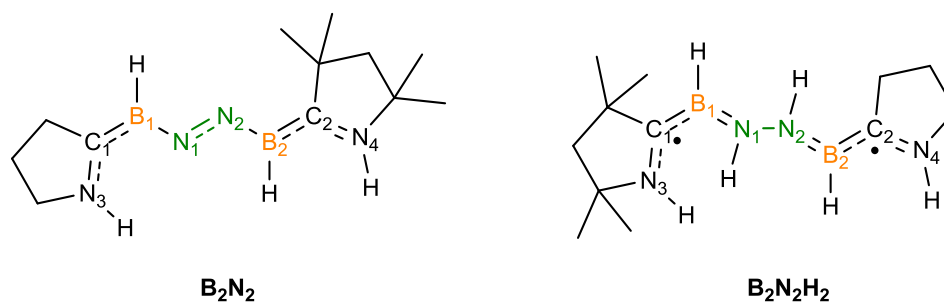
Figure 106: Numeration of both model systems for the definition of the dihedrals.

By varying the three important dihedrals $\sphericalangle_{B_1N_1N_2B_2}$, $\sphericalangle_{N_3C_1B_1N_1}$ and $\sphericalangle_{N_2B_2C_2N_4}$ between 0°, 90° and 180°, the detailed influence of the geometry on the electronic properties was investigated. For the model systems, the orthogonal structure ($\sphericalangle_{B_1N_1N_2B_2}$ = 90°) exhibits the most favorable one for the smallest substructures of **B₂N₂H₂**. However, with a difference of only 8 kcal/mol compared to the all coplanar geometry and no substantial differences regarding the KS orbitals, the size of the energy gap can be reduced to interaction effects caused by hydrogen bonds, which can also be formed in the orthogonal case. On the contrary, the conjugation of the B-N-N-B bridge with the carbenes and thus the planarity of the $\sphericalangle_{N_3C_1B_1N_1}$ dihedrals play a more important role regarding the electronic properties. When the carbene ligands arrange orthogonally to the B-N part, the bonding pattern is shifted resulting in a near B=N double bond and a C-B single bond. Consequently, in **B₂N₂H₂** the spin density is mainly localized on the carbon. This kind of bonding pattern reveals a destabilization of the system up to 40 kcal/mol.

The substructures of **B₂N₂** illustrate that the system has to arrange orthogonally regarding the $\sphericalangle_{B_1N_1N_2B_2}$ dihedral to form the N=N double bond. By forcing the system to a coplanar structure, the nitrogen bond becomes a single bond with a triplet ground state. If the carbenes are twisted out-of-plane, the singlet and triplet get highly unfavorable, in particular for

$\sphericalangle_{B_1N_1N_2B_2}$ = 90°. Caused by the missing conjugation from boron to carbon, the p-orbital of the boron donates electron density only to nitrogen leading to a B=N double bond and a N-N single bond.

Derivatives of these molecules were synthesized in the Braunschweig group with two carbon atoms instead of dinitrogen forming a double bond in between the boron atoms. As seen in Figure 107 (left), the systems for alkyl substituents R on the bridging carbon and chlorides on the boron atoms forming systems **A1** and **A2**, tend to arrange as open shell molecules with a high biradical character. Since the ST gap is less than 1 kcal/mol, a clear definition of the ground state multiplicity is not possible. The alkyl substituted systems **A1** and **A2** exhibit a C=C double bond with a planar orientation of the B-C-C-B unit. However, the carbene is twisted out-of-plane and no conjugation is obtained between the CAAC ligand and the C=C double bond. Between N-C-B, a multiple bond character is observed combined with the spin densities for the triplet being located on all three atoms. There is no difference seen in the substitution of methyl **A1** to ethyl **A2**. However, substituting the bridging carbon atoms by hydrogens leads to a slightly different picture. This appears for the molecules **H1** and **H2**, which are completely substituted by hydrogen atoms.

A1/A2　　　　　**H1/H2**
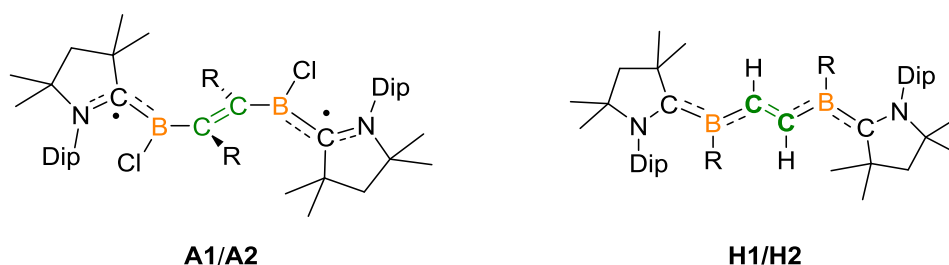
Figure 107: Basic structure of the CAAC stabilized diborylalkenes with the alkyl substituted ones **A1** (R: methyl) and **A2** (R: ethyl) on the left, the hydrogen substituted **H1** (R: hydrogen) and the "all"-hydrogen system **H2** on the right.

On the first look, **H1** and **H2** are very close in energy and both systems show a singlet with a ST gap of 8-10 kcal/mol. The different bonding pattern can be explained by completely coplanar systems, in which the C-C bond order decreases and shows only a slight multiple bond character, while the B-C bond illustrates nearly double bond character. Both systems exhibit almost the same geometry and electronic properties. However, experimentally they differ substantially, with **H2** being a singlet and **H1** appearing as a triplet. This can be attributed to the close lying diabatic triplet of **H1** to the singlet minimum structure, which is highly

increased for **H2**. Thus, by substituting boron with hydrogen, it gets less electropositive, which results in a slight destabilization of the triplet.

The difference between **H1** and **A1** consists only in the substituent bound to the carbon atom in the center of the molecule. Since both systems arrange differently concerning the B-C-C-B bridge, even this small steric influence resulting from the substitution of a hydrogen to a methyl is enough to cause this change. Besides the steric effects, the hydrogen bond of chloride, which can be formed in the planar **H1**, is one of the significant differences, since it cannot be formed in **A1**.

The idea of attaching bulkier substituents, as iPropyl or phenyl, to the carbon atoms could not be realized in the laboratory so far. An analysis of the stability of these compounds shows that the increase of system size with iPropyl destabilizes the ground state about 10 kcal/mol, while a substitution with phenyl leads to a more stable compound of about 20 kcal/mol. Nevertheless, both systems are found to be stable and should be synthesizable in the laboratory. In particular, the phenyl substituted system seems to be a very interesting molecule to study in future works.

9   Zusammenfassung

In dieser Arbeit werden biradikalische Bor-Systeme mit unterschiedlichen Strukturen untersucht, um die Abhängigkeit des biradikalischen Charakter von der Carben-Einheit, die am Bor (NHC, CAAC) gebunden ist, und den sterischen Anspruch der Substituenten zu analysieren. Eine Übersicht aller untersuchten Systeme, einschließlich der Multiplizität ihres Grundzustands, der geometrischen Parameter und des ST Gaps, ist in Tabelle 1 gezeigt. Um die biradikalischen Systeme in korrekter Weise zu beschreiben, werden präzise und robuste theoretische Methoden benötigt, weshalb zunächst ein Benchmark durchgeführt wird.
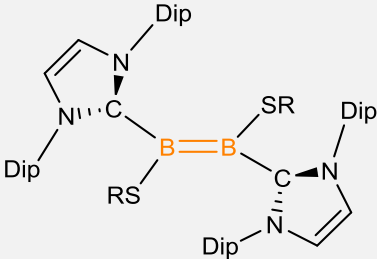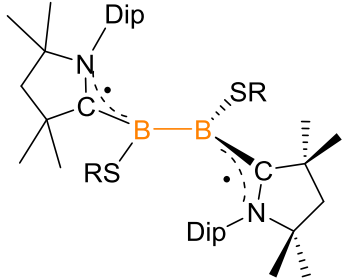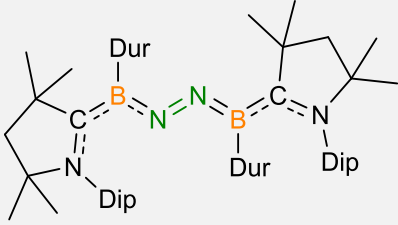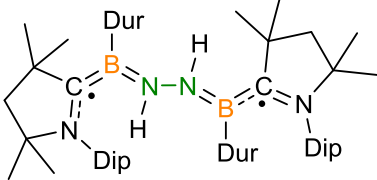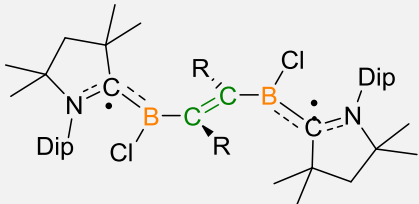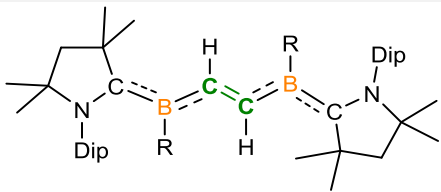
Aus den erhaltenen Ergebnissen des Benchmarks konnte gefolgert werden, dass konventionelle DFT-Methoden in der Regel zufriedenstellende und präzise Resultate für die Berechnung von Triplett-Zuständen der Diboran-Systeme liefern. Im Gegensatz dazu werden Singulett Zustände mit steigendem Biradikalcharakter von den meisten DFT-Funktionalen nur unzureichend beschrieben, da bereits die Geometrien der Singulett Biradikale fehlerhaft dargestellt wird. Indem man den Broken-Symmetrie (BS)-Ansatz mit DFT verwendet kann dieser Fehler immens verkleinert werden. So liegt die mittlere absolute Abweichung für fast alle DFT-Funktionale unterhalb 5kcal/mol. Funktionale, wie MN12L, MN12SX, M06L, M062X, M08HX, SVWN, PW6B95D3 und SOGGA11, sind am besten geeignet, da diese nur einen geringfügigen Fehler von < 1 kcal/mol in der Berechnung des ST Gaps aufzeigen.

Neben der Berechnung mit DFT-Funktionalen mithilfe des (BS) Ansatzes, wurde auch Spin-Flip (SF)-DFT verwendet. Insbesondere dieser Ansatz ist in der Lage, sowohl closed-shell als auch open-shell Systeme mit Multireferenzcharakter korrekt zu beschreiben. Ein weiterer Vorteil von SF-DFT ist die Anwendung in Kombination mit anderen DFT-Funktionalen, die es auch ermöglicht, größere Systeme zu berechnen. Hier muss jedoch beachtet werden, dass die Qualität der SF-Ergebnisse von der Güte des berechneten Tripletts abhängt.

Es ist bereits Literatur bekannt, dass CCSD(T) in der Regel präzisere Ergebnisse als CCSD, dem Coupled-Cluster Funktional ohne Berücksichtigung der Triplett Anregungen, erzielt. Allerdings können die Coupled-Cluster Methoden für größere Systeme nur unter Einbeziehung der DLPNO Näherung verwendet werden.

Tabelle 1: Übersicht der untersuchten Systeme mit Aussage über ihre Multiplizität, die Geometrie des Grundzustandes und die berechneten ST Gaps.

Moleküle	R	Grundzustand	ΔE_{ST} [kcal/mol]	Dieder-winkel [°]
	Phenyl Methyl *n*-Butyl	closed-shell Singulett	22-30	SBBS: 160 NCBB: 100
	Phenyl Methyl *n*-Butyl	Triplett	6-7	SBBS: 90 NCBB 170
		closed-shell Singulett	12	BNNB: 110 NCBN: 160
		Triplett	0.1	BNNB: 170 NCBN: 170
	Methyl Ethyl	Biradikal Singulett	0.3	BCCB: 180 CBCC: 90
	Wasserstoff Chlorid	Singulett	8	BCCB: 180 CBCC: 180

Diese Näherung ermöglicht zwar die Berechnung von größeren Systemen, führt jedoch im Vergleich zum Experiment oder den NEVPT2 Ergebnissen auch zu einem höheren Fehler bei den berechneten ST Gaps. Es hat sich gezeigt, dass Complete Active Space (CAS) Methoden mit störungstheoretischen Korrekturtermen für die dynamische Korrelation, wie z.B. NEVPT2 oder CASPT2, die besten Methoden zu Beschreibung von biradikalischen Systeme darstellen. Da diese Methoden signifikante Probleme mit der Größe der untersuchten, anorganischen Biradikal-Systeme aufzeigen, hat sich eine Kombination aus dem UMN12L-Funktional und SF-DFT unter Einbezug von BLYP als beste Wahl für die anspruchsvollen biradikalische Systeme bewährt.

Diese erhaltenen Ergebnisse wurden zur Berechnung von CAAC und NHC stabilisierten Diboranen bzw. Diborenen (Tabelle 1, Zeilen 1 und 2) mit verschiedenen Substituenten am Schwefel-Liganden der Bor-Atome herangezogen. Die Grundstruktur beider Systeme ist in Abbildung 1 gezeigt.
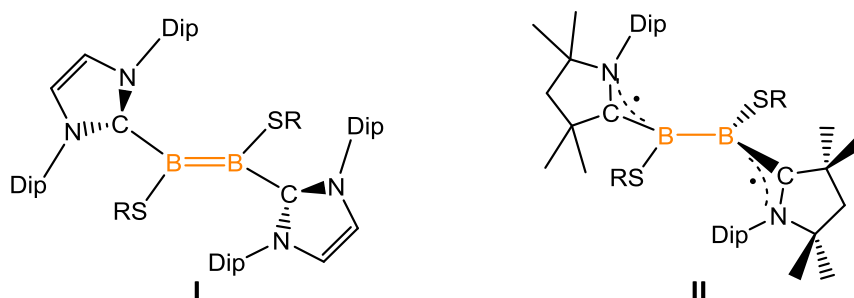
Abbildung 1: Basisstruktur der untersuchten Diborene/Diborane, die mit NHC Carbenen (links) und CAAC Carbenen (rechts) substituiert sind (R: Methyl, *n*-Butyl oder Phenyl).

Die CAAC stabilisierten Diborane **II** bilden Biradikale mit einer orthogonalen C-B-B-C Ebene. Dadurch kann keine Konjugation zwischen den Boratomen entstehen, was zu einer B-B Einfachbindung führt. Im Gegensatz dazu bilden die Diborene mit NHC Liganden **I** eine planare C-B-B-C Ebene mit einer B=B Doppelbindung. Dies führt dazu, dass die NHC stabilisierten Diborene einen closed-shell Singulett als Grundzustand ohne Biradikalcharakter besitzen. Dahingegen weisen die CAAC substituierten Diborane einen Triplett Grundzustand mit einem energetisch nahe liegenden Singulett Zustand mit einen hohen Biradikalcharakter auf. Die Triplett Zustände der CAAC-Systeme zeigen eine Konjugation des Bors über die Carben Liganden (N-C-B). Dies führt zu einer Delokalisation der Spindichte des ungepaarten Elektrons über das Kohlenstoffatom und den Stickstoff des CAAC Liganden, sowie zu einem kleinen Anteil über das Bor Atom. Da im Falle des NHC substituierten Diborenes die C-B-B-C Einheit

planar vorliegt, werden die NHC Liganden aus sterischen Gründen aus der Ebene gedreht, wodurch eine Konjugation über die Carben-Einheiten verhindert wird. Durch eine Variation der am Schwefel gebundenen Reste mit unterschiedlichen Substituenten wurde gezeigt, dass diese Gruppen keinen Einfluss auf die elektronische Struktur besitzen. Dies ist auch der Fall für die CAAC stabilisierten Moleküle.

Wenn die Größe der Substituenten am Schwefel und Stickstoff verkleinert wird, hat dies eine Planarisierung der CAAC und NHC stabilisierten Systeme zur Folge. Für den Fall, dass ein fehlender sterischer Anspruch die Moleküle nicht aus der Ebene zwingt, bilden beide Systeme ein Diboren. Dieses Verhalten führt zur Annahme, dass mit zunehmendem sterischen Anspruch die Moleküle gezwungen werden, entweder die Konjugation der C-B-B-C Einheit oder die der N-C-B Komponente, welche mit dem Carben gebildet wird, aufzulösen. Mit Hilfe der Modellsysteme **I´** und **II´** wurde untersucht, weshalb die CAAC stabilisierten Diborane die C-B-B-C Ebene verdrehen und somit die Konjugation aufgeben, wohingegen die NHC Systeme die Konjugation mit den Carbenen durch Verdrehen dieser Ebene (B-B-C-N) auflösen. In Abbildung 2 werden die beiden Modellsysteme **I´** und **II´** gezeigt, bei denen sämtliche Substituenten durch Wasserstoff ersetzt wurden.
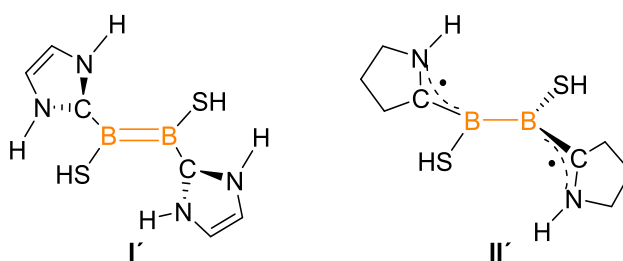
Abbildung 2: Modellsysteme zur Analyse des Einflusses der unterschiedlichen Carben Liganden NHC (links) **I** und CAAC (rechts) **II`**.

Indem die beiden wichtigen Diederwinkel, CBBC und BBNC, in eine planare (180°, 0°) oder verdrehte (90°) Anordnung gebracht werden, wird entweder eine Konjugation ermöglicht oder verhindert. Offensichtlich kann der Triplett Grundzustand von **II** erreicht werden, da in diesem CAAC System das HL Gap im Vergleich zu **I** sehr klein ist. Dieser Trend setzt sich auch im Modellsystem **II´** fort, wodurch ebenfalls ein minimal verkleinertes ST Gap entsteht. Der Energieunterschied des HL Gaps zwischen **I´** und **II´** kann darauf zurückgeführt werden, dass die HOMOs der beiden Systeme energetisch gesehen keine Unterschiede aufzeigen. Das LUMO von **I** hingegen liegt energetisch höher als das von **II**. Betrachtet man die LUMOs der

beiden Systeme, so ist eine Knotenebene zwischen dem Kohlenstoff und dem Stickstoff des Carbens erkennbar. Da CAAC nur ein Stickstoff, NHC jedoch zwei Stickstoff Atome besitzt, ist es naheliegend, dass der Energieanstieg des LUMOs von NHC auf den durch die doppelte Anzahl an Stickstoff Atomen verursachten stärkeren antibindenden Charakter zurückzuführen ist. Ein weiterer wichtiger Faktor, der in diese Betrachtung miteinbezogen werden muss, ist die Rotation um die B-B-Bindung, da das ST Gap des jeweiligen Systems, I` oder II`, in etwa der für eine Rotation um die B-B-Bindung benötigten Energie entspricht. Mit dieser Beobachtung kann das relativ kleine ST Gap für die B-B-Einfachbindung in **II** erklärt werden, während das Gap für die B=B-Doppelbindung von **I** einen größeren Wert besitzt. Abbildung 3 verdeutlicht die verschiedenen Stabilisierungsmöglichkeiten der beiden Carben Liganden. Durch Rotation der B-B-Bindung erhält man ein Biradikal mit einer Bor Einfachbindung, welches aufgrund der unterschiedlichen Verhaltensweisen der zwei Carben Liganden entweder stabil (CAAC) oder instabil (NHC) ist.
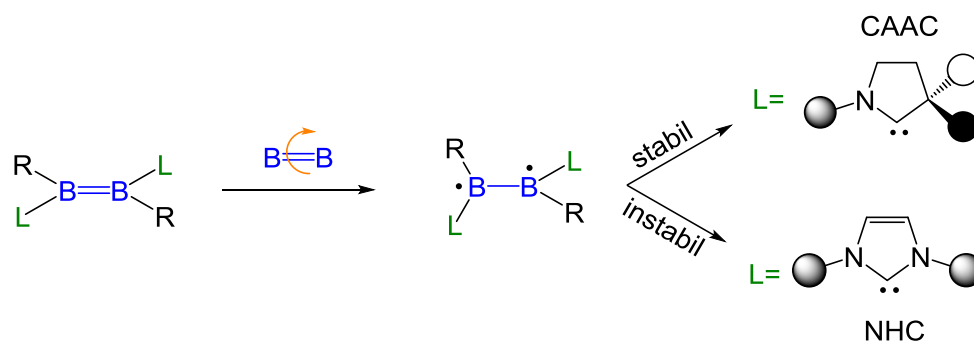
Abbildung 3: Durch die Drehung der B=B Doppelbindung um 90° entsteht eine B-B-Einfachbindung, die nur mit CAAC stabil ist.

Eine weitere vom Arbeitskreis Braunschweig synthetisierte Bor -Molekülklasse, die ein ähnliches Verhalten zu dem der Diborane und Diborene zeigt, enthält eine zusätzlich Distickstoffbrücke zwischen den beiden Bor Atomen (Tabelle 1, Zeilen 3 und 4). Durch diese Modifikationen bezüglich der strukturellen und elektronischen Eigenschaften kann ein unterschiedliches Verhalten beobachtet werden.

Abbildung 4: Zwei unterschiedliche Distickstoff-Verbindungen ohne Wasserstoff (links) und mit Wasserstoff (rechts) gebunden an die Stickstoff Atome der Brücke.

Auf der einen Seite ordnet sich das **B₂N₂** Molekül als closed-shell Singulett mit einer verdrehten BNNB Geometrie an. Durch diese Verdrehung können die leeren p-Orbitale des einen Stickstoffs mit dem sp²-Orbital des anderen Stickstoffs, welches das freie Elektronenpaar beinhaltet, wechselwirken, wodurch diese Verbindung eine Doppelbindung besitzt. Zudem entsteht im restlichen System aufgrund der geometrischen Anordnung ein Mehrfachbindungscharakter zwischen CAAC und Bor (Abbildung 4, links).

Auf der anderen Seite ordnet sich das hydrierte Gegenstück, **B₂N₂H₂,** vollständig planar an und besitzt einen Triplett Grundzustand mit einem energetisch sehr naheliegenden, biradikalischen Singulett Zustand. Durch die Wasserstoffbrückenbindung zum Stickstoff entsteht an jedem Stickstoff jeweils ein freies Elektron, welche zusammen das antibindende π^*-Orbital besetzen, woraus eine N-N-Einfachbindung resultiert.

Da der Anteil der Elektrondichte, die auf der B-N-N-B -Brücke lokalisiert ist, eine zentrale Rolle spielt, werden beide Substituenten, die am Bor und am Stickstoff des Carbens gebunden sind, variiert. Somit werden sowohl der sterische, als auch der elektronische Einfluss dieser zwei Substituenten untersucht. Hierbei hat sich herausgestellt, dass bei **B₂N₂** die Substituenten nur eine untergeordnete Rolle spielen. Die geringfügigen Geometrieänderungen der Untersysteme werden hauptsächlich von anderen elektronischen Effekten, wie Wasserstoffbrückenbindungen (N···H) oder π-Stacking der Phenyl-Gruppen dominiert. Das globale Minimum bleibt stets der closed-shell Singulett. Im Gegensatz dazu verändert sich die Geometrie von **B₂N₂H₂** bei Verkleinerung der Substituenten signifikant. So verdreht sich das sonst planare Molekül um den BNNB Diederwinkel und zeigt folglich einen Singulett Grundzustand. Eine ausführliche Analyse zeigt jedoch, dass die Veränderung nicht durch elektronische Effekte der Substituenten, sondern auch hier durch andere Wechselwirkungen (Wasserstoffbrückenbindungen, π-Stacking) bestimmt wird. Da **B₂N₂H₂** eine N-N-

Einfachbindung besitzt, die bei Raumtemperatur frei drehbar ist, kann vor allem in kleineren Systemen jede mögliche Konformation bezüglich der N-N-Rotation angenommen werden. Zum besseren Verständnis werden Testsysteme, welche inklusive verwendeter Nummerierung in Abbildung 5 dargestellt sind, genauer analysiert.

Abbildung 5: Modellsysteme von **B₂N₂** und **B₂N₂H₂** mit Nummerierung zur Definition der Diederwinkel.

Durch Variation der drei wichtigen Diederwinkel $\sphericalangle_{B_1N_1N_2B_2}$, $\sphericalangle_{N_3C_1B_1N_1}$ und $\sphericalangle_{N_2B_2C_2N_4}$ zwischen 0°, 90° und 180°, wird wieder eine Konjugation dieser bestimmten Abschnitte ermöglicht oder verhindert. Somit wird ein Überblick über den Einfluss der elektronischen Parameter erhalten, der unabhängig von sterischen Effekten ist. Wie bei den verschieden Untersystemen zuvor bereits festgestellt, besitzt das um den Winkel $\sphericalangle_{B_1N_1N_2B_2}$ verdrehte Konformer ($\sphericalangle_{B_1N_1N_2B_2}$ = 90°) von **B₂N₂H₂** die niedrigste Energie. Da der energetische Unterschied zum komplett planaren System lediglich 8 kcal/mol beträgt und die KS Orbitale keinen Unterschied aufweisen, kann der energetische Unterschied zwischen den Konformeren auf andere Wechselwirkungseffekte zurückgeführt werden. So können beim verdrehten System Wasserstoffbrückenbindungen ausgebildet werden, was beim planaren System nicht möglich ist. Im Gegensatz dazu spielt der Diederwinkel ($\sphericalangle_{N_3C_1B_1N_1}$), der die Anordnung zwischen B-N-Einheit und Carben festlegt, eine wichtigere Rolle in Bezug auf die elektronischen Eigenschaften der Systeme. Die Verdrehung der Carben Liganden aus der B-N-Ebene ($\sphericalangle_{N_3C_1B_1N_1}$ = 90°) hat einen erheblichen Einfluss auf das Bindungsmuster des restlichen Systems. Folglich kommt es zu einer Doppelbindung zwischen der B=N Einheit und einer C-B-Einfachbindung. Dieses veränderte Bindungsverhalten hat eine Lokalisation des freien Elektrons auf den Carben Kohlenstoff zur Folge, was zu Destabilisierungen von bis zu 40 kcal/mol führen kann. Im Gegensatz zur freien Rotation um die N-N-Bindung beim **B₂N₂H₂** Systems, muss sich das **B₂N₂** Molekül orthogonal bezüglich des Diederwinkels $\sphericalangle_{B_1N_1N_2B_2}$ anordnen, um eine N=N-Doppelbindung ausbilden zu können. Zwingt man das System in eine

komplett planare Struktur, wird die N=N-Doppelbindung zu einer Einfachbindung reduziert und es wird ein Triplett Grundzustand berechnet. Durch eine orthogonale Anordnung der Carben Liganden werden sowohl der Singulett, als auch der Triplett Zustand energetisch stark destabilisiert. Dieser Trend wird ausgehend von der bereits verdrehten Struktur nochmals verstärkt. Durch die fehlende Konjugation zwischen den Carben Liganden und den Bor Atomen kommt es zu einer B=N-Doppelbindung, wodurch die N-N-Einfachbindung weiter geschwächt wird. Mit Hilfe dieser Analyse konnte gezeigt werden, dass **$B_2N_2H_2$** durch die sterischen Hinderungen starrer wird, während **B_2N_2** in der Lage sein muss, sich verdreht anzuordnen, um die stabilisierende N=N-Doppelbindung auszubilden. Beide Moleküle müssen wie erwartet in der Lage sein, mit dem Carben Liganden wechselzuwirken, was durch eine planare Geometrie gegeben ist.

Neben den Systemen mit einer Distickstoffbrücke zwischen den Bor Atomen wurden im Arbeitskreis Braunschweig auch Moleküle synthetisiert, die anstelle des N_2 eine Ethylenbrücke besitzen (Tabelle 1, Zeilen 5 und 6). Die Alkyl-substituierten Moleküle **A1** und **A2** (Abbildung 6, links) besitzen ein sehr kleines ST Gap (<1 kcal/mol), wodurch es sich schwierig gestaltet, eine allgemein gültige Aussage über die Multiplizität des Grundzustandes zu treffen. Während sich die B-C-C-B-Einheit planar anordnet und eine C=C Doppelbindung formt, besteht mit den Carben Liganden keine Konjugation, was durch die orthogonale Anordnung der Liganden zur B-C-C-Ebene und die Bindungsordnung bestätigt wird. Zwischen den N-C-Atomen des Carbens und dem Bor tritt ein Mehrfachbindungs-charakter auf, was zu einer Delokalisation der berechneten Spindichte über diese drei Atome führt. Durch Austauschen des Methyl- mit einem Ethyl-Substituenten ist kein Unterschied zwischen den beiden Systemen erkennbar.
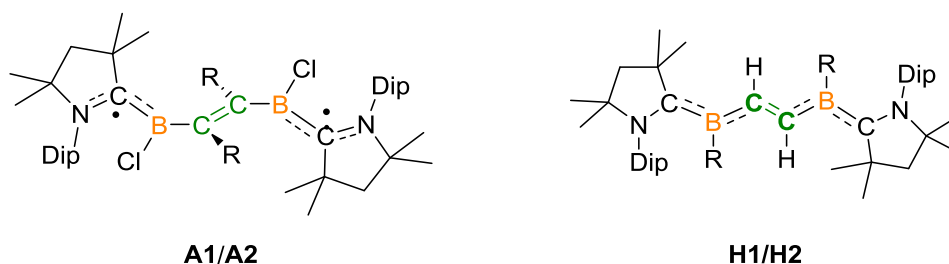
Abbildung 6: Basisstruktur der mit CAAC stabilisierten Diborylalkene. Die Alkyl-substituierten Moleküle **A1** (R: Methyl) und **A2** (R: Ethyl) befinden sich auf der linken Seiten. Die Moleküle **H1** mit Chlor am Bor und **H2** mit Wasserstoff am Bor (rechts) haben Wasserstoff an der Ethylenbrücke gebunden.

Die Moleküle **H1** und **H2** (siehe Abbildung 6, rechts) besitzen Wasserstoffatome, die an den Kohlenstoffatomen der Ethylenbrücke gebunden sind. Dies führt im Gegensatz zu **A1** und **A2**

zu einer Änderung des chemischen Verhaltens. Der Unterschied zwischen **H1** und **H2** besteht im am Bor gebundenen Rest. Analog zu den Alkyl-Molekülen, **A1** und **A2**, hat **H1** ein Chloratom am Bor gebunden, während **H2** mit Wasserstoff substituiert ist. **H1** und **H2** verhalten sich auf den ersten Blick sehr ähnlich, da beide Moleküle einen closed-shell Singulett Grundzustand aufweisen mit einem ST Gap von 8-10 kcal/mol. Im Gegensatz zu **A1** und **A2** zeigen diese Systeme eine komplett planare Struktur, was zu einer verringerten C=C Bindungsordnung führt, da nun auch ein starker Mehrfachbindungscharakter zwischen Bor und Kohlenstoff zu finden ist (siehe Abbildung 6, rechts). Experimente deuten bei **H1** auf einen Triplett Grundzustand oder einen sehr naheliegenden Triplett hin, was bei **H2** nicht der Fall ist. Betrachtet man die diabatischen ST Gaps ohne Geometrieänderung von **H1**, so fällt auf, dass der Triplett Zustand im Vergleich zu **H2** energetisch nahezu identisch ist. Es scheint, als ob eine Substitution des Bors mit Wasserstoff anstelle von Chlor zu einem weniger elektropositiven Boratom führt, was eine Destabilisierung des Tripletts zur Folge hat. Dieser Unterschied wird durch den Austausch der Substituenten am Bor Atom verursacht. Im Fall von **H1** und **A1** wird der Bindungspartner der Ethylenbrücke ausgetauscht. Auch wenn der sterische Unterschied zwischen Methyl (**A1**) und Wasserstoff (**H1**) sehr gering ist, reicht es dennoch aus, um die strukturelle Veränderung zu bedingen, da die untersuchten elektronischen Effekte keinen großen Einfluss aufweisen. Neben dem sterischen Unterschied, kann **H1** im Gegensatz zu **A1** in der planaren Struktur Wasserstoffbrücken mit Chlor ausbilden, weswegen die planare Struktur bevorzugt gebildet wird.

Im Labor wurde versucht, sterisch anspruchsvollere Reste, wie iPropyl oder Phenyl, an die Ethylenbrücke zu binden. Dies konnte jedoch bis heute noch nicht realisiert werden. Die theoretische Analyse der beiden Systeme hat ergeben, dass durch die Substitution mit iPropyl eine um etwa 10 kcal/mol instabilere Verbindung als **A1** und **A2** entsteht. Das Anbringen von Phenyl-Liganden an die Ethylen-Brücke stabilisiert das Molekül im Vergleich zu **A1/A2** um 20 kcal/mol. Der Einfluss des wachsenden sterischen Anspruchs könnte bei der Synthese der Moleküle eine Rolle spielen. Dies wurde im Rahmen dieser Arbeit jedoch nicht berücksichtigt. Nichtsdestotrotz sollten beide Moleküle als isolierbare und stabile Komponenten synthetisiert werden können. Insbesondere das mit Phenyl substituierte Molekül scheint ein sehr interessantes Verhalten für zukünftige Arbeiten zu besitzen.

10 References

1.   D. V. Loshadkin, *Des. Monomers Polym.*, 2001, **4**, 281-300.
2.   A. Wurtz, *Justus Liebigs Ann. Chem.*, 1855, **96**, 364-375.
3.   M. Gomberg, *J. Am. Chem. Soc.*, 1900, **22**, 752-757.
4.   W. Schlenk, M. Brauns, *Ber. Dtsch. Chem. Ges.*, 1915, **48**, 661-669.
5.   G. Kothe, K.-H. Denkel, W. Sümmermann, *Angew. Chem., Int. Ed.*, 1970, **9**, 906-907.
6.   D. C. Reitz, S. I. Weissman, *J. Chem. Phys.*, 1960, **33**, 700-704.
7.   P. Baumgartner, E. Weltin, G. Wagnière, E. Heilbronner, *Helv. Chim. Acta*, 1965, **48**, 751-764.
8.   M. Abe, *Chem. Rev.*, 2013, **113**, 7011–7088.
9.   F. Breher, *Coord. Chem. Rev.*, 2007, **251**, 1007-1043.
10.   P. Muller, in *Pure and Applied Chemistry*, eds. H. v. Burrows and J. Stohner, Walter de Gruyter GmbH, Berlin, 1994, vol. 66, pp. 1077-1100.
11.   P. Muller, in *Pure and Applied Chemistry*, eds. H. v. Burrows and J. Stohner, Walter de Gruyter GmbH, Berlin, 1994, vol. 66, pp. 1101-1184.
12.   G. P. Moss, P. A. S. Smith, D. Tavernier, in *Pure and Applied Chemistry*, eds. H. v. Burrows and J. Stohner, Glossary of class names of organic compounds and reactivity intermediates based on structure (IUPAC Recommendations 1995), Berlin, 1995, vol. 67, pp. 1307-1375.
13.   D. A. Dougherty, *Acc. Chem. Res.*, 1991, **24**, 88-94.
14.   G. Bertrand, *Carbene Chemistry: From Fleeting Intermediates to Powerful Reagents*, Marcel Dekker, New York, 2002.
15.   Y. Morita, S. Suzuki, K. Sato, T. Takui, *Nat. Chem.* , 2011, **3**, 197-204.
16.   C. Wentrup, *Science*, 2002, **295**, 1846-1847.
17.   W. T. Borden, H. Iwamura, J. A. Berson, *Acc. Chem. Res.*, 1994, **27**, 109-116.
18.   J. A. Berson, *Science*, 1994, **266**, 1338-1339.
19.   D. A. Shultz, R. M. Fico, S. H. Bodnar, R. K. Kumar, K. E. Vostrikova, J. W. Kampf, P. D. Boyle, *J. Am. Chem. Soc.*, 2003, **125**, 11761-11771.
20.   M. L. Kirk, D. A. Shultz, E. C. Depperman, C. L. Brannen, *J. Am. Chem. Soc.*, 2007, **129**, 1937-1943.
21.   M. G. Bonini, R. Radi, G. Ferrer-Sueta, A. M. D. C. Ferreira, O. Augusto, *J. Biol. Chem.*, 1999, **274**, 10802-10806.
22.   D. A. Dougherty, in *Kinetics and Spectroscopy of Carbenes and Biradicals*, ed. M. S. Platz, Springer US, Boston, MA, 1990, pp. 117-142.
23.   R. Jain, G. J. Snyder, D. A. Dougherty, *J. Am. Chem. Soc.*, 1984, **106**, 7294-7295.
24.   R. Jain, M. B. Sponsler, F. D. Coms, D. A. Dougherty, *J. Am. Chem. Soc.*, 1988, **110**, 1356-1366.
25.   L. Salem, C. Rowland, *Angew. Chem., Int. Ed.*, 1972, **11**, 92-111.
26.   C. Doubleday, N. J. Turro, J. F. Wang, *Acc. Chem. Res.*, 1989, 199-205.
27.   F. Kita, W. Adam, P. Jordan, W. M. Nau, J. Wirz, *J. Am. Chem. Soc.*, 1999, **121**, 9265-9275.
28.   W. T. Borden, E. R. Davidson, *Acc. Chem. Res.*, 1981, **14**, 69-76.
29.   W. T. Borden, E. R. Davidson, *Annu. Rev. Phys. Chem.*, 1979, **30**, 125-153.
30.   C. F. Lovitt, H. Dong, D. A. Hrovat, R. Gleiter, W. T. Borden, *J. Am. Chem. Soc.*, 2010, **132**, 14617-14624.

31.   M. Dračínský, in *Annual Reports on NMR Spectroscopy*, ed. G. A. Webb, Academic Press, 2017, vol. 90, pp. 1-40.

32.   M. Abe, C. Ishihara, M. Nojima, *J. Org. Chem.*, 2003, **68**, 1618-1621.

33.   R. Hoffmann, *J. Am. Chem. Soc.*, 1968, **90**, 1475-1485.

34.   R. Hoffmann, *Acc. Chem. Res.*, 1971, **4**, 1-9.

35.   N. C. Baird, *J. Am. Chem. Soc.*, 1972, **94**, 4941-4948.

36.   R. Breslow, *Acc. Chem. Res.*, 1973, **6**, 393-398.

37.   P. v. R. Schleyer, C. Maerker, A. Dransfeld, H. Jiao, N. J. R. van Eikema Hommes, *J. Am. Chem. Soc.*, 1996, **118**, 6317-6318.

38.   Z. Chen, C. S. Wannere, C. Corminboeuf, R. Puchta, P. v. R. Schleyer, *Chem. Rev.*, 2005, **105**, 3842-3888.

39.   H. Möllerstedt, M. C. Piqueras, R. Crespo, H. Ottosson, *J. Am. Chem. Soc.*, 2004, **126**, 13938-13939.

40.   C. Dahlstrand, M. Rosenberg, K. Kilså, H. Ottosson, *J. Phys. Chem. A*, 2012, **116**, 5008-5017.

41.   V. Gogonea, P. v. R. Schleyer, P. R. Schreiner, *Angew. Chem., Int. Ed.*, 1998, **37**, 1945-1948.

42.   N. S. Goroff, *Acc. Chem. Res.*, 1996, **29**, 77-83.

43.   T. Saito, S. Nishihara, S. Yamanaka, Y. Kitagawa, T. Kawakami, S. Yamada, H. Isobe, M. Okumura, K. Yamaguchi, *Theor. Chem. Acc.*, 2011, **130**, 749-763.

44.   S. Fujii, T. Enoki, *Acc. Chem. Res.*, 2013, **46**, 2202-2210.

45.   A. Konishi, Y. Hirao, K. Matsumoto, H. Kurata, R. Kishi, Y. Shigeta, M. Nakano, K. Tokunaga, K. Kamada, T. Kubo, *J. Am. Chem. Soc.*, 2013, **135**, 1430-1437.

46.   T. Enoki, K. Takai, M. Kiguchi, *Bull. Chem. Soc. Jpn.*, 2012, **85**, 249-264.

47.   A. E. Tschitschibabin, *Ber. Dtsch. Chem. Ges.*, 1907, **40**, 1810-1819.

48.   J. Thiele, H. Balhorn, *Ber. Dtsch. Chem. Ges.*, 1904, **37**, 1463-1470.

49.   P. Ravat, M. Baumgarten, *Phys. Chem. Chem. Phys.*, 2015, **17**, 983-991.

50.   L. K. Montgomery, J. C. Huffman, E. A. Jurczak, M. P. Grendze, *J. Am. Chem. Soc.*, 1986, **108**, 6004-6011.

51.   H. M. McConnell, *J. Chem. Phys.*, 1960, **33**, 1868-1869.

52.   H. Stieger, H.-D. Brauer, *Chem. Ber.*, 1970, **103**, 3799-3810.

53.   Y. Kanzaki, D. Shiomi, K. Sato, T. Takui, *J. Phys. Chem. B*, 2012, **116**, 1053-1059.

54.   D. R. McMasters, J. Wirz, *J. Am. Chem. Soc.*, 2001, **123**, 238-246.

55.   A. Rajca, *Chem. Rev.*, 1994, **94**, 871-893.

56.   Z. Sun, Q. Ye, C. Chi, J. Wu, *Chem. Soc. Rev*, 2012, **41**, 7857-7889.

57.   C. J. Cramer, *J. Chem. Soc., Perkin Trans. 2*, 1998, 1007-1014.

58.   V. I. Minkin, in *Pure and Applied Chemistry*, eds. H. v. Burrows and J. Stohner, Glossary of terms used in theoretical organic chemistry, Berlin, 1999, vol. 71, p. 1919.

59.   P. Dowd, *J. Am. Chem. Soc.*, 1966, **88**, 2587-2589.

60.   P. Dowd, *Acc. Chem. Res.*, 1972, **5**, 242-248.

61.   P. Dowd, *J. Am. Chem. Soc.*, 1970, **92**, 1066-1068.

62.   E. R. Davidson, W. T. Borden, *J. Am. Chem. Soc.*, 1977, **99**, 2053-2060.

63.   W. T. Borden, *Qualitative Methods for Predicting the Ground States of Non-Kekule Hydrocarbons and the Effects of Heteroatom Substitution on the Ordering of the Electronic States*, Taylor & Francis, 1993.

64.   W. T. Borden, in *The Foundations of Physical Organic Chemistry: Fifty Years of the James Flack Norris Award*, American Chemical Society, 2015, vol. 1209, ch. 11, pp. 251-303.

65.   J. A. Berson, *Acc. Chem. Res.*, 1997, **30**, 238-244.
66.   T. Ikeda, H. Ikeda, Y. Takahashi, M. Yamada, K. Mizuno, S. Tero-Kubota, S. Yamauchi, *J. Am. Chem. Soc.*, 2008, **130**, 2466-2472.
67.   Y. Kano, K. Mizuno, H. Ikeda, *J. Phys. Org. Chem.*, 2011, **24**, 921-928.
68.   Q. Fu, J. Yang, X.-B. Wang, *J. Phys. Chem. A*, 2011, **115**, 3201-3207.
69.   B. A. Jazdzewski, W. B. Tolman, *Coord. Chem. Rev.*, 2000, **200-202**, 633-685.
70.   V. Bachler, G. Olbrich, F. Neese, K. Wieghardt, *Inorg. Chem.*, 2002, **41**, 4179-4193.
71.   T. Petrenko, K. Ray, K. E. Wieghardt, F. Neese, *J. Am. Chem. Soc.*, 2006, **128**, 4422-4436.
72.   D. Herebian, K. E. Wieghardt, F. Neese, *J. Am. Chem. Soc.*, 2003, **125**, 10997-11005.
73.   R. A. Moss, M. S. Platz, M. J. Jones, in *Reactive Intermediate Chemistry*, John Wiley & Sons, Inc., New York, 2004.
74.   P. G. Wenthold, W. C. Lineberger, *Acc. Chem. Res.*, 1999, **32**, 597-604.
75.   W. C. Lineberger, W. T. Borden, *Phys. Chem. Chem. Phys.*, 2011, **13**, 11792-11813.
76.   M. S. Robinson, M. L. Polak, V. M. Bierbaum, C. H. DePuy, W. C. Lineberger, *J. Am. Chem. Soc.*, 1995, **117**, 6766-6778.
77.   F. Z. Hund, *Phys. Chem. Chem. Phys.*, 1925, **33**, 345-371.
78.   J. Kolc, J. Michl, *J. Am. Chem. Soc.*, 1973, **95**, 7391-7401.
79.   J. Michl, V. Bonačić-Koutecký, *Tetrahedron*, 1988, **44**, 7559-7585.
80.   D. Doehnert, J. Koutecky, *J. Am. Chem. Soc.*, 1980, **102**, 1789-1796.
81.   Z. Sun, J. Wu, *J. Mater. Chem.*, 2012, **22**, 4151-4160.
82.   C. Lambert, *Angew. Chem., Int. Ed.*, 2011, **50**, 1756-1758.
83.   E. Miliordos, K. Ruedenberg, S. S. Xantheas, *Angew. Chem.*, 2013, **125**, 5848-5851.
84.   J. M. Bofill, P. Pulay, *J. Chem. Phys.*, 1989, **90**, 3637-3646.
85.   P. Pulay, T. P. Hamilton, *J. Chem. Phys.*, 1988, **88**, 4926-4933.
86.   R. G. A. Bone, P. Pulay, *Int. J. Quantum Chem.*, 1993, **45**, 133-166.
87.   K. Yamaguchi, F. Jensen, A. Dorigo, K. N. Houk, *Chem. Phys. Lett.*, 1988, **149**, 537-542.
88.   S. Yamanaka, M. Okumura, M. Nakano, K. Yamaguchi, *J. Mol. Struct. (Theochem)*, 1994, **310**, 205-218.
89.   K. Yamaguchi, Y. Takahara, T. Fueno, K. N. Houk, *Theor. Chim. Acta*, 1988, **73**, 337-364.
90.   K. Yamaguchi, K. Ohta, S. Yabushita, T. Fueno, *Chem. Phys. Lett.*, 1977, **49**, 555-559.
91.   M. M. Hansmann, M. Melaimi, D. Munz, G. Bertrand, *J. Am. Chem. Soc.*, 2018, **140**, 2546-2554.
92.   S. Styra, M. Melaimi, C. E. Moore, A. L. Rheingold, T. Augenstein, F. Breher, G. Bertrand, *Chem. Eur. J.*, 2015, **21**, 8441-8446.
93.   J. K. Mahoney, D. Martin, C. E. Moore, A. L. Rheingold, G. Bertrand, *J. Am. Chem. Soc.*, 2013, **135**, 18766-18769.
94.   J. K. Mahoney, D. Martin, F. Thomas, C. E. Moore, A. L. Rheingold, G. Bertrand, *J. Am. Chem. Soc.*, 2015, **137**, 7519-7525.
95.   J. K. Mahoney, R. Jazzar, G. Royal, D. Martin, G. Bertrand, *Chem. Eur. J.*, 2017, **23**, 6206-6212.
96.   E. Schrödinger, *Ann. Phys.*, 1926, **384**, 361-376.
97.   L. d. Broglie, *Phil. Mag.*, 1924, **47**, 446-458.
98.   W. A. Fedak, J. J. Prentis, *Am. J. Phys.*, 2009, **77**, 128-139.
99.   M. Born, P. Jordan, *Z. Phys.*, 1925, **34**, 858-888.
100.   M. Born, *Z. Phys.*, 1924, **26**, 379-395.
101.   F. Jensen, *Introduction to Computational Chemistry*, Wiley & Sons Ltd, 2017.
102.   J. M. Combes, presented in part at the The Schrödinger Equation, Vienna, 1977.
103.   W. Pauli, *Z. Phys.*, 1925, **31**, 765-783.

104. D. Serwer, *Hist. Stud. Phys. Sci.*, 1977, **8**, 189-256.
105. J. C. Slater, *Phys. Rev.*, 1951, **81**, 385-390.
106. A. Szabo, N. S. Ostlund, *Modern Quantum Chemistry: Introduction to Advanced Electronic Structure Theory*, 1989.
107. C. J. Cramer, *Essentials of Computational Chemistry*, John Wiley & Sons Ltd., Chichester, 2003.
108. A. Halkier, T. Helgaker, P. Jørgensen, W. Klopper, J. Olsen, *Chem. Phys. Lett.*, 1999, **302**, 437-446.
109. C. W. Bauschlicher, P. R. Taylor, *J. Chem. Phys.*, 1986, **85**, 6510-6512.
110. C. W. Bauschlicher, P. R. Taylor, *Theor. Chim. Acta*, 1987, **71**, 263-276.
111. L. Brillouin, *Act. Sci. Ind.*, 1934, **159**.
112. F. Grein, T. C. Chang, *Chem. Phys. Lett.*, 1971, **12**, 44-48.
113. A. Dreuw, M. Head-Gordon, *Chem. Rev.*, 2005, **105**, 4009-4037.
114. J. Čížek, in *Advances in Chemical Physics*, eds. R. LeFebvre and C. Moser, 1969, vol. 14, p. 35.
115. J. Čížek, *J. Chem. Phys.*, 1966, **45**, 4256-4266.
116. J. Čížek, J. Paldus, *Int. J. Quantum Chem.*, 1971, **5**, 359-379.
117. R. J. Bartlett, M. Musiał, *Rev. Mod. Phys.*, 2007, **79**, 291-352.
118. A. Veillard, E. Clementi, *Theor. Chim. Acta*, 1967, **7**, 133-143.
119. P. R. Taylor, in *Lecture Notes in Quantum Chemistry II: European Summer School in Quantum Chemistry*, ed. B. O. Roos, Springer Berlin Heidelberg, Berlin, Heidelberg, 1994, pp. 125-202.
120. R. J. Bartlett, *Ann. Rev. Phys. Chem.*, 1981, **32**, 359-401.
121. R. J. Bartlett, J. D. Watts, S. A. Kucharski, J. Noga, *Chem. Phys. Lett.*, 1990, **165**, 513-522.
122. M. Urban, J. Noga, S. J. Cole, R. J. Bartlett, *J. Chem. Phys.*, 1985, **83**, 4041-4046.
123. K. Raghavachari, G. W. Trucks, J. A. Pople, M. Head-Gordon, *Chem. Phys. Lett.*, 1989, **157**, 479-483.
124. T. J. Lee, J. E. Rice, G. E. Scuseria, H. F. Schaefer, *Theor. Chim. Acta*, 1989, **75**, 81-98.
125. T. J. Lee, P. R. Taylor, *Int. J. Quantum Chem.*, 1989, **36**, 199-207.
126. W. D. Laidig, G. D. Purvis, R. J. Bartlett, *Chem. Phys. Lett.*, 1983, **97**, 209-214.
127. G. D. Purvis, R. J. Bartlett, *J. Chem. Phys.*, 1982, **76**, 1910-1918.
128. G. E. Scuseria, H. F. Schaefer, *Chem. Phy. Lett.*, 1987, **142**, 354-358.
129. C. L. Janssen, I. M. B. Nielsen, *Chem. Phys. Lett.*, 1998, **290**, 423-430.
130. I. M. B. Nielsen, C. L. Janssen, *Chem. Phys. Lett.*, 1999, **310**, 568-576.
131. W. Jiang, N. J. DeYonker, A. K. Wilson, *J. Chem. Theory Comput.*, 2012, **8**, 460-468.
132. T. Korona, H.-J. Werner, *J. Chem. Phys.*, 2003, **118**, 3006-3019.
133. D. Kats, T. Korona, M. Schütz, *J. Chem. Phys.*, 2007, **127**, 064107.
134. M. Schütz, F. R. Manby, *Phys. Chem. Chem. Phys.*, 2003, **5**, 3349-3358.
135. F. Claeyssens, J. N. Harvey, F. R. Manby, R. A. Mata, A. J. Mulholland, K. E. Ranaghan, M. Schütz, S. Thiel, W. Thiel, H. J. Werner, *Angew. Chem.*, 2006, **118**, 7010-7013.
136. D. Kats, M. Schütz, *Local Time-Dependent Coupled Cluster Response for Properties of Excited States in Large Molecules*, Oldenbourg Wissenschaftsverlag, Regensburg, 2010.
137. Y. Guo, C. Riplinger, U. Becker, D. G. Liakos, Y. Minenkov, L. Cavallo, F. Neese, *J. Chem. Phys.*, 2018, **148**, 011101.
138. Y. Minenkov, E. Chermak, L. Cavallo, *J. Chem. Theory Comput.*, 2015, **11**, 4664-4676.
139. D. G. Liakos, A. Hansen, F. Neese, *J. Chem. Theory Comput.*, 2011, **7**, 76-87.
140. M. Sparta, F. Neese, *Chem. Soc. Rev*, 2014, **43**, 5032-5041.

141. C. Riplinger, B. Sandhoefer, A. Hansen, F. Neese, *J. Chem. Phys.*, 2013, **139**, 134101.
142. S. Saebo, P. Pulay, *Ann. Rev. Phys. Chem.*, 1993, **44**, 213-236.
143. S. Saebo, P. Pulay, *Chem. Phys. Lett.*, 1985, **113**, 13-18.
144. G. Rauhut, P. Pulay, H.-J. Werner, *J. Comp. Chem.*, 1998, **19**, 1241-1254.
145. P. Pulay, S. Saebo, W. Meyer, *J. Chem. Phys.*, 1984, **81**, 1901-1905.
146. J. W. Boughton, P. Pulay, *J. Comput. Chem.*, 1993, **14**, 736-740.
147. S. Saebo, J. Almlof, *Chem. Phys. Lett.*, 1989, **154**, 83-89.
148. P.-O. Löwdin, *Phys. Rev.*, 1955, **97**, 1474-1489.
149. C. Edmiston, M. Krauss, *J. Chem. Phys.*, 1966, **45**, 1833-1839.
150. C. Edmiston, M. Krauss, *J. Chem. Phys.*, 1965, **42**, 1119-1120.
151. W. Meyer, *Int. J. Quantum Chem.*, 1971, **5**, 341-348.
152. P. R. Taylor, *J. Chem. Phys.*, 1981, **74**, 1256-1270.
153. C. Kollmar, F. Neese, *J. Chem. Phys.*, 2011, **135**, 084102.
154. F. Neese, F. Wennmohs, A. Hansen, *J. Chem. Phys.*, 2009, **130**, 114108.
155. F. Neese, A. Hansen, F. Wennmohs, S. Grimme, *Acc. Chem. Res.*, 2009, **42**, 641-648.
156. C. Riplinger, F. Neese, *J. Chem. Phys.*, 2013, **138**, 034106.
157. A. K. Dutta, F. Neese, R. Izsák, *J. Chem. Phys.*, 2016, **145**, 034102.
158. D. G. Liakos, F. Neese, *J. Phys. Chem. A*, 2012, **116**, 4801-4816.
159. D. G. Liakos, M. Sparta, M. K. Kesharwani, J. M. L. Martin, F. Neese, *J. Chem. Theory Comput.*, 2015, **11**, 1525-1539.
160. D. G. Liakos, F. Neese, *J. Chem. Theory Comput.*, 2011, **7**, 1511-1523.
161. M. Saitow, U. Becker, C. Riplinger, E. F. Valeev, F. Neese, *J. Chem. Phys.*, 2017, **146**, 164105.
162. A. Hansen, D. G. Liakos, F. Neese, *J. Chem. Phys.*, 2011, **135**, 214102.
163. D. G. Liakos, F. Neese, *J. Chem. Theory Comput.*, 2015, **11**, 2137-2143.
164. Y. Guo, U. Becker, F. Neese, *J. Chem. Phys.*, 2018, **148**, 124117.
165. D. Datta, S. Kossmann, F. Neese, *J. Chem. Phys.*, 2016, **145**, 114101.
166. M. S. Gordon, J. M. Mullin, S. R. Pruitt, L. B. Roskop, L. V. Slipchenko, J. A. Boatz, *J. Phys. Chem. B*, 2009, **113**, 9646-9663.
167. Z. Ni, S. Li, *Mol. Phys.*, 2016, **114**, 1447-1460.
168. Y. Guo, W. Li, S. Li, *J. Phys. Chem. A*, 2014, **118**, 8996-9004.
169. S. Li, J. Shen, W. Li, Y. Jiang, *J. Chem. Phys.*, 2006, **125**, 074109.
170. H. J. Silverstone, O. Sinanoğlu, *J. Chem. Phys.*, 1966, **44**, 1899-1907.
171. D. K. W. Mok, R. Neumann, N. C. Handy, *J. Phys. Chem.*, 1996, **100**, 6225-6230.
172. A. D. Walsh, *J. Chem. Soc.*, 1953, 2260-2266.
173. M. W. Schmidt, M. S. Gordon, *Annu. Rev. Phys. Chem.*, 1998, **49**, 233-266.
174. T. Helgaker, P. Jørgensen, J. Olsen, in *Molecular Electronic-Structure Theory*, John Wiley & Sons, Ltd 2014.
175. K. Kirby-Docken, B. Liu, *J. Chem. Phys.*, 1977, **66**, 4309-4316.
176. G. C. Lie, J. Hinze, B. Liu, *J. Chem. Phys.*, 1973, **59**, 1872-1886.
177. A. D. McLean, B. Liu, *J. Chem. Phys.*, 1973, **58**, 1066-1078.
178. B. O. Roos, P. R. Taylor, P. E. M. Siegbahn, *Chem. Phy.s*, 1980, **48**, 157-173.
179. P. E. M. Siegbahn, J. Almlöf, A. Heiberg, B. O. Roos, *J. Chem. Phys.*, 1981, **74**, 2384-2396.
180. B. O. Roos, in *Advances in Chemical Physics*, ed. K. P. Lawley, John Wiley & Sons, Inc, 2007.
181. P. A. Malmqvist, A. Rendell, B. O. Roos, *J. Phys. Chem.*, 1990, **94**, 5477-5482.

10. References

182. B. O. Roos, in *Lecture Notes in Quantum Chemistry: European Summer School in Quantum Chemistry*, ed. B. O. Roos, Springer Berlin Heidelberg, Berlin, Heidelberg, 1992, pp. 177-254.
183. B. O. Roos, in *In Advances in Chemical Physics*, ed. K. P. Lawley, John Wiley & Sons, Inc, 2007.
184. B. O. Roos, P. R. Taylor, P. E. M. Siegbahn, *Chem. Phys.*, 1980, **48**, 157-173.
185. J. Olsen, B. O. Roos, P. Jørgensen, H. Jensen, *J. Chem. Phys.*, 1988, **89**, 2185-2192.
186. F. Krausbeck, D. Mendive-Tapia, A. J. W. Thom, M. J. Bearpark, *Comput. Theor. Chem.*, 2014, **1040-1041**, 14-19.
187. C. J. Stein, M. Reiher, *J. Chem. Theory Comput.*, 2016, **12**, 1760-1771.
188. C. Camacho, S. Yamamoto, H. A. Witek, *Phys. Chem. Chem. Phys.*, 2008, **10**, 5128-5134.
189. V. Veryazov, P. Å. Malmqvist, B. O. Roos, *Int. J. Quantum Chem.*, 2011, **111**, 3329-3338.
190. M. G. Delcey, T. B. Pedersen, F. Aquilante, R. Lindh, *J. Chem. Phys.*, 2015, **143**, 044110.
191. K. K. Docken, J. Hinze, *J. Chem. Phys.*, 1972, **57**, 4928-4936.
192. H. J. Werner, W. Meyer, *J. Chem. Phys.*, 1981, **74**, 5794-5801.
193. K. Ruedenberg, L. M. Cheung, S. T. Elbert, *Int. J. Quantum Chem.*, 1979, **16**, 1069-1101.
194. D. L. Yeager, P. Jørgensen, *Mol. Phys.*, 1980, **39**, 587-596.
195. D. R. Yarkony, in *Modern Electronic Structure Theory*, World Scientific Publishing Company, 1995, pp. i-xiii.
196. B. O. Roos, R. Lindh, P. A. Malmqvist, V. Veryazov, P.-O. Widmark, *Multiconfigurational Quantum Chemistry*, John Wiley & Sons, Hoboken, New Jersey, 216.
197. C. Møller, M. S. Plesset, *Phys. Rev.*, 1934, **46**, 618-622.
198. R. J. Buenker, S. D. Peyerimhoff, *Theor. Chem. Acc.*, 1974, **35**, 33-58.
199. R. J. Buenker, S. D. Peyerimhoff, in *Excited States in Quantum Chemistry: Theoretical and Experimental Aspects of the Electronic Structure and Properties of the Excited States in Atoms, Molecules and Solids*, eds. C. A. Nicolaides and D. R. Beck, Springer Netherlands, Dordrecht, 1979, pp. 45-61.
200. R. Preuss, R. J. Buenker, S. D. Peyerimhoff, *J. Mol. Struc.*, 1978, **49**, 171-179.
201. R. J. Buenker, S. D. Peyerimhoff, W. Butscher, *Mol .Phys.*, 1978, **35**, 771-791.
202. M. Schnell, J. S. Francisco, S. D. Peyerimhoff, *Phys. Chem. Chem. Phys.*, 2005, **7**, 1912-1917.
203. U. S. Mahapatra, B. Datta, D. Mukherjee, *J. Chem. Phys.*, 1999, **110**, 6171-6188.
204. P. G. Szalay, R. J. Bartlett, *Chem. Phys. Lett.*, 1993, **214**, 481-488.
205. S. Pal, M. Rittby, R. J. Bartlett, D. Sinha, D. Mukherjee, *J. Chem. Phys.*, 1988, **88**, 4357-4366.
206. B. A. Hess, U. Kaldor, *J. Chem. Phys.*, 2000, **112**, 1809-1813.
207. P. Pulay, *Int. J. Quantum Chem.*, 2011, **111**, 3273-3279.
208. C. Angeli, R. Cimiraglia, J.-P. Malrieu, *J. Chem. Phys.*, 2002, **117**, 9138-9153.
209. C. Angeli, R. Cimiraglia, J.-P. Malrieu, *Chem. Phys. Lett.*, 2001, **350**, 297-305.
210. C. Angeli, R. Cimiraglia, S. Evangelisti, T. Leininger, J.-P. Malrieu, *J. Chem. Phys.* , 2001, **114**, 10252-10264.
211. B. O. Roos, K. Andersson, M. P. Fülscher, P.-â. Malmqvist, L. Serrano-Andrés, K. Pierloot, M. Merchán, *Multiconfigurational Perturbation Theory: Applications in Electronic Spectroscopy*, John Wiley & Sons, Inc., 2007.
212. B. O. Roos, *Acc. Chem. Res.*, 1999, **32**, 137-144.
213. B. O. Roos, in *Theory and Applications of Computational Chemistry*, eds. C. E. Dykstra, G. Frenking, K. S. Kim and G. E. Scuseria, Elsevier, Amsterdam, 2005, pp. 725-764.

214. M. Merchán, L. Serrano-Andrés, M. P. Fülscher, B. O. Roos, in *Recent Advances in Multireference Methods*, World scientific, 1999, vol. Volume 4, pp. 161-195.
215. L. Gagliardi, B. O. Roos, *Chem. Soc. Rev.*, 2007, **36**, 893-903.
216. T. Bally, W. T. Borden, in *Reviews in Computational Chemistry*, eds. K. B. Lipkowitz and D. B. Boyd, Wiley-VCH, Inc., 2007.
217. J. Finley, P.-Å. Malmqvist, B. O. Roos, L. Serrano-Andrés, *Chem. Phys. Lett.*, 1998, **288**, 299-306.
218. P. Celani, H.-J. Werner, *J. Chem. Phys.*, 2000, **112**, 5546-5557.
219. M. Sejpal, R. P. Messmer, *J. Chem. Phys.*, 2001, **114**, 4796-4804.
220. F. W. Bobrowicz, W. A. Goddard, in *Methods of Electronic Structure Theory*, ed. H. F. Schaefer, Springer US, Boston, MA, 1977, pp. 79-127.
221. D. L. Cooper, M. Raimondi, J. Gerratt, in *Advances in Chemical Physics*, ed. K. P. Lawley, Wiley-Interscience, 2007.
222. J. Gerratt, D. L. Cooper, P. B. Karadakov, M. Raimondi, *Chem. Soc. Rev.*, 1997, **26**, 87-100.
223. J.-P. Malrieu, J.-L. Heully, A. Zaitsevskii, *Theor. Chem. Acc.*, 1995, **90**, 167-187.
224. J. L. Heully, J. P. Malrieu, A. Zaitsevskii, *J. Chem. Phys.*, 1996, **105**, 6887-6891.
225. K. G. Dyall, *J. Chem. Phys.*, 1995, **102**, 4909-4918.
226. K. Andersson, B. O. Roos, *Int. J. Quantum Chem.*, 1993, **45**, 591-607.
227. C. Angeli, M. Pastore, R. Cimiraglia, *Theor. Chem. Acc.*, 2007, **117**, 743-754.
228. R. W. A. Havenith, P. R. Taylor, C. Angeli, R. Cimiraglia, K. Ruud, *J. Chem. Phys.*, 2004, **120**, 4619-4625.
229. E. Fermi, *Rend. Accad. Naz. Lincei.*, 1927, **6**, 602–607.
230. L. H. Thomas, *Math. Proc. Cambridge Philos. Soc.*, 1927, **23**, 542-548.
231. E. Teller, *Rev. Mod. Phys.*, 1962, **34**, 627-631.
232. W. Kohn, L. J. Sham, *Phys. Rev.*, 1965, **140**, A1133-A1138.
233. P. Hohenberg, W. Kohn, *Phys. Rev.*, 1964, **136**, B864.
234. R. Peverati, D. G. Truhlar, *Phil.l Trans. R. Soc. A*, 2014, **372**, 1-52.
235. S. Kümmel, L. Kronik, *Rev. Mod. Phys.*, 2008, **80**, 3-60.
236. P.-F. Loos, P. M. W. Gill, *WIREs Comput. Mol. Sci.*, 2016, **6**, 410-429.
237. A. Sommerfeld, *Zeits. fur Physik*, 1928, **47**, 1-32.
238. R. Gáspár, *Acta Phys. Hung.*, 1974, **35**, 213-218.
239. D. M. Ceperley, B. J. Alder, *Phys. Rev. Lett.*, 1980, **45**, 566-569.
240. D. Ceperley, *Phys. Rev. B*, 1978, **18**, 3126-3138.
241. S. H. Vosko, L. Wilk, M. Nusair, *Can. J. Phys.*, 1980, **58**, 1200-1211.
242. J. P. Perdew, *Unified Theory of Exchange and Correlation beyond the Local Density Approximation*, Akademic Verlag, Berlin, 1991.
243. J. P. Perdew, J. Tao, S. Kümmel, in *Electron Correlation Methodology*, American Chemical Society, 2007, vol. 958, ch. 2, pp. 13-25.
244. J. Sun, J. P. Perdew, M. Seidl, *Phys. Rev. B*, 2010, **81**, 085123.
245. N. Mardirossian, M. Head-Gordon, *Mol. Phys.*, 2017, **115**, 2315-2372.
246. S. F. Sousa, P. A. Fernandes, M. J. Ramos, *J. Phys. Chem. A*, 2007, **111**, 10439-10452.
247. J. P. Perdew, W. Yue, *Phys. Rev. B*, 1989, **40**, 3399-3399.
248. F. Herman, I. B. Ortenburger, J. P. Van Dyke, *J. Quant. Chem.*, 1969, **4**, 827-846.
249. F. Herman, J. P. Van Dyke, I. B. Ortenburger, *Phys. Rev. Lett.*, 1969, **22**, 807-811.
250. J. P. Perdew, K. Burke, M. Ernzerhof, *Phys. Rev. Lett.*, 1996, **77**, 3865-3868.
251. A. D. Becke, *J. Chem. Phys.*, 1986, **84**, 4524-4529.
252. A. D. Becke, *J. Chem. Phys.*, 1997, **107**, 8554-8560.

253. A. D. Becke, *Phy. Rev. A*, 1988, **38**, 3098-3100.
254. C. Lee, W. Yang, R. G. Parr, *Phy. Rev. B*, 1988, **37**, 785-789.
255. J. P. Perdew, K. Burke, M. Ernzerhof, *Phys. Rev. Lett.*, 1997, **78**, 1396-1396.
256. A. D. Boese, N. C. Handy, *J. Chem. Phys.*, 2001, **114**, 5497-5503.
257. J. P. Perdew, A. Ruzsinszky, G. I. Csonka, O. A. Vydrov, G. E. Scuseria, L. A. Constantin, X. Zhou, K. Burke, *Phys. Rev. Lett.*, 2008, **101**, 239702.
258. Y. Zhao, D. G. Truhlar, *J. Chem. Phys.*, 2008, **128**, 184109.
259. R. Peverati, Y. Zhao, D. G. Truhlar, *J. Phys. Chem. Lett.*, 2011, **2**, 1991-1997.
260. P. R. Antoniewicz, L. Kleinman, *Phys. Rev. B*, 1985, **31**, 6779-6781.
261. S.-K. Ma, K. A. Brueckner, *Phys. Rev.*, 1968, **165**, 18-31.
262. R. Peverati, D. G. Truhlar, *J. Chem. Phys.*, 2012, **136**, 134704.
263. A. D. Becke, *J. Chem. Phys.*, 1996, **104**, 1040-1046.
264. C. Adamo, V. Barone, *J. Chem. Phys.*, 1998, **108**, 664-675.
265. Y. Zhao, D. G. Truhlar, *Acc. Chem. Res.*, 2008, **41**, 157-167.
266. J. P. Perdew, L. A. Constantin, *Phys. Rev. B*, 2007, **75**, 155109.
267. J. P. Perdew, A. Ruzsinszky, G. I. Csonka, L. A. Constantin, J. Sun, *Phys. Rev. Lett.*, 2009, **103**, 026403.
268. J. P. Perdew, S. Kurth, A. Zupan, P. Blaha, *Phys. Rev. Lett.*, 1999, **82**, 2544-2547.
269. Y. Zhao, D. G. Truhlar, *J. Chem. Phys.*, 2006, **125**, 194101.
270. Y. Zhao, N. E. Schultz, D. G. Truhlar, *J. Phys. Chem.*, 2005, **123**, 161103.
271. T. Van Voorhis, G. E. Scuseria, *J. Chem. Phys.*, 2008, **129**, 219901.
272. A. D. Boese, N. C. Handy, *J. Chem. Phys.*, 2002, **116**, 9559-9569.
273. R. Peverati, D. G. Truhlar, *J. Chem. Theory Comput.*, 2012, **8**, 2310-2319.
274. J. P. Perdew, Y. Wang, *Phys. Rev. B*, 2018, **98**, 079904.
275. R. Peverati, D. G. Truhlar, *Phys. Chem. Chem. Phys.*, 2012, **14**, 13171-13174.
276. H. S. Yu, X. He, S. L. Li, D. G. Truhlar, *Chem. Sci.*, 2016, **7**, 5032-5051.
277. H. S. Yu, X. He, D. G. Truhlar, *J. Chem. Theory Comput.*, 2016, **12**, 1280-1293.
278. J. P. Perdew, S. Kurth, in *A Primer in Density Functional Theory*, eds. C. Fiolhais, F. Nogueira and M. A. L. Marques, Springer Berlin Heidelberg, Berlin, Heidelberg, 2003, pp. 1-55.
279. A. J. Cohen, P. Mori-Sánchez, W. Yang, *J. Chem. Phys.*, 2008, **129**, 121104.
280. J. P. Perdew, A. Zunger, *Phys. Rev. B*, 1981, **23**, 5048-5079.
281. J. P. Perdew, A. Ruzsinszky, J. Tao, V. N. Staroverov, G. E. Scuseria, G. I. Csonka, *J. Chem. Phys.*, 2005, **123**, 062201.
282. A. D. Becke, *J. Chem. Phys.*, 1993, **98**, 5648-5652.
283. P. Stephens, F. Devlin, C. Chabalowski, M. J. Frisch, *J. Phys. Chem.*, 1994, **98**, 11623-11627.
284. T. W. Keal, D. J. Tozer, *J. Chem. Phys.*, 2005, **123**, 121103.
285. R. Peverati, D. G. Truhlar, *J. Chem. Phys.*, 2011, **135**, 191102.
286. C. Adamo, V. Barone, *J. Chem. Phys.*, 1999, **110**, 6158-6170.
287. Y. Zhao, D. G. Truhlar, *Theor. Chem. Acc.*, 2008, **120**, 215-241.
288. Y. Zhao, D. G. Truhlar, *J. Chem. Theory Comput.*, 2008, **4**, 1849-1868.
289. Y. Zhao, D. G. Truhlar, *J. Phys. Chem. A*, 2005, **109**, 5656-5667.
290. S. Grimme, *J. Comp. Chem.*, 2004, **25**, 1463-1473.
291. S. Grimme, J. Antony, S. Ehrlich, H. Krieg, *J. Chem. Phys.*, 2010, **132**.
292. S. Grimme, S. Ehrlich, L. Goerigk, *J. Comp. Chem.*, 2011, **32**, 1456-1465.
293. T. Tsuneda, K. Hirao, *Wiley Interdiscip. Rev. Comput. Mol. Sci.*, 2014, **4**, 375-390.
294. H. Iikura, T. Tsuneda, T. Yanai, K. Hirao, *J. Chem. Phys.*, 2001, **115**, 3540-3544.

295. A. Savin, United States, 1996.
296. T. Yanai, D. P. Tew, N. C. Handy, *Chem. Phys. Lett.*, 2004, **393**, 51-57.
297. J.-D. Chai, M. Head-Gordon, *Phys. Chem. Chem. Phys.*, 2008, **10**, 6615-6620.
298. R. Peverati, D. G. Truhlar, *J. Phys. Chem. Lett.*, 2011, **2**, 2810-2817.
299. J.-D. Chai, M. Head-Gordon, *J. Chem. Phys.*, 2008, **128**, 084106.
300. R. Peverati, D. G. Truhlar, *Phys. Chem. Chem. Phys.*, 2012, **14**, 16187-16191.
301. L. Goerigk, S. Grimme, *J. Chem. Theory Comput.*, 2011, **7**, 291-309.
302. S. Grimme, *J. Comp. Chem.*, 2006, **27**, 1787-1799.
303. S. Kozuch, J. M. L. Martin, *Phys. Chem. Chem. Phys.*, 2011, **13**, 20104-20107.
304. O. Gunnarsson, B. I. Lundqvist, *Phys. Rev. B*, 1976, **13**, 4274-4298.
305. O. Gunnarsson, B. I. Lundqvist, *Phys. Rev. B*, 1977, **15**, 6006-6006.
306. J. Toulouse, K. Sharkas, E. Brémond, C. Adamo, *J. Chem. Phys.*, 2011, **135**, 101102.
307. S. M. O. Souvi, K. Sharkas, J. Toulouse, *J. Chem. Phys.*, 2014, **140**, 084107.
308. K. Sharkas, J. Toulouse, A. Savin, *J. Chem. Phys.*, 2011, **134**, 064113.
309. É. Brémond, J. C. Sancho-García, Á. J. Pérez-Jiménez, C. Adamo, *J. Chem. Phys.*, 2014, **141**, 031101.
310. V. Bonačić-Koutecký, J. Koutecký, J. Michl, *Angew. Chem., Int. Ed.*, 1987, **26**, 170-189.
311. K. Ruedenberg, M. W. Schmidt, M. M. Gilbert, S. T. Elbert, *Chem. Phys.*, 1982, **71**, 41-49.
312. P. M. Kozlowski, M. Dupuis, E. R. Davidson, *J. Am. Chem. Soc.*, 1995, **117**, 774-778.
313. W. T. Borden, E. R. Davidson, *Acc. Chem. Res.*, 1996, **29**, 67-75.
314. E. R. Davidson, *J. Phys. Chem.*, 1996, **100**, 6161-6166.
315. A. I. Krylov, *Chem. Phy. Lett.*, 2001, **338**, 375-384.
316. A. I. Krylov, *Chem. Phys. Lett.*, 2001, **350**, 522-530.
317. A. I. Krylov, C. D. Sherrill, *J. Chem. Phys.*, 2002, **116**, 3194-3203.
318. L. Slipchenko, A. Krylov, *J. Chem. Phys.*, 2002, **117**, 4694-4708.
319. Y. Shao, M. Head-Gordon, A. I. Krylov, *J. Chem. Phys.*, 2003, **118**, 4807-4818.
320. F. Wang, T. Ziegler, *J. Chem. Phys.*, 2004, **121**, 12191-12196.
321. F. Wang, T. Ziegler, *J. Chem. Phys.*, 2005, **122**, 074109.
322. E. Runge, E. K. U. Gross, *Phys. Rev. Lett.*, 1984, **52**, 997-1000.
323. M. Petersilka, U. J. Gossmann, E. K. U. Gross, *Phys. Rev. Lett.*, 1996, **76**, 1212-1215.
324. O. V. Gritsenko, P. R. T. Schipper, E. J. Baerends, *J. Chem. Phys.*, 1997, **107**, 5007-5015.
325. D. Cremer, *Mol. Phys.*, 2001, **99**, 1899-1940.
326. R. Pollet, A. Savin, T. Leininger, H. Stoll, *J. Chem. Phys.*, 2002, 1250-1258.
327. J. Gräfenstein, D. Cremer, *Phys. Chem. Chem. Phys.*, 2000, **2**, 2091-2103.
328. F. Weigend, M. Haser, *Theor. Chem. Acc.*, 1997, **97**, 331-340.
329. S. Grimme, M. Waletzke, *J. Chem. Phys.*, 1999, **111**, 5645-5655.
330. J. Gräfenstein, D. Cremer, *Chem. Phys. Lett.*, 2000, **316**, 569-577.
331. J. M. L. Martin, J. El-Yazal, J.-P. François, *Mol. Phys.*, 1995, **86**, 1437-1450.
332. M. E. Casida, in *Recent Advances in Density Functional Methods*, World Scientific, 1995, pp. 155-192.
333. S. Hirata, M. Head-Gordon, *Chem. Phys. Lett.*, 1999, **314**, 291-299.
334. W. Kohn, A. D. Becke, R. G. Parr, *J. Phys. Chem.*, 1996, **100**, 12974-12980.
335. Y. Tawada, T. Tsuneda, S. Yanagisawa, T. Yanai, K. Hirao, *J. Chem. Phys.*, 2004, **120**, 8425-8433.
336. S. Hirata, M. Head-Gordon, *Chem. Phys. Lett.*, 1999, **302**, 375-382.
337. L. Noodleman, *J. Chem. Phys.*, 1981, **74**, 5737-5743.
338. L. Noodleman, E. R. Davidson, *Chem. Phys.*, 1986, **109**, 131-143.

339. F. Neese, *J. Phys. Chem. Solids*, 2004, **65**, 781-785.

340. C. Herrmann, M. Reiher, B. A. Hess, *J. Chem. Phys.*, 2005, **122**, 034102.

341. K. Yamaguchi, Y. Takahara, T. Fueno, presented in part at the Applied Quantum Chemistry, Dordrecht, 1986.

342. T. Soda, Y. Kitagawa, T. Onishi, Y. Takano, Y. Shigeta, H. Nagao, Y. Yoshioka, K. Yamaguchi, *Chem. Phys. Lett.*, 2000, **319**, 223-230.

343. H. F. King, R. E. Stanton, H. Kim, R. E. Wyatt, R. G. Parr, *J. Chem. Phys.*, 1967, **47**, 1936-1941.

344. A. T. Amos, G. G. Hall, *Proc. R. Soc. Ser. A*, 1961, **263**, 483-493.

345. K. Yamaguchi, Y. Yoshioka, T. Takatsuka, T. Fueno, *Theor. Chim. Acta*, 1978, **48**, 185-206.

346. R. Shepard, *The Multiconfiguration Self-Consistent Field Method*, Wiley-Interscience, New York, 2007.

347. B. O. Roos, *John Wiley & Sons, Inc.: 2007*, 2007, DOI: doi:10.1002/9780470142943.ch7, 399–445.

348. P. G. Szalay, T. Müller, G. Gidofalvi, H. Lischka, R. Shepard, *Chem. Rev.*, 2012, **112**, 108-181.

349. F. A. Evangelista, W. D. Allen, H. F. Schaefer, *J. Chem. Phys.*, 2007, **127**, 024102.

350. K. Hirao, in *Recent Advances in Computational Chemistry*, World Scientific, 1999, vol. 4, p. 224.

351. P. G. Wenthold, R. R. Squires, W. C. Lineberger, *J. Am. Chem. Soc.*, 1998, **120**, 5279-5290.

352. D. Kaiser, E. Reusch, P. Hemberger, A. Bodi, E. Welz, B. Engels, I. Fischer, *Phys. Chem. Chem. Phys.*, 2018, **20**, 3988-3996.

353. S. R. Gwaltney, E. F. C. Byrd, T. V. Voorhis, M. Head-Gordon, *Chem. Phys. Lett.*, 2002, **353**, 359-367.

354. T. Van Voorhis, M. Head-Gordon, *Chem. Phys. Lett.*, 2000, **330**, 585-594.

355. A. I. Krylov, C. D. Sherrill, E. F. C. Byrd, M. Head-Gordon, *J. Chem. Phys.*, 1998, **109**, 10669-10678.

356. A. I. Krylov, C. D. Sherrill, M. Head-Gordon, *J. Chem. Phys.*, 2000, 6509-6527.

357. M. Wladyslawski, M. Nooijen, in *Low-Lying Potential Energy Surfaces*, American Chemical Society, 2002, vol. 828, ch. 4, pp. 65-92.

358. B. K. Carpenter, J. Pittner, L. Veis, *J. Phys. Chem. A*, 2009, **113**, 10557-10563.

359. L. Noodleman, E. J. Baerends, *J. Am. Chem. Soc.*, 1984, **106**, 2316-2327.

360. L. Noodleman, D. A. Case, A. Aizman, *J. Am. Chem. Soc.*, 1988, **110**, 1001-1005.

361. T. Kawakami, R. Takeda, S. Nishihara, T. Saito, M. Shoji, S. Yamada, S. Yamanaka, Y. Kitagawa, M. Okumura, K. Yamaguchi, *J. Phys. Chem. A*, 2009, **113**, 15281-15297.

362. H. B. Schlegel, *J. Chem Phys.*, 1986, **84**, 4530–4534.

363. B. H. Schlegel, J. M. Wittbrodt, *J. Chem. Phys.*, 1996, **105**, 6574–6577.

364. D. H. Ess, E. R. Johnson, X. Hu, W. Yang, *J. Phys. Chem. A*, 2011, **115**, 76-83.

365. D. Peng, X. Hu, D. Devarajan, D. H. Ess, E. R. Johnson, W. Yang, *J. Chem. Phys.*, 2012, **137**, 114112.

366. A. J. Cohen, P. Mori-Sánchez, W. Yang, *Chem. Rev.*, 2012, **112**, 289-320.

367. A. J. Cohen, P. Mori-Sánchez, W. Yang, 2008, **321**, 792-794.

368. A. I. Krylov, *Chem. Phys. Lett.*, 2001, **338**, 375-384.

369. A. I. Krylov, *Acc. Chem. Res.*, 2006, **39**, 83-91.

370. D. Casanova, M. Head-Gordon, *Phys. Chem. Chem. Phys.*, 2009, **11**, 9779-9790.

371. P. M. Zimmerman, F. Bell, M. Goldey, A. T. Bell, M. Head-Gordon, *J. Chem. Phys.*, 2012, **137**, 164110.

372. S. V. Levchenko, A. I. Krylov, *J. Chem. Phys.*, 2003, **120**, 175-185.

373. L. V. Slipchenko, A. I. Krylov, *J. Chem. Phys.*, 2005, **123**, 084107.

374. P. U. Manohar, A. I. Krylov, *J. Chem. Phys.*, 2008, **129**, 194105.

375. V. Pless, H. U. Suter, B. Engels, *J. Phys. Chem.*, 1994, **101**, 4042-4048.

376. V. Settels, W. Liu, J. Pflaum, R. F. Fink, B. Engels, *J. Comput. Chem.*, 2012, **33**, 1544-1553.

377. M. Peric, B. Engels, S. D. Peyerimhoff, *J. Mol. Spectrosc.*, 1991, **150**, 70-85.

378. B. Engels, *Theor. Chem. Acc.*, 1993, **86**, 429-437.

379. B. Engels, S. D. Peyerimhoff, *Mol. Phys.*, 1989, **67**, 583-600.

380. L. Ji, R. M. Edkins, A. Lorbach, I. Krummenacher, C. Bruckner, A. Eichhorn, H. Braunschweig, B. Engels, P. J. Low, T. B. Marder, *J. Am. Chem. Soc.*, 2015, **137**, 6750-6753.

381. C. Brückner, F. Wuerthner, K. Meerholz, B. Engels, *J. Phys. Chem. C*, 2017, **121**, 4-25.

382. M. M. Francl, W. J. Pietro, W. J. Hehre, J. S. Binkley, M. S. Gordon, D. J. Defrees, J. A. Pople, *J. Chem. Phys.*, 1982, **77**, 3654-3665.

383. J. A. Pople, M. Headgordon, K. Raghavachari, *J. Chem. Phys.*, 1987, **87**, 5968-5975.

384. A. D. McLean, G. S. Chandler, *J. Chem. Phys.*, 1980, **72**, 5639-5648.

385. T. Clark, J. Chandrasekhar, G. W. Spitznagel, P. V. R. Schleyer, *J. Chem. Phys.*, 1983, **4**, 294-301.

386. M. J. Frisch, J. A. Pople, J. S. Binkley, *J. Chem. Phys.*, 1984, **80**, 3265-3269.

387. K. B. Wiberg, *J. Comp. Chem.*, 2004, **25**, 1342-1346.

388. M. Klene, M. A. Robb, M. J. Frisch, P. Celani, *J. Chem. Phys.*, 2000, **113**, 5653-5665.

389. M. Frisch, I. N. Ragazos, M. A. Robb, B. H. Schlegel, *Chem. Phys. Lett.*, 1992, **189**, 524-528.

390. F. Bernardi, A. Bottoni, J. J. W. McDouall, M. A. Robb, H. B. Schlegel, *Faraday Symp. Chem. Soc.*, 1984, **19**, 137-147.

391. H. B. Schlegel, M. A. Robb, *Chem. Phys. Lett.*, 1982, **93**, 43-46.

392. R. H. A. Eade, M. A. Robb, *Chem. Phys. Lett.*, 1981, **83**, 362-368.

393. F. Weigend, R. Ahlrichs, *Phys. Chem. Chem. Phys.*, 2005, **7**, 3297-3305.

394. F. Weigend, *Phys. Chem. Chem. Phys.*, 2006, **8**, 1057-1065.

395. M. Schütz, *Phys. Chem. Chem. Phys.*, 2002, **4**, 3941-3947.

396. C. Hampel, H. J. Werner, *J. Chem. Phys.*, 1996, **104**, 6286-6297.

397. M. Schütz, H.-J. Werner, *Chem. Phys. Lett.*, 2000, **318**, 370-378.

398. R. T. McGibbon, A. G. Taube, A. G. Donchev, K. Siva, F. Hernández, C. Hargus, K.-H. Law, J. L. Klepeis, D. E. Shaw, *J. Chem. Phys.*, 2017, **147**, 161725.

399. D. P. Tew, B. Helmich, C. Hättig, *J. Chem. Phys.*, 2011, **135**, 074107.

400. C. Hättig, D. P. Tew, B. Helmich, *J. Chem. Phys.*, 2012, **136**, 204105.

401. S. Grimme, L. Goerigk, R. F. Fink, *Wiley Interdiscip. Rev. Comput. Mol. Sci.*, 2012, **2**, 886-906.

402. T. H. Dunning, *J. Chem. Phys.*, 1989, **90**, 1007-1023.

403. R. A. Kendall, T. H. D. Jr., R. J. Harrison, *J. Chem. Phys.*, 1992, **96**, 6796-6806.

404. T. GmbH,TURBOMOLE V7.1 2016, University of Karlsruhe and Forschungszentrum Karlsruhe GmbH, Karlsruhe, 2016.

405. M. J. Frisch, G. W. Trucks, H. B. Schlegel, G. E. Scuseria, M. A. Robb, J. R. Cheeseman, G. Scalmani, V. Barone, G. A. Petersson, H. Nakatsuji, X. Li, M. Caricato, A. V. Marenich, J. Bloino, B. G. Janesko, R. Gomperts, B. Mennucci, H. P. Hratchian, J. V. Ortiz, A. F.

Izmaylov, J. L. Sonnenberg, Williams, F. Ding, F. Lipparini, F. Egidi, J. Goings, B. Peng, A. Petrone, T. Henderson, D. Ranasinghe, V. G. Zakrzewski, J. Gao, N. Rega, G. Zheng, W. Liang, M. Hada, M. Ehara, K. Toyota, R. Fukuda, J. Hasegawa, M. Ishida, T. Nakajima, Y. Honda, O. Kitao, H. Nakai, T. Vreven, K. Throssell, J. A. Montgomery Jr., J. E. Peralta, F. Ogliaro, M. J. Bearpark, J. J. Heyd, E. N. Brothers, K. N. Kudin, V. N. Staroverov, T. A. Keith, R. Kobayashi, J. Normand, K. Raghavachari, A. P. Rendell, J. C. Burant, S. S. Iyengar, J. Tomasi, M. Cossi, J. M. Millam, M. Klene, C. Adamo, R. Cammi, J. W. Ochterski, R. L. Martin, K. Morokuma, O. Farkas, J. B. Foresman, D. J. Fox, Gaussian 16 Rev. B.01 Wallingford, CT, 2016.

406. F. Neese, *Wiley Interdiscip. Rev. Comput. Mol. Sci.*, 2012, **2**, 73-78.

407. E. D. Glendening, J. K. Badenhoop, A. E. Reed, J. E. Carpenter, J. A. Bohmann, C. M. Morales, C. R. Landis, F. Weinhold, NBO 6.0.Theoretical Chemistry Institute, University of Wisconsin, Madison, 2013.

408. J. Böhnke, T. Dellermann, M. A. Celik, I. Krummenacher, R. D. Dewhurst, S. Demeshko, W. C. Ewing, K. Hammond, M. Heß, E. Bill, E. Welz, M. I. S. Röhr, R. Mitrić, B. Engels, F. Meyer, H. Braunschweig, *Nat. Commun.*, 2018, **9**, 1197.

409. N. Orms, D. R. Rehn, A. Dreuw, A. I. Krylov, *J. Chem. Theory Comput.*, 2018, **14**, 638-648.

410. Y. Shoji, T. Matsuo, D. Hashizume, M. J. Gutmann, H. Fueno, K. Tanaka, K. Tamao, *J. Am. Chem. Soc.*, 2011, **133**, 11058-11061.

411. M.-A. Légaré, G. Bélanger-Chabot, R. D. Dewhurst, E. Welz, I. Krummenacher, B. Engels, H. Braunschweig, *Science*, 2018, **359**, 896-900.

412. E. Welz, J. Böhnke, R. D. Dewhurst, H. Braunschweig, B. Engels, *J. Am. Chem. Soc.*, 2018, **140**, 12580-12591.

413. Y. Wang, X. Wang, D. G. Truhlar, X. He, *J. Chem. Theory Comput.*, 2017, **13**, 6068-6077.

414. H. W. Wanzlick, *Angew. Chem.*, 1962, **74**, 129-134.

415. R. Breslow, *J. Am. Chem. Soc.*, 1958, **80**, 3719-3726.

416. H.-W. Wanzlick, E. Schikora, *Chem. Ber.*, 1961, **94**, 2389-2393.

417. H. W. Wanzlick, *Angew. Chem., Int. Ed.*, 1962, **1**, 75-80.

418. A. Igau, H. Grutzmacher, A. Baceiredo, G. Bertrand, *J. Am. Chem. Soc.*, 1988, **110**, 6463-6466.

419. A. J. Arduengo, R. L. Harlow, M. Kline, *J. Am. Chem. Soc.*, 1991, **113**, 361-363.

420. W. A. Herrmann, D. Mihalios, K. Öfele, P. Kiprof, F. Belmedjahed, *Chem. Ber.*, 1992, **125**, 1795-1799.

421. K. Öfele, W. A. Herrmann, D. Mihalios, M. Elison, E. Herdtweck, W. Scherer, J. Mink, *J. Organomet. Chem.*, 1993, **459**, 177-184.

422. W. A. Herrmann, K. Öfele, M. Elison, F. E. Kühn, P. W. Roesky, *J . Organomet. Chem.*, 1994, **480**, c7-c9.

423. K. Öfele, W. A. Herrmann, D. Mihalios, M. Elison, E. Herdtweck, T. Priermeier, P. Kiprof, *J. Organomet. Chem.*, 1995, **498**, 1-14.

424. W. A. Herrmann, O. Runte, G. Artus, *J. Organomet. Chem.*, 1995, **501**, c1-c4.

425. W. A. Herrmann, *Angew. Chem., Int. Ed.*, 2002, **41**, 1290-1309.

426. A. J. Arduengo, J. R. Goerlich, W. J. Marshall, *J. Am. Chem. Soc.*, 1995, **117**, 11027-11028.

427. R. W. Alder, P. R. Allen, M. Murray, A. G. Orpen, *Angew. Chem., Int. Ed.*, 1996, **35**, 1121-1123.

428. R. W. Alder, M. E. Blake, C. Bortolotti, S. Bufali, C. P. Butts, E. Linehan, J. M. Oliva, A. Guy Orpen, M. J. Quayle, *Chem. Commun.*, 1999, 241-242.

429. D. Enders, K. Breuer, G. Raabe, J. Runsink, J. H. Teles, J.-P. Melder, K. Ebel, S. Brode, *Angew. Chem., Int. Ed.*, 1995, **34**, 1021-1023.

430. A. J. Arduengo, J. R. Goerlich, W. J. Marshall, *Liebigs Ann.*, 2006, **1997**, 365-374.

431. R. W. Alder, C. P. Butts, A. G. Orpen, *J. Am. Chem. Soc.*, 1998, **120**, 11526-11527.

432. M. Iglesias, D. J. Beetstra, J. C. Knight, L.-L. Ooi, A. Stasch, S. Coles, L. Male, M. B. Hursthouse, K. J. Cavell, A. Dervisi, I. A. Fallis, *Organometallics*, 2008, **27**, 3279-3289.

433. M. Melaimi, R. Jazzar, M. Soleilhavoup, G. Bertrand, *Angew. Chem., Int. Ed.*, 2017, **56**, 10046-10068.

434. M. Melaimi, M. Soleilhavoup, G. Bertrand, *Angew. Chem., Int. Ed.*, 2010, **49**, 8810-8849.

435. M. N. Hopkinson, C. Richter, M. Schedler, F. Glorius, *Nature*, 2014, **510**, 485.

436. V. Lavallo, Y. Canac, C. Präsang, B. Donnadieu, G. Bertrand, *Angew. Chem., Int. Ed.*, 2005, **44**, 5705-5709.

437. R. H. Grubbs, *Angew. Chem., Int. Ed.*, 2006, **45**, 3760-3765.

438. W. A. Herrmann, M. Elison, J. Fischer, C. Köcher, G. R. J. Artus, *Angew. Chem., Int. Ed.*, 1995, **34**, 2371-2374.

439. U. Frenzel, T. Weskamp, F. J. Kohl, W. C. Schattenmann, O. Nuyken, W. A. Herrmann, *J. Organomet. Chem.*, 1999, **586**, 263-265.

440. T. Weskamp, V. P. W. Böhm, W. A. Herrmann, *J . Organomet. Chem.*, 2000, **600**, 12-22.

441. C. Yang, H. M. Lee, S. P. Nolan, *Org. Lett.*, 2001, **3**, 1511-1514.

442. D. S. McGuinness, K. J. Cavell, *Organometallics*, 2000, **19**, 741-748.

443. E. Peris, J. A. Loch, J. Mata, R. H. Crabtree, *Chem. Commun.*, 2001, 201-202.

444. S. Caddick, F. G. N. Cloke, G. K. B. Clentsmith, P. B. Hitchcock, D. McKerrecher, L. R. Titcomb, M. R. V. Williams, *J. Organomet. Chem.*, 2001, **617-618**, 635-639.

445. T. M. Trnka, R. H. Grubbs, *Acc. Chem. Res.*, 2001, **34**, 18-29.

446. A. K. Chatterjee, J. P. Morgan, M. Scholl, R. H. Grubbs, *J. Am. Chem. Soc.*, 2000, **122**, 3783-3784.

447. A. K. Chatterjee, R. H. Grubbs, *Org. Lett.*, 1999, **1**, 1751-1753.

448. C. L. Yang, S. P. Nolan, *Synlett*, 2001, 1539-1542.

449. J. Huang, S. P. Nolan, *J. Am. Chem. Soc.*, 1999, **121**, 9889-9890.

450. V. P. W. Böhm, T. Weskamp, C. W. K. Gstöttmayr, W. A. Herrmann, *Angew. Chem., Int. Ed.*, 2000, **39**, 1602-1604.

451. G. A. Grasa, S. P. Nolan, *Org. Lett.*, 2001, **3**, 119-122.

452. A. K. Phukan, A. K. Guha, S. Sarmah, R. D. Dewhurst, *J. Org. Chem.*, 2013, **78**, 11032-11039.

453. B. Borthakur, T. Rahman, A. K. Phukan, *J. Org. Chem.*, 2014, **79**, 10801-10810.

454. M. Z. Kassaee, F. A. Shakib, M. R. Momeni, M. Ghambarian, S. M. Musavi, *J. Org. Chem.*, 2010, **75**, 2539-2545.

455. M. Arrowsmith, J. D. Mattock, J. Bohnke, I. Krummenacher, A. Vargas, H. Braunschweig, *Chem. Commun.*, 2018, **54**, 4669-4672.

456. M. Arrowsmith, H. Braunschweig, T. E. Stennett, *Angew. Chem., Int. Ed.*, 2017, **56**, 96-115.

457. J. Böhnke, H. Braunschweig, T. Dellermann, W. C. Ewing, T. Kramer, I. Krummenacher, A. Vargas, *Angew. Chem., Int. Ed.*, 2015, **54**, 4469-4473.

458. P. Bissinger, H. Braunschweig, A. Damme, I. Krummenacher, A. K. Phukan, K. Radacki, S. Sugawara, *Angew. Chem., Int. Ed.*, 2014, **53**, 7360-7363.

459. M. Arrowsmith, J. Böhnke, H. Braunschweig, M. A. Celik, T. Dellermann, K. Hammond, *Chem. Eur. J.*, 2016, **22**, 17169-17172.

460. R. Jazzar, J.-B. Bourg, R. D. Dewhurst, B. Donnadieu, G. Bertrand, *J. Org. Chem.*, 2007, **72**, 3492-3499.

461. X. Zeng, G. D. Frey, R. Kinjo, B. Donnadieu, G. Bertrand, *J. Am. Chem. Soc.*, 2009, **131**, 8690-8696.

462. K. Denk, P. Sirsch, W. A. Herrmann, *J. Organomet. Chem.*, 2002, **649**, 219-224.

463. V. Lavallo, Y. Canac, A. DeHope, B. Donnadieu, G. Bertrand, *Angew. Chem., Int. Ed.*, 2005, **44**, 7236-7239.

464. C. A. Tolman, *Chem. Rev.*, 1977, **77**, 313-348.

465. K. Verlinden, H. Buhl, W. Frank, C. Ganter, *Eur. J. Inorg. Chem.*, 2015, **2015**, 2416-2425.

466. A. Liske, K. Verlinden, H. Buhl, K. Schaper, C. Ganter, *Organometallics*, 2013, **32**, 5269-5272.

467. R. R. Rodrigues, C. L. Dorsey, C. A. Arceneaux, T. W. Hudnall, *Chem. Commun.*, 2014, **50**, 162-164.

468. O. Back, M. Henry-Ellinger, C. D. Martin, D. Martin, G. Bertrand, *Angew. Chem., Int. Ed.*, 2013, **52**, 2939-2943.

469. U. S. D. Paul, U. Radius, *Eur. J. Inorg. Chem.*, 2017, **2017**, 3362-3375.

470. B. Rao, H. Tang, X. Zeng, L. Liu, M. Melaimi, G. Bertrand, *Angew. Chem., Int. Ed.*, 2015, **54**, 14915-14919.

471. Z. R. McCarty, D. N. Lastovickova, C. W. Bielawski, *Chem. Commun.*, 2016, **52**, 5447-5450.

472. L. Wang, S. Y. Lim, Y. Li, R. Ganguly, R. Kinjo, *Molecules*, 2016, **21**, 990.

473. T. Kosai, S. Ishida, T. Iwamoto, *Angew. Chem., Int. Ed.*, 2016, **55**, 15554-15558.

474. M. Arrowsmith, J. Böhnke, H. Braunschweig, M. A. Celik, *Angew. Chem., Int. Ed.*, 2017, **56**, 14287-14292.

475. M. Arrowsmith, H. Braunschweig, T. E. Stennett, *Angew. Chem., Int. Ed.*, 2016, **56**, 96-115.

476. P. Bissinger, H. Braunschweig, A. Damme, T. Kupfer, A. Vargas, *Angew. Chem., Int. Ed.*, 2012, **51**, 9931-9934.

477. H. Braunschweig, R. D. Dewhurst, K. Hammond, J. Mies, K. Radacki, A. Vargas, *Science*, 2012, **336**, 1420.

478. H. Klusik, A. Berndt, *Angew. Chem., Int. Ed.*, 1981, **20**, 870-871.

479. A. Moezzi, M. M. Olmstead, P. P. Power, *J. Am. Chem. Soc.*, 1992, **114**, 2715-2717.

480. P. P. Power, *Inorg. Chim. Acta*, 1992, **198-200**, 443-447.

481. A. Moezzi, R. A. Bartlett, P. P. Power, *Angew. Chem., Int. Ed.*, 1992, **31**, 1082-1083.

482. Y. Wang, B. Quillian, P. Wei, C. S. Wannere, Y. Xie, R. B. King, H. F. Schaefer, P. v. R. Schleyer, G. H. Robinson, *J. Am. Chem. Soc.*, 2007, **129**, 12412-12413.

483. Y. Wang, B. Quillian, P. Wei, Y. Xie, C. S. Wannere, R. B. King, H. F. Schaefer, P. v. R. Schleyer, G. H. Robinson, *J. Am. Chem. Soc.*, 2008, **130**, 3298-3299.

484. Y. Wang, G. H. Robinson, *Inorg. Chem.*, 2011, **50**, 12326-12337.

485. P. Bissinger, H. Braunschweig, A. Damme, R. D. Dewhurst, T. Kupfer, K. Radacki, K. Wagner, *J. Am. Chem. Soc.*, 2011, **133**, 19044-19047.

486. W. J. Grigsby, P. P. Power, *J. Am. Chem. Soc.*, 1996, **118**, 7981-7988.

487. L. C. Ducati, N. Takagi, G. Frenking, *J. Phys. Chem. A*, 2009, **113**, 11693-11698.

488. J. Böhnke, H. Braunschweig, P. Constantinidis, T. Dellermann, W. C. Ewing, I. Fischer, K. Hammond, F. Hupp, J. Mies, H.-C. Schmitt, A. Vargas, *J. Am. Chem. Soc.*, 2015, **137**, 1766-1769.

489. M. M. Hansmann, M. Melaimi, D. Munz, G. Bertrand, *J. Am. Chem. Soc.*, 2018, **140**, 2546-2554.

490. C. M. Weinstein, G. P. Junor, D. R. Tolentino, R. Jazzar, M. Melaimi, G. Bertrand, *J. Am. Chem. Soc.*, 2018, **140**, 9255-9260.

491. H. G. Viehe, Z. Janousek, R. Merenyi, L. Stella, *Acc. Chem. Res.*, 1985, **18**, 148-154.

492. D. Griller, K. U. Ingold, *Acc. Chem. Res.*, 1976, **9**, 13-19.

493. H. Fischer, *Chem. Rev.*, 2001, **101**, 3581-3610.

494. I. Degirmenci, M. L. Coote, *J. Phys. Chem. A*, 2016, **120**, 7398-7403.

495. K. U. Ingold, in *The Foundations of Physical Organic Chemistry: Fifty Years of the James Flack Norris Award*, American Chemical Society, 2015, vol. 1209, ch. 10, pp. 223-250.

496. L. Stella, Z. Janousek, R. Merényi, H. G. Viehe, *Angew. Chem., Int. Ed.*, 1978, **17**, 691-692.

497. C. D. Martin, M. Soleilhavoup, G. Bertrand, *Chem. Sci.*, 2013, **4**, 3020-3030.

498. H. Jacobsen, A. Correa, A. Poater, C. Costabile, L. Cavallo, *Coord. Chem. Rev.*, 2009, **253**, 687-703.

499. H. Jacobsen, A. Correa, C. Costabile, L. Cavallo, *J. Organomet. Chem.*, 2006, **691**, 4350-4358.

500. D. M. Khramov, V. M. Lynch, C. W. Bielawski, *Organometallics*, 2007, **26**, 6042-6049.

501. B. Tumanskii, D. Sheberla, G. Molev, Y. Apeloig, *Angew. Chem., Int. Ed.*, 2007, **46**, 7408-7411.

502. J. A. S. Roberts, J. A. Franz, E. F. van der Eide, E. D. Walter, J. L. Petersen, D. L. DuBois, R. M. Bullock, *J. Am. Chem. Soc.*, 2011, 14593-14603.

503. C. Chen, H. Qiu, W. Chen, D. Wang, *J. Organomet. Chem.*, 2008, **693**, 3273-3280.

504. M. M. Hansmann, M. Melaimi, G. Bertrand, *J. Am. Chem. Soc.*, 2018, **140**, 2206-2213.

505. D. Munz, J. Chu, M. Melaimi, G. Bertrand, *Angew. Chem., Int. Ed.*, 2016, **55**, 12886-12890.

506. H. Braunschweig, I. Krummenacher, M.-A. Légaré, A. Matler, K. Radacki, Q. Ye, *J. Am. Chem. Soc.*, 2017, **139**, 1802-1805.

507. H. Braunschweig, R. D. Dewhurst, *Angew. Chem., Int. Ed.*, 2013, **52**, 3574-3583.

508. W. Lu, Y. Li, R. Ganguly, R. Kinjo, *J. Am. Chem. Soc.*, 2017, **139**, 5047-5050.

509. W. Lu, Y. Li, R. Ganguly, R. Kinjo, *Angew. Chem.*, 2017, **129**, 9961-9964.

510. C. M. Weinstein, G. P. Junor, D. R. Tolentino, R. Jazzar, M. Melaimi, G. Bertrand, *J. Am. Chem. Soc.*, 2018, **140**, 9255-9260.

511. M. Soleilhavoup, G. Bertrand, *Acc. Chem. Res.*, 2015, **48**, 256-266.

512. Y. Katsuma, N. Tsukahara, L. Wu, Z. Lin, M. Yamashita, *Angew. Chem., Int. Ed.*, 2018, **57**, 6109-6114.

513. N. Tsukahara, H. Asakawa, K.-H. Lee, Z. Lin, M. Yamashita, *J. Am. Chem. Soc.*, 2017, **139**, 2593-2596.

514. J. Böhnke, H. Braunschweig, T. Dellermann, W. C. Ewing, T. Kramer, I. Krummenacher, A. Vargas, *Angew. Chem.*, 2015, **127**, 4551-4555.

515. J. Wolff, *Starch - Stärke*, 1985, **37**, 176-176.

516. G. Frenking, R. Tonner, S. Klein, N. Takagi, T. Shimizu, A. Krapp, K. K. Pandey, P. Parameswaran, *Chem. Soc. Rev.*, 2014, **43**, 5106-5139.

517. G. Frenking, M. Hermann, D. M. Andrada, N. Holzmann, *Chem. Soc. Rev.*, 2016, **45**, 1129-1144.

518. D. Martin, M. Melaimi, M. Soleilhavoup, G. Bertrand, *Organometallics*, 2011, **30**, 5304-5313.

519. M. Arrowsmith, J. Böhnke, H. Braunschweig, A. Deißenberger, R. D. Dewhurst, W. C. Ewing, C. Hörl, J. Mies, J. H. Muessig, *Chem. Commun.*, 2017, **53**, 8265-8267.

520. M. Arrowsmith, J. Böhnke, H. Braunschweig, M. A. Celik, C. Claes, W. C. Ewing, I. Krummenacher, K. Lubitz, C. Schneider, *Angew. Chem., Int. Ed.*, 2016, **55**, 11271-11275.

521. J. Seufert, E. Welz, I. Krummenacher, V. Paprocki, J. Böhnke, S. Hagspiel, R. D. Dewhurst, R. Tacke, B. Engels, H. Braunschweig, *Angew. Chem.*, 2018, **130**, 10912-10915.

522. M. Hidai, Y. Mizobe, *Chem. Rev.*, 1995, **95**, 1115-1133.

523. B. A. MacKay, M. D. Fryzuk, *Chem. Rev.*, 2004, **104**, 385-402.

524. N. Hazari, *Chem. Soc. Rev.*, 2010, **39**, 4044-4056.

525. R. R. Schrock, *Acc. Chem. Res.*, 2005, **38**, 955-962.

526. F. Haber, G. van Oordt, *Z. Anorg. Chem.*, 1905, **44**, 341-378.

527. O. Lemmermann, *Z. Pflanzenernaehr. Dueng. Bodenk.*, 1951, **55**, 258-258.

528. R. Schlögl, *Angew. Chem.*, 2003, **115**, 2050-2055.

529. P. P. Power, *Nature*, 2010, **463**, 171.

530. D. Martin, M. Soleilhavoup, G. Bertrand, *Chem. Sci.*, 2011, **2**, 389-399.

531. O. Back, B. Donnadieu, M. von Hopffgarten, S. Klein, R. Tonner, G. Frenking, G. Bertrand, *Chem. Sci.*, 2011, **2**, 858-861.

532. M. M. Hansmann, M. Melaimi, G. Bertrand, *J. Am. Chem. Soc.*, 2017, **139**, 15620-15623.

533. A. J. Arduengo, G. Bertrand, *Chem. Rev.*, 2009, **109**, 3209-3210.

534. S. Raoufmoghaddam, Y.-P. Zhou, Y. Wang, M. Driess, *J. Organomet. Chem.*, 2017, **829**, 2-10.

535. M. Asay, C. Jones, M. Driess, *Chem. Rev.*, 2011, **111**, 354-396.

536. C. Marschner, *Eur. J. Inorg. Chem.*, 2015, **2015**, 3805-3820.

537. F. Dielmann, O. Back, M. Henry-Ellinger, P. Jerabek, G. Frenking, G. Bertrand, *Science*, 2012, **337**, 1526.

538. M. M. Hansmann, G. Bertrand, *J. Am. Chem. Soc.*, 2016, **138**, 15885-15888.

539. L. Liu, David A. Ruiz, D. Munz, G. Bertrand, *Chem*, 2016, **1**, 147-153.

540. H. Braunschweig, C. Kollann, U. Englert, *Angew. Chem., Int. Ed.*, 1998, **37**, 3179-3180.

541. H. Braunschweig, R. D. Dewhurst, V. H. Gessner, *Chem. Soc. Rev.*, 2013, **42**, 3197-3208.

542. H. Braunschweig, R. D. Dewhurst, A. Schneider, *Chem. Rev.*, 2010, **110**, 3924-3957.

543. M. Krasowska, H. F. Bettinger, *J. Am. Chem. Soc.*, 2012, **134**, 17094-17103.

544. M. Krasowska, M. Edelmann, H. F. Bettinger, *J. Phys. Chem. A*, 2016, **120**, 6332-6341.

545. C. Buron, H. Gornitzka, V. Romanenko, G. Bertrand, *Science*, 2000, **288**, 834.

546. S. Solé, H. Gornitzka, W. W. Schoeller, D. Bourissou, G. Bertrand, *Science*, 2001, **292**, 1901.

547. M. Krasowska, M. Edelmann, H. F. Bettinger, *J. Chem. Phys. A*, 2016, **120**, 6332-6341.

548. M. Krasowska, H. F. Bettinger, *Chem. Eur. J.*, 2016, **22**, 10661-10670.

549. P. Bissinger, H. Braunschweig, K. Kraft, T. Kupfer, *Angew. Chem., Int. Ed.*, 2011, **50**, 4704-4707.

550. H. Braunschweig, C. Claes, A. Damme, A. Deißenberger, R. D. Dewhurst, C. Hörl, T. Kramer, *Chem. Commun.*, 2015, **51**, 1627-1630.

551. M. Soleilhavoup, G. Bertrand, *Angew. Chem., Int. Ed.*, 2017, **56**, 10282-10292.

552. G. D. Frey, V. Lavallo, B. Donnadieu, W. W. Schoeller, G. Bertrand, *Science*, 2007, **316**, 439.

553. M. R. Momeni, E. Rivard, A. Brown, *Organometallics*, 2013, **32**, 6201-6208.

554. S. Würtemberger-Pietsch, U. Radius, T. B. Marder, *Dalton Trans.*, 2016, **45**, 5880-5895.

555. H. Braunschweig, R. D. Dewhurst, F. Hupp, M. Nutz, K. Radacki, C. W. Tate, A. Vargas, Q. Ye, *Nature*, 2015, **522**, 327.

556. H. Braunschweig, M. A. Celik, R. D. Dewhurst, K. Ferkinghoff, A. Hermann, J. O. C. Jimenez-Halla, T. Kramer, K. Radacki, R. Shang, E. Siedler, F. Weißenberger, C. Werner, *Chem. Eur. J.*, 2016, **22**, 11736-11744.

557. P. M. W. Gill, B. G. Johnson, J. A. Pople, M. J. Frisch, *Chem. Phys. Lett.*, 1992, **197**, 499-505.

558. B. G. Johnson, P. M. W. Gill, J. A. Pople, *J. Chem. Phys.*, 1993, **98**, 5612-5626.

559. R. Kinjo, B. Donnadieu, M. A. Celik, G. Frenking, G. Bertrand, *Science*, 2011, **333**, 610-613.

560. M. Balci, in *Basic 1H- and 13C-NMR Spectroscopy*, ed. M. Balci, Elsevier Science, Amsterdam, 2005, pp. 283-292.

561. C. A. Hunter, J. K. M. Sanders, *J. Am. Chem. Soc.*, 1990, **112**, 5525-5534.

562. C.-W. Chiu, F. P. Gabbaï, *Angew. Chem., Int. Ed.*, 2007, **46**, 1723-1725.

563. S.-H. Ueng, M. Makhlouf Brahmi, É. Derat, L. Fensterbank, E. Lacôte, M. Malacria, D. P. Curran, *J. Am. Chem. Soc.*, 2008, **130**, 10082-10083.

564. A. Deissenberger, E. Welz, R. Drescher, I. Krummenacher, R. D. Dewhurst, B. Engels, H. Braunschweig, *Angew. Chem., Int. Ed.*, 2019, **58**, 1842-1846.

565. J. Böhnke, H. Braunschweig, W. C. Ewing, C. Hörl, T. Kramer, I. Krummenacher, J. Mies, A. Vargas, *Angew. Chem., Int. Ed.*, 2014, **53**, 9082-9085.

566. J. Böhnke, H. Braunschweig, T. Dellermann, W. C. Ewing, K. Hammond, J. O. C. Jimenez-Halla, T. Kramer , J. Mies, *Angew. Chem., Int. Ed.*, 2015, **54**, 13801-13805.

567. Z. Zhu, X. Wang, Y. Peng, H. Lei, J. C. Fettinger, E. Rivard, P. P. Power, *Angew. Chem., Int. Ed.*, 2009, **48**, 2031-2034.

568. T. Agou, K. Nagata, T. Sasamori, N. Tokitoh, *Phosphorus Sulfur Silicon Relat. Elem.*, 2016, **191**, 588-590.

569. E. Breitmaier, G. Jung, *Organische Chemie: Grundlagen, Stoffklassen, Reaktionen, Konzepte, Molekülstrukturen*, Thieme, Stuttgart; New York, 2005.

570. R. Ziessel, C. Stroh, H. Heise, F. H. Köhler, P. Turek, N. Claiser, M. Souhassou, C. Lecomte, *J. Am. Chem. Soc.*, 2004, **126**, 12604-12613.

571. C. Stroh, R. Ziessel, P. Turek, *Chem. Commun.*, 1998, 2337-2338.

572. J. Seufert, E. Welz, I. Krummenacher, V. Paprocki, J. Böhnke, S. Hagspiel, R. D. Dewhurst, R. Tacke, B. Engels, H. Braunschweig, *Angew. Chem., Int. Ed.*, 2018, **57**, 10752-10755.